

Gas Hydrate Studies for Carbon Dioxide Capture and Methane Recovery

Thesis Submitted to AcSIR For the Award of
the Degree of
DOCTOR OF PHILOSOPHY
in **CHEMICAL SCIENCES**



By
Asheesh Kumar
10EC13J26043

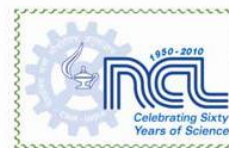
Under the guidance of
Dr. Rajnish Kumar

CSIR-National Chemical Laboratory, Pune (INDIA)

December 2015



राष्ट्रीय रासायनिक प्रयोगशाला
(वैज्ञानिक तथा औद्योगिक अनुसंधान परिषद)
डॉ. होमी भाभा रोड, पुणे - 411 008. भारत
NATIONAL CHEMICAL LABORATORY
(Council of Scientific & Industrial Research)
Dr. Homi Bhabha Road, Pune - 411008. India



Certificate

This is to certify that the work incorporated in this Ph.D. thesis entitled “*Gas Hydrate Studies for Carbon Dioxide Capture and Methane Recovery*” submitted by *Mr. Asheesh Kumar* to Academy of Scientific and Innovative Research (AcSIR) in fulfillment of the requirements for the award of the Degree of *Doctor of Philosophy in Chemical Sciences*, embodies original research work under my/our supervision/guidance.

I/We further certify that this work has not been submitted to any other University or Institution in part or full for the award of any degree or diploma. Research material obtained from other sources has been duly acknowledged in the thesis. Any text, illustration, table etc., used in the thesis from other sources, have been duly cited and acknowledged.

Asheesh Kumar

(Research Scholar)
Mr. Asheesh Kumar
CEPD Division
CSIR-NCL, Pune

Dr. Rajnish Kumar

(Supervisor)
Dr. Rajnish Kumar
Senior Scientist, CEPD Division
CSIR-NCL, Pune

Dr. Rajnish Kumar

Sr. Scientist
Chemical Engineering & Process Development Division
National Chemical Laboratory
Dr. Homi Bhabha Road, Pune-411 008.

Communications Channels +91 20 25902000
+91 20 25893300
+91 20 25893400

Fax +91 20 25902601 (Director)
+91 20 25902660 (Admin.)
+91 20 25902639 (Business Development)

URL : www.ncl-india.org

Declaration by Research Scholar

I hereby declare that the thesis “*Gas Hydrate Studies for Carbon Dioxide Capture and Methane Recovery*” submitted for the degree of Doctor of Philosophy to the AcSIR has been carried out by me at the Chemical Engineering and Process Development Division, CSIR-National Chemical Laboratory, Pune – 411 008, India, under the supervision of *Dr. Rajnish Kumar*. Research material obtained from other sources has been duly acknowledged in the thesis. I declare that the present work has not been submitted to any other University for the award of any other degree or diploma.



Mr. Asheesh Kumar

Research Scholar

Chemical Engineering and Process Development Division

CSIR-National Chemical Laboratory

Dr. Homi Bhabha Road, Pune-411 008, Maharashtra, India

& Academy of Scientific & Innovative Research (AcSIR)-CSIR, India

Acknowledgements

*It gives me immense pleasure to extend my warm appreciation to all those who helped me in pursuing my work contained in this thesis. I take this opportunity to express my deepest sense of appreciation and reverence towards my research supervisor **Dr. Rajnish Kumar** for effortlessly guiding me throughout the course of this work. His experience and expertise helped me immensely.*

*To my family (Specially my parents, **Dr. Virendra Singh** and **Rashmi Singh**), thank you for your support and encouragement throughout the years, and for providing the basic foundations which have enabled my success. I am truly indebted.*

I find this an exceptional opportunity to be glad about and acknowledge the enormous support of my wife for her belief and affection in me that drove me to stand out even under problematic situations.

*I am grateful to **Dr. Sourav Pal, Dr. V. V. Ranade and Dr. Vijaymohan**, Directors, CSIR-NCL, Pune for allowing me to carry out the research work in India's most prestigious, well-equipped and biggest chemical laboratory. I would like to acknowledge the members of my Doctoral Advisory Committee (DAC), **Dr. Kumar Vanka, Dr. Sanjay P Kamble, Dr. S Mayadevi and Dr. Sudip Roy** for their sincere comments, suggestions and constant support.*

I am indebted to many present and past colleagues at NCL: Tushar Sakpal, Nilesh Choudhary, Gaurav Bhattacharjee, Omkar singh, Vivek, Mrunali, Aneesh, Anuj, Anupam, Amit and Dishant for providing a stimulating and fun environment in which to learn and grow. I am grateful to my dear friends Bhanu, Rajendra, Rajeshwari, Geeta, Vijay Rana and Jugal for their constant encouragement and for being always with me in my difficult times.

*I would like to acknowledge our collaborators across the globe, **Drs. Praveen Linga, Sudip Roy, JuDong Lee, Sanjay Kamble, Pushendra Kumar and Chandrajit Balomajumder** for their timely help, comments, provocative ideas and encouraging suggestions towards improvement of the thesis and framing it in right direction.*

I would also like to thank Council of Scientific and Industrial Research (CSIR), Department of science and technology (DST) for providing funding for this project.

Asheesh Kumar

*Dedicated to my Parents
and
My Wife Rekha*

Abstract

Carbon dioxide (CO_2) is one of the major greenhouse gases, which anthropologically gets released into the earth's atmosphere. Use of conventional and un-conventional fossil fuels for energy production is set to continue for the foreseeable future and one needs to develop strategies to contain the emission of CO_2 from point sources such as coal based thermal power station. One of the novel approaches to mitigate CO_2 emission into the atmosphere is CO_2 capture through clathrate hydrate crystallization also known as the hydrate based gas separation (HBGS) process. While separation and capture the CO_2 is one aspect of the study, a complete solution comes from safely sequestering the captured CO_2 for geologically significant time periods.

The main objective of this dissertation is to study the feasibility of the Hydrate Based Gas Separation (HBGS) process for CO_2 capture from point sources such as coal based thermal power stations followed by simultaneous sequestration of the captured CO_2 in hydrate form. The proposed method also allows methane or natural gas recovery from natural gas hydrate reserves (energy production with CO_2 sequestration).

Literature suggests that while hydrate based separation is thermodynamically feasible, there is a good scope in improving the kinetics of hydrate growth while being economical in doing so. This thesis examines the kinetics of hydrate formation and separation of gas mixture by utilizing an effective fixed bed media for enhanced hydrate formation kinetics. Suitable additives (surfactant) were utilized to further enhance the hydrate growth by ensuring better gas/liquid contact. Nonporous metallic (SS-316) mesh arrangements, copper foam and non-structured brass packing having high thermal conductivity compared to conventional packing media such as silica sand and silica gel were used as packing materials in a fixed bed setup to obtain faster hydrate growth kinetics. Sodium dodecyl sulfate (SDS) was found to be an effective kinetic promoter. The amount of CO_2 gas captured "per mass/volume" of packing material was significantly higher for metallic packing media as compared to silica sand and silica gel, which is an important parameter for evaluating a hydrate crystallization process using fixed bed media.

Conventional process of CO_2 capture is highly sensitive to the presence of other acidic impurities in the flue gas stream. In this work, the impact of impurities like fly ash, SO_2 and H_2S on the separation efficiency of the HBGS process for separation and capture of CO_2 from flue gas and fuel gas mixture was also investigated. It was observed that the hydrate equilibrium conditions did not change in the presence of fly ash but hydrate equilibrium shifts to milder conditions in presence of both SO_2 and H_2S . Based on the experimental results obtained in this study, a conceptual process flow diagram for the successful scale-up and commercialization of the HBGS process for CO_2 capture/ separation from fuel gas mixture has been proposed.

Economically viable sequestration of the captured CO_2 through lab scale experimentation was performed in which CO_2 was injected into methane hydrate sediment. The injection of carbon dioxide (CO_2), into hydrate bearing sediments preferentially liberates some of the enclathrated methane (CH_4), by replacing them in the hydrate cages."Additionally, kinetics of methane hydrate formation was investigated in a test sediment of sand and clay.

Table of Contents

Title Page	i
Certificate	ii
Declaration By Research Scholar	iii
Acknowledgements	iv
Dedication	v
Abstract	vi
Table of contents	vii
List of tables	xi
List of figures	xiii

Chapter 1

1. Literature Review	1
1.1. Carbon dioxide capture and storage or sequestration (CCS)	2
<i>1.1.1. Carbon dioxide capture systems</i>	3
<i>1.1.2. Carbon dioxide capture technologies</i>	5
<i>1.1.3. Carbon dioxide sequestration</i>	8
1.2. Background on gas hydrates	10
<i>1.2.1. Gas hydrate structures</i>	13
<i>1.2.2. Thermodynamic of gas hydrates (Gas hydrate phase equilibrium)</i>	15
<i>1.2.3. Kinetics of gas hydrate formation</i>	18
<i>1.2.4. Surface active agents (Surfactants) and their role in gas hydrate studies</i>	20
<i>1.2.5. Surfactants as kinetic hydrate promoters</i>	21
1.3. Research Objectives	24
1.4. Thesis Organization	24

Chapter 2

2. Selection of Suitable Porous Fixed Bed media and Surfactants to Enhance the Carbon Dioxide Hydrate formation Kinetics	26
2.1. Introduction	27
2.2. Experimental Section	28
<i>2.2.1. Materials</i>	28
<i>2.2.2. Apparatus used for surfactant selection with silica gel as fixed bed media</i>	28
<i>2.2.3. Experimental procedure for hydrate formation in silica gel/surfactant system</i>	29
<i>2.2.4. Calculation for the amount of gas consumed</i>	30
<i>2.2.5. Water to hydrate conversion calculation</i>	30
2.3. Results and discussion	31

2.3.1.	Effect of silica gels on hydrate formation kinetics	31
2.3.2.	Effect of surfactants on hydrate formation kinetics in silica gel media	35
2.4.	Conclusion	41

Chapter 3

3.	Impact of fly ash, SO₂ and H₂S impurities on the hydrate based gas separation process for carbon dioxide capture from flue and fuel gas mixtures	42
3.1.	Introduction	43
3.2.	Experimental Section	44
3.2.1.	Materials	44
3.2.2.	Experimental apparatus	45
3.2.2.1.	Stirred tank setup	45
3.2.2.2.	Fixed bed setup	45
3.3.	Impact of Fly ash on HBGS Process	47
3.3.1.	Experimental procedure for finding incipient phase equilibrium data	47
3.3.2.	Experimental procedure for hydrate formation (Kinetics measurements)	48
3.3.3.	Calculation for the amount of gas consumed	49
3.3.4.	Calculation for water to hydrate conversion	49
3.3.5.	Calculation for the rate of hydrate formation	50
3.3.6.	Experimental Procedure for hydrate dissociation	50
3.3.7.	Separation efficiency	51
3.4.	Results and discussion (fly ash impact)	52
3.4.1.	Effect of fly ash impurity on the thermodynamics of hydrate formation	52
3.4.2.	Kinetics of hydrate formation and decomposition in presence of 1 mol% THF and its significance for HBGS process	55
3.4.3.	Effect of fly ash impurity on the hydrate formation kinetics of flue gas mixture and its impact on HBGS process	57
3.4.4.	Effect of two anionic surfactants on gas hydrate formation kinetics and its synergistic effects on kinetics of hydrate formation in presence of fly ash	60
3.4.5.	Gas phase analysis and separation efficiency	63
3.5.	Impact of SO ₂ impurity on HBGS Process	65
3.5.1.	Kinetics of Hydrate Formation in the Presence of kinetic promoter (SDS) for CO ₂ +N ₂ +SO ₂ system	65
3.5.2.	Kinetics of Hydrate Formation in the Presence of THF for CO ₂ +N ₂ +SO ₂ system	67
3.5.3.	Safety concerns in the use of gas mixture containing SO ₂	69
3.6.	Impact of H ₂ S impurity on the hydrate formation (thermodynamics /kinetics of fuel gas mixture and its impact on the HBGS process)	70
3.6.1.	Effect of H ₂ S impurity on the thermodynamics of hydrate formation	70
3.6.2.	Effect of H ₂ S impurity on the kinetics of hydrate formation	71

3.6.2.1.	Kinetics of hydrate formation in STR (CO ₂ + H ₂ + H ₂ S+ STR system)	71
3.6.2.2.	Kinetics of hydrate formation in a fixed bed of silica sand and impact of H ₂ S on silica sand	73
3.6.2.3.	Kinetics of hydrate formation in a fixed bed of silica gel	77
3.7.	Conclusions	79

Chapter 4

4.	Metallic fixed bed media for enhanced gas hydrate formation kinetics: application to carbon dioxide capture from fuel gas mixture	81
4.1.	Introduction	82
4.2.	Experimental Section:	83
4.2.1.	Materials	83
4.2.2.	Procedure for saturating various packing with SDS solution (Pure CO ₂ system)	83
4.2.3.	Apparatus and hydrate formation procedure for experiment conducted with various fixed bed media in batch mode (Pure CO ₂ system)	84
4.2.4.	Apparatus (for Fuel gas system)	84
4.3.	Experimental Procedure (for Fuel gas system)	86
4.3.1.	Preparation of Silica sand Bed	86
4.3.2.	Preparation of metallic Bed:	86
4.3.3.	Hydrate formation/dissociation procedure	86
4.4.	Calculation for the amount of gas consumed during hydrate formation	87
4.5.	Water to hydrate conversion calculation	87
4.6.	Calculation for the rate of hydrate formation	88
4.7.	Results and discussion (for Pure CO ₂ system)	88
4.7.1.	Comparison of CO ₂ hydrate formation kinetics for various fixed bed media (Silica sand, silica gel, SSP-1 and SSP-2)	88
4.8.	Results and discussion (for Fuel gas (CO ₂ + H ₂) system)	97
4.8.1.	Hydrate formation kinetics of fuel gas mixture in silica sand and SSP packing	97
4.8.2.	Hydrate formation kinetics of fuel gas mixture in Copper Foam and Brass packing	106
4.8.3.	Hydrate dissociation kinetics of fuel gas mixture in silica sand, Copper Foam and Brass packing	111
4.9.	Conclusions	116

Chapter 5

5.	Carbon dioxide sequestration by replacement of methane from natural gas hydrate reservoir	117
5.1.	Introduction	118
5.2.	Methane hydrate formation	119

5.2.1.	Materials	119
5.2.2.	Preparation of silica sand/clay bed	120
5.2.3.	Apparatus and hydrate formation procedure	120
5.2.4.	Calculation for the amount of gas consumed during hydrate formation	122
5.2.5.	Water to hydrate conversion calculation	123
5.2.6.	Calculation of rate of hydrate formation	124
5.3.	Results and discussion	124
5.3.1.	Methane hydrate formation in test sediment	124
5.4.	CO ₂ Sequestration and Methane recovery from marine gas hydrates through carbon dioxide replacement	131
5.4.1.	Thermodynamic Feasibility of Replacement	131
5.4.2.	CH ₄ hydrate formation and CH ₄ -CO ₂ hydrate replacement procedure	133
5.4.3.	Calculations for CH ₄ release and CO ₂ consumed during replacement process	134
5.5.	Methane – carbon dioxide replacement	134
5.6.	Conclusion	137

Chapter 6

6.	Summary of Conclusions, Recommendations for Future Work and CSIR-800 project	138
6.1.	Summary of Conclusions	138
6.2.	Conceptual protocol for potential application (continuous removal of carbon dioxide from a fuel gas mixture)	140
6.3.	Recommendations for Future Work	142
6.4.	CSIR-800 Project: A novel approach for seawater desalination: Hydrate based desalination (HBD) process	143
7.	References	144
8.	Appendix A	151
9.	Appendix B	154
10.	Appendix C	156
11.	Appendix D	161
12.	Curriculum Vitae	165

List of Tables

1.1.	Size ratio for CO ₂ , N ₂ , CH ₄ and H ₂	15
2.1.	Comparison of gas uptake in different type of silica gels at constant pressure P _{exp} 3.55 MPa, Driving Force ^a 2.14 MPa and temperature 274 K (Experiments were conducted in semi-batch mode)	34
2.2.	Effect of Surfactants (Tween-80, SDS and DTACl) on hydrate formation in C type of silica gel kinetics at constant pressure P _{exp} 3.55 MPa, Driving Force 2.14 MPa and temperature 274 K (Experiments were conducted in semi-batch mode)	39
3.1.	Summary of experimental conditions and observations; Table shows gas consumption, water to hydrate conversion (mol %), induction time and hydrate dissociation condition. Gas uptake experiments were conducted at 3.75 MPa, and 274.5 K. Data shown in the table is for 5h run.	58
3.2.	Influence of anionic surfactants; SDS (500 ppm), SDBS (500 ppm) and fly ash impurity (0.25 wt %) on gas uptake kinetics at 3.75 MPa and 274.5 K. Table shows experimental condition, induction time and water to hydrate conversion (mol %).	59
3.3.	Gas phase CO ₂ composition for different systems showed in table 3.1 and 3.2. CO ₂ recovery and separation factor were calculated as per equation 5-7.	64
3.4.	CO ₂ recovery data in the presence of thermodynamic and kinetic additives used for CO ₂ capture through HBGS process in reported. For better comparison only the results from stirred tank reactors are presented.	64
3.5.	Summary of experiments, gas consumption; experimental pressure and temperature Amount of water used for all the experiment was 50 cm ³	66
3.6.	Summary of experiments, gas consumption and induction time in STR and fixed bed of silica gel and silica sand	74
4.1.	Summary of experiments, induction time, gas consumption and water to hydrate conversion; experimental pressure and temperature used was 3.0 MPa and 274.65 K respectively. Amount of water used for all the experiment was 50 cm ³ . (Experiments were conducted in batch mode)	89
4.2.	Comparison of gas uptake measurement and initial rate of hydrate growth for STR (stirred tank reactor) and other fixed bed media, relevant experimental details are also included.	90
4.3.	Summary of experiments, induction time, gas consumption and water to hydrate	99

conversion; experimental pressure and temperature used was 7.0 MPa and 273.65 K respectively (CO₂+H₂ gas mixture). Amount of water used for all the experiment was 27 cm³.

- 4.4.** Comparison of gas uptake measurement for stirred tank reactor and fixed bed media, relevant experimental details are also included. Data presented is for 120 minutes of hydrate growth (after induction time) 105
- 4.5.** Summary of experiments, gas consumption and water to hydrate conversion; experimental pressure and temperature used was 7.0 MPa and 273.65 K respectively. 107
- 5.1.** Summary of all the systems used for hydrate formation experiments along with water saturation level. 121
- 5.2.** Hydrate formation experiments performed at experimental temperature 274.5 K. Hydration number used for hydrate conversion calculation was 6.10. 125
- 5.3.** Properties of methane hydrates and carbon dioxide hydrates 132
- 5.4.** Summary of CH₄-CO₂ replacement experiments 135

List of Figures

1.1. Human activities for global anthropogenic green house gas emissions along with world CO ₂ emission by sectors.	3
1.2. Pre-combustion and Post combustion capture	4
1.3. Oxy-fuel combustion capture	5
1.4. Various CO ₂ capture techniques from fuel/flue gas mixture (Data adopted from Aaron and Tsouris, 2005) (Note: energy cost is given for CO ₂ /N ₂ gas mixture)	6
1.5. Schematic diagram of possible CCS systems showing the sources for which CCS might be relevant, transport of CO ₂ and storage options (Courtesy of Intergovernmental Panel on Climate Change, Special report on CO ₂ Capture and Storage, IPCC, 2005)	9
1.6. Various applications of gas hydrates	12
1.7. Potential deposits of gas hydrate over the world and regional area of gas hydrate in India. Location of the sites within the Mahanadi Basin, Andaman Sea and Kerala Konkan Basin along with the location of the 15 sites located within Krishna Godavari Basin	13
1.8. Gas hydrate structures	14
1.9. Hydrate phase equilibrium of pure gases (CO ₂ , H ₂ , N ₂ and CH ₄)	16
1.10. Hydrate phase equilibrium of fuel & flue gas mixture along with different concentrations of CO ₂ .	17
1.11. A typical gas uptake curve along with temperature profile showing the induction time for gas hydrate formation. Inset figures: (A) showing the gas dissolution, (B) hydrate nucleation and (C) hydrate growth.	19
1.12. (a) A surfactant molecule with hydrophilic and lipophilic groups and (b) Micelle formation in aqueous media through association of surfactant molecules	20
1.13. Different classes of surfactants and their corresponding structures	21
2.1. Schematic of the experimental apparatus used for surfactant selection using silica gel as fixed bed media.	29
2.2. Kinetics of the CO ₂ hydrates formation with various silica gels under the same driving force. The axis title and units of the inset are the same as figure 2.2. Inset corresponds to the induction time comparison of silica gels (for B type of silica gel ~ 35 min)	33

2.3. A typical gas uptake measurement curve together with the temperature profile (induction time ~ 35 min using 100-200 mesh type silica gel) and Comparison of water to hydrate conversion for CO ₂ hydrate formation conducted in the same apparatus with and without the presence of silica gel (100-200 mesh)	35
2.4. Effect of surfactants on hydrate growth for CO ₂ /water system in silica gels at 500, 2000 and 4000 ppm concentration of surfactants (a) Non ionic surfactant Tween-80 (b) Cationic surfactant DTACl (c) Anionic surfactant SDS	38
2.5. Comparison of rate CO ₂ uptake with and without the presence of silica gel (230-400 mesh) and in presence of SDS	40
2.6. Comparison of water to hydrate conversion for CO ₂ hydrate formation for 10 hr	41
3.1. Schematic of Experimental Setup: Stirred Tank Reactor along with window showing the CO ₂ /N ₂ /THF Hydrates	46
3.2. Schematic of the experimental apparatus (fixed bed reactor) used for experiments conducted in batch mode	47
3.3. Incipient equilibrium hydrate formation conditions for the CO ₂ (16.1%) / N ₂ (83.9%) / 1 mol% THF and CO ₂ (16.1%) / N ₂ (83.9%) / 1 mol% THF system with 0.25 wt % flyash impurity. Incipient hydrate formation conditions from literature is plotted for similar system, (CO ₂ :N ₂ =17:83 mol %) in presence / absence of THF (1 mol %) (Kang et al., 2001) and 16.9 mol% CO ₂ /1 mol% THF (Linga et al 2008). Y-axis on the right hand side shows the hydrate formation pressure of CO ₂ /N ₂ mixture	53
3.4. Clausius–Clapeyron plot based on the hydrate equilibrium data (a) CO ₂ (16.1%)/N ₂ /H ₂ O/THF (1mol%)/ Flyash (0.25 wt%) System (b) CO ₂ (16.1%)/N ₂ /H ₂ O/THF (1mol%) System (c) CO ₂ (17 %)/N ₂ /H ₂ O/THF (1mol%) System (Kang et al., 2001)	54
3.5. Typical gas uptake curve along with temperature profile for both fresh and memory conditions (Experiment T-1, T-2 and T-4). Inset figure shows the normalized hydrate growth, where time zero corresponds to nucleation point (induction time).	56
3.6. Average gas uptake curve for hydrate growth with and without fly ash (0.25 wt%) in presence of 1 mol% THF. Time zero in the graph corresponds to nucleation point (induction time) for the experiments. The standard deviation for selective data points are presented as error bars	57
3.7. Comparison of (a) average gas consumption (mol of gas/mol of water) for hydrate	61

growth and (b) rate of gas uptake with and without surfactants (SDS and SDBS) in presence of 1 mol% THF; Time zero in the graph corresponds to nucleation point (induction time) for the experiments. The standard deviation for selective data points are presented as error bars

- 3.8.** Comparison of (a) average gas consumption (mol of gas/mol of water) for hydrate growth and (b) rate of gas uptake with and without surfactants (SDS) in presence of 1 mol% THF and 0.25wt% fly ash; Time zero in the graph corresponds to nucleation point (induction time) for the experiments. The standard deviation for selective data points are presented as error bars. 62
- 3.9.** (a) Typical gas uptake measurement curve along with temperature profile at 9.5 MPa and 273.65K. (b) Comparison of gas consumption for hydrate growth (In ~10h from induction time) measured in presence of 1wt% SDS. 67
- 3.10.** (a) Comparison of gas consumption (mol of gas/mol of water) for hydrate growth measured for different amount of THF (3 and 5.56 mol%) at 2.45 MPa and 273.65K. Time zero in the graph corresponds to nucleation point (induction time) for the experiments. (b) Comparison of gas consumption (mol of gas/mol of water) for hydrate growth with literature (1 mol% THF) 69
- 3.11.** Image of rupture disc, damaged by the action of SO₂ 70
- 3.12.** Incipient equilibrium hydrate formation conditions for the CO₂ (40.9%) / H₂ (58.05%) / H₂S (1.05%), CO₂ (39.2%) / H₂ (60.8%) system and pure CO₂. Y-axis on the right hand side shows the hydrate formation pressure of pure CO₂ system 71
- 3.13.** (a) Hydrate formation-dissociation curve for CO₂/H₂/H₂S system, along with temperature profile at 8.5 MPa and 274.65-293.15K. (b) Gas uptake profile (c) pressure drop data for two fresh experimental runs 72
- 3.14.** (a) Hydrate growth curves at 7.8 MPa and 274.15K for CO₂+H₂+H₂S/Sand System (fresh and memory run). Time zero in the graph corresponds to the nucleation point (b) Colour of silica sand before and after hydrate formation using CO₂+H₂+H₂S gas mixture. 75
- 3.15.** Raman spectra of pure silica sand and silica sand after reaction with H₂S. 76
- 3.16.** Typical gas uptake measurement curve for Silica gel /CO₂/H₂/H₂S system (experiment G2) along with the temperature profile at 8 MPa and 274.65 K 77
- 3.17.** Effect of driving force on the gas uptake curve in silica gel bed for CO₂/H₂/H₂S gas mixture, Time zero corresponds to the induction time for the experiment. 78
- 3.18.** Comparison of gas uptake data at different experimental pressures and different reactor configurations for CO₂+H₂ (obtained from literature Babu et al., 2013; Linga et al., 2007) and CO₂+H₂+H₂S (present study) gas mixtures. Gas uptake after 120 minutes from hydrate nucleation has been plotted. 79

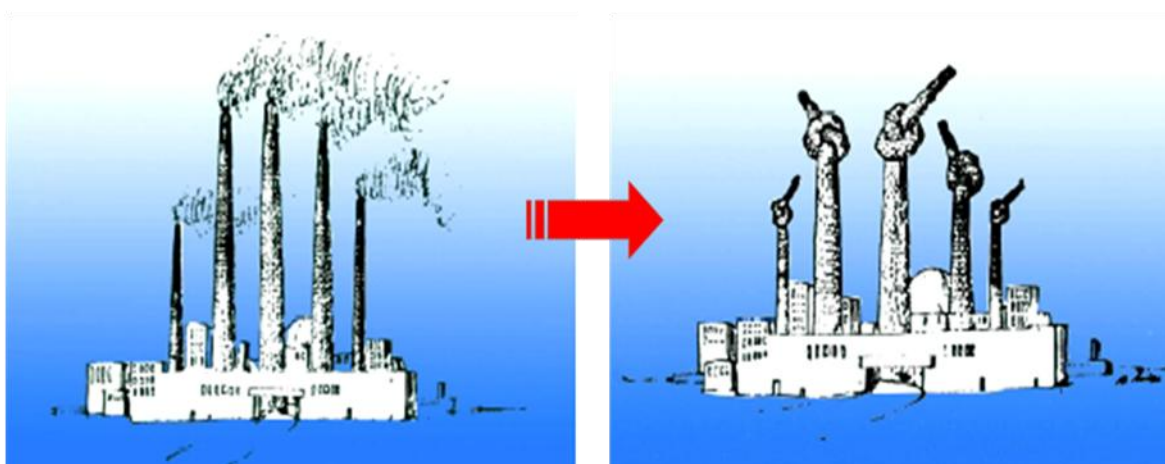
4.1. Schematic of the experimental apparatus along with the location of thermocouples in the crystallizer and bed height for both packing media	85
4.2. Typical gas uptake measurement curve (water to hydrate conversion %) along with temperature profile at 3.0 MPa and 274.65K. (SSP-2/SDS/water system, exp. 3d)	91
4.3. Comparison of gas consumption for hydrate growth measured for different fixed bed media. Time zero in the graph corresponds to nucleation point (induction time) for the experiments.	92
4.4. Hydrate growth curves (Fresh and memory runs) for SSP-2/SDS system. Time zero in the graph corresponds to nucleation point (induction time) for the experiments. (Experiment No. 3a, 3b and 3c)	93
4.5. Normalized rate of hydrate formation for different fixed bed media, calculated for first 30 min after nucleation.	94
4.6. Comparison of gas consumption for hydrate growth (average CO ₂ uptake) in mg of CO ₂ consumed per unit mass of material (g), per unit volume of material (cm ³) and per unit mass of water (g) used for hydrate formation. The data shown is for the first 30 min of hydrate growth from induction time (Per unit mass of material includes mass of packing material (g) and water (g) similarly per unit volume of material includes volume of packing material (cm ³) and water (cm ³).	95
4.7. Comparison of induction time for different fixed bed media and no media system for hydrate formation	96
4.8. A typical hydrate formation (pressure drop) – dissociation (pressure rise at 293.15K) curve along with temperature profile at 7.0 MPa and 273.65 K (Experiments4)	98
4.9. Comparison of gas consumption for hydrate growth measured for different concentration of SDS (1, 0.5, 0.1 wt%) in silica sand media. Time zero in the graph corresponds to nucleation point	101
4.10. Comparison of gas consumption for hydrate growth measured for two different fixed bed media in presence of 1wt% SDS. Time zero in the graph corresponds to nucleation point	103
4.11. Normalized rate of hydrate formation for different fixed bed media with different concentration of SDS, calculated for first 30 minutes after nucleation	103
4.12. Comparison of gas uptake as a function of driving force for different fixed bed media and stirred tank reactor. The data presented is for 120 minutes of hydrate growth	104

4.13. Hydrate formation-dissociation curve for copper foam and brass packing in presence of 1wt% SDS, along with temperature profile at 7.0 MPa and 273.65 K	108
4.14. Blooming of Hydrates during formation in copper foam at 7.0 MPa and 273.65K	109
4.15. Typical gas uptake measurement curve for Brass/1wt% SDS system together with the temperature profile at 7 MPa and 273.65 K	110
4.16. (a) Comparison of gas uptake for hydrate growth measured for different fixed bed media (Brass, copper and sand). Time zero in the graph corresponds to nucleation point (induction time) (b) Normalized rate of hydrate formation with 1wt% of SDS, calculated for first 30 min after nucleation.	111
4.17. (a) Normalized gas release curves for hydrate decomposition in silica sand, copper foam and brass bed. The results are normalized at the dissociation time of 50min for all the experiments. (b) Normalized rate of hydrate dissociation for different fixed bed media with 1wt% of SDS, calculated for first 20 min after nucleation (NR ₂₀).	113
4.18. Sequential images of hydrate formation and dissociation in copper foam bed along with the pressure and temperature profile during hydrate dissociation by thermal stimulation	114
4.19. Sequential images of hydrate formation and dissociation in brass bed along with the pressure and temperature profile during hydrate dissociation by thermal stimulation	115
5.1. Schematic of experimental setup along with location of thermocouples within the reactor	122
5.2. Methane hydrates in silica sand (Brown=silica sand, white=hydrates)	126
5.3. Typical gas uptake curve along with temperature profile for hydrate formation in 100% water saturated silica sand (Experiment 1).	126
5.4. Comparison of gas uptake (water to hydrate conversion) for methane hydrate formation with pure silica sand at three different water saturation levels (100, 75 and 50 %, Experiment 1, 5 and 7) (b) Comparison of the rate of methane uptake for the three system	127
5.5. (a) Comparison of gas uptake (water to hydrate conversion) for methane hydrate formation conducted with Silica sand-clay mixture (75:25 ratio) at three different water saturation levels (100, 75 and 50 %, experiment 9,12 and 14) (b) Comparison of the rate of methane uptake for the three system	128
5.6. (a) Comparison of gas uptake (water to hydrate conversion) for methane hydrate formation conducted with Silica sand-clay mixture (50:50 ratio) at two water saturation levels (75 and 50 %, experiment 15, 17 and18) (b) Comparison of the rate of methane uptake for the same system	130

5.7. Comparison of water to hydrate conversion for methane hydrate formation conducted in same apparatus with silica sand-clay mixtures and pure silica sand at different water saturation levels	131
5.8. Hydrate formation conditions of carbon dioxide and methane modified from Goel,2006	132
5.9. Release of methane due to hydrate dissociation and CO ₂ consumption due to CO ₂ hydrate formation (silica sand and clay mixture (75:25) at 75% water saturation) (experiment 1b) and its comparison with S-75 system (Exp. 1a)	137
6.1. (a) Schematic flow sheet for CO ₂ capture and separation using HBGS process	141
1. H ₂ gas, 2. Membrane separator, 3 &4. Metallic packing bed, 5. Feed gas (CO ₂ +H ₂), 6. Throttling process, 7. CO ₂ gas	
6.2. Schematic of the apparatus for hydrate-based desalination (HBD) process	143

Chapter 1

Literature Review



1. Literature Review¹

¹“A version of this chapter has been published.

Kumar A, Bhattacharjee G, Kulkarni B D, Kumar R. Role of surfactants in promoting gas hydrate formation, Ind Eng Chem Res 2015, DOI: 10.1021/acs.iecr.5b03476

1.1. Carbon dioxide capture and storage or sequestration (CCS)

Carbon dioxide (CO₂) emission into the atmosphere is a major concern due to its potential role in global warming and climate change. While CO₂ gets emitted naturally into the atmosphere due to the earth's carbon cycle; anthropological emissions of CO₂ are responsible for increase in atmospheric CO₂ levels that has occurred since the industrial revolution (Diwan and Yaqoot, 2010). Figure 1.1 shows the shares of human activities which are responsible for global anthropogenic green house gas emissions. As can be seen in figure 1.1, the use of energy represents the largest source of emission (69%) compare to industrial processes, agriculture and other human activities. CO₂ emission was found to be a major contributor (90%) compare to other green house gases such as methane (CH₄) and nitrous oxide (N₂O). The electricity and heat generation are the two major sectors which produces 42% of global CO₂ emissions. They have been considered as largest contributor compared to transport (23%), industries (20%), residential (6%) and 9% from other sectors (IEA, 2014). Use of conventional and un-conventional fossil fuel for energy production is going to continue in foreseeable future and one need to identify ways to contain the emission of CO₂ from point sources like a coal based thermal power plant. An efficient CO₂ capture and storage (CCS) technology is required to tackle the environmental concerns safely (Kumar et al., 2015).

Carbon capture and storage or sequestration (CCS) covers a diverse range of technologies that are being developed to capture and sequester the CO₂ safely. CCS is a process consisting of the separation of CO₂ from industrial and energy-related sources, transport to a storage location and sequester it for long-term isolation from the atmosphere. IPCC report even almost a decade old is still relevant which deals with the climate change and strategies for future. According to the report, CCS will play an important role among mitigation strategies for global warming. This report provides a detailed assessment of the current state of knowledge regarding the technical, scientific, environmental, economic and societal dimensions of CCS (IPCC, 2005).

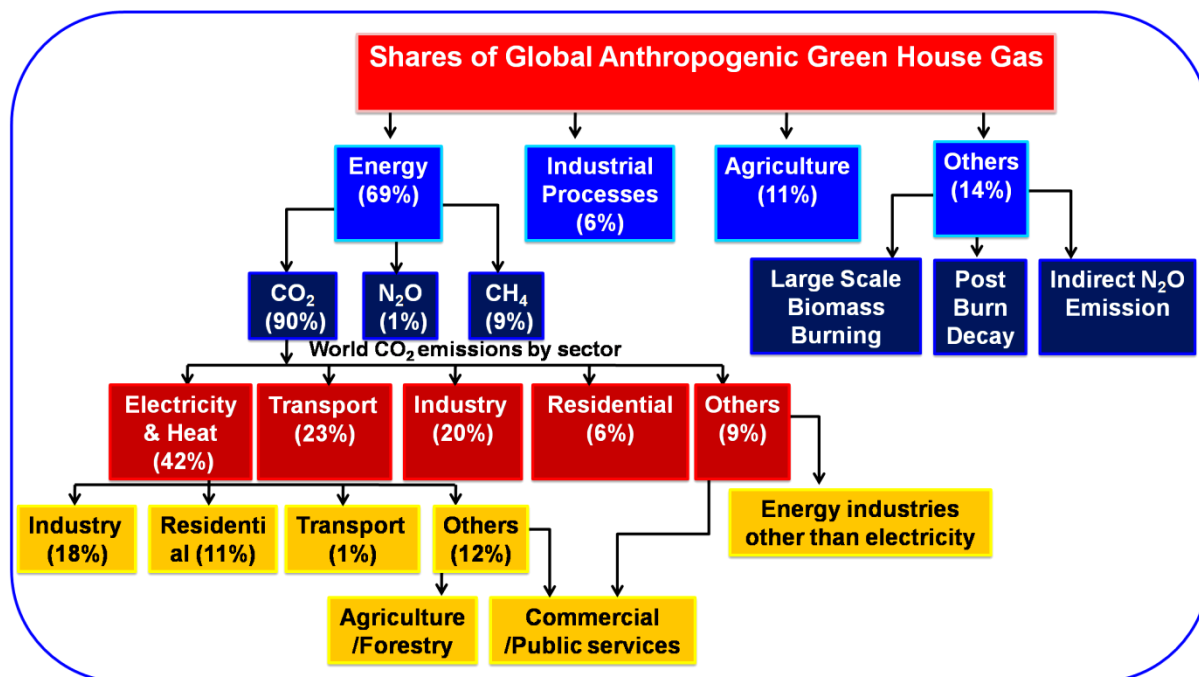


Figure 1.1. Human activities for global anthropogenic green house gas emissions along with world CO₂ emission by sectors. (Data adopted from CO₂ emissions from fuel combustion Highlights (2014 Edition), International Energy Agency (IEA), France. (www.iea.org))

1.1.1. Carbon dioxide capture systems

There are three major routes to capture CO₂ coming from various human activities.

(i). Pre-combustion capture: Pre-combustion capture of CO₂ and utilization of H₂ to produce electricity through coal gasification is a suitable approach for a green field projects (Spencer et al., 2002, Klara and Srivastava, 2002). This approach is also known as integrated coal gasification combined cycle (IGCC), where a fossil fuel is gasified and catalytically converted in presence of water to a mixture of CO₂ and H₂ (Fuel gas). Carbon dioxide can then be captured while hydrogen can be used as the fuel. In IGCC plant, generation of electricity is possible during the coal gasification step and also from the produced H₂ gas, resulting in a combined efficiency of 60% (<http://www.netl.doe.gov>). Furthermore, the above processes produce a fuel gas mixture at high pressure resulting in an economical CO₂ separation step (Barchas and Davis, 1992). Shifted synthesis gas of an IGCC power station comprises approximately 40% CO₂ and 60% H₂ coming out at a pressures of 2-7 MPa. (Klara and Srivastava, 2002; Deaton and Frost, 1946). In an IGCC plant, fuel gas may also contain a trace amount of hydrogen sulfide (H₂S), carbon monoxide (CO), ammonia (NH₃), coal dust

(Particulate matter) and so forth (Stephen et al., 1977). These impurities have to be removed from the system. Another application, utilizes the H_2 to power solid oxide fuel cells (SOFCs) or other fuel cell technologies to significantly increase the overall plant efficiency. A detailed schematic of IGCC plant for electricity generation and pre-combustion CO_2 capture is shown in figure 1.2.

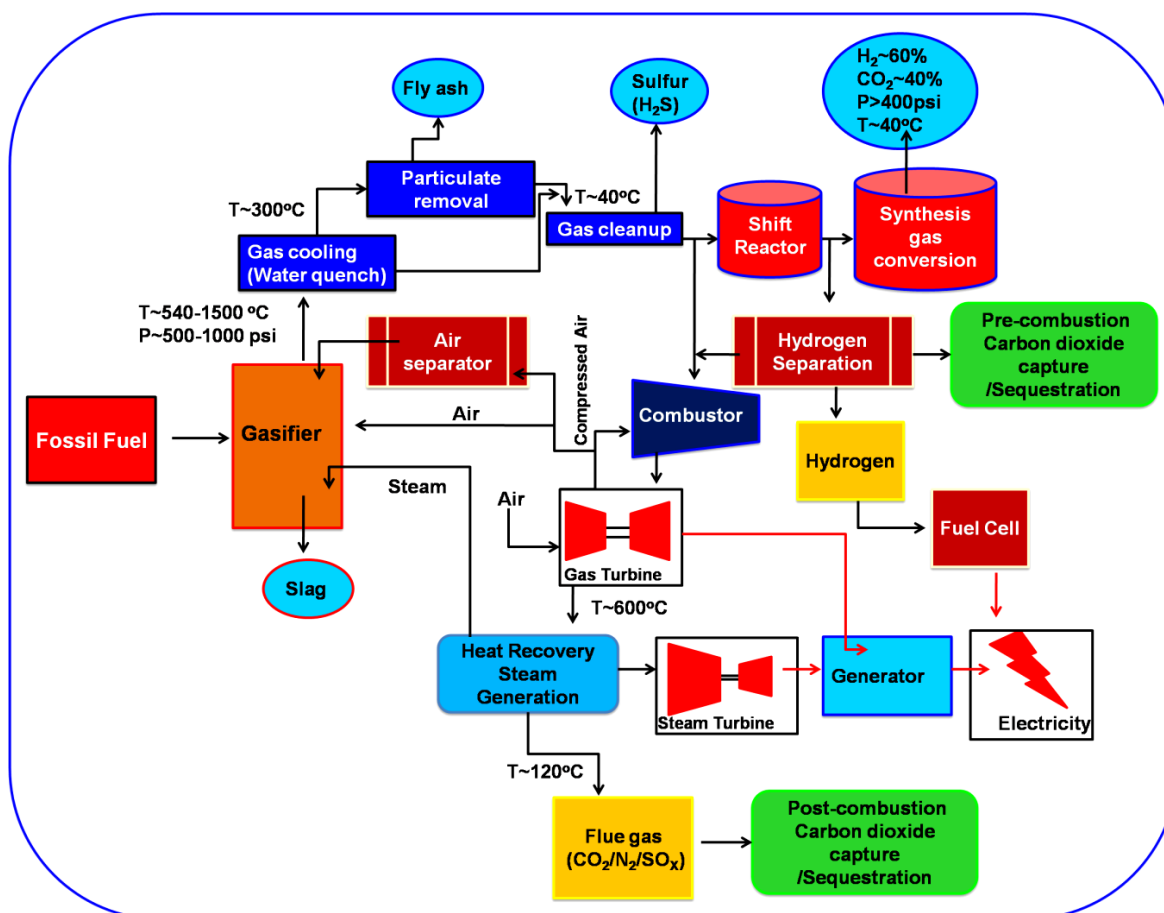


Figure 1.2. Pre-combustion and Post combustion capture

(ii). Post-combustion capture: CO_2 capture from flue gases produced by combustion of fossil fuels and biomass in air is referred to as post-combustion capture. Schematic of flue gas production can be seen in the figure 1.2. It's a mixture of carbon dioxide (10-15 mol%) and nitrogen along with trace gases like oxygen, nitrogen oxides (NO_x), sulfur oxides (SO_x) and fly ash as particulate matter. The flue gas is usually at low pressure (low CO_2 partial pressure) which provide low driving force for CO_2 capture technologies such as adsorption or absorption. Other challenges are low concentration of CO_2 (10-15%), high temperature of the flue gases and high capital costs.

(iii). **Oxy-fuel combustion capture:** In this process, during combustion pure oxygen is used in place of air resulting in a nitrogen free flue gas mixture. CO_2 is separated by condensing the water produced during combustion of hydrocarbons in the fuel. Figure 1.3 shows the schematic of oxy-fuel combustion capture. The main advantage of this process is that the concentration of CO_2 is high with values of up to 80%. The disadvantage is the higher cost of cryogenic separation of O_2 and N_2 by the air separation unit and high temperature during combustion of fuel in presence of oxygen.

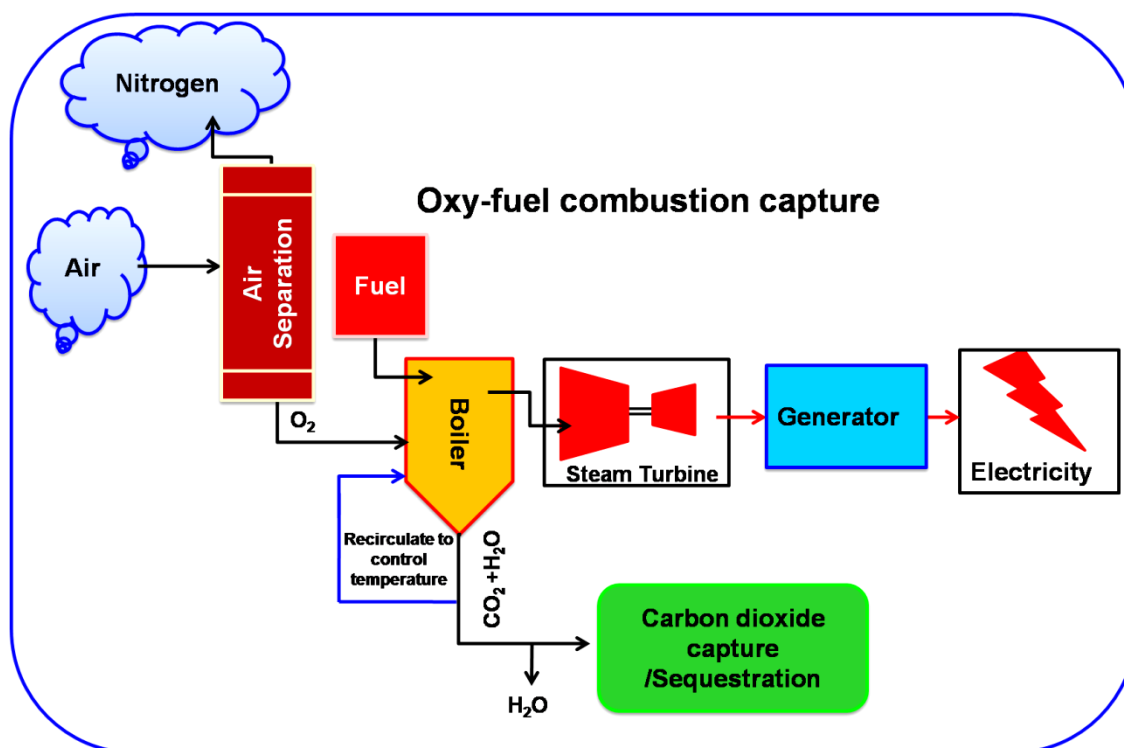


Figure 1.3. *Oxy-fuel combustion capture*

1.1.2. Carbon dioxide capture technologies

CO_2 capture systems discussed in section 1.1.1 can utilize many of the known technologies for gas separation. A summary of these separation techniques is given in figure 1.4 which includes leading commercial options like physical absorption & adsorption, chemical absorption, separation through membrane diffusion and cryogenic distillation. In addition many promising techniques based on new liquid sorbents or solid sorbents and hydrate based gas separation process are under development stage.

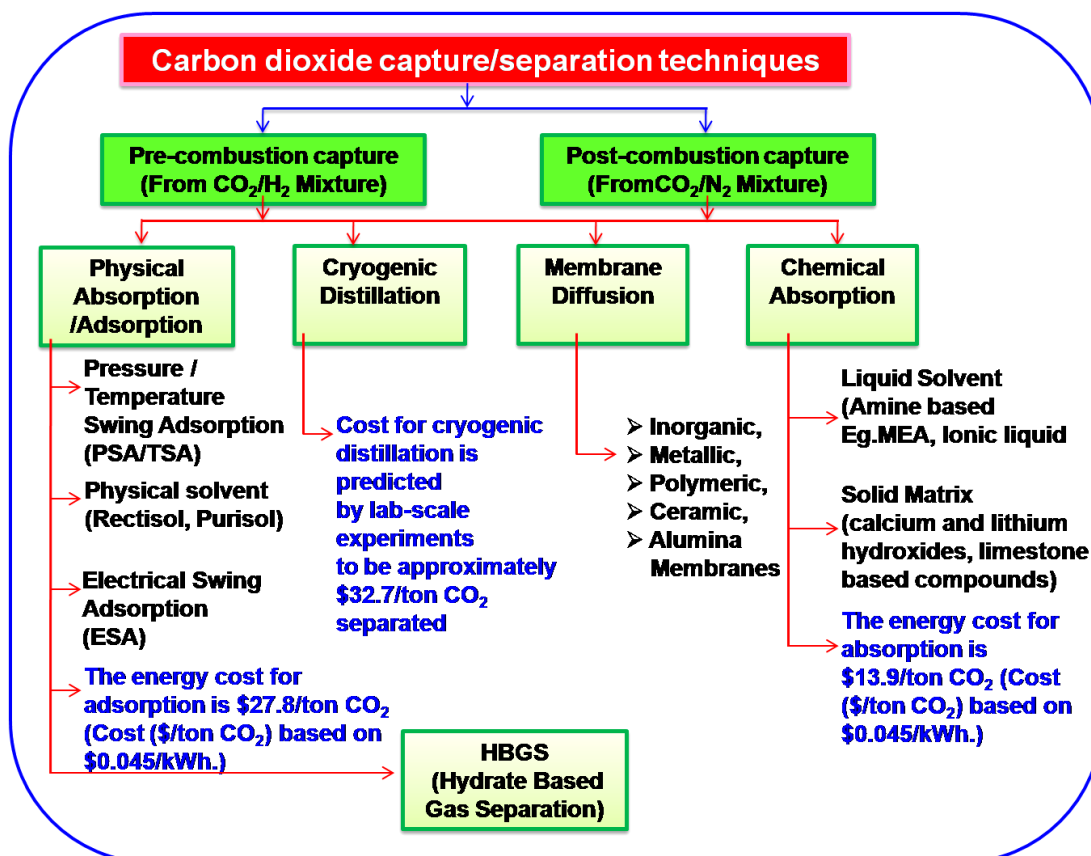


Figure 1.4. Various CO₂ capture techniques from fuel/flue gas mixture (Data adopted from Aaron and Tsouris, 2005) (Note: energy cost is given for CO₂/N₂ gas mixture)

As seen in figure 1.4, cryogenic separation of CO₂ from CO₂/N₂ (post combustion capture) is highly energy intensive. This is because of low concentration and partial pressure of CO₂ in the flue gas mixture (Aaron and Tsouris, 2005; Barchas and Davis, 1992).

Physical adsorption or absorption is a way to capture CO₂ through temperature/pressure/electrical swing adsorption (TSA /PSA/ESA) or using typical solvents such as Selexol (dimethyl ether of polyethylene glycol) and Rectisol (cold methanol) (Sweny and Valentine, 1970). Low partial pressure of CO₂ in flue gas mixture is not conducive for physical separation and can be a costly affair.

Chemical absorption involves use of a solvent that absorbs carbon dioxide by chemically binding the CO₂ molecule. This CO₂ rich solvent is typically regenerated at elevated temperature and the solvent is recycled. Amines such as mono-ethanolamine (MEA), Ionic liquids (ILs) are the most common examples of CO₂ absorption. MEA having the highest theoretical absorption capacity for carbon dioxide (Herzog et al., 1997) while operating in the pressure range of 10-80 bar and temperature range of 303 to 343 K (Aaron and Tsouris, 2005).

Challenges for using chemical solvents as CO₂ capture media

- The large amount of utility steam required for solvent regeneration de-rates the power plant significantly.
- Energy required to heat, cool, and pump non-reactive components like N₂, H₂O are quite significant.
- Vacuum stripping can reduce regeneration steam requirements but is prohibitively expensive to scale one such operation
- Separation efficiency is very sensitive to impurities such as fly ash, SO_x and NO_x.
- Corrosion problems
- Use of toxic, volatile and flammable chemicals (*Source: U.S. Department of Energy, DOE/NETL Carbon Dioxide Capture R&D Annual Technology Update, Draft, National Energy Technology Laboratory, Pittsburgh, PA, April 2010; hereafter "DOE, Carbon Dioxide Capture"*)

Challenges for Solid Sorbent as CO₂ Capture media

- Heat required to reverse chemical reaction (although generally less than for wet-scrubbing).
- Heat management in solid systems is difficult. This can limit capacity and/or create operational issues for exothermic absorption reactions.
- Pressure drop can be large in a fixed bed arrangement for flue gas separation.
- Sorbent attrition may be high and thus makeup adsorbent would be prohibitively expensive.
- Impurities such as fly ash, SO_x, NO_x and H₂S may affect the separation efficiency of the process (*Source: DOE, "Carbon Dioxide Capture"*)

Selective absorption and diffusion through membrane is one of the promising approaches for CO₂ capture/separation. Membranes effectively act as a filter, allowing only CO₂ to pass through the material. The driving force for this separation process is a pressure differential (ΔP) across a membrane, which can be created either by compressing the gas on one side of the membrane or by creating a vacuum on the opposite side (Folger, 2013). The advantage of the process is no requirement of toxic chemicals and no steam load assuming membranes can be reused without regeneration. Compared to absorption separation, the other advantages of the membrane process are as follows: (i) it does not require a separating agent, thus no regeneration is required; and (ii) it has low maintenance requirements because there are no moving parts in the membrane unit.

Challenges for Membrane-Based approaches to CO₂ Capture (Folger, 2013)

- Membranes tend to be more suitable for processes which generate a high-pressure flow stream such as IGCC, for post combustion CO₂ capture a compressor would be required thus reducing the efficiency Tradeoff between recovery rate and product purity (difficulty to meet both at the same time).
- Require high selectivity (due to CO₂ concentration and low pressure ratio).
- Good pre-treatment required
- Poor economies of scale
- Multiple stages and recycle streams may be required.

There are several other emerging techniques for CO₂ separation from flue gas (post combustion) and fuel gas (pre combustion). Hydrate based gas separation (HBGS) process is one such promising approaches (Linga et al., 2007a,b, 2008, 2010; Yang et al., 2008, 2011). However, further development is required for economically capturing CO₂ from flue/fuel gas on a large scale. Clathrate or gas hydrates are crystals formed by water and substances such as CO₂, N₂, O₂, H₂, and natural gas components (Davidson, 1973, Englezos, 1993; Ripmeester, 2000; Sloan and Koh, 2008). During hydrate formation most of the liquid water converts into solid hydrate phase through selective enclathration of CO₂ from fuel/flue gas mixture (H₂ rich gas), followed by a hydrate decomposition stage which converts the solid hydrate phase back into liquid water and CO₂ rich gas. This is the basis for the utilization of clathrate hydrate formation/decomposition as a separation process (Makogon, 1981; Englezos, 1993). Similar to physical absorption, hydrate based technology needs to be operated at lower temperature and higher pressure, which makes it more suitable for pre-combustion capture where a CO₂ rich mixture (~40:60 mixture of CO₂/H₂) is obtained at 2-7 MPa (IPCC, 2005).

1.1.3. Carbon dioxide sequestration:

The target of CCS is not only to capture the CO₂ but also to store or sequester the captured CO₂ for long-term isolation from the atmosphere. There are various approaches considered for permanent storage of CO₂. The earth's major potential storage options for CO₂ sequestration that was reported in IPCC report is as follows and shown in figure 1.5:

1. Mineral carbonation:(i) Natural silicate minerals
(ii) Waste materials

2. Ocean Storage: (i) Direct injection (dissolution type)
(ii) Direct injection (lake type)
3. Geological storage: (i) Enhanced Oil Recovery (EOR)
(ii) Depleted Oil and Gas Reservoirs
(iii) Deep Saline Formations
(iv) Enhanced Coal Bed Methane recovery (ECBM)

In sequestration process, the compressed CO₂ is injected deep into the underground porous rock, such as sandstone, shale, dolomite, basalt, or deep coal seams. Suitable formations for CO₂ sequestration are located under one or more layers of cap rock, which trap the CO₂ and prevent upward migration. These sites are then rigorously monitored to ensure that the CO₂ remains stable there. The safety and security of CO₂ geologic sequestration is one of the major concerns (<http://www.epa.gov/climatechange/ccs/>), apart from that cost of transportation and storage is the other concern.

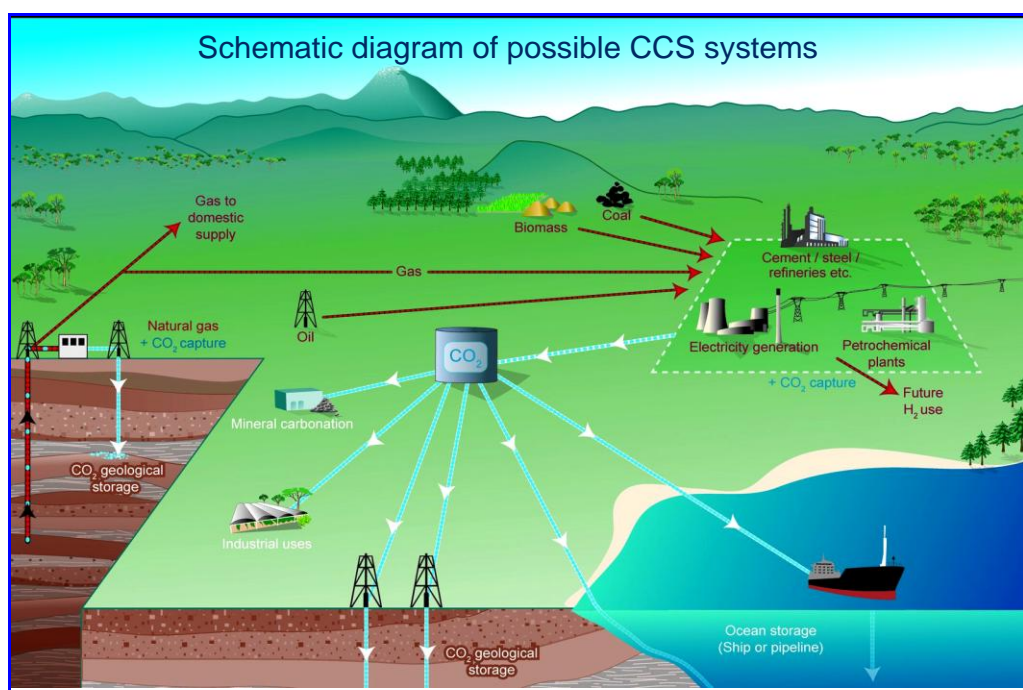


Figure 1.5. Schematic diagram of possible CCS systems showing the sources for which CCS might be relevant, transport of CO₂ and storage options (Courtesy of Intergovernmental Panel on Climate Change, Special report on CO₂ Capture and Storage, IPCC, 2005)

One of the emerging options for CO₂ sequestration is gas hydrate based sequestration where disposal of CO₂ takes place in the ocean or in deep saline aquifers in the form of CO₂ hydrate (Takahashi et al., 2000; Yamasaki, 2000). In particular, the injection of carbon dioxide (CO₂),

into ocean (hydrate bearing sediments) can preferentially liberate some of the enclathrated methane (CH_4), and simultaneously sequester CO_2 in hydrate form. Thus this approach offers twin advantages (i) reducing carbon dioxide emissions into the atmosphere (ii) assisting gas hydrate exploitation, thereby overcoming the economic barrier of carbon dioxide sequestration and methane recovery. It is thus a carbon dioxide sequestration with energy production process. *The goal of this thesis is to study the feasibility of the Hydrate Based Gas Separation (HBGS) process for CO_2 capture from point sources such as coal based thermal power stations and CO_2 sequestration by replacement of methane from natural gas hydrate reserves.*

Next, the thesis presents a basic description of gas hydrates which is followed by a discussion on work already done for hydrate based gas separation (HBGS) process & methane replacement and challenges of HBGS process for CO_2 capture/separation. Later in this chapter the objectives of the thesis are presented followed by the organization of the thesis.

1.2. Background on gas hydrates

Gas hydrates or clathrate hydrates are non-stoichiometric, ice like crystalline compounds formed by water (host) and smaller gas molecules (guest). Most of the gases like methane, carbon dioxide, hydrogen and some of the low molecular weight hydrocarbons including Tetrahydrofuran (THF), neo-hexane (NH) and other hydrocarbon of similar size can form clathrates (Davidson, 1973; Sloan and Koh, 2008). Thermodynamic requirement for gas hydrate formation, which is typically high pressure and low temperature are frequently encountered in nature, like under the sea bed and in the permafrost. Clathrate hydrate formation is also encountered quite frequently in the oil and gas industries and can lead to serious problems due to blockages of pipelines by solid hydrate formation (Sloan and Koh, 2008).

Gas hydrate formation / decomposition studies on natural gas hydrate is mainly driven by its potential as methane resource, whereas, hydrate formation/decomposition mechanism in the oil and gas pipelines are studied due its nuisance nature. Oil and gas industries are forced to use expensive gas hydrate inhibitor in certain doses to stop hydrate formation in the pipelines. Formation and decomposition studies of gas hydrate is thus very important in both the cases explained above and in many other applications like storage and transport of natural gas, carbon dioxide capture and sequestration, hydrogen storage etc. Hydrate based gas separation process is one of the emerging approaches. Figure 1.6 represents the various applications of gas hydrates in different field of research.

The fact that 164 cubic meters of methane gas is trapped in one cubic meter of gas hydrate and large area of deep water have favorable conditions for gas hydrate formation, makes it a suitable candidate for methane recovery. Natural gas hydrates are known to occur naturally in the earth and potential reserves of natural gas hydrates are over $1.5 \times 10^{16} \text{ m}^3$ which are distributed all over the earth in the Arctic on land and offshore (figure 1.7) (Makogon et. al., 1971, 2007; Klauda and Sandler, 2005; Milkov et al., 2004, Kvenvolden, 1993).

India is fourth largest energy consumer in the world, just behind US of America, China and Russia. Energy consumption in India has doubled in last one decade and Indian government want to become energy independent by 2030 by tapping conventional and un-conventional hydrocarbon resources. Potential hydrate deposits have been found in Andaman-Nicobar Island, Krishna Godavari basin, Konkan and Kutch offshore (Chopra, 1985). Gas hydrate resource identification and delineation of such resources is an ongoing work and National Gas Hydrate Program (NGHP) has been quite instrumental in this respect. Gas hydrates are known to occur in numerous marine environment around Indian offshore, however little is known about the technology necessary to produce gas hydrates.

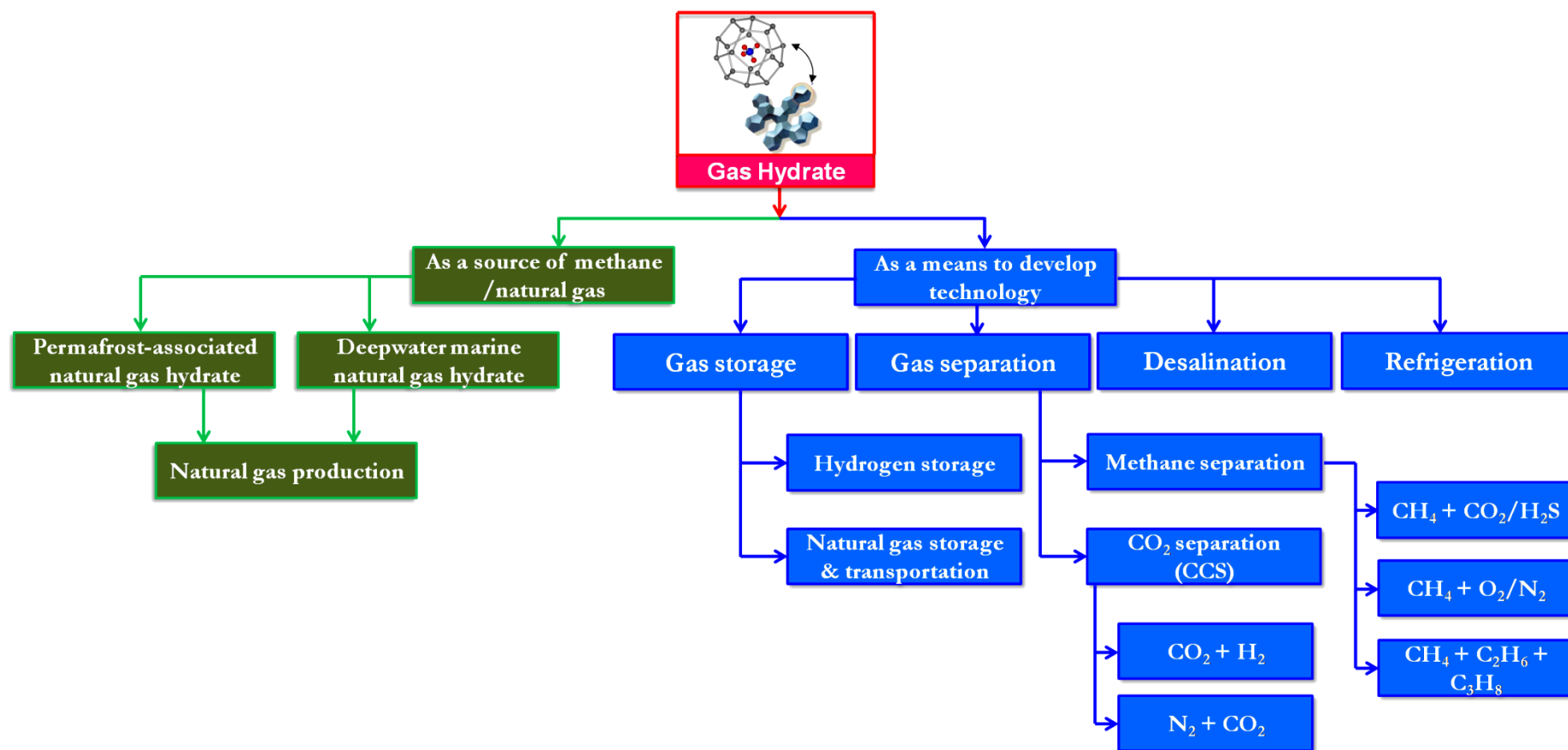


Figure 1.6. Various applications of gas hydrates

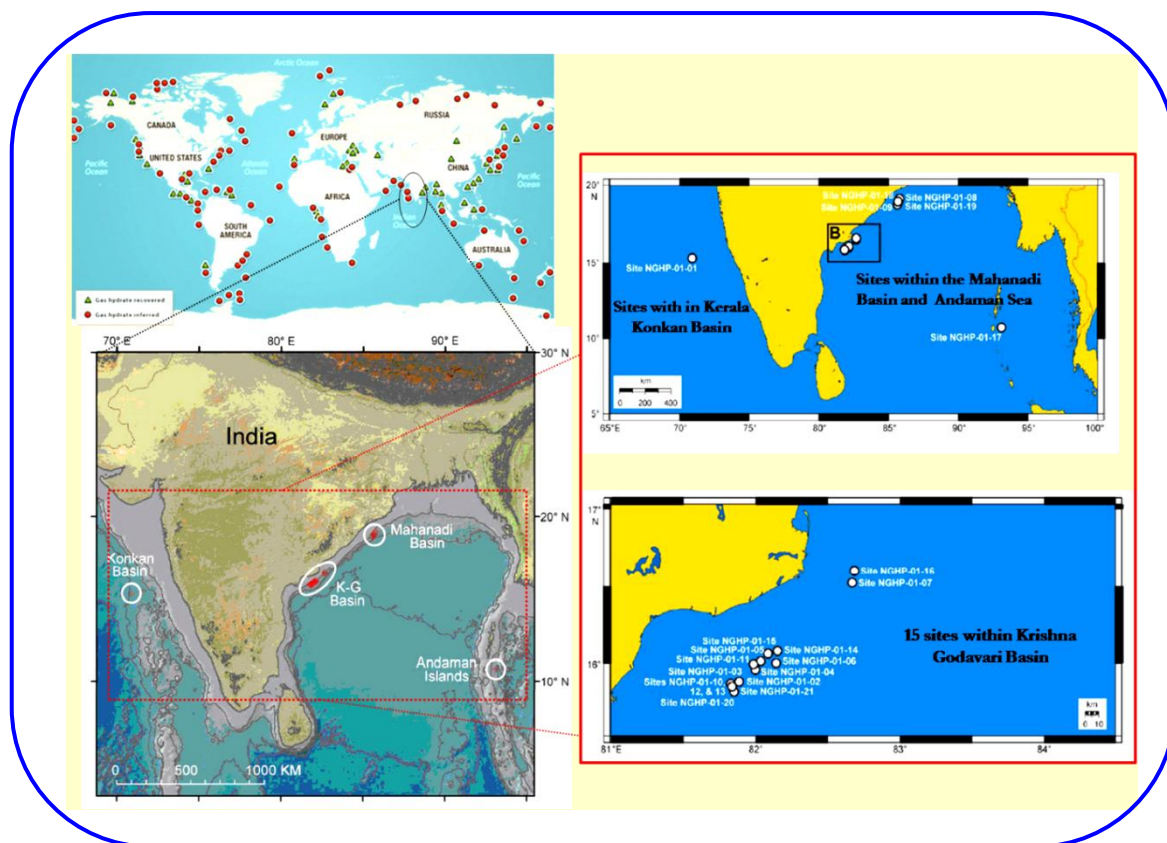


Figure 1.7. Potential deposits of gas hydrate over the world and regional area of gas hydrate in India. Location of the sites within the Mahanadi Basin, Andaman Sea and Kerala Konkan Basin along with the location of the 15 sites located within Krishna Godavari Basin (Adopted from Collett *et al.*, 2008, USGS, ICICI Securities and <http://www.naturalgaseurope.com/methane-hydrates-and-the-potential-natural-gas-boom>)

1.2.1. Gas hydrate structures

The structure of gas hydrate cavity depends on the size and chemical properties of guest molecules. In nature, gas hydrates usually form two crystallographic cubic structures (i) structure I (sI) and (ii) structure II (sII) of space groups $Pm\bar{3}n$ and $Fd\bar{3}m$, respectively. However, a third hexagonal structure of space group $P6/mmm$ may be observed (structure H or sH) (Ripmeester *et al.*, 1987, Udachin and Ripmeester 1999).

Structure I hydrates consist of two different types of cavities. The first cavity is formed when water molecules comes together through hydrogen bond in such a way that they form a structure with 12 pentagonal faces called a pentagonal dodecahedron (5^{12}). This cavity or cage is present in all three gas hydrate structures mentioned above (sI, sII and sH).

When the pentagonal dodecahedra link together by their vertices they create a second type of cavity, a polyhedron with 12 pentagonal and 2 hexagonal faces ($5^{12}6^2$) called a tetrakaidecahedron, which is larger than the dodecahedron. A unit cell of structure I hydrate consists of six large $5^{12}6^2$ cavities, and two small 5^{12} cavities created by 46 water molecules. Structure I is formed with molecules which are of size between 4- 6 Å, such as methane, ethane, carbon dioxide, and hydrogen sulfide. Nitrogen and other small molecules like hydrogen ($d < 4.2$ Å) forms structure II by single guest or multiple guests in each cage (Sloan and Koh, 2008). When, the pentagonal dodecahedra link together through face sharing, not by the vertices as in structure I, then the structure formed is known as structure II. By linking together through face sharing, they create a hexakaidecahedron, a polyhedron with 12 pentagonal and 4 hexagonal faces. Because of bending in the hydrogen bonding the large cavity structure II is bigger than the large cavity in structure I, while the small cavity in structure II is slightly smaller than the small cavity in structure I. Structure II hydrate consists of 16 small and 8 large cavities made up by 136 water molecules. Molecules forming structure II have diameters less than 4.2 Å or greater than 6 Å up to 7 Å. Hydrogen, nitrogen and propane are some of the structure II forming gases.

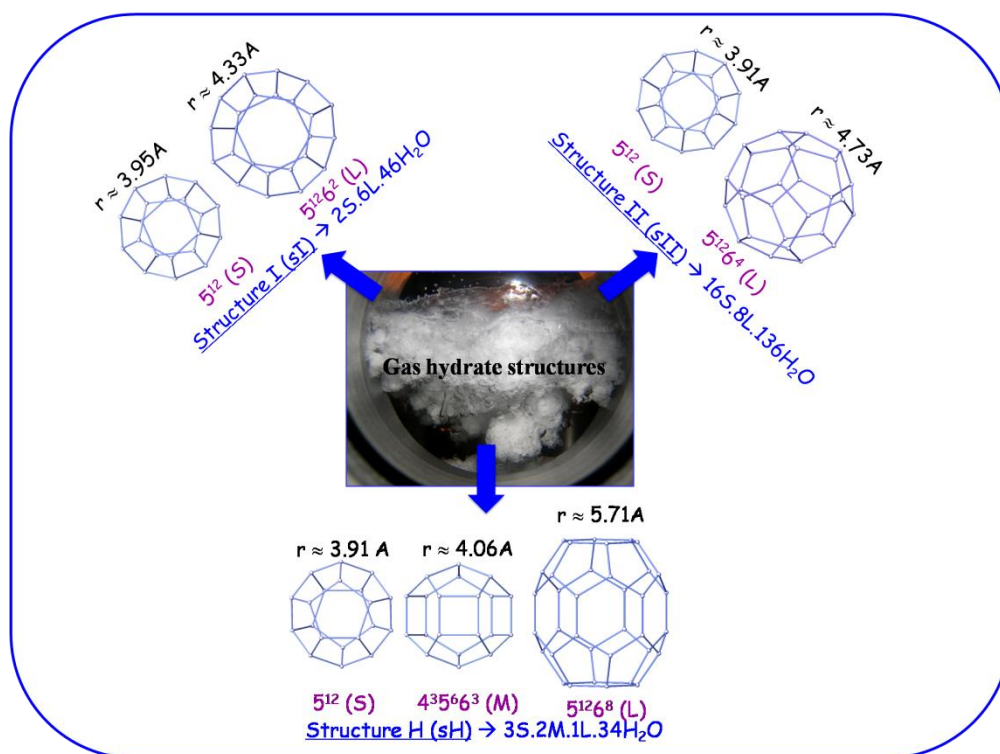


Figure 1.8. Gas hydrate structures

Structure H was discovered in 1987 at National Research Council in Canada (Ripmeester et al., 1987). It consists of three different types of crystal cavities, two of which are small and one large non-spherical cavity. Similar to structure I and structure II, structure H has the basic 5^{12} cage. However, it is unique compared to the two previous structures because it requires molecules of at least two different sizes to stabilize the crystal. The two other cavities consist of a $4^35^66^3$ cage which has three fairly strained square faces, six pentagonal and three hexagonal faces and a large $5^{12}6^8$ cage made up of twelve pentagonal and eight hexagonal faces. The latter cavity is the largest hydrate cavity of any of the structures and is estimated to fit guests up to 9 Å in diameter (Ripmeester et al., 1994). Small molecules, known as help guests, such as methane, xenon or hydrogen sulfide, can occupy the two small cages in structure H, while intermediate sized hydrocarbons such as cycloheptane or 2,2-dimethylbutane (neohexane) can fill the large cavity of structure H. The shapes of all the cavities formed in structure I, Structure II and structure H are shown in fig 1.8. It was observed that the size ratio of the guest molecule to the cavity determines whether the guest can form a stable hydrate structure. In order to obtain a stable hydrate structure, the ratio needs to be approximately 0.9. If the ratio is significantly less or above unity, stable hydrates structure will not be formed (table 1.1).

Table 1.1: Size ratio for CO₂, N₂, CH₄ and H₂ (data adapted from Sloan and Koh, 2008)

Guest Molecules	Guest diameter (Å)	Guest diameter (Å)/Actual cavity diameter (Å)*			
		Structure I		Structure II	
		5^{12}	$5^{12}6^2$	5^{12}	$5^{12}6^4$
CO ₂	5.12	1	0.83	1.02	0.769
H ₂	2.72	0.533	0.46	0.542	0.408
N ₂	4.1	0.804	0.7	0.817	0.616
CH ₄	4.36	0.855	0.744	0.808	0.655

*Actual cavity diameter (Å) = Cavity diameter - Diameter of water (2.8 Å)

1.2.2. Thermodynamic of gas hydrates (Gas hydrate phase equilibrium/Incipient hydrate formation conditions)

The phase equilibria of gas hydrates have the most important set of properties which differentiate it from physically similar ice crystals. The thermodynamics of gas hydrate has been studied extensively over the years. Experimental data on the thermodynamics of gas hydrate formation has been obtained for many systems. Studies on hydrate equilibrium are

focused on gathering incipient equilibrium hydrate formation data as well as developing predictive methods for the calculation of phase equilibria. Incipient hydrate formation conditions refer to the situation in which an infinitesimal amount of the hydrates are present in equilibrium with the fluid phases (Kumar et al., 2006). Figure 1.9 represents the hydrate phase equilibrium (Incipient hydrate formation conditions) of pure gases such as CO_2 , N_2 , H_2 and CH_4 . At 275.6 K, the minimum pressure required to form pure CO_2 and CH_4 is ~ 1.6 and 3.4 MPa respectively however for pure H_2 and N_2 hydrate, it was significantly high 366 and ~ 21 MPa respectively (figure 1.9).

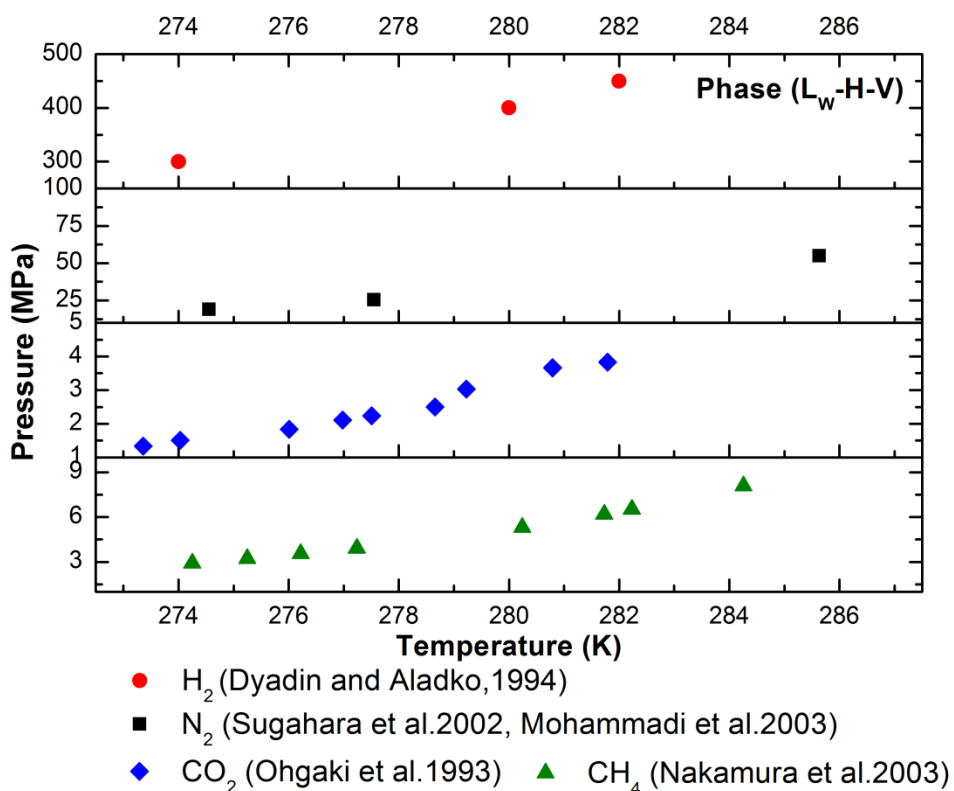


Figure 1.9. Hydrate phase equilibrium of pure gases (CO_2 , H_2 , N_2 and CH_4)

This significant difference in equilibrium hydrate formation condition forms the basis for HBGS process. The hydrate phase equilibrium of a typical fuel gas mixture consisting of different mol% CO_2 is also shown in Figure 1.10. Typical fuel gas mixture coming out of IGCC power plant is in the range of 2.0 – 7.0 MPa. As can be seen in the figure, the fuel gas mixture can form hydrates from water in this pressure range. The minimum pressure required to form hydrate from the fuel gas mixture (39.9% CO_2 /rest H_2) at 273.9 K is 5.56 MPa (Kumar et al., 2006). It was observed that during pre-combustion capture the hydrate contains more than 80% CO_2 . Linga et al. proposed to add one more stage and obtain a further concentrated CO_2 stream

(Linga et al. 2007b). The equilibrium hydrate formation pressure of CO₂/H₂ gas mixture with 83.3% CO₂ and rest hydrogen is 1.58 MPa at 273.9 K (Kumar et al., 2006). Kumar et al characterized (structural and compositional) the hydrate samples formed from CO₂/H₂ gas mixtures using PXRD, ¹H MAS NMR (with rotor synchronized spin echoes), ¹³C MAS NMR, mass spectrometry, FTIR (with attenuated total reflection) and Raman spectroscopy. They confirmed that the hydrate prepared from the CO₂/H₂ mixture is structure I and CO₂ occupies 100% of the large cages, whereas 9.3% of the small cages are occupied by bimolecular H₂ and 6.2% by single H₂ molecules. They have also estimated the cage occupancy values and found that the hydration no is 7.09 for CO₂/H₂ gas mixture (Kumar et al., 2009). Hydration number is defined as the number of water molecules per guest molecule. For simple hydrates, the hydration number is related to the fractional occupancy of the large and small cavities, θ_L , and θ_S , and is given by equation 1 for sI hydrates (Sloan and Koh, 2008).

$$sI \text{ Hydration Number } (n) = \frac{46}{6\theta_L + 2\theta_S} \quad (1)$$

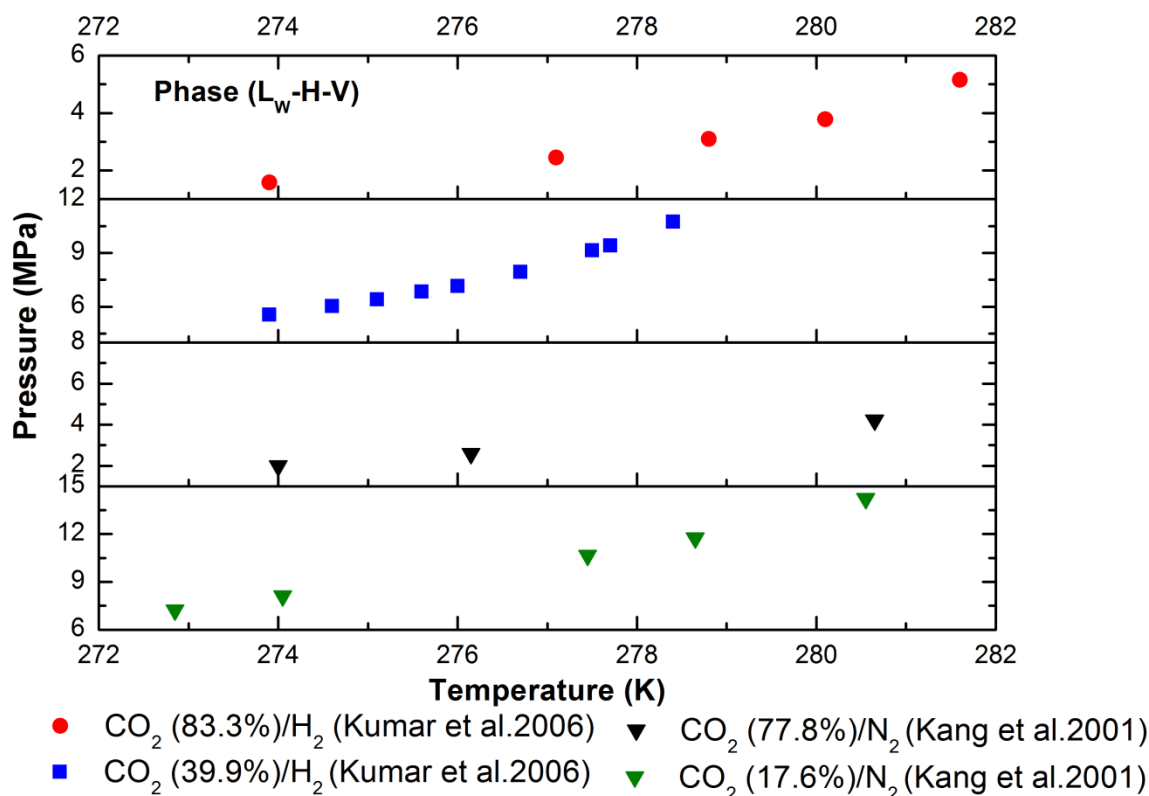


Figure 1.10. Hydrate phase equilibrium of fuel & flue gas mixture along with different concentrations of CO₂.

A conventional power plant emits flue gas of composition 15–20% CO₂, 5–9% O₂ and rest N₂. (Linga et al., 2007b) Kang et al. reported equilibrium hydrate formation data for a mixture of carbon dioxide and nitrogen with varying proportion. The equilibrium hydrate formation conditions for the mixture of carbon dioxide and nitrogen are also shown in Figure 1.10. The minimum pressure required to form hydrate from the flue gas mixture (17.6% CO₂/rest N₂) at 274.05 K is 8.12 MPa (Kang et al., 2001). The major disadvantage with flue gas is the high pressure required specially in the first stage of HBGS process. However in second and third stage a concentrated CO₂ stream can be obtained and separation can be achieved at moderate pressure compared to stage I. The equilibrium hydrate formation pressure of CO₂/N₂ gas mixture with 77.8% CO₂ and rest nitrogen is 2.0 MPa at 274 K (Kang et al., 2001). Linga et al. proposed a Hybrid hydrate-membrane processes for pre and post-combustion capture and concluded that there is a need of additives in order to improve the economics of the process (Linga et al., 2007). Seo and Lee studied the structure and guest distribution of mixed hydrates of carbon dioxide and nitrogen using X-ray diffraction and C¹³ NMR spectroscopy (Seo and Lee, 2004). The structure formed was identified as structure I. NMR spectra results revealed that carbon dioxide molecules mainly occupied the large 5¹² 6² cages of structure I when the mixed hydrate (CO₂+N₂) was formed at a vapor phase composition range of 10 – 20 mol% CO₂. Seo and Lee also reported that CO₂ molecules may occupy both large and small cavities of structure I when the CO₂ content in the gas phase exceeds 33 % (Seo and Lee, 2004).

1.2.3. Kinetics of gas hydrate formation

The hydrate based gas separation (HBGS) process for CO₂ separation from a gas mixture has been studied extensively. However, a commercially viable hydrate based CO₂ separation process demands a rapid hydrate formation rate (Linga et al., 2010). Hydrate formation is basically a crystallization process; upon successful hydrate nucleation, a thin hydrate film forms on the water-gas interface thus limiting gas to water contact (Gayet et al., 2005). It has been identified that higher solubility of hydrate forming guest in water and larger contact area between the hydrate formers and water are crucial to reduce the mass transfer resistance and thus ensure more hydrate growth (Mori et al., 2003, Linga et al., 2012). Kalogerakis et al. suggested that addition of surface active agents to water can enhance gas uptake rate during clathrate hydrate formation without affecting the three phase equilibrium (Kalogerakis et al., 1993). Recently quite a few studies have shown that presence of a small percentage of

surfactant in the hydrate forming mixture changes the hydrate growth kinetics and its morphology. This changed morphology results in better gas-water contact and thus sustains faster hydrate growth kinetics for longer periods of time resulting in better water to hydrate conversion. (Zhong et al., 2000; Kalogerakis et al., 1993; Rogers et al., 2007)

Figure 1.11 shows a typical gas uptake curve with its corresponding temperature profile and induction time. A general gas uptake curve as discussed by Natarajan et al. begins with a gas dissolution phase shown by gradual drop in pressure of the reactor (in batch mode). This is followed by hydrate nucleation, nucleation point is identified by a sudden rise in gas uptake rate and sharp exothermic peak in the temperature profile coincide. The time at which stable hydrate nucleation is observed is also known as induction time. Once nucleation occurs, hydrate formation enters into the growth phase. The growth phase continues for a certain period of time and can be concluded to have finished when no more gas uptake takes place, i.e. the hydrate growth reaches saturation. The slope of the gas uptake curve can be utilized to measure the hydrate growth rate (Natarajan et al., 1994).

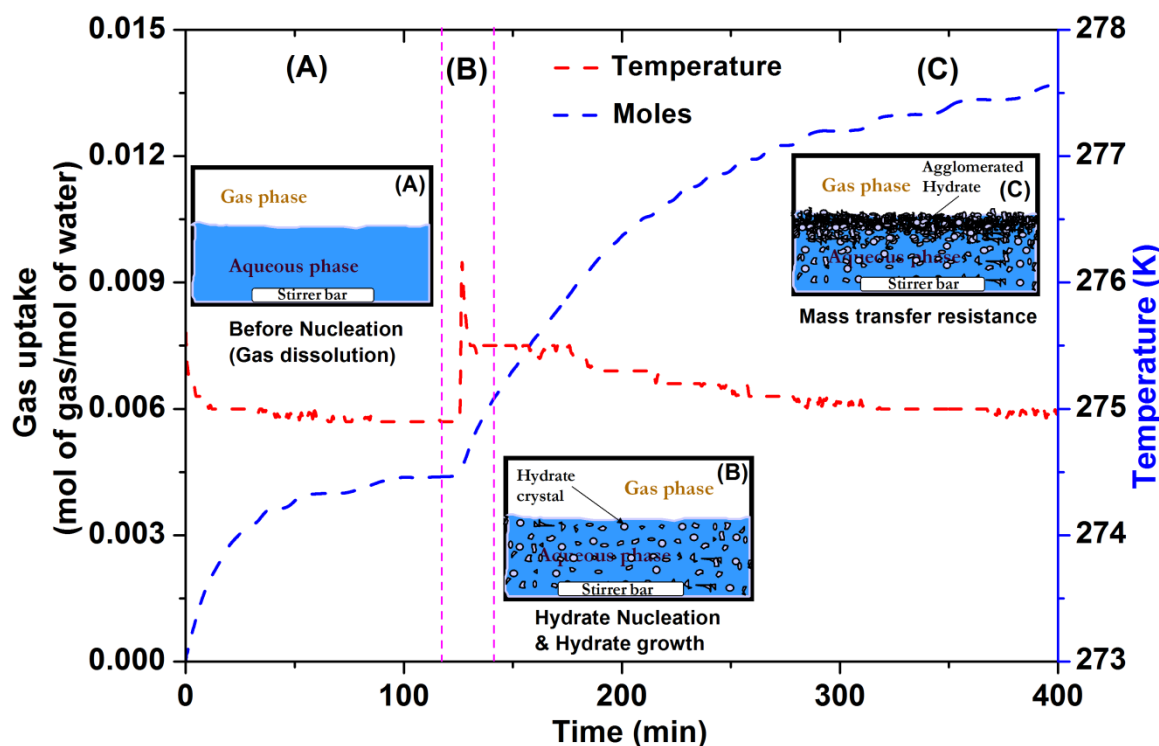


Figure 1.11. A typical gas uptake curve along with temperature profile showing the induction time for gas hydrate formation. Inset figures: (A) showing the gas dissolution, (B) hydrate nucleation and (C) hydrate growth.

Hydrate growth rate slows down with time due to a) limited heat and mass transfer in a lab scale reactor and b) drop in driving force in a batch reactor. A gas hydrate promoter is expected to reduce the induction time and sustain fast hydrate growth rate for extended period of time. Thus a classical gas uptake experiment and the ensuing gas uptake curve in a stirred tank reactor can be utilized for identifying a hydrate promoter. Fairly fast hydrate crystallization can then be utilized for several technological applications through hydrate formation and decomposition cycle.

1.2.4. Surface active agents (Surfactants) and their role in gas hydrate studies

Surface active agents (Surfactants) are compounds, whose molecules contain both lipophilic (hydrophobic) and hydrophilic moieties, i.e., they are amphiphilic (exhibit affinity for both polar and non-polar substances (Figure 1.12(a)). The lipophilic and hydrophilic groups, characteristic of each surfactant are the property determining factors. Surfactants can diffuse from the bulk phase to an interface, altering the surface or interfacial tension, modifying the contact angle between the phases and wettability of solid surfaces, and thus changing surface charge & surface viscosity (Shah; 1977). At suitable concentrations, the surfactant molecules in water aggregate to form various kinds of structures (called micelles) with diverse shapes and orientations (spherical, rod-like micelles, multilayer structures and so forth) (Figure 1.12(b)) (Vögtle, 1991; Fuhrhop and Koning, 1994).

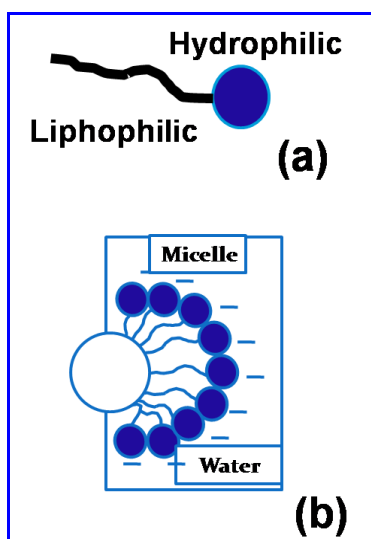


Figure 1.12. (a) A surfactant molecule with hydrophilic and lipophilic groups and (b) Micelle formation in aqueous media through association of surfactant molecules

Surfactants can mainly be classified into three categories depending on the moieties they contain, namely anionic, cationic and non-ionic surfactants. Zwitterionic surfactants are another

major class which is distinguished from others as these compounds contain both cationic and anionic centers attached to the same molecule (Figure 1.13).

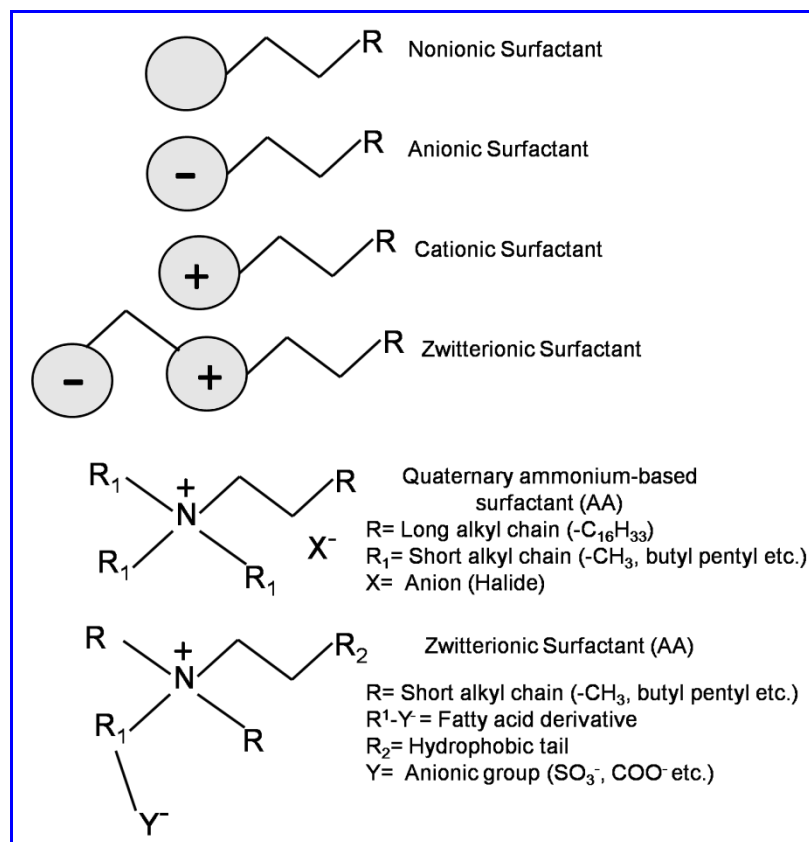


Figure 1.13. Different classes of surfactants and their corresponding structures

Use of surfactants in gas hydrate related studies has been ongoing since the early 90s (Kutergin et al., 1992; Kalogerakis, 1993; Leporcher, 1998). While certain surfactants have been recognized as kinetic promoters others have shown no such activity. A thorough search of relevant literature clearly shows that use of surfactant greatly enhances the kinetics of hydrate formation and they have been widely used in different lab scale studies. However, there is still a lot of ambiguity in determining whether a surfactant is going to work for a particular system.

1.2.5. Surfactants as kinetic hydrate promoters

Karaaslan et al. have used three different types of surfactants (anionic, cationic and nonionic); they have reported that hydrate formation kinetics was significantly better in the presence of the anionic surfactant. The effect of the nonionic surfactant was less pronounced while the cationic surfactant showed behavior exactly opposite to that of the anionic surfactant at low and high concentrations. (Karaaslan et. al., 2000 a,b). In a different work, Karaaslan et

al. studied the effect of three non-ionic surfactants, polyoxyethylene (5) nonylphenyl ether (IGEPAL-520), Brij-58 and Tween-40. The authors concluded that IGEPAL-520 is the most effective hydrate formation promoter among the three. An amount of 1 wt % IGEPAL-520 accelerates the methane hydrate formation rate by a factor of 2.4 compared to methane hydrate formation with pure water (Karaaslan et al., 2002).

Zhang et al. reported that sodium dodecyl sulfate (SDS) reduces the induction time; however a systematic trend was not observed between induction times and SDS concentrations, when the concentration of SDS was varied from 260 to 10000 ppm (Zhang et al., 2007a).

Okutani et al. studied the effects of three homologues anionic surfactants (sodium dodecyl sulfate (SDS), sodium tetradecyl sulfate (STS), sodium hexadecyl sulfate (SHS)) on methane hydrate formation. At concentrations of ~ 1000 ppm or above, SDS was found to be very effective in increasing both, the rate of pure methane hydrate formation and the final water-to-hydrate conversion. However, equivalent promotion effect was seen with STS at a much lower concentration, say ~ 100 ppm. It was concluded that, STS is more favorable than SDS as far as methane hydrate formation is concerned. SHS was found to be less effective compared to SDS and STS. (Okutani et al., 2008). According to Yoslim et. al., the addition of SDS (concentration range between 242 to 2200 ppm) increases the gas uptake rate for mixed hydrate of methane /propane ($\text{CH}_4/\text{C}_3\text{H}_8$) by 14 times as compared to that for pure water. At SDS concentrations of 2200 ppm and 645 ppm, pressure drop due to hydrate formation was found to be the maximum. They suggest that in the presence of the surfactant (SDS), thin solid hydrate film is not formed at the liquid-gas interface. Also hydrate growth was also seen on the walls of the reactor suggesting better water to gas contact by capillary effect. (Yoslim et. al, 2010).

Kang et al. through their experimental work has concluded that an optimum concentration of SDS acts as a promoter but an excess amount of the same can act an inhibitor. In the presence of SDS, initial hydrate formation rates were found to increase the gas consumption from the gas phase (Kang et. al., 2010).

Zhong et al., studied the influence of cyclopentane (CP) and SDS on methane separation from low-concentration coal mine gas. They found that the gas uptake and rate of hydrate formation were dependent on SDS concentration, but the presence of SDS did not show any clear influence on methane recovery. The methane recovery obtained in the presence of SDS was 33.3%, while that obtained without SDS was 33.1% (Zhong et al., 2013). In a similar work with other surfactant Li et al., found that methane hydrate formation rate for cyclopentane / water

emulsion with tween-80 was better than the one obtained in absence of tween-80, higher gas/liquid contact area in presence of surfactant was identified as one of the reasons for such results (Li et al., 2010).

Link et al. tested a large selection of surfactants in order to judge their kinetics promoting properties on gas hydrate formation. They used pure methane as the hydrate forming guest. The authors found that out of all the surfactants tested, SDS was the best surfactant for promoting methane hydrate formation (Link et al., 2003). Zhong and Rogers found that by adding about 284 ppm of SDS to an ethane-water system, the rate of formation of ethane hydrate could be increased by a factor greater than about 700 as compared to a system having only pure water. They also reported good reproducibility of the induction time in the surfactant solution compared with no surfactant experiment. Furthermore, they suggested that formation of micelle in presence of surfactant not only enhanced ethane solubility but the micelle itself acted as nucleating sites for faster hydrate growth (Zhong and Rogers et. al. 2000). Authors report that the CMC value of SDS-water solution decreases with pressure from 2725 ppm (at atmospheric pressure and room temperature) to 242 ppm (at hydrate forming conditions). At 242 ppm of SDS, there was a significant change in the hydrate induction time which was used to define the CMC. In another work Zhang et. al. found that the pure non-ionic surfactant Tween-40 (T40) performed better in promoting a stable crystal nuclei and shortening the induction time, compared to T40 (Tween-40)/T80 (Tween-80) (1:1) and T40/T80 (4:1) mixtures (Zhang et. al. 2008). Gayet et al. obtained the methane hydrate equilibrium conditions in presence of 0.02wt% SDS and found that SDS did not have any effect on the gas hydrate equilibrium but enhance the hydrate formation rate. In addition to this, visually they observed that for pure water system, nucleation and growth of hydrates usually occurred at the water–gas interface. After the whole interface was covered with a rigid hydrate film, hydrate formation was stopped. For Water-SDS system, they found hydrates grow as a porous structure on the reactor wall and the liquid–gas interface remained free of hydrate (liquid migrates from the bulk phase to the porous structure due to capillary forces) (Gayet et al., 2005).

From the above discussions, it can be safely concluded that the utility of surfactants as a promoter for hydrate crystallization has been clearly established. However, the qualitative knowledge obtained so far is system specific. Dependencies on the surfactant concentration for hydrate-formation rate and the final water to hydrate conversion ratio has been established for many guest species. However, it is not clear whether such dependencies actually exist or it is

more to do with different reactor configuration used in different studies. Most of the studies discussed in this section were employed in stirred tank reactors and hence the agglomeration of hydrate crystals creates a barrier for effective gas-liquid contact resulting very low gas uptake and low water conversion to hydrate even in presence of surfactant. Therefore, there is a need for innovative materials (fixed bed) which will increase the gas-liquid contact mode, enhance hydrate formation kinetics and maximize the CO₂ capture capacity.

1.3. Research Objectives

The thesis focuses on the following aspects;

1. Determine effective media (fixed bed) and additive (surfactant) for better gas/liquid contact for enhanced hydrate formation kinetics and water to hydrate conversion
2. Study the impact of impurities like fly ash, SO₂ and H₂S on the separation efficiency of HBGS process for separation and capture of CO₂ from flue gas and fuel gas mixture.
3. Suggestions for the scale-up of HBGS process for successful commercialization of CO₂ capture from fuel gas mixture
4. Identification of economically viable sequestration option for captured CO₂ through lab scale experimentation.

The above objectives will ensure sustainable utilization of available fossil fuel by allowing us to study (i) *the feasibility of Hydrate Based Gas Separation (HBGS) process for CO₂ capture from point source like coal based thermal power station in fixed bed configuration, and (ii) CO₂ sequestration by replacement of methane from natural gas hydrate reserves (energy production with CO₂ sequestration)*

1.4. Thesis Organization

CO₂ emission mitigation technologies available are discussed in chapter 1. This chapter also gives the basic information on gas hydrates and current knowledge on gas hydrate research relevant to CO₂ capture and sequestration. In addition the role of surfactants in gas hydrate studies has also been discussed in chapter 1.

Chapter 2 reports the performance of additives (surfactants) in suitable fixed bed arrangement for enhanced carbon dioxide hydrate formation kinetics.

Chapter 3 reports impact of fly ash and SO₂ impurities on the hydrate based gas separation process for carbon dioxide capture from a flue gas mixture. In addition, this chapter also presents impact of H₂S impurity on carbon dioxide capture from fuel gas mixture.

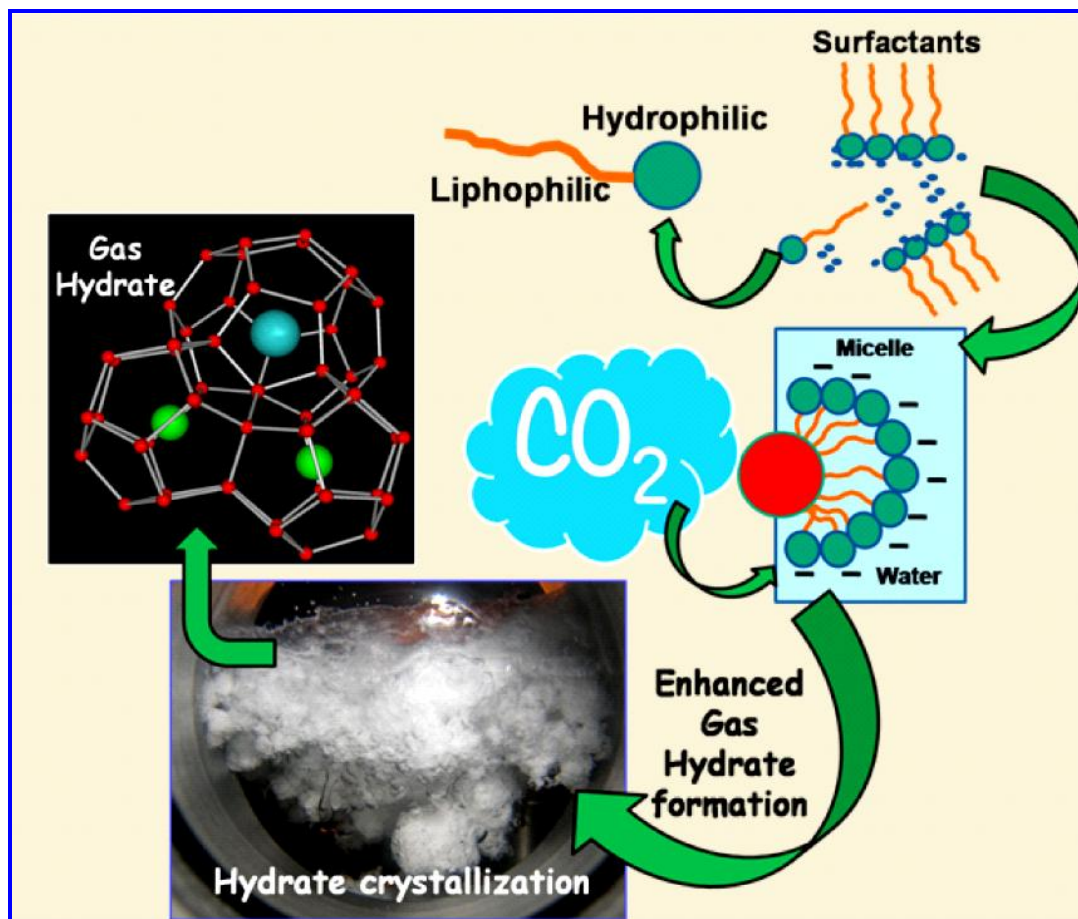
Chapter 4 reports the use of metallic fixed bed media like stainless steel packing, brass packing and copper foam packing for enhanced gas hydrate formation that is applicable to carbon dioxide capture from fuel gas mixture.

Chapter 5 reports the study of CO₂ sequestration by methane replacement in synthetic natural gas hydrate sediment through lab scale experimentation. Methane hydrate formation kinetics in test sediment and replacement kinetics is presented.

Finally, in chapter 6 the conclusions of the thesis and future directions for implementing a pilot scale HBGS process for CO₂ capture/separation in continuous mode are presented.

Chapter 2

Selection of Suitable Porous Fixed Bed Media and Surfactants to Enhance the Carbon Dioxide Hydrate Formation Kinetics



2. Selection of Suitable Porous Fixed Bed Media and Surfactants to Enhance the Carbon Dioxide Hydrate Formation Kinetics ²

²“A version of this chapter has been published.

Kumar A, Sakpal T, Linga P, Kumar R. Influence of contact medium and surfactants on carbon dioxide clathrate hydrate kinetics. *Fuel* 2013;105:664-71.

2.1. Introduction

As discussed in chapter 1, hydrate formation is essentially a gas-liquid-solid multiphase reaction and thus higher interfacial area is desirable for better gas-water contact to form solid hydrates. Employing a stirred tank reactor results in faster hydrate kinetics; however agglomeration of hydrate crystals on the interface creates a barrier for gas to come into contact with water, resulting in low water to hydrate conversion. Moreover, it has been shown that stirring cost becomes a significant portion of total process cost, thus making it a highly energy intensive process (Linga et al., 2010). In the previous chapter, a comprehensive review of gas hydrates and role of surfactants in hydrate formation were presented. As discussed, hydrate formation in a non-stirred setup is quite slow, a thin film of hydrate forms on the water surface, and mass transfer across the film become rate controlling, resulting in slower kinetics and lower water to hydrate conversion. Thus a fixed bed contact mode having a high surface to volume ratio is ideally suitable; packing material with large intra pore surface area (silica gel) has been used in fixed bed arrangement. Effect of pore size distribution of silica gel has already been studied (Adeyemo et al. 2010), however the current work complements the previous work by studying the effect of surface area. Three different silica gels, type A (60–120 mesh), type B (100–200 mesh) and type C (230–400 mesh) were chosen for this study with almost similar pore diameter and different surface area, type C having the highest surface area and type A the lowest. (Appendix A).

In addition, use of surfactant in the aqueous phase is known to reduce the surface tension and has been reported that the morphology of the hydrate formed is quite porous which assist better water and gas contact even if the interface is covered with a hydrate layer.

In this work, we have studied three types of surfactants at varying concentration to study its effect on water to hydrate conversion. SDS serves the purpose for anionic surfactant, Tween-80

a nonionic surfactant and dodecyltrimethylammonium chloride (DTACl) a cationic surfactant. This study is undertaken to help in developing a suitable surfactant aided commercial processes for carbon dioxide separation from flue and fuel gases.

2. 2. Experimental Section

2.2.1. Materials

Carbon dioxide gas with a certified purity of more than 99.9% was supplied by Vadilal Gases Ltd., India. Silica gels with the pore diameter of ~5 nm, particle size distribution in the range of 60–120, 100–200 and 230–400 mesh size having different surface area and pore volume with 99% purity (LR grade) was purchased from Rankem Ltd (Appendix table A1 and figure A1, A2). Surfactants, Tween-80 (LR Grade), dodecyl trimethyl ammonium chloride (LR Grade) and SDS (SQ Grade) with minimum 98% purity were purchased from Rankem Ltd., SRL Pvt. Ltd. and Fisher Scientific Ltd. All the materials were used without further treatment. Deionized and distilled water was used for the experiments.

2.2.2. Apparatus used for surfactant selection with silica gel as fixed bed media

The apparatus is shown in Figure 2.1. It consists of a 500 cm³ SS-316 high-pressure hydrate crystallizer (CR) equipped with an internal cooling coil. The top cover plate of the crystallizer had six ports each equipped with a Swagelok connector. These ports were used for inserting three thermocouples, supplying gas (inlet), vent and pressure transducer. Three thermocouples with ± 0.1 K accuracy are used to measure the temperature; T-1, T-2 and T-3. All pressure measurements are made with pressure transducers, with a range of 0–160 bar and accuracy of 0.075% of the span. The crystallizer is immersed in a water bath containing a 50/50 wt% methanol/ water mixture. Both the crystallizer cooling coil as well as the water bath is connected to a chiller (Julabo-FS18), which maintains the temperature in the hydrate crystallizer and the supply vessel (SV) constant. A stirrer is used inside the water bath to uniformly distribute the cooling liquid in the water bath. As we know hydrate formation predominantly depends on the degree of super-cooling, more hydrate forms near the crystallizer wall than that at the center of the crystallizer (due to heat transfer limitation). To avoid this problem, a cooling coil is provided in the fixed bed portion of the crystallizer for additional cooling. The gas-supply line connecting a high-pressure gas cylinder to the crystallizer was equipped with a pressure regulator, a mass flow controller (MFC) (Brooks model F10974-001, with a Flow rate 0–5 ml/min at operating pressure) and a digital pressure gauge (PPI model).

This allowed us to measure the instantaneous rate of gas supply into the crystallizer and the pressure inside the crystallizer. A vacuum pump (model N86KT.18) is also connected to CR to remove any contamination in the form of air from the fixed bed at the start of the reaction. The setup is equipped with a gas chromatograph GC-2014AT (Shimadzu) to measure the composition of the gas phase in the crystallizer. A representative photograph of experimental setup is presented in Appendix figure A3.

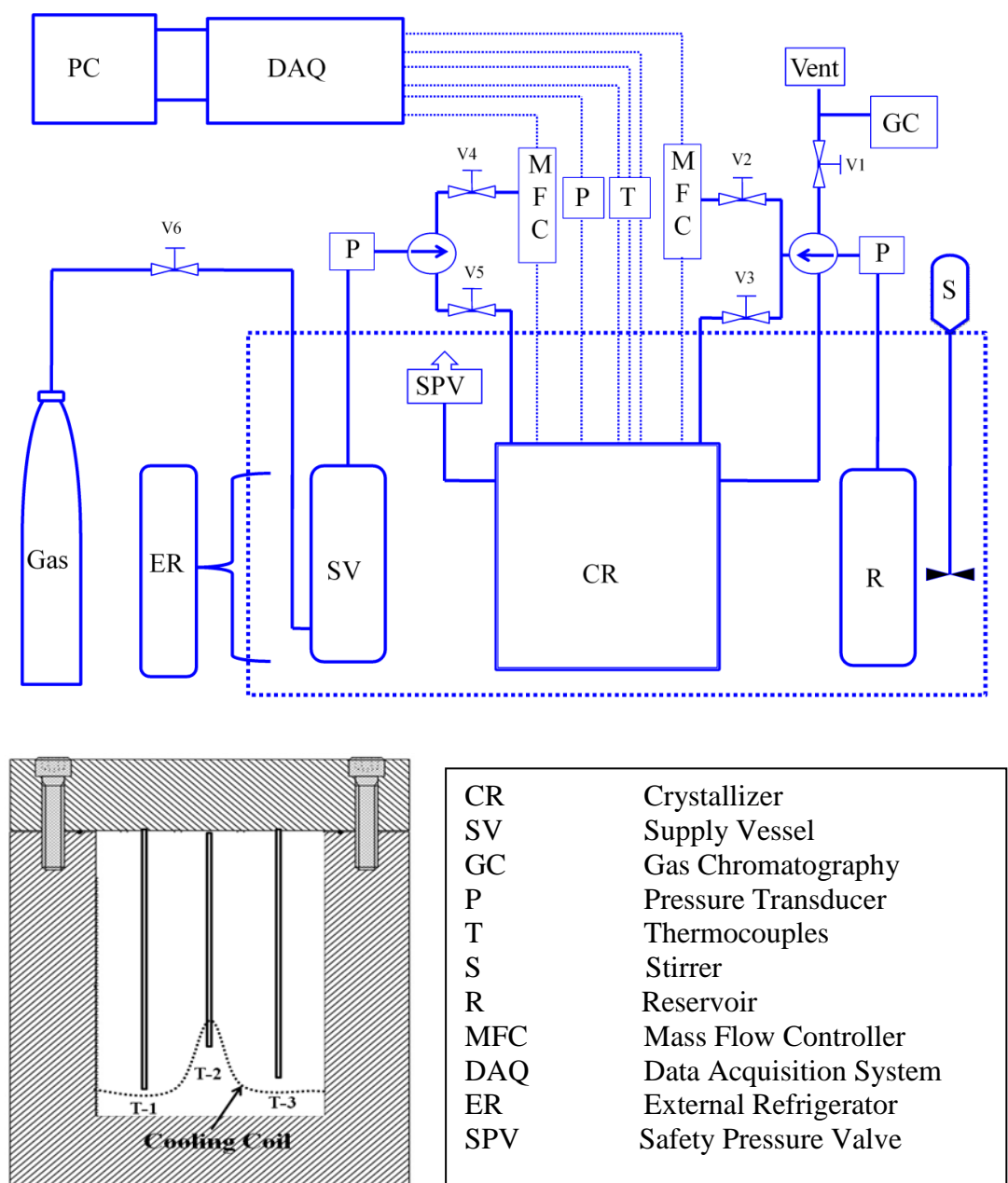


Figure 2.1. Schematic of the experimental apparatus used for surfactant selection using silica gel as fixed bed media, along with location of thermocouples within the reactor.

2.2.3. Experimental procedure for hydrate formation in silica gel/surfactant system

The amount of silica gel used for each experiment was 150 g. Silica gel was oven dried at 100 °C over night to ensure that no free water is present in the silica gel sourced from the manufacturer bottle. Water equal to the pore volume of silica gel was added to obtain pore saturated silica gel. Pore volume was determined by BET analysis. For the experiments with no surfactants, tap water was used whereas different concentrations of surfactants were mixed (refer Table 2.2) to prepare a surfactant–water solution which was used to study the effect of surfactant. Hydrate formation experiment was operated in a semi-batch mode under isothermal and isobaric conditions. The reactor (CR) was charged with 150 cm³ of water saturated silica gel and placed in the water bath, the vent line was connected to a vacuum pump and the reactor was evacuated for 10 min at 0.01 MPa. Circulating water–methanol mixture from the water bath was employed to cool the reactor to desire experimental temperature (274 K), once the desired temperature was reached the crystallizer was pressurized to the desired experimental pressure through supply vessel (SV). Constant pressure inside the reactor was maintained through mass flow controller (MFC), operating pressure for any experiment was the set point for the MFC and as the pressure inside the reactors dropped due to hydrate formation, an equal amount of gas was supplied through the MFC. The gas flow was accurately measured by the MFC and was used to determine gas uptake profile during an experiment. After the completion of hydrate formation (600 min) hydrates were decomposed by heating the hydrate sample to 288 K using the chiller. After complete decomposition a hydrate formation experiment was repeated using the method described above.

2.2.4. Calculation for the amount of gas consumed

As the gas in the crystallizer was consumed for hydrate formation, additional gas was supplied from the SV through mass flow controller, thus the pressure in the reactor was maintained constant. The number of moles of gas passing through the mass flow controller is recorded with respect to time, which basically is the rate of hydrate formation. It is important to note that, the gas in the reactor (CR) is supplied from the supply vessel (SV). The supply vessel is also equipped with the pressure gauge, the pressure difference at the start and end of a reaction is noted down to calculate the total amount of gas supplied to the reactor. For this calculation pitzer's correlation is used. The total number of moles of the gas that have been consumed from the supply vessel for hydrate formation was calculated by equation

$$n = PV / ZRT \quad (1)$$

Where Z is the compressibility factor calculated by Pitzer's correlation (Smith et al., 2001)

This value was compared with that obtained by the totalizer (this is a software which gives total numbers of gas flowing through the MFC, in a specified time) of the MFC.

2.2.5. Water to hydrate conversion calculation

Water to hydrate conversion (mole %) was calculated using the following equation (Linga et al., 2010)

$$\text{Water to hydrate conversion (mol\%)} = \frac{\Delta n_{H,\downarrow} \times \text{Hydration Number}}{n_{H_2O}} \times 100 \quad (2)$$

Where $\Delta n_{H,\downarrow}$ the number of moles of gas consumed for hydrate formation at the end of the experiment and n_{H_2O} is the total number of moles of water in the system.

Pure CO₂ hydrates is type I structure. Its unit cell contains 46 water molecules in the basic crystal with 6 large (5¹²6²) cavities (average cavity radius 4.33 Å) and 2 small (5¹²) cavities (average cavity radius 3.95 Å). The ideal unit cell formula is 6 (5¹²6²). 2 (5¹²). 46 H₂O (Sloan and Koh, 2008). For an ideal sI hydrates, if all the cavities (large and small) were fully occupied the hydration number (water molecules per guest molecule) would be 46/8. However, even partially filled small cages can stabilize a hydrate structure and the actual hydration number can vary depending upon experimental condition. Cage occupancy of pure CO₂ hydrate at moderate pressure range is reported by Kumar et al. 2009 and has been used in the current study.

For simple hydrates, the hydration number is related to the fractional occupancy of the large and small cavities, θ_L , and θ_S , respectively as

$$\text{Hydration Number } (n) = \frac{46}{6\theta_L + 2\theta_S} \quad (3)$$

Cage occupancy value for pure CO₂ hydrate obtained by combining results from infrared spectroscopy and gas chromatography were $\theta_S = 0.81$, $\theta_L = 1.0$ leading to a hydration number of 6.04 (Kumar et al. 2009).

The normalized rate of hydrate formation for hydrate growth is calculated using the following equation (Linga et al., 2010)

$$\text{Rate of hydrate formation } \left(\frac{\text{mol/mol}}{\text{min}} \right) = \frac{(\Delta n_{H,\downarrow})_t / n_{H_2O}}{t} \quad (4)$$

The average of these rates is calculated every 5 min and reported.

2.3. Results and discussion

2.3.1. Effect of silica gels on hydrate formation kinetics

Gas uptake measurements were carried out to monitor CO₂ hydrate crystallization by determining the moles of CO₂ gas consumed during an experiment. Table 2.1 summarizes all the experiments performed and their experimental conditions (experimental pressure, temperature and driving force). In addition, moles of gas consumed and final water to hydrate conversion (based on hydration number) after 10 hours of hydrate formation and induction time are also reported. Operating temperature of 274 K was chosen to ensure that hydrate formation studies are carried out at liquid-gas interface, the minimum hydrate formation pressure at the operating temperature was estimated from CSMGEM (Sloan and Koh, 2008). Figure 2.2 shows the gas uptake curves obtained for all the three types of water saturated silica gels for the period of 500 minutes. This curve represents the kinetics of hydrate formation. The general shape of the curve agrees with the gas uptake curve described in detail by Natarajan et al, however, the dispersed state of water in the silica gel pores allows for enhanced gas consumption due to better gas-water contact. As shown in Figure 2.2 the gas uptake is highest in type C silica gel (230-400 mesh) compared to type A and type B silica gel (60-120 and 100-200 mesh respectively). Pore sizes of all the three types of silica gel used in this study were quite similar, however it differs in particle size and exposed surface area. Results suggest that type C silica gel which has smaller particle size but higher surface area (compared to type A and B silica gel) has highest water to hydrate conversion ratio. It is noted that water to hydrate conversion (mol %) with type C silica gel is ~50.0% after 200 minutes compared to A and B type of silica gel having ~15.0% and 30.0% conversion respectively. The percentage conversion from water to hydrate was determined from Equation 2 using a hydration number of 6.04. Adeyemo et al. has reported that for favorable hydrate formation (water to hydrate conversion ratio) larger pore diameter is more important than larger particle size, however, they could not compare the effects of exposed surface area. The results obtained in this study clearly suggests that if pore diameter is kept constant, larger surface area is the most important factor for enhancing the water to hydrate conversion ratio. As shown in Figure 2.2 with increasing surface area, water to hydrate conversion ratio increases. Thus a combination of larger pore diameter and higher surface area should enhance the rate of hydrate formation and water to hydrate conversion ratio significantly. In a porous matrix, hydrates are formed within the pores as well as between the

interstitial sites (Seo et al., 2005, Natarajan et al., 1994). While larger pores enhances the diffusion of gases into the interstitial sites, higher surface area allows more contact between the water and gas thus resulting in better water to hydrate conversion.

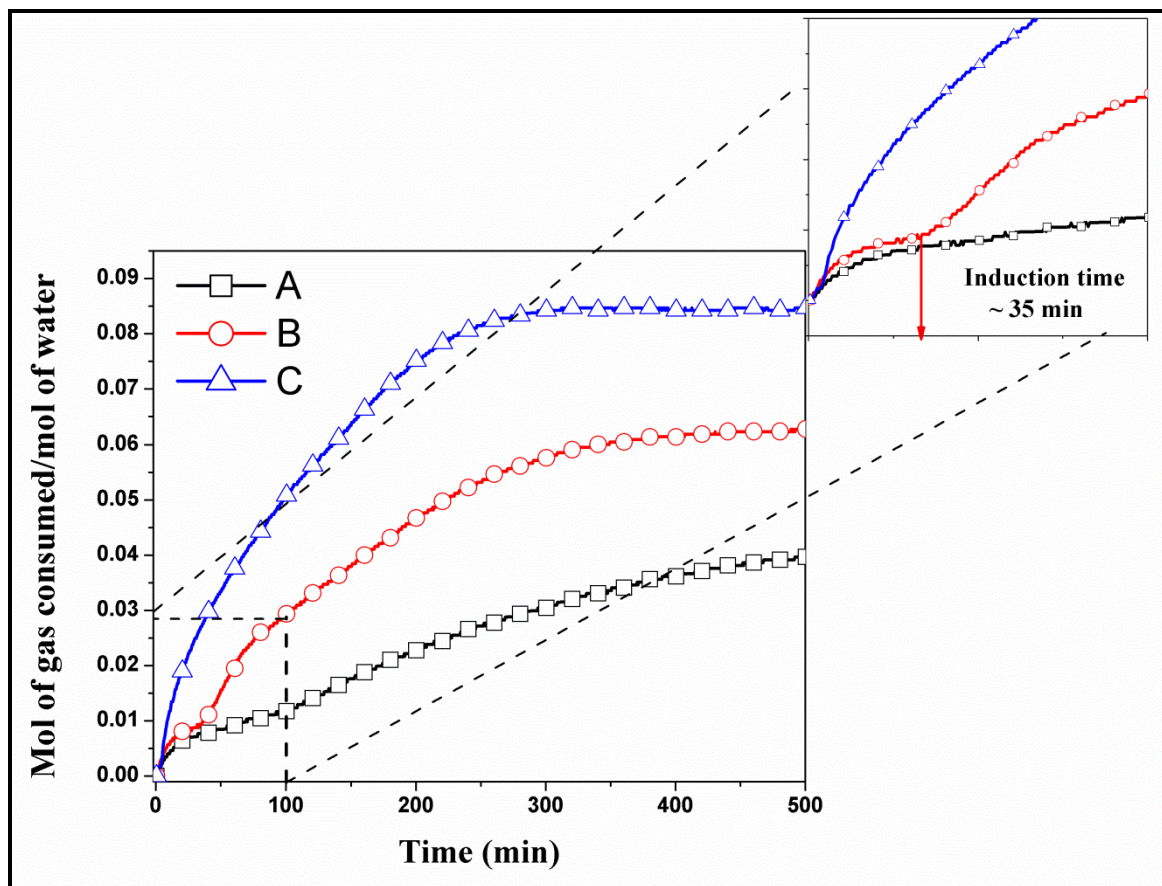


Figure 2.2. Kinetics of the CO_2 hydrates formation with various silica gels under the same driving force. The axis title and units of the inset are the same as figure 2.2. Inset corresponds to the induction time comparison of silica gels (for B type of silica gel ~ 35 min)

The induction time in gas hydrate crystallization is an important characteristic of the kinetic studies, as seen the induction time in the three systems is quite different; type C silica gel with higher surface area has the shortest induction time followed by type B and type A silica gel (Table 2.1). Induction time is a stochastic phenomena and in gas hydrate crystallization, it has been found that higher the pressure, lower the induction time (higher pressure is a measure of super-saturation). Though this work was done at constant pressure, different induction time observed for three different systems is not surprising, type C silica gel with higher surface area compared to others, allowed a better contact between the gas and water

phase resulting in lower induction time. Shorter induction time is favorable for a hydrate based separation process where CO₂ is to be separated from its mixture.

Table 2.1 Comparison of gas uptake in different type of silica gels at constant pressure P_{exp} 3.55 MPa, Driving Force ^a2.14 MPa and temperature 274 K (Experiments were conducted in semi-batch mode)

System	Silica gel type	Exp. No.	CO ₂ consumed (mol of gas/mol of water)	CO ₂ consumed (gas mol)	Final conversion of water to hydrate ^c (mol %)	Induction Time (Min)
CO ₂ /H ₂ O	A	A-1	0.041	0.277	25.15	95
		A-2	0.040	0.267	24.25	98
	B	B-1	0.059	0.396	35.96	35
		B-2	0.062	0.415	37.65	38
	C	C-1	0.085	0.566	51.41	6
		C-2	0.083	0.549	51.14	5
	Quiescent Water	D-1	0.008	0.053	4.82	*

^a Driving Force $P_{\text{exp}} - P_{\text{eq}}$ (P_{exp} = experimental pressure, P_{eq} = equilibrium pressure^b)

^b From CSMGEM (Sloan and Koh, 2008)

*Was not identified in the current study

^c Hydration number of 6.04 was used for water to hydrate conversion (Kumar et al., 2009)

To compare the enhancement factor in presence of silica gel one experiment was performed in the reactor without silica gel (under quiescent conditions). A volume of 130 cm³ of water was placed in CR, keeping the temperature and pressure condition similar. Figure 2.3 shows the comparison of water to hydrate conversion for CO₂ hydrate in quiescent condition and type B silica gel. As seen in the figure, water to hydrate conversion in the quiescent water / CO₂ system is almost 8 times less compared with silica gel / water / CO₂ system. In quiescent water / CO₂ system, once the gas water interface gets converted into CO₂ hydrates, either CO₂ has to diffuse through the hydrate layer to come in contact with fresh water or water has to travel through the hydrate film, resulting in a mass transfer controlled reaction and hence the rate of hydrate formation reduces to a great extent. It has been reported that the obstructing hydrate film does not develop if a surfactant is added to the aqueous phase, eliminating the mass transfer limitation to a greater extent, thus enhancing the rate of hydrate formation. Figure 2.3 also shows a comparison of the temperature profiles as a function of time for the two

systems, the extent of heat released is quite high for the experiment carried out in silica gel medium for hydrate formation. At least, couple of large temperature spikes can be seen in a silica gel system, a high yield of hydrates is usually associated with a large magnitude of temperature spike accompanied by a higher magnitude of gas uptake (as seen in Figure 2.3).

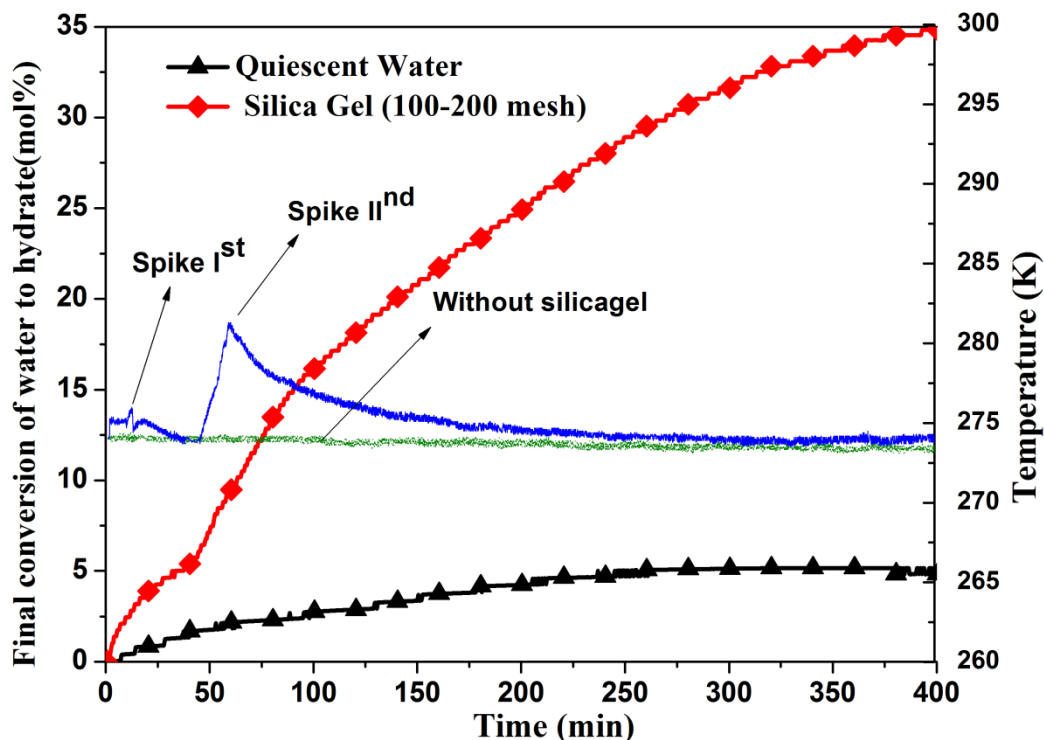


Figure 2.3. A typical gas uptake measurement curve (red and black) together with the temperature profile (blue and green) (induction time ~ 35 min using 100-200 mesh type silica gel) and Comparison of water to hydrate conversion for CO_2 hydrate formation conducted in the same apparatus with and without the presence of silica gel (100-200 mesh)

2.3.2. Effect of surfactants on hydrate formation kinetics in silica gel media

To evaluate the effect of surfactants on the formation kinetics of CO_2 hydrates in a fixed bed setup, three different surfactants were chosen, tween-80 (a nonionic surfactant), dodecyltrimethylammonium chloride (DTACl) (a cationic surfactant) and SDS (an anionic surfactant). Type C silica gel (230-400 mesh) having the maximum surface area (see the supplementary data) was used in all the experiments, silica gel was saturated with surfactant-water solution and this pore saturated silica gel was used for gas uptake measurement as described before.

Table 2.2 summarizes all the results obtained in presence of different surfactant. These data show that, at optimum concentrations of surfactant, the water to hydrate formation is

higher for anionic and nonionic surfactant (4000 ppm and 2000 ppm respectively) compared to cationic surfactant. However, in general the final water to hydrate conversion in presence of anionic and nonionic surfactants was found to be almost same compared to conversion in absence of surfactant. It can be clearly seen that induction time for hydrate formation reduces upon increasing the SDS concentration (Table 2.2).

Figure 2.4a shows the observed mol of gas consumed (per mol of water used) with respect to time for different concentrations of Tween-80 solution (Hydrate growth after induction time is plotted). As seen in the figure, experiments with 2000 ppm have a faster rate of hydrate formation, compared to 500 ppm. It is observed that increasing the concentration to 4000 ppm does not improve the rate of hydrate formation. Also with the three different concentrations of Tween-80 solution used for this study, no significant difference in the total moles of gas consumed (after 10 h of the experiment) was observed.

Figure 2.4b represents the effect of cationic surfactant (DTACl) on the CO₂ gas hydrate formation. As observed from the figure, DTACl has the lowest gas consumption rate compared to the other two surfactants. Karaaslan and Parlaktuna made the same observation for cationic surfactants. They observed that cationic surfactant showed opposite behavior compared to the anionic surfactant. Such deviation may be due to particle aggregation, which blocks mass transfer through the solid hydrate (Karaaslan and Parlaktuna, 2000b).

Figure 2.4c provides the effect of different concentration of SDS (anionic surfactant) on the CO₂ gas hydrate growth. It can be seen that with SDS concentration of 4000 ppm the gas consumption after 30 minutes of hydrate formation is almost twice compared to the other two surfactants used in this study. However, at lower SDS concentration no significant difference is observed either in the initial rate of hydrate formation or in the final gas consumption. This observation agrees well with the observation of Kalogerakis et al. 1993, where they have observed a noticeable increase in hydrate formation rate with an anionic surfactant. Okutani et al. & Yoslim et al. have also reported similar results in terms of higher water to hydrate conversion ratio with higher concentration of an anionic surfactant like SDS (Okutani et al. 2008; Yoslim et al. 2010)

One experiment was performed with SDS solution in absence of silica gel (under quiescent conditions). All the conditions for hydrate formation were same as shown in Table 2.2 and 4000 ppm of SDS were used for this study. As shown in the tables, there is ~ 4 times

more water to hydrate conversion with SDS compared to in absence of SDS (in quiescent condition).

Thus SDS was found to be a best surfactant which enhances the rate of hydrate formation and water to hydrate formation. Based on results obtained with silica gel and SDS; silica sand was also used as a fixed bed media in presence for SDS for enhanced hydrate formation kinetics.

Figure 2.5 shows the comparison of normalized rate (Equation 4) of hydrate formation with and without SDS (best performing surfactant) in a packed bed setup for type C silica gel (best performing silica gel) and with quiescent water. As shown in the figure, a tenfold increase in the initial rate of hydrate formation is observed by using silica gel compared to quiescent water condition. Upon addition of surfactant the initial rate of hydrate formation improves further and compared to quiescent water a 15 fold increase in the rate of hydrate formation can be achieved. It is important to note that this 15 fold increase in the initial rate of hydrate formation was achieved without stirring the system and hence will bring a significant cost advantage compared to a stirred tank reactor for hydrate formation.

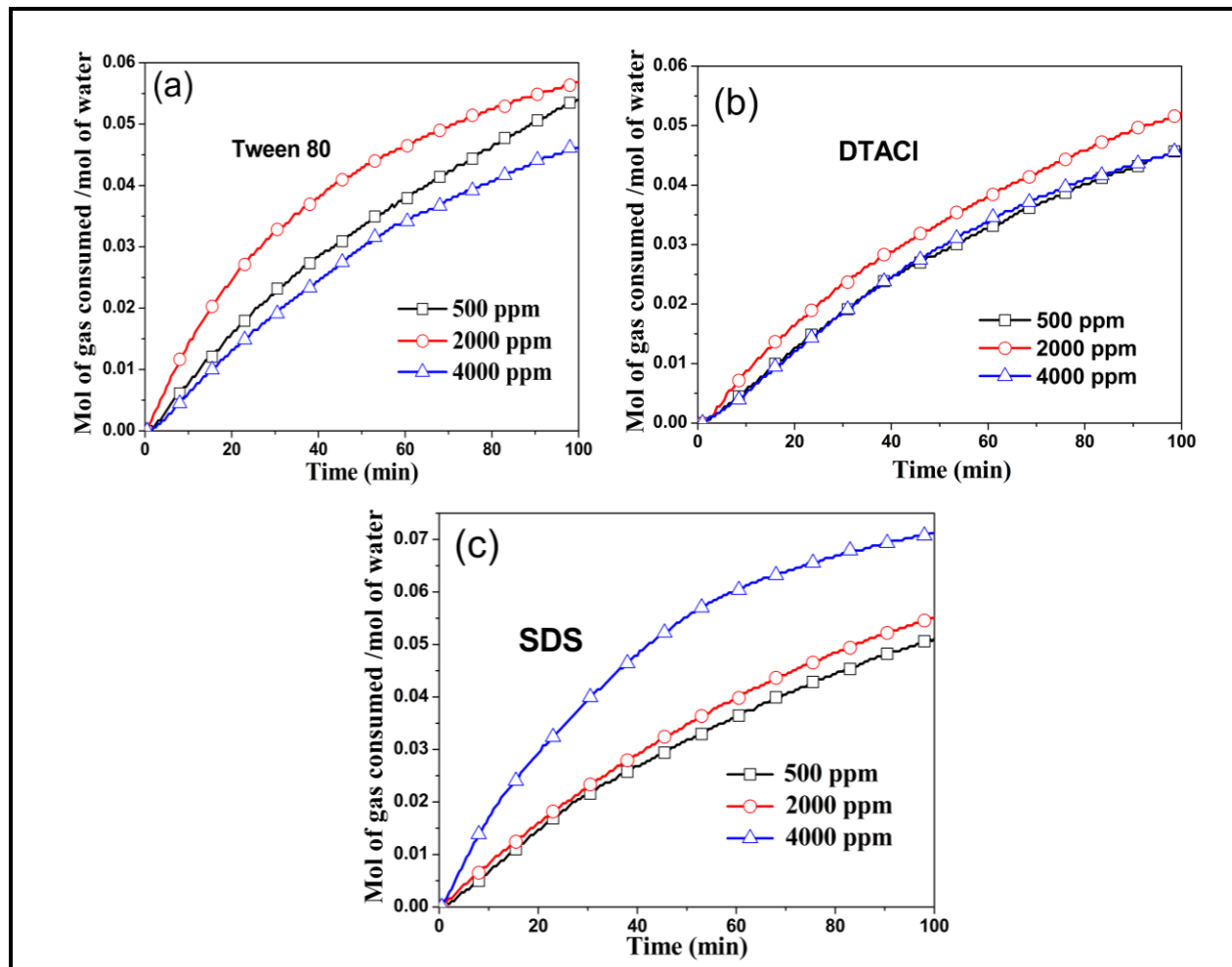


Figure 2.4. Effect of surfactants on hydrate growth for CO₂/water system in silica gels at 500, 2000 and 4000 ppm concentration of surfactants (a) Non ionic surfactant Tween-80 (b) Cationic surfactant DTACl (c) Anionic surfactant SDS

Table 2.2 Effect of Surfactants (Tween-80, SDS and DTACl) on hydrate formation in C type of silica gel kinetics at constant pressure P_{exp} 3.55 MPa, Driving Force 2.14 MPa and temperature 274 K (Experiments were conducted in semi-batch mode)

System	Surfactant concentration (ppm)	Exp. No.	CO ₂ consumed (mol of gas/mol of water)	CO ₂ consumed (gas mol)	Final conversion of water to hydrate ^c (mol%)	Induction Time (min)
CO ₂ /T-80/ H ₂ O	500	C-3	0.087	0.581	52.69	11
		C-4	0.075	0.505	48.87	12
	2000	C-5	0.085	0.569	51.66	5
		C-6	0.081	0.554	49.32	12
	4000	C-7	0.084	0.563	51.14	13
		C-8	0.067	0.451	40.98	21
CO ₂ /SDS/ H ₂ O	500	C-9	0.075	0.505	45.87	20
		C-10	0.058	0.390	35.39	22
	2000	C-11	0.089	0.595	53.98	16
		C-12	0.076	0.507	48.06	18
	4000	C-13	0.087	0.583	52.95	3
		C-14	0.079	0.529	48.00	8
CO ₂ /SDS /Quiescent Water (without silica gel)	4000	D-2	0.028	0.189	17.16	*
CO ₂ /DTACl/ H ₂ O	500	C-15	0.076	0.512	46.80	14
		C-16	0.062	0.415	37.65	8
	2000	C-17	0.074	0.496	45.07	14
		C-18	0.053	0.355	32.23	15
	4000	C-19	0.0785	0.523	47.44	18
		C-20	0.0761	0.508	46.10	20

*Was not identified in the current study

^cHydration number of 6.04 was used for water to hydrate conversion (Kumar et al., 2009)

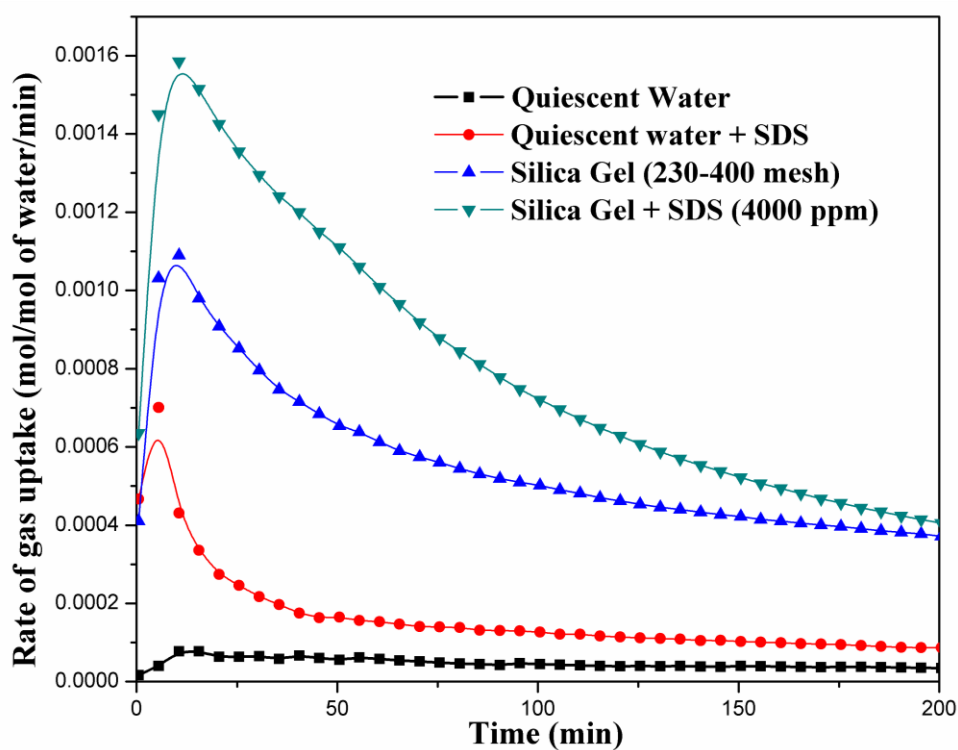


Figure 2.5. Comparison of rate CO_2 uptake with and without the presence of silica gel (230-400 mesh) and in presence of SDS

Figure 2.6 summarizes the results obtained for water to hydrates conversion ratio of all the experiments performed during this study. All the experiments were run for 10 h, after which the reaction was stopped. A comparison between the three gels shows that type C gel gave the highest water to hydrate conversion. The water to hydrate conversion of type C gel was found to be ~ 36 % higher than that of type B gel and ~ 100% higher than that of type A Gel. On the other hand when surfactants was added to the fixed bed set up consisting of type C gel, two surfactants (SDS and Tween) were found to provide more or less the same water to hydrate conversions compared to similar experiments without any surfactants. However, DTACI was found to hinder the hydrate growth suggesting it may act like a hydrate kinetic inhibitor. This also resulted in a lower conversion of water to hydrates compared to the control experiment (type C gel without the surfactant). It is noted that a detail study is required to suggest the potential applicability of DTACI as a hydrate kinetic inhibitor. Comparing the three different silica gels studied in this work, it can be said that higher surface area not only enhances the rate of hydrate formation (Figure 2.2), it also improves water to hydrate conversion. Since equal amount of water was used for hydrate formation in all the three silica gel, higher surface area ensure better distribution and contact of water and gas resulting in higher conversion. From this study, it can be concluded that larger pore diameter and higher surface area enhances the rate of

hydrate formation and water to hydrate conversion. Figure 2.6 also suggests that using a surfactant solution is better for hydrate formation compared to pure water alone; however it cannot be a viable option for a commercial hydrate formation unless the system is stirred or a fixed bed setup is used.

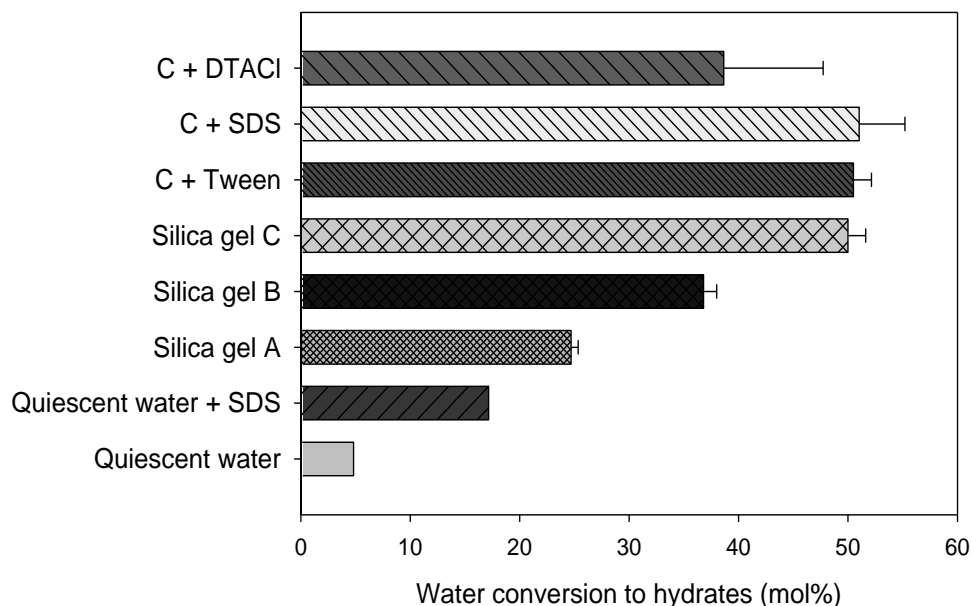


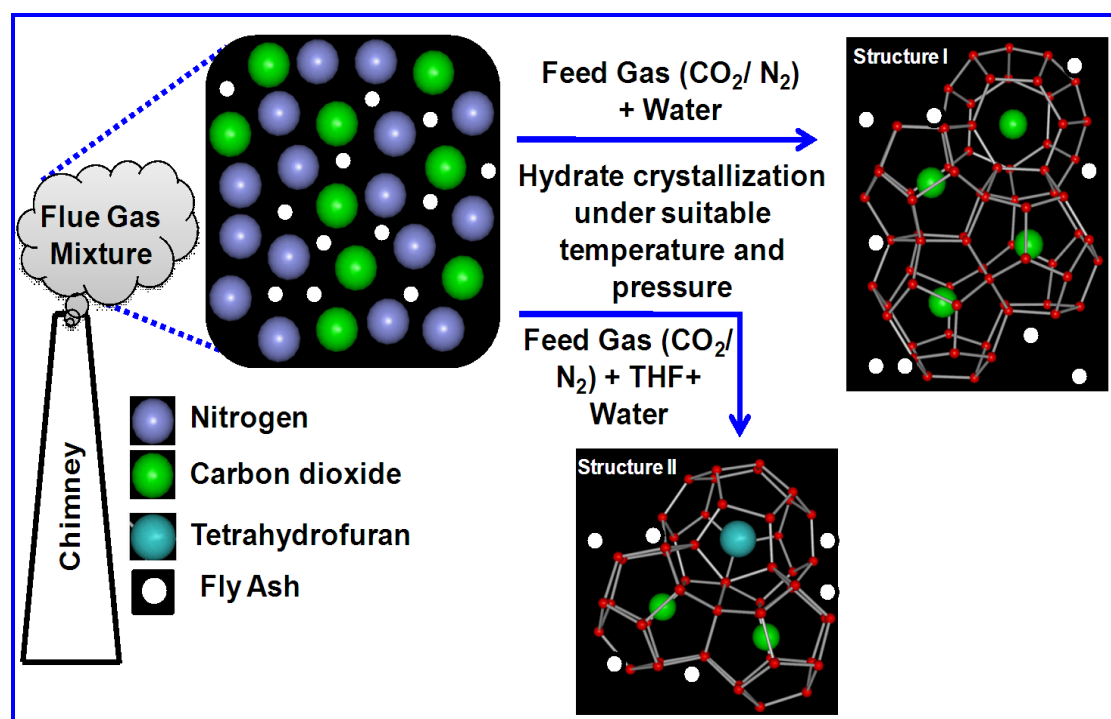
Figure 2.6. Comparison of water to hydrate conversion for CO_2 hydrate formation for 10 hr

2.4. Conclusion

The effect of different silica gels, nonionic, cationic and anionic surfactant on CO_2 gas hydrate formation has been investigated experimentally. The presence of silica gel with high surface area has significant effect on the rate of hydrate formation. Among the three surfactants anionic (SDS) and nonionic (tween-80) are substantially more effective than the cationic surfactant (DTACI). Compared to tween-80, presence of SDS shows higher hydrate formation rate and slightly better hydrate yield. Final water to hydrate conversion results suggests that surfactants have little effect on total amount of CO_2 enclathration (important for flue gas separation through hydrate formation/decomposition process) moreover, with certain surfactant, hydrate formation can be inhibited. Finally it is concluded that in presence of silica gel the rate of gas uptake considerably enhanced and anionic surfactant can be used as a kinetic promoter. For a commercial hydrate formation process, a fixed bed reactor is more economical compared to a stirred tank reactor and this study along with an earlier published study conclusively proves that bigger pores and higher surface area are two important parameters while selecting a fixed bed packing for such a hydrate forming reactor.

Chapter 3

Impact of fly ash, SO₂ and H₂S impurities on the hydrate based gas separation process for carbon dioxide capture from flue and fuel gas mixtures



3. Impact of fly ash, SO₂ and H₂S impurities on the hydrate based gas separation process for carbon dioxide capture from a flue and fuel gas mixtures³

³“A version of this chapter has been published.

Kumar A, Sakpal T, Linga P, Kumar R. Impact of Fly Ash Impurity on the Hydrate-Based Gas Separation Process for Carbon Dioxide Capture from a Flue Gas Mixture. *Ind Eng Chem Res* 2014;53:9849–59.

Kumar A, Sakpal T, Bhattacharjee G, Kumar A, Kumar R. Impact of H₂S Impurity on Carbon Dioxide Hydrate Formation Kinetics in Fixed Bed Arrangements, *Ind Eng Chem Res* 2015 (DOI: 10.1021/acs.iecr.5b04079)

3.1. Introduction

As discussed in chapter 1, hydrate based gas separation (HBGS) process for a gas mixture of CO₂ & N₂ (flue gas) has proven to be very efficient and highly selective for CO₂ capture. In addition to CO₂ & N₂, flue gas coming out of a coal based thermal power station may contain impurities like nitrogen oxides (NO_x), sulfur oxides (SO_x) and fly ash. Large-scale implementation of carbon capture is not possible if the technology cannot withstand minor loads of fly ash and other acidic gases in the flue gas stream. It has been recognized that the advanced/novel CO₂ capture technologies has not been optimized in the presence of other acidic gases or fly ash and thus shows a dip in performance in real life application (Chapel et al. 1999; Nohra et al. 2012).

The flue gas mixture employed by most of the researchers for gas hydrate formation is a model flue gas (CO₂/N₂ gas mixture) which is essentially free of any acidic gases and fly ash (Kang et al. 2000; Linga et al. 2007a,b; Li et al.2011; Seo et al. 2005; Yang, 2013). Effect of acidic gases and fly ash on gas hydrate based separation process is not yet well understood. Recently, the impact of SO₂ (an acidic gas) on post combustion carbon dioxide capture was investigated and was found to shift the equilibrium to milder conditions but the kinetics was very slow (Daraboina et al. 2013). In the present work, the impact of fly ash on the HBGS process efficiency was investigated. Two different anionic surfactants; sodium lauryl sulphate (SLS or SDS) and sodium dodecyl benzene sulphonate (SDBS) were used in combination with 1 mol% THF (Thermodynamic promoter). In addition to this we also present enhanced kinetics of hydrate formation for the clathrate process in the presence of kinetic and thermodynamic promoters namely SDS (sodium dodecyl sulphate) and THF (tetrahydrofuran, 3 and 5.5 mol%)

in a fixed bed reactor for post-combustion capture of CO₂ in presence of SO₂ impurity. Silica sand was used as a fixed bed medium to capture CO₂ from CO₂/N₂/SO₂ (17.7 mol% CO₂, 1.05 mol % SO₂ and rest N₂) gas mixture by hydrate crystallization. Experiments were performed at a constant temperatures (273.65 K) and at different pressures (9.5 and 2.45 MPa) in batch mode.

As discussed in chapter 1, an alternate method to utilize coal for power generation is through coal gasification. This however, requires a green field power station, but has two major advantages compared to conventional power station based on coal combustion. 1) Coal Gasification route for power generation is more efficient 2) The effluent gas mixture comes at significantly high pressure which is also rich in CO₂ thus reducing the cost of capture. Shifted synthesis gas coming out of an IGCC power station comprises approximately 40% CO₂ and 60% H₂. (Klara, 2002; Deaton, 1946) However in an IGCC plant, fuel gas may also contain a trace amount of hydrogen sulfide (H₂S), Carbon monoxide (CO), ammonia (NH₃), coal dust etc (Stephen, 1977). The impact of these impurities on the thermodynamics and kinetics of hydrate formation needs to be studied. The impact of H₂S on the thermodynamics and kinetics of hydrate formation has not been studied. Therefore, in this work, the impact of H₂S in the fuel gas stream was also studied for the HBGS process. A ternary gas mixture of 40.9% CO₂, 58.05% H₂ and 1.05% H₂S was used for thermodynamic and kinetic experiments.

3.2. Experimental Section

3.2.1. Materials

The flue gas mixture of 16.1 mol% CO₂ and 83.9 mol% N₂ (with 99.9% purity) was supplied by De-luxe Industrial Gases, India. CO₂/N₂/SO₂ gas mixture contains 17.7% by mole CO₂, 1.05 % SO₂ and rest N₂ was supplied by Vadilal Gases Ltd. Pune, India. CO₂ (40.9%) + H₂ (58.05%) + H₂S (1.05%) gas mixture corresponding to a typical composition of a fuel gas mixture from an integrated coal gasification cycle was also supplied by Vadilal Gases Ltd., India. Silica sand was purchased from Sakalchand & Company Pune, India. Tetrahydrofuran (THF) (with 99.5% purity), sodium lauryl sulphate (SLS or SDS) (with 98% purity) and sodium dodecyl benzene sulphonate (SDBS) (with 99.9% purity) were purchased from S.D Fine Chem. Ltd. Mumbai, Fisher Scientific Mumbai, India and Sigma Aldrich respectively. Fly ash used for this work was donated to us by Tata Power (Maithon Power Limited, Dhanbad, India). Figure B1, B2 and B3 in appendix B represents the SEM image of fly ash, spherical silica gel (100 nm pore size) and silica sand.

3.2.2. Experimental apparatus

3.2.2.1. Stirred tank setup

Figure 3.1 shows the schematic of the experimental setup. It consists of a 400 cm³ SS-316 stirred tank high-pressure hydrate crystallizer (CR) (Berghof Germany). The top cover plate of the crystallizer has six ports each equipped with a Swagelok connector. These ports were used for inserting a thermocouple, supplying gas (inlet), vent & safety valve, gas sample extraction, liquid sample extraction and pressure transducer. The resistance temperature detectors (RTD, Pt-100) with ± 0.1 K accuracy are used to measure the temperature of the reactor contents in the liquid phase. All pressure measurements are made with pressure transducers (Wika), with a range of 0-2.5MPa bar and accuracy of 0.075% of the span. The crystallizer is immersed in a temperature controlled water bath containing a 40/60 wt% ethylene glycol /water mixture, which maintains the temperature in the hydrate crystallizer constant. The setup is equipped with a gas chromatography GC-2014AT (Shimadzu) to measure the composition of the gas phase in the crystallizer. Hydrate phase equilibria of flue gas mixture in presence of fly ash were measured through another high pressure stirred tank reactor of 90 cm³ capacity as it is equipped with a set polycarbonate windows for visual identification of hydrate crystals to visually observe the presence of infinitesimal crystals in the aqueous solution at equilibrium point.

3.2.2.2. Fixed bed setup

Detail description of the fixed bed apparatus (Figure 3.2) and the procedure for hydrate formation are given as follow. A fixed quantity of liquid solution was used along with calculated amount of packing material (silica gel and silica sand) in a SS-316 crystallizer (CR). CR was tightly closed and placed inside the temperature controlled water bath. CR was flushed out with the experimental gas mixture by repeating pressurization (~ 0.5 MPa) and depressurization sequence prior to the experiment. Circulating ethylene glycol / water mixture from the water bath was employed to cool the CR at experimental temperature. Once the desired temperature is reached, the CR is pressurized by gas mixture to pre determined experimental pressure. At this point, gas uptake measurement was initiated. All the gas uptake measurements were carried out in batch mode. CR is equipped with pressure transducer (WIKA) of 0-20 MPa range; drop in the reactor pressure was measured to calculate the gas consumption during a gas uptake measurement. Temperature and pressure of the reactor were recorded every 5 seconds through a data acquisition system connected to a computer. The

pressure of the CR starts to drop upon hydrate formation, which was used to measure the moles of gas uptake for hydrate formation experiment. It is noted that experiment was done in a batch mode and thus effective driving force changes as hydrate formation proceeds, as more and more CO_2 from the gas phase occupies the solid hydrate phase.

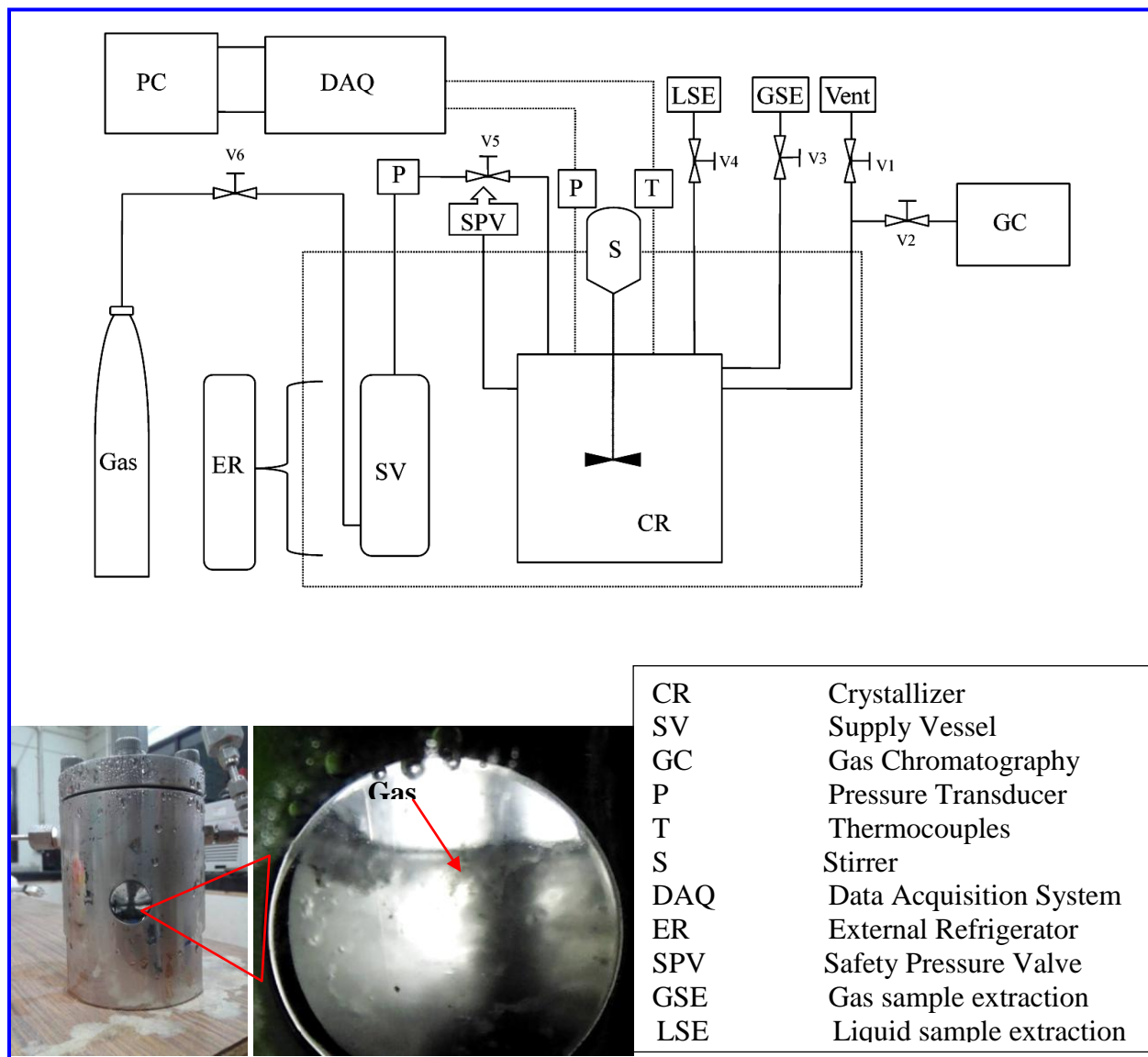


Figure 3.1. Schematic of Experimental Setup: Stirred Tank Reactor along with window showing the $\text{CO}_2/\text{N}_2/\text{THF}$ Hydrates

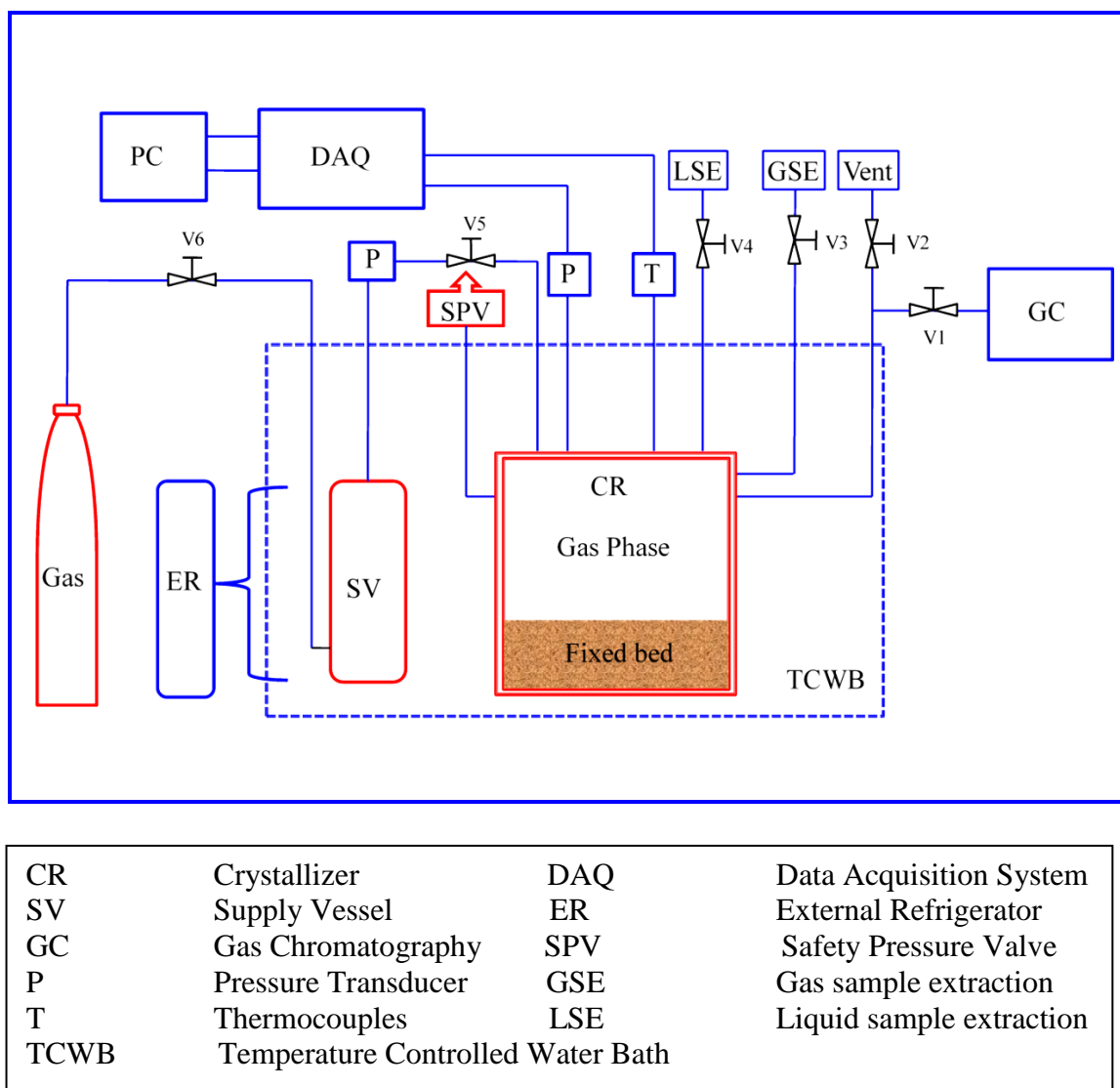


Figure 3.2. Schematic of the experimental apparatus (fixed bed reactor) used for experiments conducted in batch mode

3.3. Impact of Fly ash on HBGS Process

3.3.1. Experimental procedure for finding incipient phase equilibrium data

The isothermal pressure search method to determine the incipient equilibrium hydrate formation pressure was followed (Kumar et al. 2006; Englezos et al. 1994). At a given experimental temperature the crystallizer (capacity 90 cm³) was filled with 30 cm³ of water. For experiments in presence of fly ash, a known amount of fly ash was added in the crystallizer containing water, the content was homogenized by a spatula. Once the temperature of the water (inside the crystallizer) reached the desired temperature, gas from the supply vessel (SV) was

used to clean the reactor of any air impurity by pressurizing and depressurizing the reactor. This process was repeated three times to ensure air free flue gas mixture for hydrate formation. Subsequently, the crystallizer was pressurized with gas from the SV to a pressure well above the expected equilibrium hydrate formation pressure (~ 2 MPa in excess). After ensuring that there are no thermal fluctuations in the RTD reading of the reactor content, the overhead stirrer was started and set at 200 RPM. Content of the reactor was continuously monitored and once a small amount of hydrate crystals formed and were visible through the viewing window, stirrer was stopped and pressure inside the reactor was reduced to a pressure well below the expected equilibrium hydrate formation pressure (~ 1 MPa lower). The process of hydrate formation and decomposition was repeated three times, each subsequent hydrate formation pressure was kept below the previous run and each subsequent hydrate decomposition pressure was above the previous run. Subsequently, the pressure of the system was increased slowly to approximately 0.15 MPa above the estimated equilibrium value in order to form a small amount of hydrate. Once a small amount of hydrate formed the pressure was slowly reduced by ~ 0.05 MPa and the reactor was left running for 4–5 h. If there was still very small (infinitesimal) amount of hydrate left in the system, the pressure was reduced further by an educated guess and the system was left to run for the next 4-5 h. If after 4 h no hydrate crystals are seen inside the reactor it can be safely said that the current pressure of the system was below the actual equilibrium pressure. Consequently, the pressure of the system was increased and small amount of hydrate was allowed to form. The process was repeated till an infinitesimal amount of hydrate was found to exist in equilibrium with water and gas phase for at least 4 h. The temperature and pressure along with the gas phase composition of the reactor was recorded and the entire process was repeated for a new temperature.

3.3.2. Experimental procedure for hydrate formation (Kinetics measurements)

Clathrate hydrate formation experiments were carried out in batch mode with a fixed amount of water (120 cm^3) in 400 cm^3 reactor. Gas uptake measurements were done at constant temperature of ~ 274.5 K and drop in the pressure was measured to calculate the gas consumption. In $\text{CO}_2/\text{N}_2/\text{H}_2\text{O}/\text{THF}$ system, 1 mol% THF solution was used. Reactor was flushed out with the flue gas mixture (at 274.5 K) by repeating a pressurization and depressurization sequence prior to the experiment. Circulating ethylene glycol /water mixture from the water bath was employed to cool the reactor at experimental temperature of 274.5 K. Once the desired temperature (inside the crystallizer) was reached (measured through RTD);

the crystallizer was pressurized to the experimental pressure. At this point, hydrate formation was initiated; the stirrer was switched on and was set to 200 RPM. Temperature and pressure of the reactor were recorded every 5 seconds. The pressure of the crystallizer starts to drop upon hydrate formation, which was used to measure the gas uptake. It is noted that effective driving force changes as hydrate formation proceeds due to preferential enclathration of CO₂ into the solid hydrate phase. To check the influence of surfactants, 500 ppm of anionic surfactants were added in the water-THF solution used for hydrate formation. For experiments with fly ash, 0.25 wt% fly ash is added to the water-THF solution prior to pressurization by the flue gas mixture (CO₂ & N₂), which was stirred at 200 RPM to achieve a homogenous mixture. For simplicity, fly ash was added in the liquid solution rather than the flue gas mixture. Moreover, impact of fly ash content on gas hydrate formation kinetics can be understood better if fly ash is uniformly mixed in the aqueous phase.

3.3.3 Calculation for the amount of gas consumed

As the gas in the crystallizer was consumed for hydrate formation the pressure in the reactor dropped. The total number of moles of the gas that have been consumed for hydrate formation was calculated by equation

$$(\Delta n_{H,\downarrow}) = V_{CR} \left(\frac{P}{zRT} \right)_0 - V_{CR} \left(\frac{P}{zRT} \right)_t \quad (1)$$

Where z is the compressibility factor calculated by Pitzer's correlation (Smith et al., 2001); z is the function of time which is obtained by the gas uptake data, composition of the gas phase is analyzed by gas chromatography. V_{CR} is the volume of the gas phase of the crystallizer; P & T are pressure and temperature of the crystallizer.

3.3.4. Calculation for water to hydrate conversion

In the absence of THF, water to hydrate conversion (mol %) can be calculated using following equation (Linga et al., 2010).

$$\text{Water to hydrate conversion (mol\%)} = \frac{\Delta n_{H,\downarrow} \times \text{Hydration Number}}{n_{H_2O}} \times 100 \quad (2)$$

Where $\Delta n_{H,\downarrow}$ the number of moles of gas consumed for hydrate formation at the end of the experiment and n_{H_2O} is the total number of moles of water in the system.

However, in presence of THF, water to hydrate conversion was calculated by using the following equation (Linga, et al., 2010).

$$\text{Water to hydrate conversion (mol\%)} = \frac{(\Delta n_{H,\downarrow} + \Delta n_{THF}) \times \text{Hydration Number}}{n_{H_2O}} \times 100 \quad (3)$$

Where Δn_{THF} is the number of moles of THF used in the water phase; with limited supply of THF and negligible mass transfer resistance it can be safely assumed that all the THF would occupy the hydrate phase. Hydration number is defined as the number of water molecules per guest molecule (Sloan and Koh, 2008). Unlike simple hydrates of pure gas molecules, the hydration numbers of mixed gas molecules encaged in small and large cavities of a hydrate lattice are difficult to determine. For mixed hydrate, molecular level measurement is required for accurate cage occupancy data; it can be determined experimentally by doing a low temperature solid state NMR spectroscopy on solid hydrate phase (Kumar et al. 2009). In this work, hydration number of 5.71 was taken from literature where similar gas mixture and experimental conditions (2.3 MPa & 273.7K) were used (Linga et al., 2010; Kang 2001).

3.3.5. Calculation for the rate of hydrate formation

The rate of hydrate formation is calculated through the forward difference method outlined by equation (4) (Linga et al. 2012).

$$\left(\frac{d\Delta n_{H,\downarrow}}{dt} \right)_t = \frac{\Delta n_{H,\downarrow(t+\Delta t)} - \Delta n_{H,\downarrow(t)}}{\Delta t}, \Delta t = 30 \text{ min} \quad (4)$$

3.3.6. Experimental Procedure for hydrate dissociation

At the end of the gas uptake measurement with fresh water-THF solution, hydrates were decomposed and gases from the solid hydrates are released to the atmosphere. Resulting aqueous solution in the reactor is again used for memory runs. In this study, hydrate crystals were decomposed by thermal as well as depressurization methods at a stirring speed of 200 RPM. During thermal decomposition, the water bath was heated from 274.5 K to a desired temperature as shown in table 3.1. With rise in the experimental temperature, slow rise in pressure inside the reactor is observed. Once the temperature crosses the equilibrium phase boundary, hydrates starts to decompose resulting in significant pressure rise in the reactor. Hydrate dissociation is continued till a constant pressure profile is obtained in the reactor. At

this point the pressure of the crystallizer was slowly brought down to the atmospheric pressure and stirring of the reactor is continued (for 2 h) with the vent valve in open position. At the end of the two hour period, water bath is again set at formation temperature of 274.5 K for a repeat run (memory experiment). Desired experimental temperature of 274.5 K for a gas uptake measurement is typically achieved in 2 h, stirrer is stopped and the reactor is pressurized with the flue gas mixture for the gas uptake measurement.

Hydrate dissociation at relatively low temperature of 278.15 & 281.15 K (Table 1) was done through depressurization method. Upon completion of a gas uptake measurement for fresh runs, temperature of the reactor is increased to a desired temperature of 278.15 or 281.15 K. Gradual rise in the reactor pressure is observed due to rise in the experimental temperature, however no further change in pressure is observed as the new temperature and pressure is within the three phase boundary and hydrates are stable. Pressure in the reactor is brought down to atmospheric pressure by quickly opening the vent valve to atmosphere and then closing it down. Hydrates are decomposed at 200 RPM while keeping the vent valve closed. Hydrates are decomposed till no further rise in pressure is recorded and at this point, decomposed gas is released into the atmosphere while stirring is continued for another 2 h by keeping the vent valve open. The memory aqueous solution is again used for hydrate formation at 274.5 K by carrying out a gas uptake measurement.

3.3.7. Separation efficiency

To evaluate the separation efficiency of the hydrate based gas separation process, CO₂ recovery or split fraction (S.Fr.) was calculated by using Eq. (5) and (6) (Linga et al. 2007b)

$$S.Fr. = \frac{n_{CO_2}^H}{n_{CO_2}^{Feed}} \quad (5)$$

$$CO_2 \text{ recovery (\%)} = 100 \times \text{split fraction} \quad (6)$$

$n_{CO_2}^H$ is the number of moles of CO₂ in the hydrate phase at the end of the experiment and $n_{CO_2}^{Feed}$ is the number of moles of CO₂ in the feed gas. Split fraction which can range from 0 to 1 is essentially a function of water to hydrate conversion ratio. Split fraction of 1 would mean that all the CO₂ from the gas phase has been converted to solid hydrate phase. The separation factor (S.F.) was determined from the following Eq. (7) (Linga et al. 2007b)

$$S.F. = \frac{n_{CO_2}^H \times n_{N_2}^{gas}}{n_{N_2}^H \times n_{CO_2}^{gas}} \quad (7)$$

Where $n_{CO_2}^{gas}$ and $n_{N_2}^{gas}$ are the number of moles of CO_2 and N_2 in the gas phase at the end of the experiment and $n_{N_2}^H$ is the number of moles of N_2 in the hydrate phase. Theoretically, separation factor in a given experiment can go as high as infinity (which would be possible if at the end of the experiment there is no nitrogen in the hydrate phase). Typically a separation factor of 10 is highly desirable, which would suggest that it is 10 times more favorable for CO_2 to be occupied in the solid hydrate phase thus enriching the hydrate phase with CO_2 and enriching the gas phase with N_2 .

3.4. Results and discussion (fly ash impact)

3.4.1. Effect of fly ash impurity on the thermodynamics of hydrate formation

Figure 3.3 represents the incipient hydrate formation conditions obtained in the presence of 0.25 wt% fly ash impurity in a flue gas mixture with 1 mol% THF. Results are compared with the data available in the literature for similar systems (Linga et al., 2008, Kang et al., 2001). No significant deviation in the equilibrium formation pressure is seen due to 0.25 wt% fly ash impurity in the flue gas mixture. As seen in the figure, the equilibrium formation pressure was found to be marginally higher compared to equilibrium data of similar system obtained from literature (Kang et al., 2001). This slight difference is observed due to the difference of 1 mol% CO_2 in the flue gas mixture used in this work with that of literature.

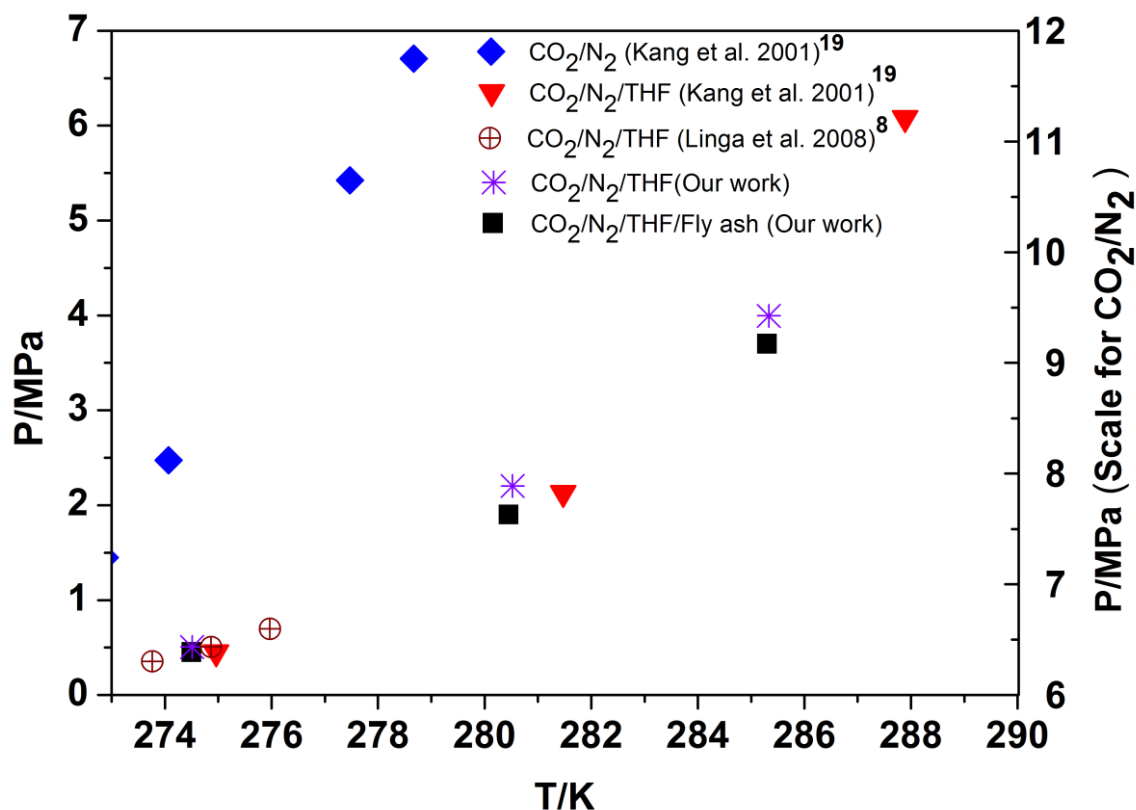


Figure 3.3. Incipient equilibrium hydrate formation conditions for the CO₂ (16.1%) / N₂ (83.9%) / 1 mol% THF and CO₂ (16.1%) / N₂ (83.9%) / 1 mol% THF system with 0.25 wt % flyash impurity. Incipient hydrate formation conditions from literature is plotted for similar system, (CO₂:N₂=17:83 mol %) in presence / absence of THF (1 mol %) (Kang et al., 2001) and 16.9 mol% CO₂/1 mol% THF (Linga et al 2008). Y-axis on the right hand side shows the hydrate formation pressure of CO₂/N₂ mixture

Sloan and Fleyfel proposed a heuristic method to estimate the heat of hydrate dissociation (ΔH_d) at temperatures above 273.2 K (Sloan and Fleyfel, 1992). They state that, to the first approximation, the heat of dissociation above 273.2 K depends upon the type of cavity occupied and is independent of the type and concentration of the guest gas, within the size constraint. The above method indirectly suggests the resultant structure formed by the mixed gas. It has been noted that the values obtained by the method are acceptable for engineering calculations (Kumar et al., 2006). The heat of hydrate dissociation can be calculated by using Clausius–Clapeyron equation, shown below:

$$\frac{d \ln P}{d(1/T)} = -\frac{\Delta H_d}{zR} \quad (8)$$

Where P and T are absolute pressure and temperatures of hydrate equilibrium with vapor and liquid water, R is the universal constant and z is the gas compressibility factor calculated by

Pitzer's correlation. Eq. (8) indicates that the slope of the logarithm of the hydrate dissociation pressure plotted against reciprocal temperature will give the negative heat of dissociation divided by the product of the compressibility factor and gas constant.

Figure 3.4 shows the Clausius–Clapeyron plots based on the hydrate equilibrium data and the straight lines represent the best linear fit of the experimental data for CO_2 (16.1%)/ N_2 / H_2O / THF(1mol%), CO_2 (17%)/ N_2 / H_2O / THF(1mol%) (Kang et al., 2001), and CO_2 (16.1%)/ N_2 / H_2O / THF (1mol%)/ Fly ash (0.25 wt%). Clausius–Clapeyron plots for all the hydrate forming mixture containing THF is plotted in figure 3.4a-c. As seen from the figure, the slopes for these gas mixtures are almost same which indicates a constant heat of dissociation. Based on the slope, the heat of dissociation was found to be ~ 120 kJ/mol. This suggests that 0.25 wt% fly ash impurity does not affect the resultant hydrate structure and the resultant hydrate is structure II hydrate. However, a confirmation of structure II hydrate formation can only be obtained by powder XRD which is out of scope of this work.

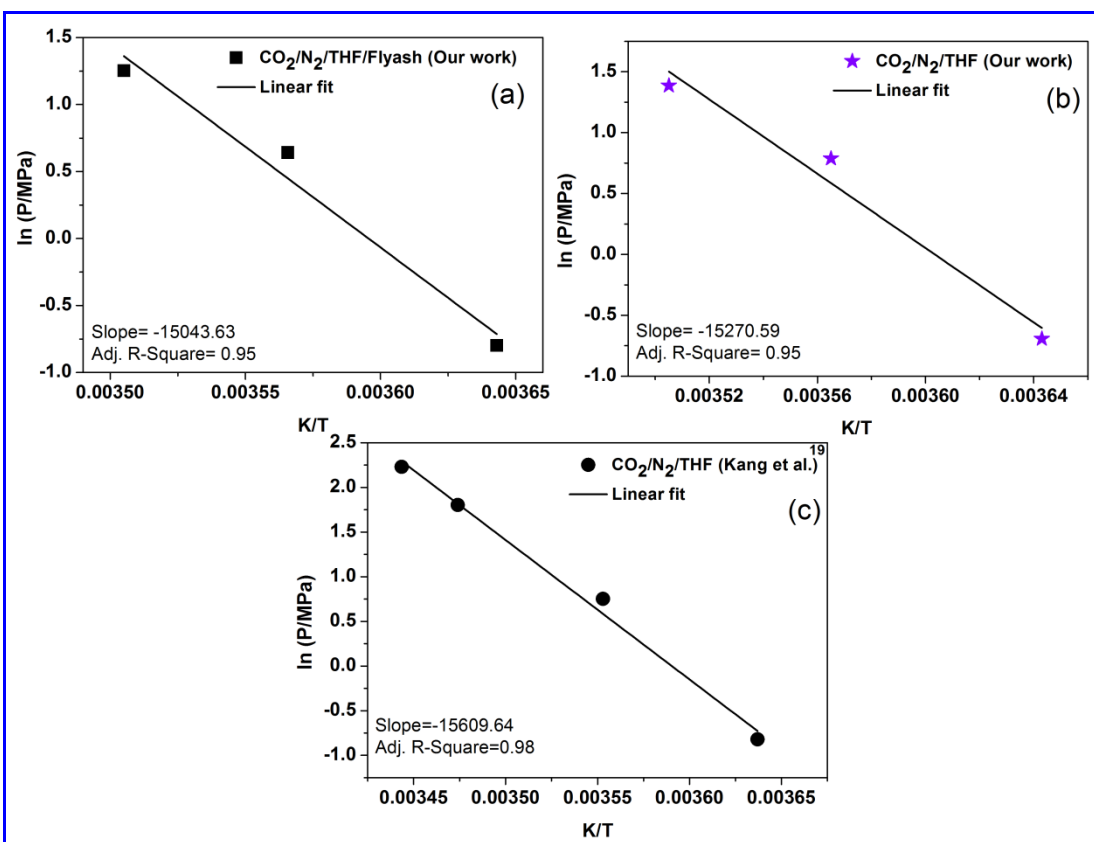


Figure 3.4. Clausius–Clapeyron plot based on the hydrate equilibrium data (a) CO_2 (16.1%)/ N_2 / H_2O /THF (1mol%)/ Flyash (0.25 wt%) System (b) CO_2 (16.1%)/ N_2 / H_2O /THF (1mol%) System (c) CO_2 (17 %)/ N_2 / H_2O /THF (1mol%) System (Kang et al., 2001)

3.4.2. Kinetics of hydrate formation and decomposition in presence of 1 mol% THF and its significance for HBGS process

As discussed in the last section use of 1 mol% THF helps the HBGS process by bringing down the hydrate formation pressure. However, water to hydrate conversion rate and ratio is very important for increasing the efficiency of HBGS process. This information was obtained through a gas uptake measurement with 1 mol% THF–water solution and is summarized in table 3.1. The gas hydrates were formed from the flue gas mixture with composition of CO₂ 16.1% and N₂ 83.9%. Table 3.1 shows the experimental conditions, gas consumption, water to hydrate conversion, induction time and hydrate dissociation conditions. Experimental pressure of 3.75 MPa was chosen to give a significant driving force (Linga et al., 2007b) for hydrate formation; equilibrium pressure was estimated from literature (Kang et al., 2001) at 274.5 K. Hydrate formation experiments were carried out at a constant temperature of 274.5 K. As shown in the table, experiment no. T-1 to T-7 were conducted to investigate the influence of repeated hydrate formation and dissociation cycle on the overall kinetics of hydrate formation. It was observed that the induction time for gas hydrate formation (for memory experiments) were consistently higher than that of fresh measurements, however the initial hydrate growth rate after hydrate nucleation were similar (shown in figure 3.5).

This result is quite important for a HBGS process (Babu et al., 2013a,b; Ho et al., 2013). In the HBGS process it is envisioned that following a hydrate formation stage, a CO₂ rich gas is obtained by decomposing the hydrate formed in the first stage and will be subjected to further CO₂ enrichment in the second stage of hydrate formation / dissociation cycle. THF solution thus obtained after hydrate decomposition (in each stage) will be reused for fresh hydrate formation. During experiment T-1 and T-3, the gas hydrates were dissociated at 293.15 K and 298.15 K respectively, the same solution was used for the repeat runs (memory experiment). For a consistent comparison, repeat runs were done with the same solution as was used in T-1 and T-3. It was observed that for repeat runs the induction time is consistently higher (Refer exp T1 to T4). Takeya et al. have shown that the memory effect generally vanishes when hydrates were dissociated at 298.15K (Takeya et al., 2000). Thus it is possible that when hydrate formation was repeated with memory water, it behaved like a fresh run showing no drop in induction time compared to previous run. A set of experiments were performed to ascertain the memory effect by performing the dissociation experiment at a lower temperature by depressurization method (Haligva et al., 2010). Three gas uptake measurements were done, a

fresh run followed by two repeat runs. Hydrates were decomposed at a lower temperature (of 281.15 K & 278.15 K); it was observed that induction time of repeat runs reduced significantly (Experiments T-5, T-6 and T-7). It is important to note that decomposition at lower temperature helps the kinetics of hydrate formation process by keeping the memory effect intact for the next cycle of hydrate formation experiments. However, rate of hydrate decomposition at lower temperature or lower ΔT will be comparatively slow (Linga et al., 2009).

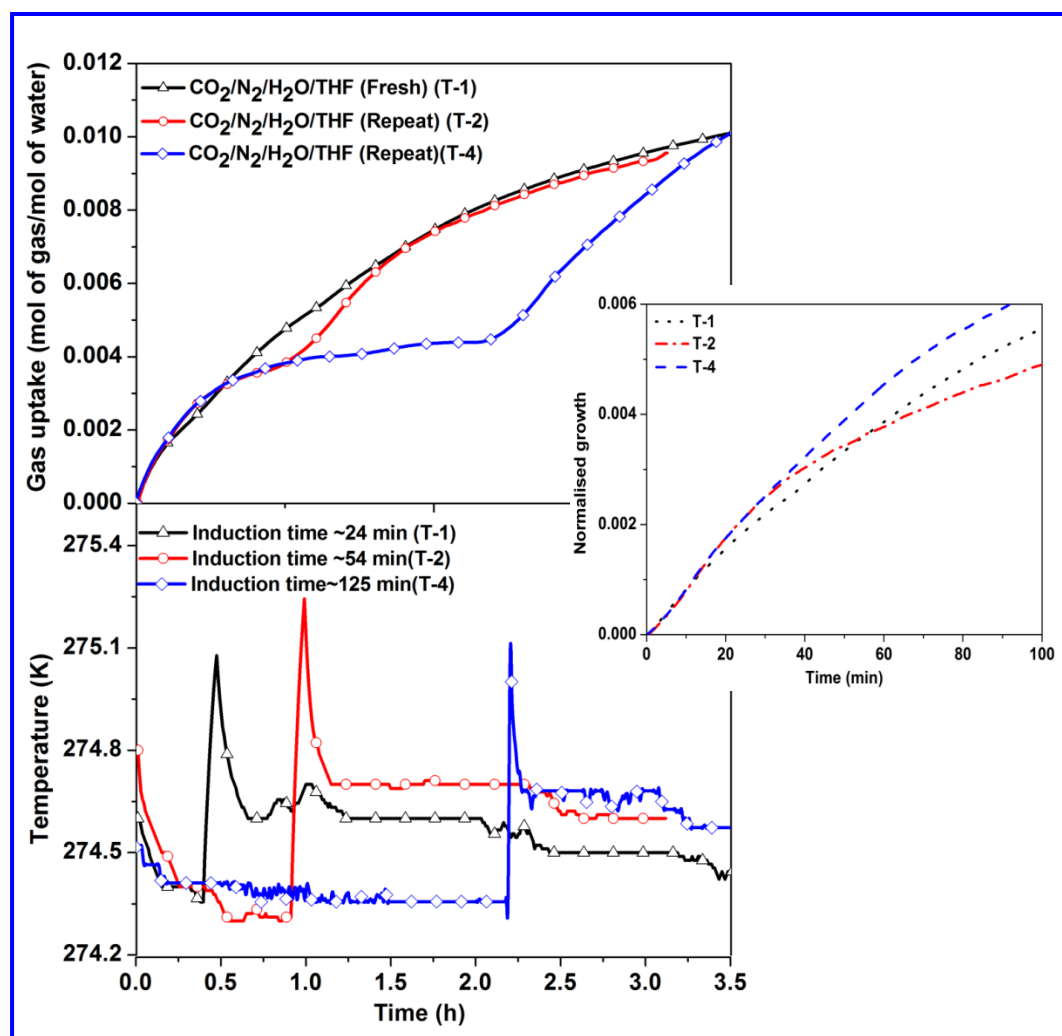


Figure 3.5. Typical gas uptake curve along with temperature profile for both fresh and memory conditions (Experiment T-1, T-2 and T-4). Inset figure shows the normalized hydrate growth, where time zero corresponds to nucleation point (induction time).

3.4.3. Effect of fly ash impurity on the hydrate formation kinetics of flue gas mixture and its impact on HBGS process

To evaluate the influence of fly ash on gas hydrate formation kinetics in a stirred tank reactor a small amount (0.25 wt %) of dry fly ash was used. Experiments F-1 to F-3 is reported in Table 3.1, in the presence of fly ash, induction time reduced significantly, whereas water to hydrate conversion was almost similar to the experiments performed with no fly ash. Figure 3.6 shows the observed mol of gas consumed per mol of water (for hydrate growth) with respect to time with and without fly ash. As seen in the figure, initial rate of hydrate formation in presence of fly ash is higher; however final water to hydrate conversion (after 5h) is almost same in both the cases (table 3.1). The observed catalytic effect of fly ash for the initial rate of hydrate formation can be explained by the fact that, small spherical fly ash ranging from 0.5 μm to 50 μm acts as a surface for heterogeneous nucleation and growth of gas hydrate crystals. Thus, this study clearly shows that presence of 0.25 wt% fly ash impurity had no negative impact on the thermodynamics and the kinetics of hydrate formation. This is an important finding; a significant load of fly ash coming out of a coal based thermal power station can be efficiently used for CO_2 capture in a HBGS process.

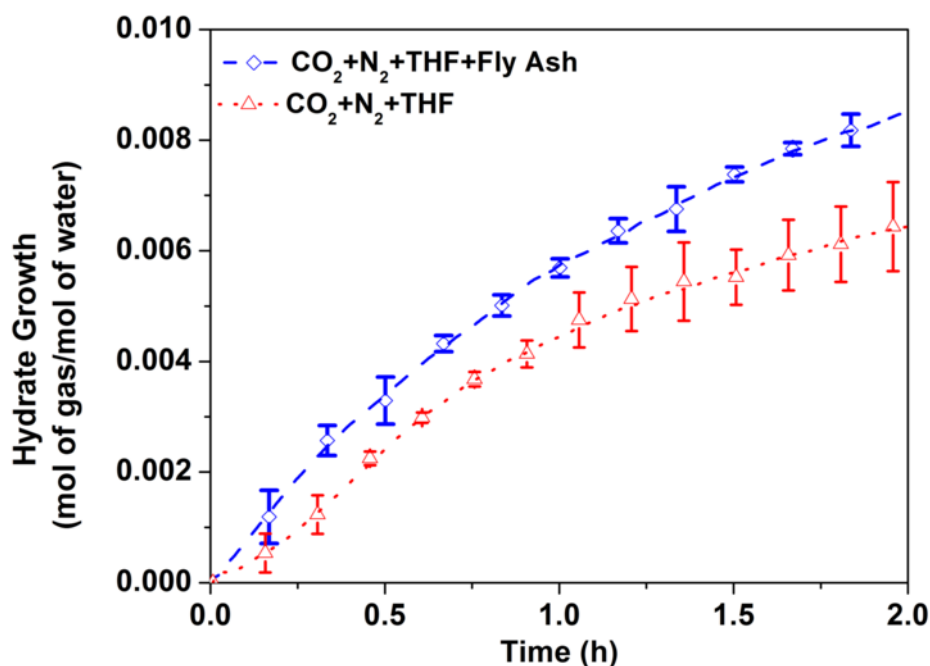


Figure 3.6. Average gas uptake curve for hydrate growth with and without fly ash (0.25 wt%) in presence of 1 mol% THF. Time zero in the graph corresponds to nucleation point (induction time) for the experiments. The standard deviation for selective data points are presented as error bars

Table 3.1. Summary of experimental conditions and observations; Table shows gas consumption, water to hydrate conversion (mol %), induction time and hydrate dissociation condition. Gas uptake experiments were conducted at 3.75 MPa, and 274.5 K. Data shown in the table is for 5h run.

System	Exp. no.	Sample state	Hydrate Dissociation condition	Induction time (IT) (min)	Gas consumed from IT (mol of gas/mol of water)	Final Water to hydrate conversion (mol %)*
CO ₂ /N ₂ /H ₂ O/T HF (1mol%)	T-1	Fresh	Thermal(293.15 K)	24.3	0.0092	10.95
	T-2	Memory (120min)		54.2	0.0054	8.80
	T-3	Fresh	Thermal(298.15K)	18.24	0.0133	13.42
	T-4	Memory (180 min)		125.34	0.0088	10.71
	T-5	Fresh	Depressurization at 281.15 K	37.7	0.0130	13.11
	T-6	Memory-1	Depressurization at 278.15 K	31.5	0.0132	13.21
	T-7	Memory-2		18.5	0.0123	12.71
CO ₂ /N ₂ /H ₂ O/T HF (1mol%)/ Fly ash (0.25 wt%)	F-1	Fresh	Thermal(288.15K)	9.2	0.0131	13.15
	F-2	Memory		11.5	0.0117	12.42
	F-3	Fresh		12.7	0.0092	11.00

* Water to hydrate conversion for 5h from IT, calculated using equation 3.

Table 3.2. Influence of anionic surfactants; SDS (500 ppm), SDBS (500 ppm) and fly ash impurity (0.25 wt %) on gas uptake kinetics at 3.75 MPa and 274.5 K. Table shows experimental condition, induction time and water to hydrate conversion (mol %).

System	Exp. no.	Sample state	Induction time (IT) (~min)	Gas consumed from IT (mol of gas/mol of water)	Final Water to hydrate conversion (mol %)*
CO ₂ /N ₂ /H ₂ O/THF (1mol%)/SDS	TS-1	Fresh	8.14	0.0115	12.26
	TS-2	Memory	6.84	0.0116	12.37
	TS-3	Fresh	5.2	0.0093	11.02
CO ₂ /N ₂ /H ₂ O/THF (1mol%)/ Fly ash (0.25 wt%)/SDS	TFS-1	Fresh	9.21	0.0121	12.62
	TFS-2	Memory	10.1	0.0116	12.33
	TFS-3	Fresh	6.5	0.0109	11.87
CO ₂ /N ₂ /H ₂ O/THF (1mol%)/SDBS	TSB-1	Fresh	6.2	0.0116	12.86
	TSB-2	Memory	3.5	0.0113	12.68
	TSB-3	Fresh	7.2	0.0091	10.91

* Water to hydrate conversion for 5h from IT, calculated using equation 3.

3.4.4. Effect of two anionic surfactants on gas hydrate formation kinetics and its synergistic effects on kinetics of hydrate formation in presence of fly ash

To evaluate the influence of anionic surfactants on gas hydrate formation kinetics in presence of fly ash in a stirred tank setup, two surfactants, SDS (sodium dodecyl sulphate) and SDBS (sodium dodecyl benzene sulphonate) were chosen. The idea was to check the possibility of increasing water to hydrate conversion rate and ratio. Table 3.2 summarizes the results obtained in the presence of surfactants, THF and with/without fly ash. The induction time data which is shown in table 3.2 for experiments with surfactants is lower than the induction time for similar systems without surfactants (table 3.1). However, final gas consumption (water to hydrate conversion ratio or hydrate yield) is almost same in all the experiments and we do not observe any increment in the hydrate conversion ratio as compared to data reported in table 3.1. Figure 3.7a shows the effect of surfactants on gas hydrate formation kinetics of our model flue gas mixture in absence of fly ash. It can be seen from the figure that, for the first 2h the gas consumption (mol of gas /mol of water) is ~40% higher compared to in absence of surfactants and effect of both the surfactants is almost same. Similar behavior has been reported in literature for methane hydrate formation in presence of anionic surfactants (Kalogerakis et al., 1993; Okutani et al., 2008; Yoslim et al., 2010). Figure 3.7b represents the rate of gas hydrate formation which was determined by using forward difference method (Eq. 4). The rate is normalized by taking into account the amount of water used for each experiment (mol of gas/mol of water/hr). Figure 3.7b shows the comparison of rate of gas uptake with and without surfactants. As seen from the figure in presence of both SDS and SDBS, the rate of gas hydrate formation is almost twice compared to without surfactants. Torre et al. in their work has also observed similar results in presence of promoters like THF and SDS. According to them, the action of these additives confers a porous structure to the hydrates formed in the bulk, which are permeable to gas (Torre et al., 2012). According to Zhang et al. the dodecyl sulphate anion gets adsorbed on the THF hydrate and keeps this hydrate in dispersed form due to electrostatic repulsion between hydrate particles (Zhang et al., 2008, 2010). Better kinetics of hydrate growth in presence of surfactants can also be explained by the observation made by two different groups, Caskey & Barlage and Hanwright, they have tried to explain the phenomena by taking into account the better mass transfer effects in presence of surfactants. They have observed that the water soluble surfactants produce a significantly lower resistance to

interfacial mass transfer. The dynamic adsorption and desorption of the surfactant molecules at the gas-liquid interface creates short term vacancies, which presumably permit the unrestricted transfer of the gas molecules through the interface (Caskey& Barlage, 1972; Hanwright et al., 2005). Thus the use of surfactants helps by increasing the water to gas contact and enhance the rate of gas hydrate formation.

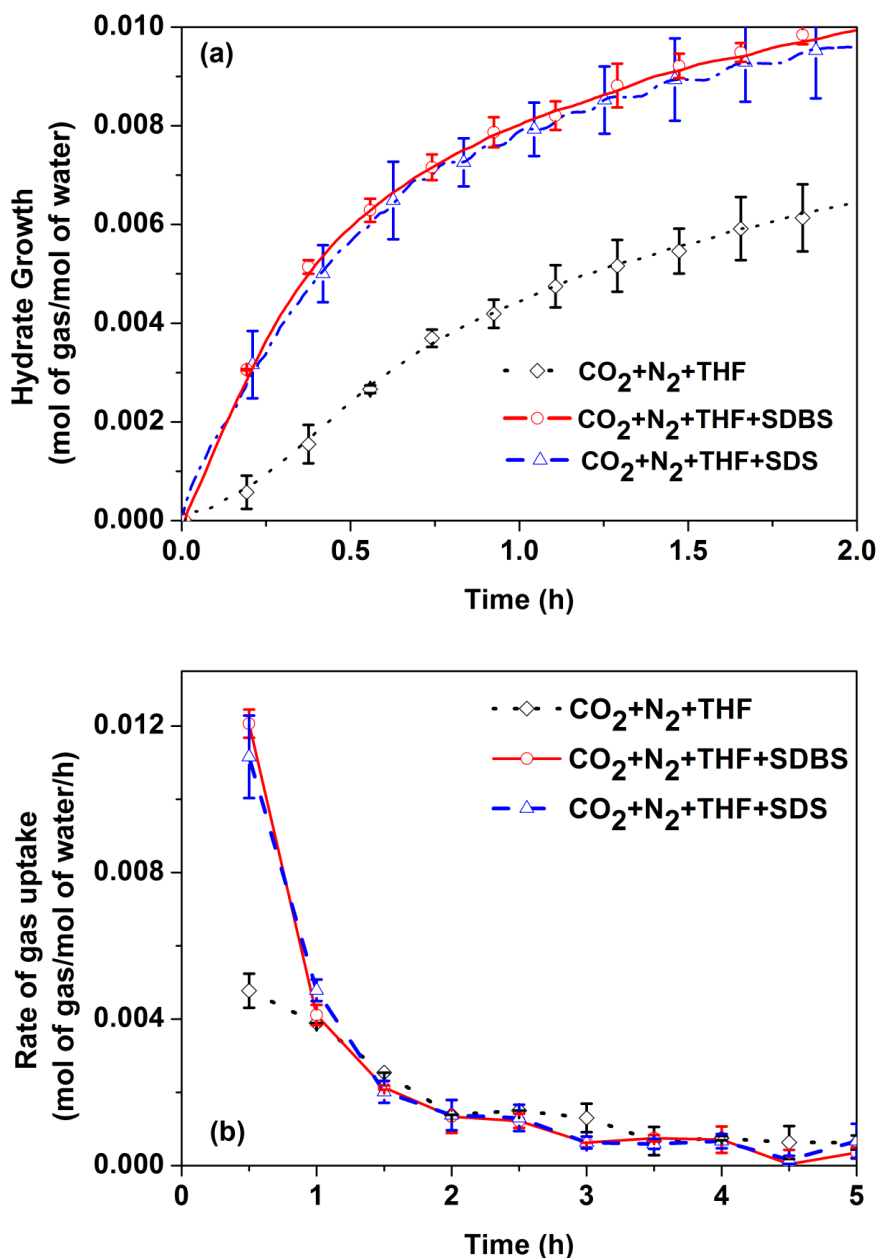


Figure 3.7. Comparison of (a) average gas consumption (mol of gas/mol of water) for hydrate growth and (b) rate of gas uptake with and without surfactants (SDS and SDBS) in presence of 1 mol% THF; Time zero in the graph corresponds to nucleation point (induction time) for the experiments. The standard deviation for selective data points are presented as error bars.

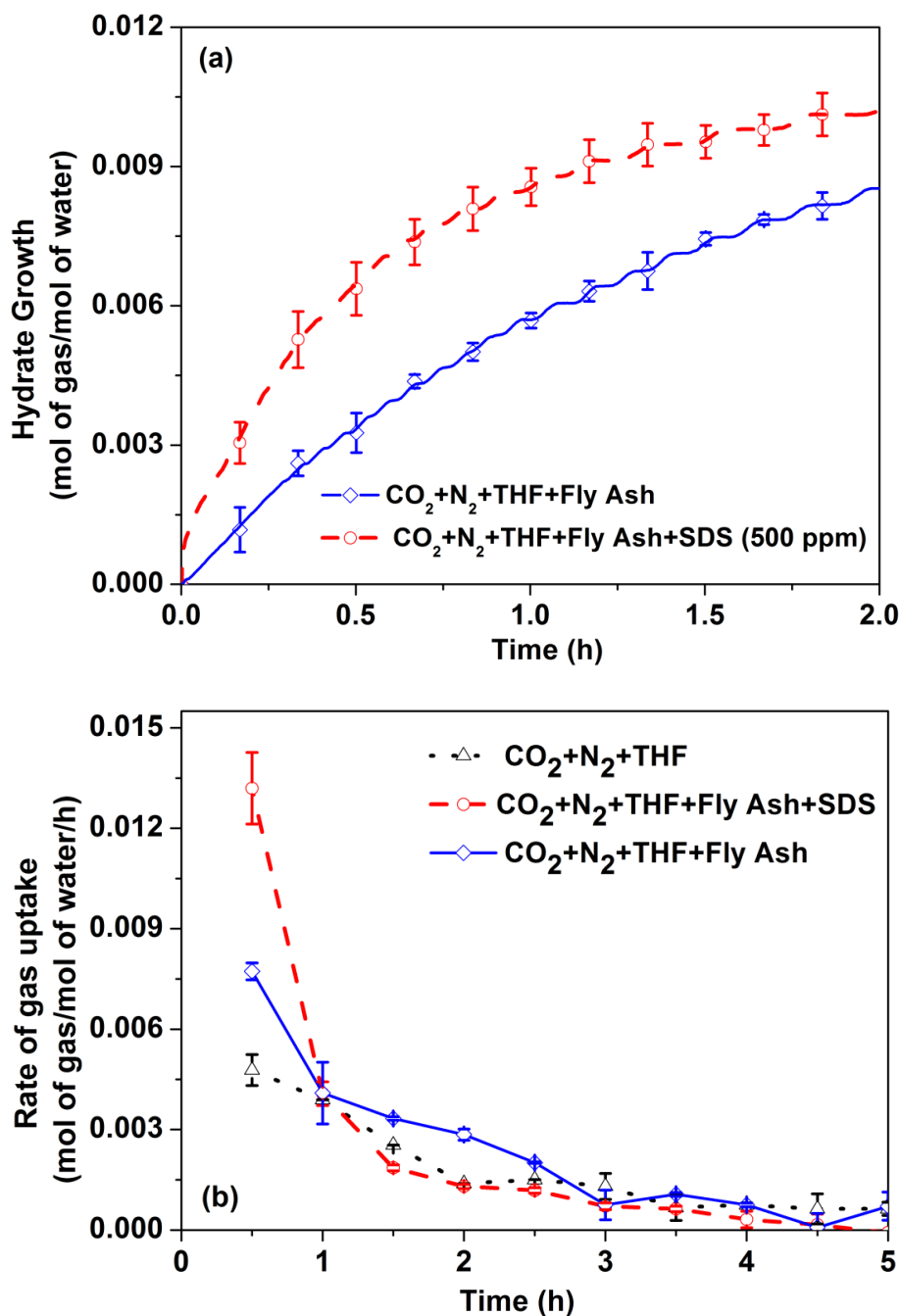


Figure 3.8. Comparison of (a) average gas consumption (mol of gas/mol of water) for hydrate growth and (b) rate of gas uptake with and without surfactants (SDS) in presence of 1 mol% THF and 0.25wt% fly ash; Time zero in the graph corresponds to nucleation point (induction time) for the experiments. The standard deviation for selective data points are presented as error bars.

Figure 3.8a provides the effect of kinetic (SDS) and thermodynamic (THF) promoter in presence of fly ash (0.25 wt %). Fly ash by itself was found to increase the initial rate of hydrate formation (refer figure 3.6) and the presence of the anionic surfactant SDS further

enhances the initial gas consumption rate (for first 50-60 min, figure 3.8a). It shows ~ 37% more consumption compared to without SDS. Figure 3.8b represents the rate of gas hydrate formation which was determined by using forward difference method (Eq. 4). It is observed that in the presence of fly ash, the rate of gas hydrate formation is slightly higher compared to hydrate formation with no fly ash (exp T-1), however in presence of SDS and fly ash the rate is almost twice compared to without fly ash and SDS experiments. This clearly shows that the presence of fly ash has no detrimental effect on the effectiveness of SDS for achieving faster hydrate growth.

It has been demonstrated in the literature that the kinetics of hydrate formation can be enhanced significantly by employing a fixed bed column which would be a favorable contact mode for carbon dioxide capture based on the HBGS process (Adeyemo et al., 2010; Seo et al., 2005; Linga et al., 2012; Babu et al., 2013). The water conversion of hydrates is generally low in the stirred tank reactors (see Table 3.1 and 3.2) due to the mass transfer limitations associated with hydrate crystal agglomeration at the gas/liquid interface (Linga et al., 2010). However, to clearly understand the impact of fly ash impurity on hydrate formation kinetics, a stirred tank reactor was employed in this work for evaluating the HBGS process for capturing carbon dioxide from flue gas.

3.4.5. Gas phase analysis and separation efficiency

Gas phase was analyzed by gas chromatography (GC-2014AT) with a thermal conductivity detector along with shin carbon micro-packed column. Table 3.3 shows the CO₂ gas composition in the gaseous phase of the crystallizer. As seen in the table, at the end of the experiment (5h) CO₂ content in the gaseous phase reduces significantly compared to initial feed gas composition, which indicates preferential incorporation of CO₂ in the solid hydrate phase. To evaluate the separation efficiency of the hydrate process, split fraction (CO₂ recovery) and separation factor were calculated using equation 5, 6 and 7 respectively. As seen in table 3.3 the CO₂ recovery calculated by eq (6) is ~60%, which means approximately 60% of the CO₂ in the feed gas is separated in the first stage of gas hydrate formation from the flue gas mixture. Separation factor for all the experiments lies in the range of 11 to 17 (table 3.3). Which shows that even in presence of 1 mol% THF, occupancy of carbon dioxide in the hydrate cages is significantly higher (11 – 17 times) than N₂. It is shown through this work that the presence of fly ash enhances the separation factor (F-1 and TSF-1, table 3.3).

Table 3.3. Gas phase CO₂ composition for different systems showed in table 3.1 and 3.2. CO₂ recovery and separation factor were calculated as per equation 5-7.

Parameter	Experiment No.				
	T-1	F-1	TS-1	TFS-1	TSB-1
Feed gas mol %	16.1	16.1	16.1	16.1	16.1
Gas phase composition at the end of the experiment mol%	8.5	7.7	8.35	8.02	7.85
CO ₂ recovery (%)	56.73	60.27	57.43	58.00	59.72
Separation factor (S.F.)	11.02	16.06	11.69	16.86	14.49

Table 3.4. CO₂ recovery data in the presence of thermodynamic and kinetic additives used for CO₂ capture through HBGS process in reported. For better comparison only the results from stirred tank reactors are presented.

CO ₂ Recovery (%)	Additive	Concentration of additives (mol%)	Experimental conditions		Ref.
			Pressure (MPa)	Temperature (K)	
46	THF	1	2.5	273.7	Linga et al. 2007
42	none	none	10	273.7	Linga et al. 2007
50	TBAB	0.29	3.5	277.5	Fan et al. 2009
42	TBAF	0.29	4	277.5	Fan et al. 2009
54	DTAC* } TBAB# }	0.028 } 0.29 }	1.7	274.9	Li et al 2011
60	THF	1	1.5	273.7	Linga et al. 2010
60	THF } Fly ash }	1 } 0.25 wt% }	3.75	274.5	This work (Exp F-1)
57	THF } SDS }	1 } 500 ppm }	3.75	274.5	This work (Exp TS-1)
57	THF	1	3.75	274.5	This work (Exp T-1)

*Dodecyl trimethyl ammonium chloride; #Tetrabutylammonium bromide

Table 3.4 summarizes the CO₂ recoveries obtained in this work and the data available in the literature at similar experimental conditions. In addition to THF, other hydrate forming hydrocarbons like TBAB, TBAF have been used as additives in HBGS process for the separation of CO₂ from flue gas mixture. As seen in the table, 1 mol % THF used in this work shows slightly better CO₂ recovery at similar operating conditions compared to other additives used in the literature. Like SDS (anionic surfactant), DTAC (a cationic surfactant) has been used to enhance the rate of hydrate formation and it was found that addition of surfactant does not enhance the separation efficiency of HBGS process (Li et al., 2010). A similar result was obtained in this work with SDS however in our work CO₂ recovery is better.

3.5. Impact of SO₂ impurity on HBGS Process

3.5.1. Kinetics of Hydrate Formation in the Presence of kinetic promoter (SDS) for CO₂/N₂/SO₂ system

Table 3.5 summarizes all the experiments performed during the course of this study and includes the experimental temperature and pressure, induction time and moles of gas consumed at the end of each experiment. Operating temperature and pressure were estimated from available literature. The driving force for hydrate formation at 273.7 K is 2.3 MPa for CO₂/N₂/SO₂ system. (Daraboina et al., 2013). Table 3.5 helps us to compare the induction time for two different systems (CO₂/N₂/SO₂/SDS and CO₂/N₂/SO₂/THF). Induction time in gas hydrate crystallization is an important characteristic of the kinetic studies. Induction time is defined as the time elapsed until the appearance of a detectable volume of hydrate phase or, equivalently, until the consumption of a detectable number of moles of hydrate forming gas. The induction time is often also termed as the hydrate nucleation or lag time. (Sloan and Koh, 2008). As can be seen in Table 3.5, the induction time in presence of THF is quite low as compared to the other system. This is an important feature that will play a huge role when finally employing the HBGS process for CO₂ capture (Babu et al., 2013).

Figure 3.9a shows the typical gas uptake curve along with the corresponding temperature profile for a CO₂/N₂/SO₂/SDS system for an experiment conducted at 273.65 K and 9.5 MPa pressure. The general shape of the curve agrees with the gas uptake profile described in detail by Natarajan et al. which involve gas dissolution, nucleation and hydrate growth (Natarajan et al. 1994). Initially, the gas diffuses into the water present between the interstitial spaces in the silica sand bed. The next stage is the super saturation and nucleation of hydrates which involves the formation of critically stable hydrate nuclei and is characterized by a sudden increase in

temperature due to the exothermic nature of hydrate crystallization. However, the crystallizer is cooled to the experimental temperature by an external refrigerator which results in the overall temperature of the crystallizer remaining essentially constant. The final stage of gas hydrate formation process is the hydrate growth, where hydrate formation continues to occur in the bed until hydrate growth reaches saturation.

Figure 3.9b represents the comparison of gas uptake (mol of gas/mol of water) in presence/absence of SDS. Data presented in the figure is for approximately 10h from induction time at approximately the same driving force (2.3 MPa). As seen in the figure, the addition of surfactant enhances the rate of hydrate formation while the final gas uptake achieved in the presence of SDS was found to be thrice of that for a system without the surfactant. In the absence of surfactant, hydrates and occluded water create a slushy hydrate mass which prevents efficient mass transfer of gas through the gas/water interface (Linga et al., 2012) However, in presence of surfactant, these mass transfer limitations can be avoided (Suradkar and Bhagwat, 2005). A water-soluble surfactant such as SDS produces a lower resistance to interfacial mass transfer. Capillary driven supply of water into the porous hydrate layers in the presence of a surfactant further enhances hydrate formation by ensuring greater gas-water contact. The use of surfactants thus in more ways than one, contributes to enhancing the kinetics of hydrate formation. (Kumar et al., 2014; Caskey et al., 1992; Hanwright et al., 2005).

Table 3.5. Summary of experiments, gas consumption; experimental pressure and temperature. Amount of water used for all the experiment was 50 cm³.

System	Pressure (MPa)	Temperature (K)	THF (mol%)	SDS (wt%)	Induction Time (min)	Gas uptake (mol of gas/mol of water)	Average Gas uptake [\pm stdev]
CO ₂ /N ₂ /SO ₂ / SDS	9.5	273.65	0	1	24	0.058	0.050 (\pm 0.007)
	9.5	273.65	0	1	342	0.047	
	9.5	273.65	0	1	104	0.045	
	2.45	273.65	3	0	5	0.0067	0.0068 (\pm 0.00066)
	2.45	273.65	3	0	7	0.0062	
	2.45	273.65	3	0	4	0.0075	
CO ₂ /N ₂ /SO ₂ / THF	2.45	273.65	5.56	0	4	0.0112	0.012 (\pm 0.00055)
	2.45	273.65	5.56	0	3	0.0121	

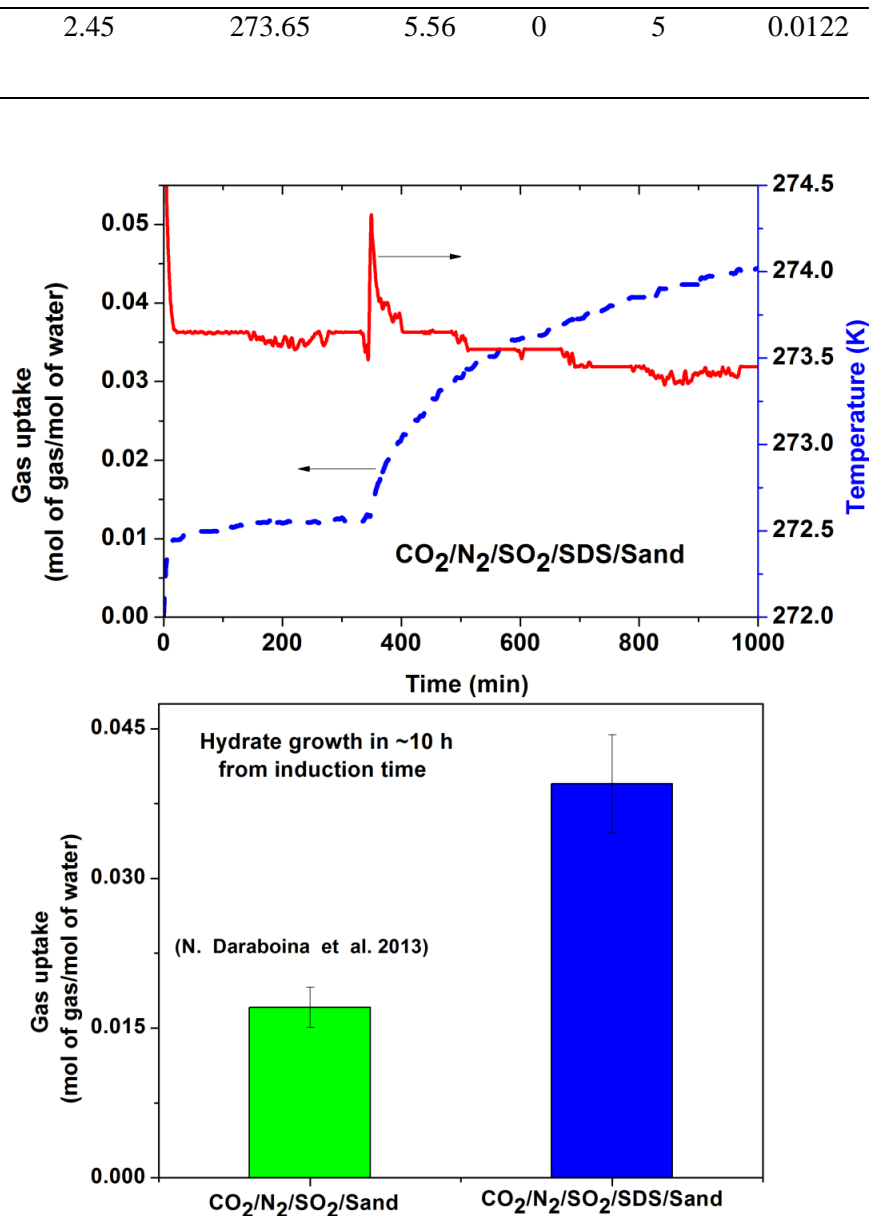


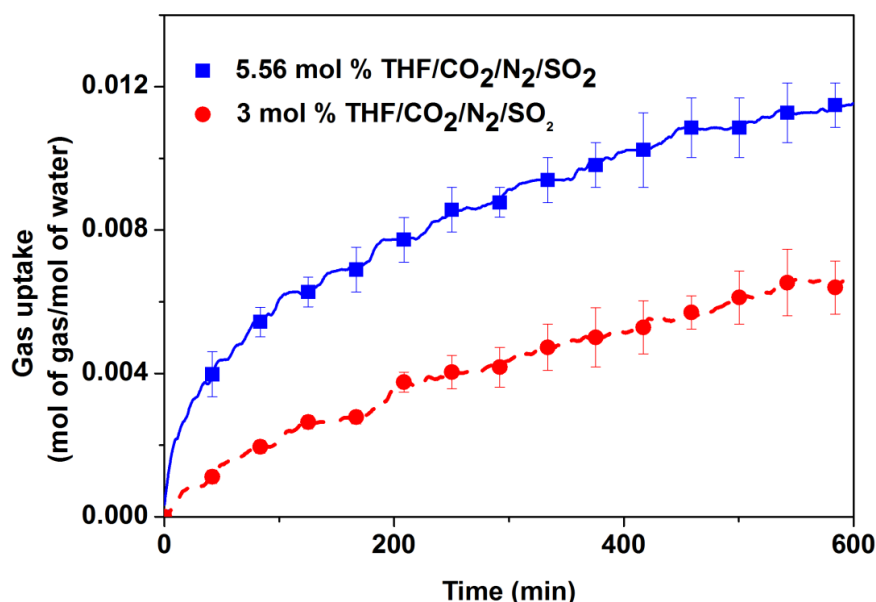
Figure 3.9 (a) Typical gas uptake measurement curve along with temperature profile at 9.5 MPa and 273.65K. (b) Comparison of gas consumption for hydrate growth (In ~10h from induction time) measured in presence of 1wt% SDS.

3.5.2. Kinetics of Hydrate Formation in the Presence of THF for CO₂/N₂/SO₂ system

Daraboina et al, reported the phase equilibria data for CO₂/N₂/SO₂ mixture in presence of 1 mol% THF. The addition of 1 mol% THF offers a huge reduction in operating pressure while a significant reduction in the induction time was also observed. On the other hand, the addition of THF also reduces the gas uptake compare to no THF system. (Linga et al., 2007; Daraboina et al., 2013). To enhance the gas uptake, in the present work, larger amounts of THF

were used (3 and 5.56 mol%). 5.56 mol% is the maximum amount of THF required to completely fill the large cages in structure II hydrates.

Figure 3.10a, compares the gas consumption (mol of gas/mol of water; hydrate growth) measured for different amounts of THF in the system (3 and 5.56 mol%) at 2.45 MPa and 273.65K pressure and temperature respectively. Time zero in the figure corresponds to nucleation point (induction time) for the experiments. Figure 3.10b shows the comparison of final gas uptake after 10 hours (mol of gas/mol of water; hydrate growth) obtained in the present work with different amounts of THF in the system with that already reported in literature (1 mol% THF, Daraboina et al., 2013). It has reported in the literature that the kinetics of hydrate formation may depend on the concentration of THF used and hydrate formation rate decreases with the addition of THF at higher concentrations due to the proximity of THF occupying the large cages readily and thus stabilising the structure II (sII) hydrates. This results in lower gas uptake of the guest gas due to mass transfer resistance; more specifically, guest gas molecules can no longer occupy the large cages due to the already present THF molecules in the same (Lee et al., 2010). However, in the present study, as can be seen in Figure 3.10b, the final gas uptake is higher in case of the 5.56 mol% THF system as compared to the 3 and 1 mol% THF systems. Similar results were reported by Babu et al., for pre-combustion CO₂ capture where the total hydrate growth for the experiment using 5.53 mol% THF greatly surpassed the experiment using 1 mol% THF with a 1.8 times higher yield. (Babu et al., 2014). Veluswamy et al., have also observed a similar trend with THF for H₂ storage in the form of gas hydrates (Veluswamy et al., 2014).



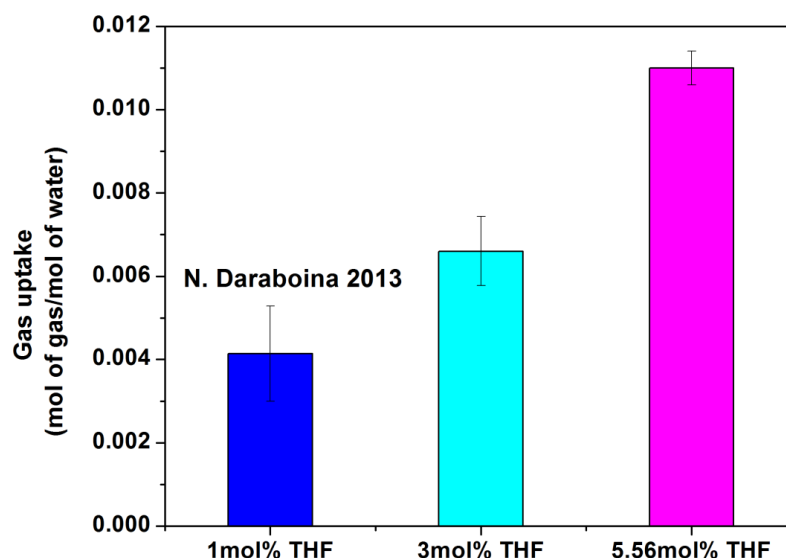
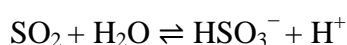


Figure 3.10. (a) Comparison of gas consumption (mol of gas/mol of water) for hydrate growth measured for different amount of THF (3 and 5.56 mol%) at 2.45 MPa and 273.65K. Time zero in the graph corresponds to nucleation point (induction time) for the experiments. (b) Comparison of gas consumption (mol of gas/mol of water) for hydrate growth with literature (1 mol% THF)

3.5.3. Safety concerns in the use of gas mixture containing SO₂

It is well known that the presence of SO₂ in the atmosphere in contact with moisture gets significantly acidic and may result in acidic rain. The corrosive action of sulfur dioxide on metallic surfaces is determined by the particular state in which the metal exists and its purity. (Mattson et al., 1963; Vannerberg et al., 1970).



SO₂ molecules present in the gas phase, adsorb onto the surface of the metals and reduces them. For example, Fe³⁺ is reduced by SO₂ to Fe²⁺ ions. Teresa et al., have observed that a SO₂ complex forms when a water surface is exposed to an atmosphere of SO₂ gas (Teresa et al., 2005). Figure 3.11 shows the image of a rupture disc from our crystallizer which was corroded by the action of SO₂ present in the gas mixture used in this study. Rupture disc was made up of Monel, a nickel alloy comprising nickel (67%) and copper with some amount of iron and other trace elements. As can be seen in the figure, the action of SO₂ has had a major impact on the state of the rupture disc corroding the alloy to a large extent. Hydrate formation and dissociation conditions (temperature transitions from low to high temperature) are believed to be favorable for the corrosive action of SO₂ further aiding in the corrosion of the rupture disc which took place during our experiments.

Corrode rupture disc by the reaction of SO₂
(CO₂/N₂/SO₂ Gas mixture)



Figure 3.11. Image of rupture disc, damaged by the action of SO₂

3.6. Impact of H₂S impurity on the hydrate formation (thermodynamics /kinetics of fuel gas mixture and its impact on the HBGS process)

3.6.1. Effect of H₂S impurity on the thermodynamics of hydrate formation

Figure 3.12 shows the incipient hydrate formation conditions obtained in the presence of 1% H₂S in the fuel gas mixture. Equilibrium experiments were performed by the isothermal pressure search method (Englezos et al., 1994). As we can see, the equilibrium formation pressure is very high for CO₂/H₂ gas mixture compared to pure CO₂. However it significantly reduces in the presence of 1mol% H₂S compared to no H₂S equilibrium data given in open literature for CO₂ (39.2)/H₂ (60.8) (Kumar et al., 2006). The most likely reason for this reduction is that the hydrate formation pressure for pure H₂S is comparatively milder compared to CO₂ and H₂ at a constant temperature of interest. Nohra et al, have also reported that small amount of impurities such as SO₂ and H₂S promotes the hydrate formation (Nohra et al., 2012).

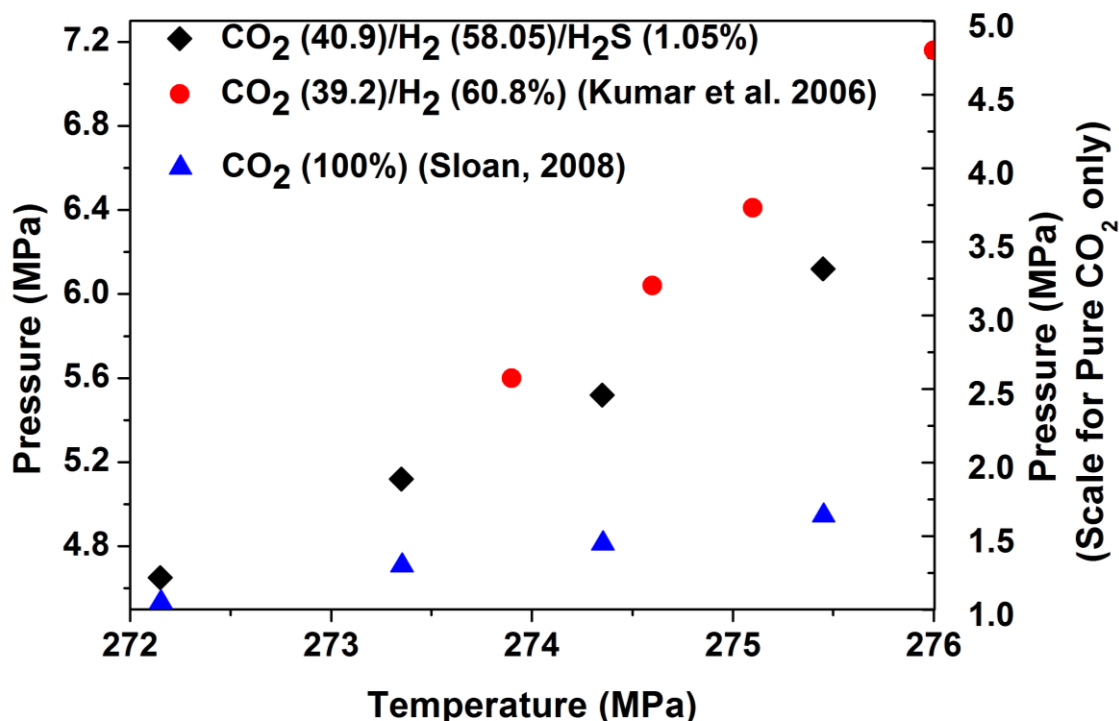


Figure 3.12. Incipient equilibrium hydrate formation conditions for the CO_2 (40.9%) / H_2 (58.05%) / H_2S (1.05%), CO_2 (39.2%) / H_2 (60.8%) system and pure CO_2 . Y-axis on the right hand side shows the hydrate formation pressure of pure CO_2 system

3.6.2. Effect of H_2S impurity on the kinetics of hydrate formation

Table 3.6 summarizes all the experiments performed with $\text{CO}_2 + \text{H}_2 + \text{H}_2\text{S}$ gas mixture in STR and fixed bed reactor during this study; relevant information including experimental pressure & temperature, induction time, duration of experiments, moles of gas consumed at induction time and at the end of the reaction have been reported. Equilibrium hydrate formation pressure at 273.35 K is 5.1 MPa.

3.6.2.1. Kinetics of hydrate formation in STR ($\text{CO}_2 + \text{H}_2 + \text{H}_2\text{S} + \text{STR}$ system)

Figure 3.13a presents the hydrate formation/dissociation curve along with temperature profiles obtained with a $\text{CO}_2 + \text{H}_2 + \text{H}_2\text{S} + \text{STR}$ system at 274.65 K (formation temperature), 293.15K (dissociation temperature) and 8.5 MPa experimental pressure. Experiments were carried out in batch mode; upon hydrate formation, pressure starts to drop which involves gas dissolution, nucleation and hydrate growth stages. As seen in the figure, the induction time is different for all three cycles (reduces from cycle 1 to 3) which represents the memory effect (figure 3.13a). Figure 3.13b and 3.13c represents the gas uptake data and pressure drop data for two fresh runs. As can be seen from these figures, two different stages of gas uptake (dissolution and hydrate nucleation followed by hydrate growth) to be observed in the experiments that had a longer

induction time (1050 min). However such these two stages were not observed for the experiments that had shorter induction times (2 min). Such a huge difference in induction time represents the stochastic nature of hydrate nucleation.

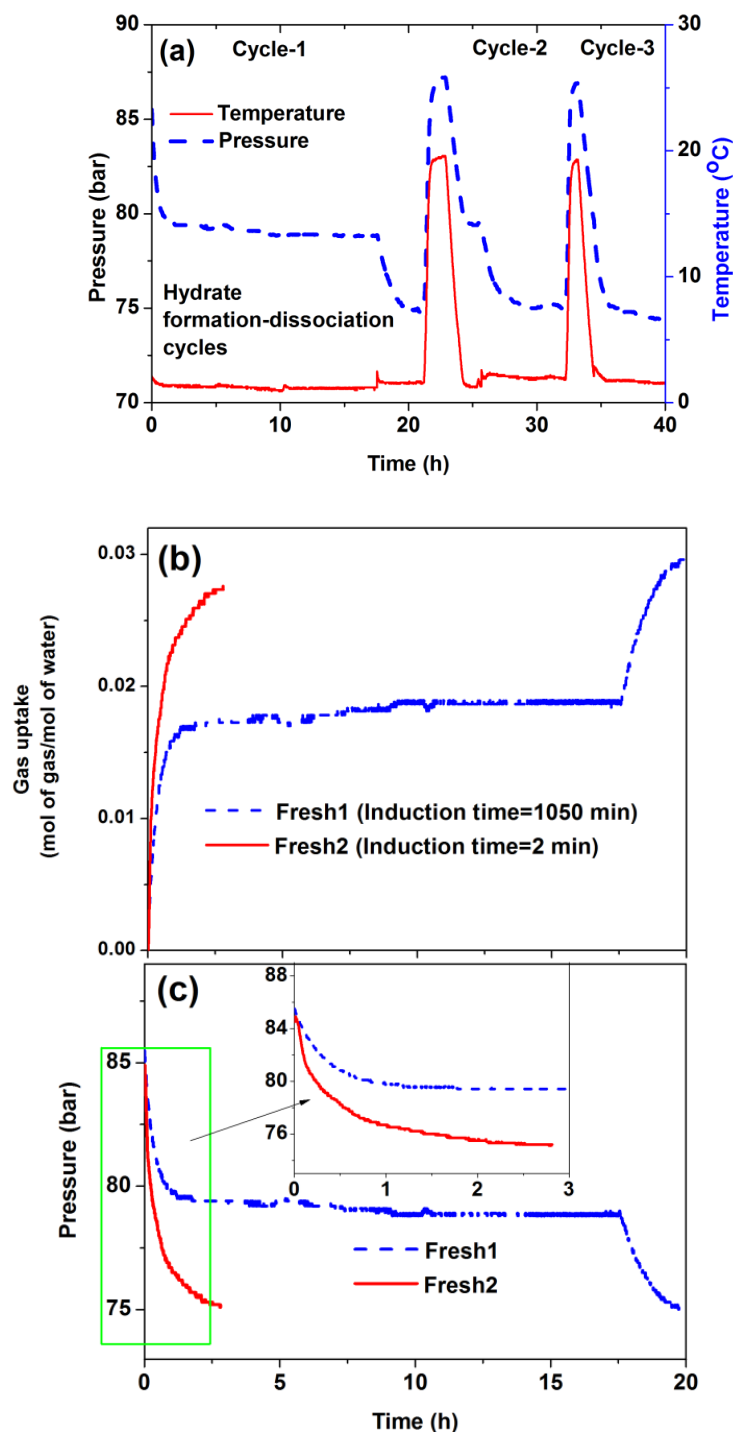


Figure 3.13. (a) Hydrate formation-dissociation curve for $\text{CO}_2/\text{H}_2/\text{H}_2\text{S}$ system, along with temperature profile at 8.5 MPa and 274.65-293.15K. (b) Gas uptake profile (c) pressure drop data for two fresh experimental runs

3.6.2.2. Kinetics of hydrate formation in a fixed bed of silica sand and impact of H₂S on silica sand

Figure 3.14 (a) presents the hydrate formation curves (gas uptake) for fresh and memory experiments obtained with silica sand for the CO₂ + H₂ + H₂S system at 274.65 K and 7.8 MPa. Equilibrium hydrate formation pressure for this particular gas mixture at 273.35 K is 5.1 MPa (Kumar et al., 2015). It can be observed that the kinetics of hydrate formation for the fresh run was much superior as compared to the memory run.

It was visually observed that after a fresh run with the CO₂+H₂+H₂S gas mixture, silica sand turns black while gradually regaining its original color when kept at room temperature (Figure 3.14(b)). This unusual behavior of silica sand was investigated upon by using Raman spectroscopy to characterize the silica sand. Figure 3.15 shows the Raman spectra for pure silica sand and silica sand immediately after reaction with the CO₂+H₂+H₂S gas mixture. Multiple peaks were observed in Raman spectra which can be attributed to large number of inorganic components in the form of Hematite (Fe₂O₃). In presence of water, Fe₂O₃ in the silica sand reacts with H₂S from the gas phase (reaction i) to form Iron (III) sulfide (Fe₂S₃), a solid black powder. While exposed at room temperature in atmospheric conditions Iron (III) sulfide again oxidizes to iron (III) oxide (Brownish in color) thus allowing the silica sand to regain its original color (reaction ii). Formation of Fe₂S₃ on reaction of silica sand with H₂S was confirmed by Raman spectroscopy (Davydov et al., 1998; Kim et al., 2007). Raman spectra obtained for silica sand after reaction with H₂S clearly shows peaks pertaining to Fe₂S₃ whereas these peaks are absent for Raman spectra obtained for pure silica sand (Figure 3.15). (Graphical representation is given below)

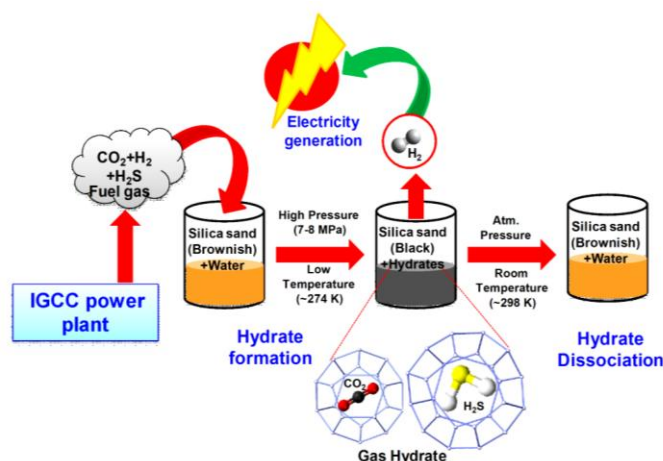


Table 3.6. Summary of experiments, gas consumption and induction time in STR and fixed bed of silica gel and silica sand

System	Exp. No.		Pressure (MPa)	Induction Time (IT) (min)	Gas Consumption at IT (mol/mol)	End of Experiment		Hydrate Growth (mol/mol)
						Final Gas Consumption (mol/mol)	Time (min)	
CO ₂ /H ₂ /H ₂ S/STR	S1	C1	8.5	1050	0.0189	0.0296	1200	0.0107
		C2	8.5	132	0.0144	0.0264	500	0.012
		C3	8.5	60	0.0167	0.0309	500	0.0142
	S2		8.5	2	0.0017	0.0273	160	0.0256
CO ₂ /H ₂ /H ₂ S/Silica Gel	G1		8.0	33.8	0.0120	0.0495	400	0.0375
	G2		8.0	367	0.0018	0.0382	900	0.0364
	G3		8.0	720	0.0042	0.0387	1200	0.0345
	G4		7.0	68.8	0.0099	0.0409	600	0.0310
	G5		7.0	2	0.0007	0.0282	300	0.0275
	G6		7.0	393	0.0042	0.0233	630	0.0191
	G7		7.0	2	0.0014	0.0296	400	0.0282
	G8		7.0	2	0.00071	0.0296	400	0.0288
	G9		6.5	1	0.00069	0.0216	300	0.0209
	G10		6.5	1.3	0.0021	0.0216	300	0.0195
	G11		6.5	1.5	0.0007	0.0237	300	0.0230
	G12		6.5	10	0.0090	0.0258	300	0.0168
CO ₂ /H ₂ /H ₂ S/Silica Sand	SS1		7.8	450	0.025	0.050	1000	0.025
	SS2		7.8	200	0.020	0.051	600	0.031
	SS3		7.8	200	0.021	0.047	600	0.026

C=Hydrate formation cycle

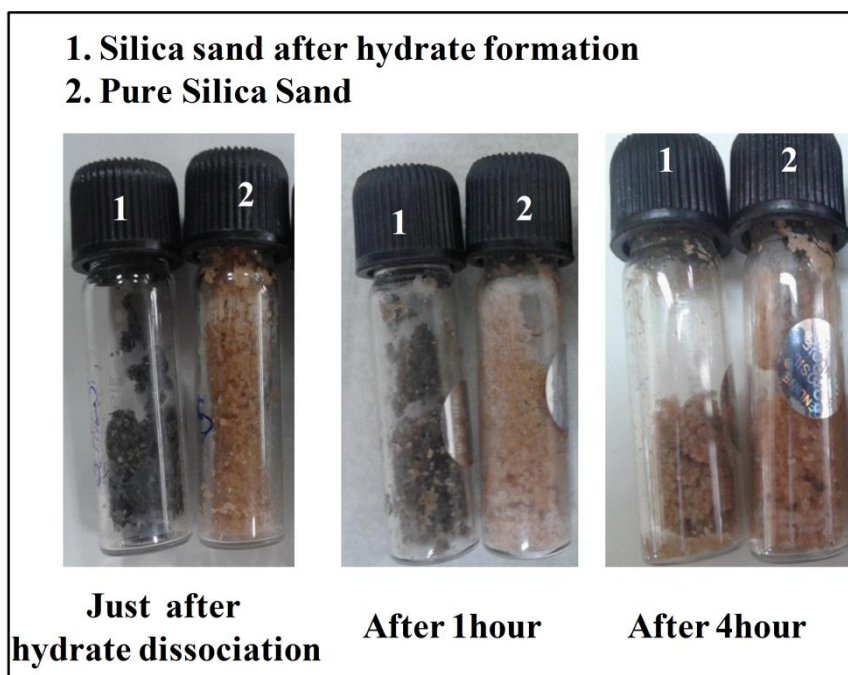
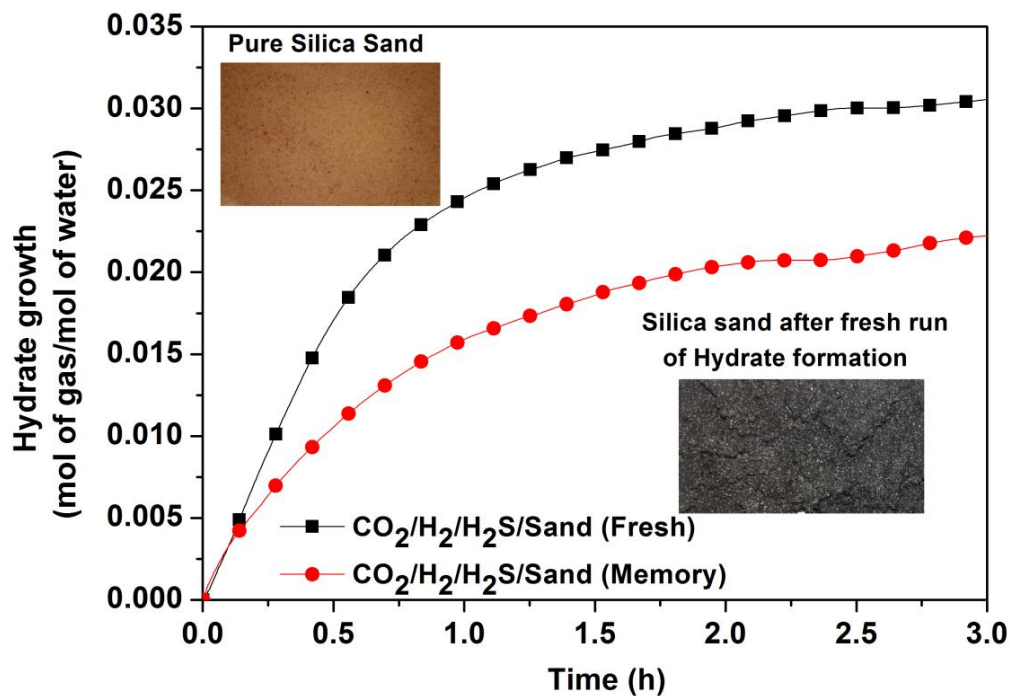


Figure 3.14. (a) Hydrate growth curves at 7.8 MPa and 274.15K for $\text{CO}_2+\text{H}_2+\text{H}_2\text{S}/\text{Sand}$ System (fresh and memory run). Time zero in the graph corresponds to the nucleation point (b) Colour of silica sand before and after hydrate formation using $\text{CO}_2+\text{H}_2+\text{H}_2\text{S}$ gas mixture.

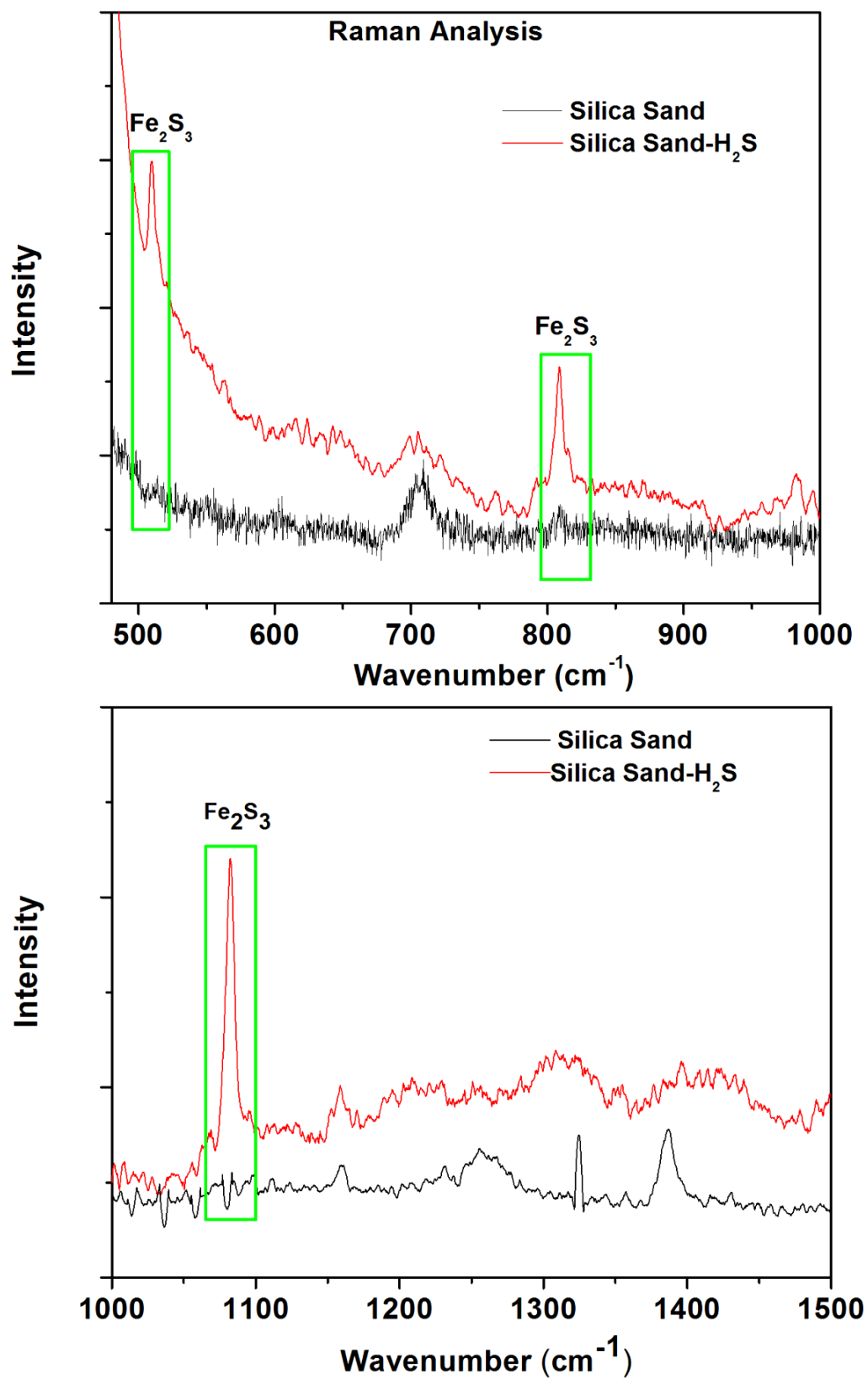


Figure 3.15. Raman spectra of pure silica sand and silica sand after reaction with H₂S.

3.6.2.3. Kinetics of hydrate formation in a fixed bed of silica gel

Due to the unusual impact of H_2S on silica sand accompanied with a significant drop in hydrate formation kinetics for memory runs in a $CO_2+H_2+H_2S$ / Silica sand system, it was decided to use silica gel with large pore diameter (~ 100 nm) as the fixed bed medium to evaluate the effect of this particular gas on hydrate formation kinetics. Table 3.6 summarizes all the experiments performed during this study with the $CO_2 + H_2 + H_2S$ gas mixture and using silica gel as the fixed bed medium; relevant information including experimental pressure & temperature, induction time, duration of experiments, moles of gas consumed at induction time and at the end of the reaction have been reported. It was visually observed that silica gel does not show any corrosive effect with $CO_2+H_2+H_2S$ gas mixture. Typical gas uptake measurement curve along with temperature profiles of the three thermocouples located in the silica gel bed is shown in Figure 3.16. It is noted that the general characteristics of the gas uptake curve resembles the one obtained in silica sand system.

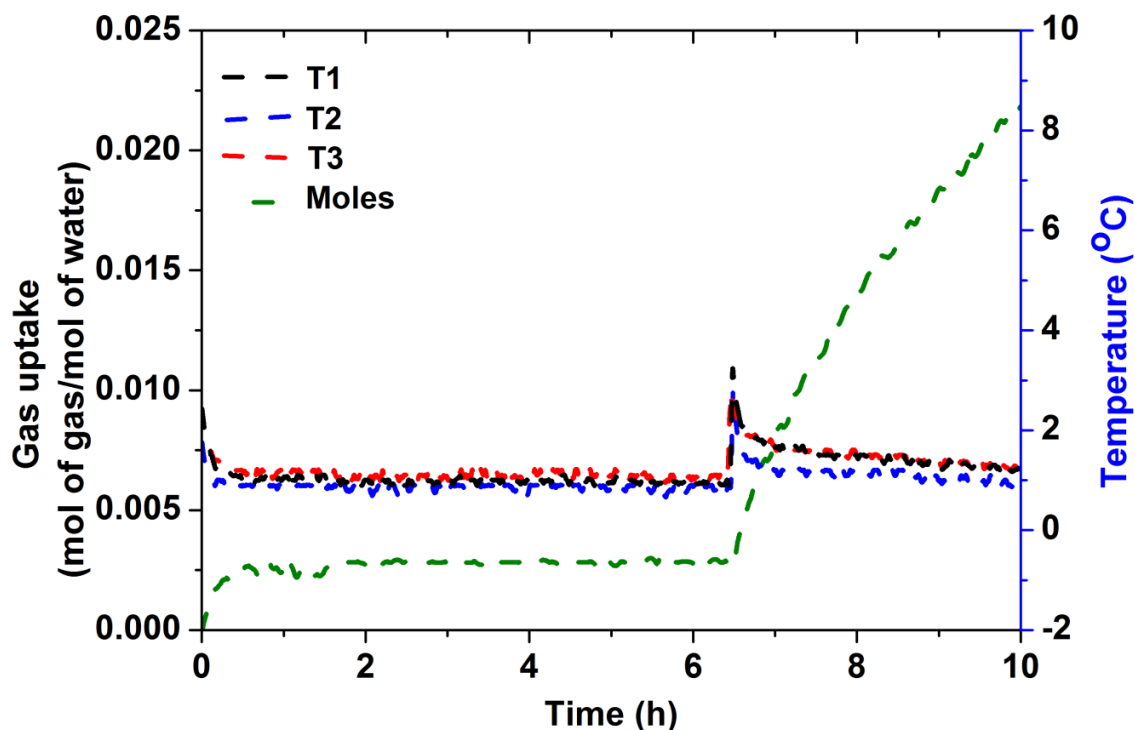


Figure 3.16. Typical gas uptake measurement curve for Silica gel / $CO_2/H_2/H_2S$ system (experiment G2) along with the temperature profile at 8 MPa and 274.65 K

The effect of driving force on hydrate formation kinetics has been investigated upon in this study, which is to say hydrate formation kinetics have been measured at three different initial experimental pressures for the same experimental temperature (274.65K). Kinetics of gas

hydrate formation and the final gas uptake are both enhanced with increase in driving force for the $\text{CO}_2+\text{H}_2+\text{H}_2\text{S}$ gas mixture. The effect of driving force on hydrate formation kinetics in silica gel bed for $\text{CO}_2+\text{H}_2+\text{H}_2\text{S}$ gas mixture has been presented figure 3.17.

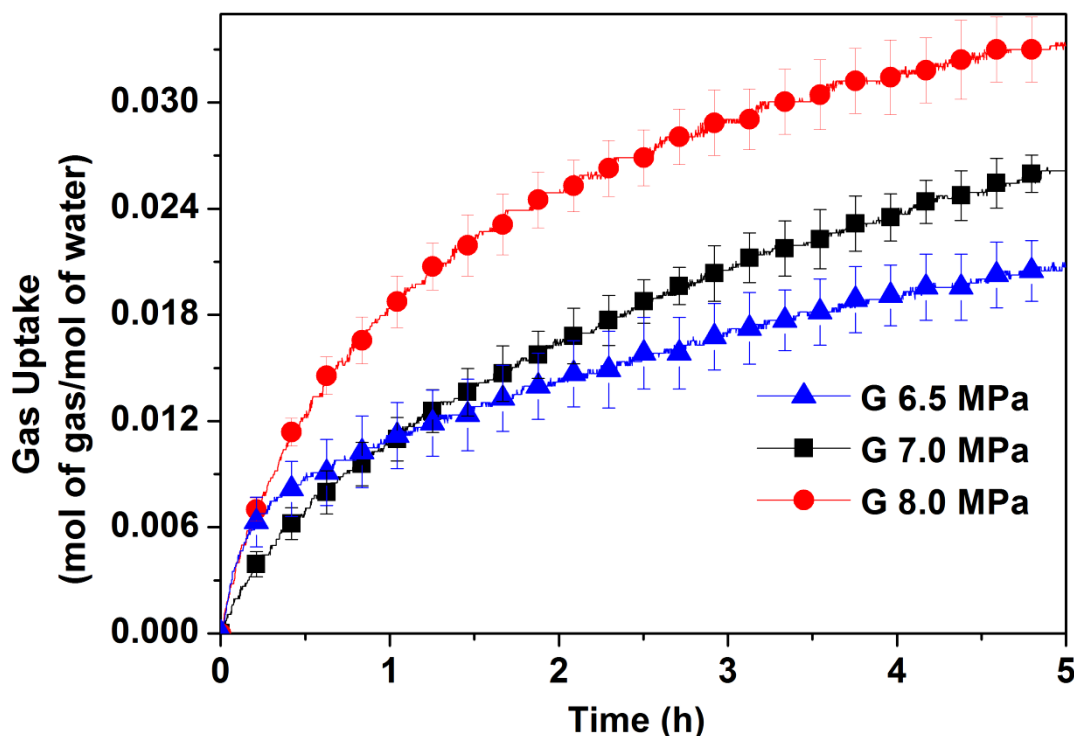


Figure 3.17. Effect of driving force on the gas uptake curve in silica gel bed for $\text{CO}_2/\text{H}_2/\text{H}_2\text{S}$ gas mixture, Time zero corresponds to the induction time for the experiment.

Figure 3.18 uses the gas uptake obtained after 120 minutes from the beginning of gas hydrate formation with the $\text{CO}_2+\text{H}_2+\text{H}_2\text{S}$ gas mixture used in this study and compares it with those obtained using a CO_2+H_2 gas mixture present in literature. The current study was performed using a fixed bed of silica gel and silica sand. Results included from literature in Figure 3.18 comprise gas uptake data obtained using both fixed bed and stirred tank reactor configurations for CO_2+H_2 gas mixture.

It can be gleaned from Figure 3.18 that the presence of H_2S impurity in the system favorably affects the gas uptake for hydrate formation. For silica gel with similar pore diameter and at much lower experimental pressures, $\text{CO}_2+\text{H}_2+\text{H}_2\text{S}$ gas mixture used in this study shows significantly higher final gas uptake (after 120 minutes) as compared to that reported in the literature using a CO_2+H_2 gas mixture. As expected, the gas uptake for a stirred tank reactor system is much lesser than that for a fixed bed system.

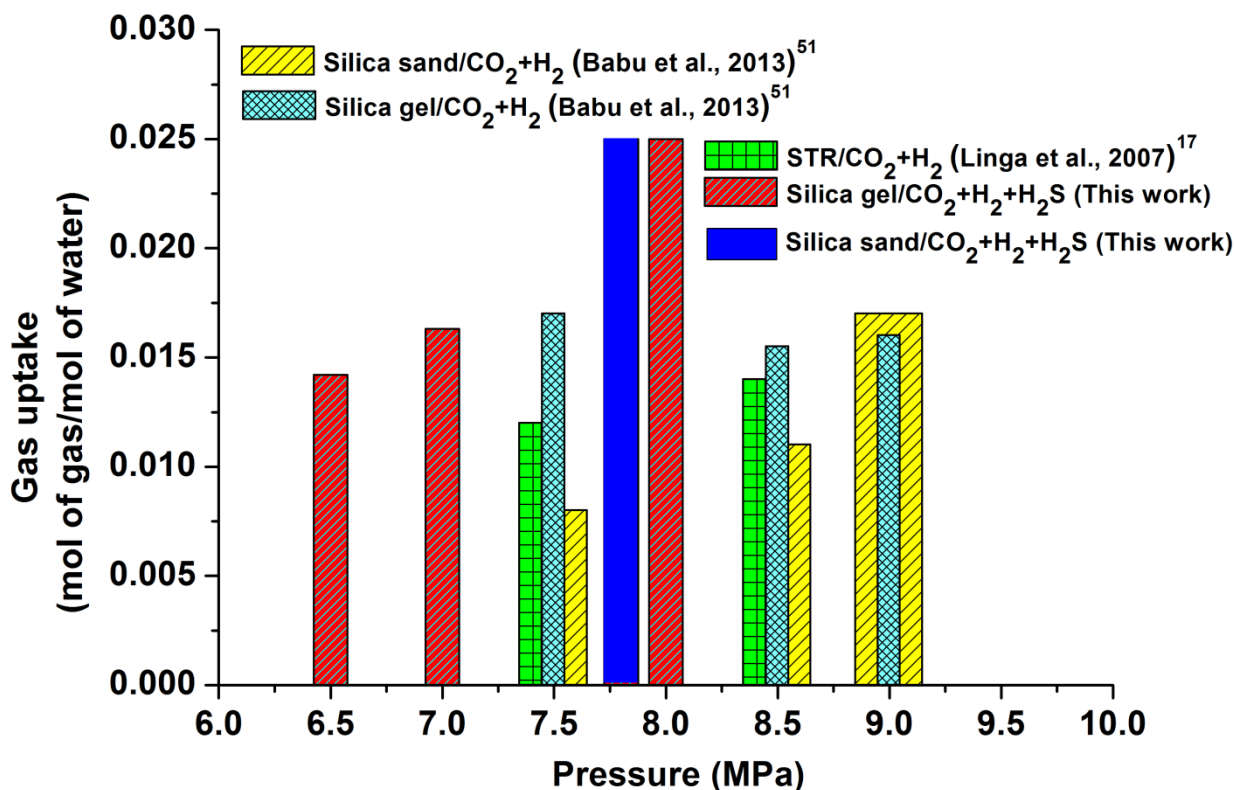


Figure 3.18. Comparison of gas uptake data at different experimental pressures and different reactor configurations for CO_2+H_2 (obtained from literature; Babu et al., 2013; Linga et al., 2007) and $\text{CO}_2+\text{H}_2+\text{H}_2\text{S}$ (present study) gas mixtures. Gas uptake after 120 minutes from hydrate nucleation has been plotted.

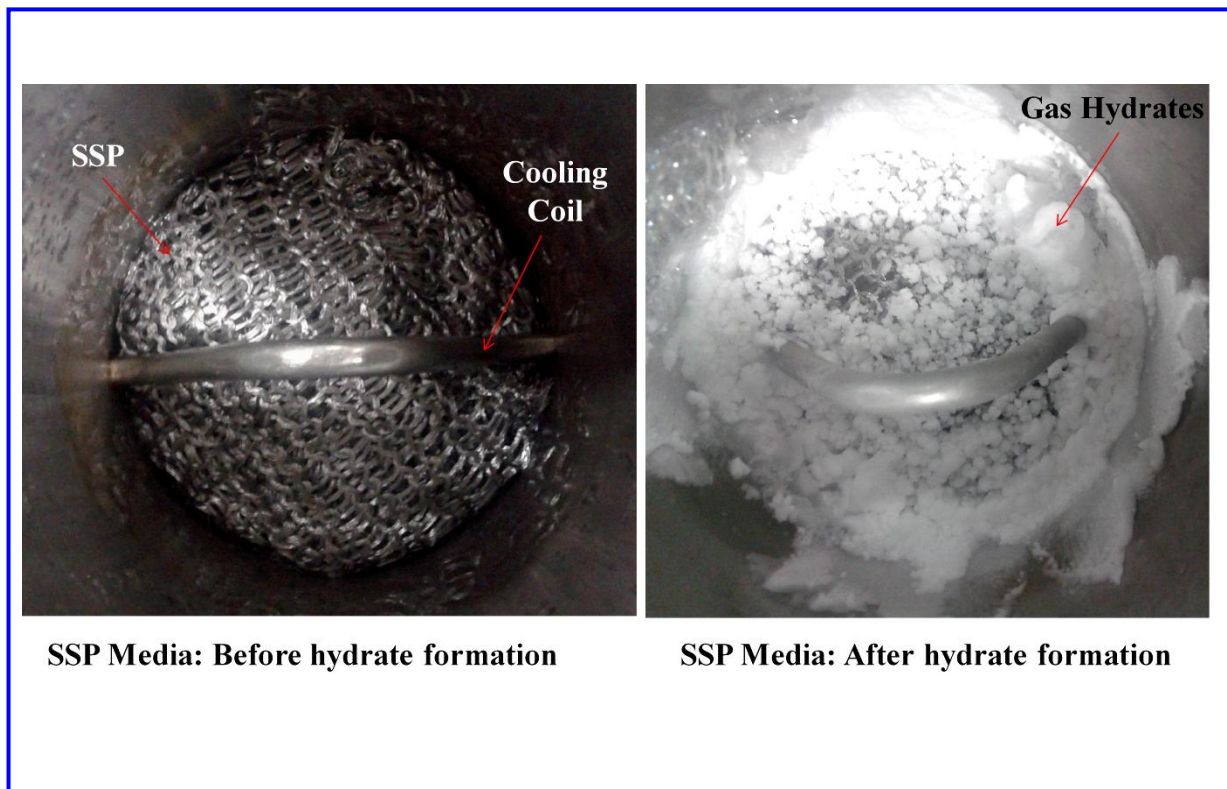
3.7. Conclusions

Gas hydrate formation experiments from flue gas mixtures (CO_2/N_2 / fly ash and $\text{CO}_2/\text{N}_2/\text{SO}_2$) and fuel gas mixture ($\text{CO}_2+\text{H}_2+\text{H}_2\text{S}$) were carried out to study the impact of these impurities (fly ash, SO_2 and H_2S) on the thermodynamics and kinetics of hydrate formation. Additional kinetic & thermodynamic promoters were added in the liquid phase to reduce the operating pressure and enhance the hydrate formation kinetics. In the presence of fly ash impurity no significant shift in the hydrate equilibrium pressure was observed. An analysis of the equilibrium data shows that flue gas mixture in presence of THF and fly ash forms structure II hydrate. It was found that HBGS process can be effective in presence of impurities like fly ash in the flue gas mixture. The two additives used in this work, a thermodynamic promoter (THF) and a kinetic promoter (SDS) showed a synergic effect on hydrate formation kinetics at a comparatively lower operating pressure of 3.75 MPa. The kinetic promoter enhances the rate of gas hydrate formation significantly, while final water to hydrate conversion is not affected. It was found that an increase in THF concentration enhances the kinetics of hydrate formation. The impact of SO_2 on post-combustion capture of CO_2 has already been investigated and it was found that the presence of SO_2 shifts the hydrate equilibrium to milder conditions. Hconditions.

However, the rate of hydrate formation was very slow which was enhanced in the present study using a thermodynamic promoter (5.56 mol% THF) and a kinetic promoter (SDS). It was also found that H₂S also shifts the hydrate formation equilibrium condition to the milder conditions (shifting towards the high temperature and low pressure). However presence of 1 mol% H₂S in the gas mixture does not enhance the overall kinetics of hydrate formation, thus would not impact the overall efficiency of HBGS process. However, it was noted that suitable material of construction needs to be selected to avoid corrosive effect of H₂S and SO₂ on the packing medium if a fixed bed arrangement is being utilized for such separation. Due to the corrosive and toxic nature of H₂S and SO₂, it is highly recommended to follow standard safety precautions in the laboratory.

Chapter 4

Metallic fixed bed media for enhanced gas hydrate formation kinetics: application to carbon dioxide capture from fuel gas mixture



4. Metallic fixed bed media for enhanced gas hydrate formation kinetics: application to carbon dioxide capture from fuel gas mixture⁴

⁴A version of this chapter has been published.

A Kumar, T Sakpal, P Linga, R Kumar, Enhanced carbon dioxide hydrate formation kinetics in a fixed bed reactor filled with metallic packing, *Chemical Engineering Science*, 2015, 122, 78-85

Kumar A, Kumar R. Role of Metallic Packing and Kinetic Promoter in Designing a Hydrate Based Gas Separation Process *Energy Fuels*, 2015, 29 (7), 4463–4471.

4.1. Introduction

As discussed in the last two chapters, a suitable surfactant like SDS can significantly improve the hydrate formation kinetics even in a fixed bed arrangement by enhancing mass transfer. However, enhanced heat transfer would also be essential during exothermic hydrate formation stage. In this work we study two metallic packing in order to study the kinetics of CO₂ hydrate formation in a fixed bed arrangement. Initially Pure CO₂ was chosen for this work for simplicity, as the focus was to compare the hydrate formation kinetics in different metallic packing, afterward fuel gas mixture was used. For exothermic hydrate crystallization, better growth kinetics can be achieved by efficient removal of localized heat from the crystallizer, thus a metallic packing with high thermal conductivity should be ideal. Yang et al., have used aluminum foam (AF, average pore size of 1000 μm) as a media to study the kinetics of methane hydrate formation. It was observed that AF not only reduces the induction time but also enhance the formation and growth significantly (Yang et al., 2011). Out of the two packing used for this work, one resembles a random packing (SS-316 fillings, SSP-1) and the other, structured packing (SS-316 wire mesh, SSP-2), photographs of the packing materials are included in the Appendix C, figure C1 and C2). SS-316 has a density of ~8000 kg/m³ which is approximately 4-times higher than the silica sand density (1560 kg/m³) (Dawson, 2004; Jones and Schoonover, 2002). Thus a very dense metallic packing might unnecessarily increase the column weight resulting in lesser CO₂ capture capacity per unit mass. To evaluate the effectiveness of such packing material, CO₂ capture capacity under similar experimental condition for CO₂ consumption per unit mass of water, per unit mass of material (combined mass of packing and water) and per unit volume of material (combined volume occupied by the packing and the water) were done and compared. Other fixed bed media such as brass packing and copper foam was also studied.

4.2. Experimental Section:

4.2.1. Materials

CO₂ (40.9%) + H₂ (58.05%) + H₂S (1.05%) gas mixture and CO₂ + H₂ mixture containing 40.4% by mole CO₂ and rest H₂ corresponding to a typical composition of a fuel gas mixture from an integrated coal gasification cycle was supplied by Vadilal Gases Ltd., India. SSP-1 is a SS-316 fillings fabricated on request at the workshop of National Chemical Laboratory. SSP-2 (SSP) is a SS-316 structured packing bought from LELESIL, Mumbai. The specific volume of SSP was found to be 0.83 cm³/g (volume of water required to fill the void spaces of SSP). A representative photograph of the SSP (SS-316) structured packing used in this study has been presented in Appendix C (Figure C1 and C2). Brass packing is fabricated on request at the workshop of National Chemical Laboratory. Copper foam was supplied by Nanoshel LLC Intelligent Materials Pvt Ltd. India. The specifications of copper foam are as follows: Number of pores per inch (PPI): 5-120, Density (g/cm³): 0.15-0.45, Thickness: 0.5-30mm. A representative photograph of the Cu foam and brass packing used in this study has been presented in Figure C3 and C4 of the Appendix C respectively. Sodium dodecyl sulphate (SQ Grade) with minimum 98% purity was purchased from Fisher Scientific Ltd. India. Silica sand was purchased from Sakalchand & Company Pune, India. The particle size distribution of silica sand is in the range of 30-400 μm. The volume of the water required to completely fill the void space between the sand particles was ~0.20 cm³/g. Silica gel with the pore diameter of ~5 nm, particle size distribution 40-65 μm and pore volume of 0.92 cm³/g with 99% purity (LR grade) was purchased from Rankem Ltd. Deionized and distilled water was used for the experiments.

4.2.2. Procedure for saturating various packing with SDS solution (Pure CO₂ system)

SDS is a white powdered solid at room temperature and pressure. To prepare the SDS-water solution, 1 wt% equivalent of SDS was weighed on a mass balance and transferred into a volumetric flask with 1000 cm³ of distilled water. The solution (SDS solution) was then thoroughly mixed before using it for hydrate formation. Quiescent hydrate formation experiment was done with 50 cm³ of SDS solution without any packing. Suitable amount of silica sand and silica gel were calculated from the specific pore volume information and each time 50 cm³ of SDS solution was used for an experiment. Silica sand and silica gel was uniformly mixed with SDS solution in a 500 cm³ beaker before transferring it into the reactor for gas uptake measurement. Specific volume of two metal packing SSP-1 and SSP-2 were

calculated by tightly filling the packing in a transparent beaker and sufficient amount of water was filled till it completely gets saturated (showing no extra layer of water above the SSP). Specific volume based on this measurement was calculated to be $3.45 \text{ cm}^3/\text{g}$ of material for SSP-1 and $0.83 \text{ cm}^3/\text{g}$ of material for SSP-2. During a gas uptake measurement with metallic packing, calculated amount of packing was tightly filled in the SS-316 reactor which was then filled with 50 cm^3 of liquid solution.

4.2.3. Apparatus and hydrate formation procedure for experiment conducted with various fixed bed media in batch mode (Pure CO₂ system)

Detail description of the fixed bed apparatus (Figure 4.1) and the procedure for hydrate formation are given as follow. A fixed quantity of liquid solution (50 cm^3) was used along with calculated amount of packing material (silica gel, silica sand, SSP-1 and SSP-2) in a 400 cm^3 SS-316 crystallizer (CR). CR was tightly closed and placed inside the temperature controlled water bath. CR was flushed out with the pure CO₂ gas (at 274.65 K) by repeating pressurization (~0.5 MPa) and depressurization sequence prior to the experiment. Circulating ethylene glycol / water mixture from the water bath was employed to cool the CR at experimental temperature of 274.65 K. Once the desired temperature is reached, the CR is pressurized by pure CO₂ gas to pre determined experimental pressure (3.0 MPa). At this point, gas uptake measurement was initiated. All the gas uptake measurements were carried out in batch mode with a pure carbon dioxide and fixed amount of SDS solution (50 cm^3) at a constant temperature of ~274.65 K. CR is equipped with pressure transducer (WIKA) of 0-20 MPa range; drop in the reactor pressure was measured to calculate the gas consumption during a gas uptake measurement. Temperature and pressure of the reactor were recorded every 5 seconds through a data acquisition system connected to a computer. The pressure of the CR starts to drop upon hydrate formation, which was used to measure the moles of gas uptake for hydrate formation experiment. It is noted that experiment was done in a batch mode and thus effective driving force changes as hydrate formation proceeds, as more and more CO₂ from the gas phase occupies the solid hydrate phase.

4.2.4. Apparatus (for Fuel gas system)

Detail description of the fixed bed apparatus and the procedure for hydrate formation are given in 4.2.3 section. Figure 4.1 shows the schematic of the experimental setup. It consists of a $\sim 500 \text{ cm}^3$ SS-316 crystallizer, CR (ID = 7.6 cm, Height = 11 cm); which is immersed in a

temperature controlled water bath. The temperature of the water bath is controlled by an external refrigerator (Make: Kumar sales corporation, Mumbai). A pressure transducer (Make: Wika) is employed for pressure measurement with a maximum uncertainty of 0.1% of the span (range 0-16 MPa). The temperature of the hydrate phase in the crystallizer is measured using RTDs with an uncertainty of ± 0.1 K. Three thermocouples were used to measure the temperature profile of the fixed bed setup during hydrate formation and decomposition runs. Locations of the three thermocouples placed in the crystallizer are shown in Figure 4.1.

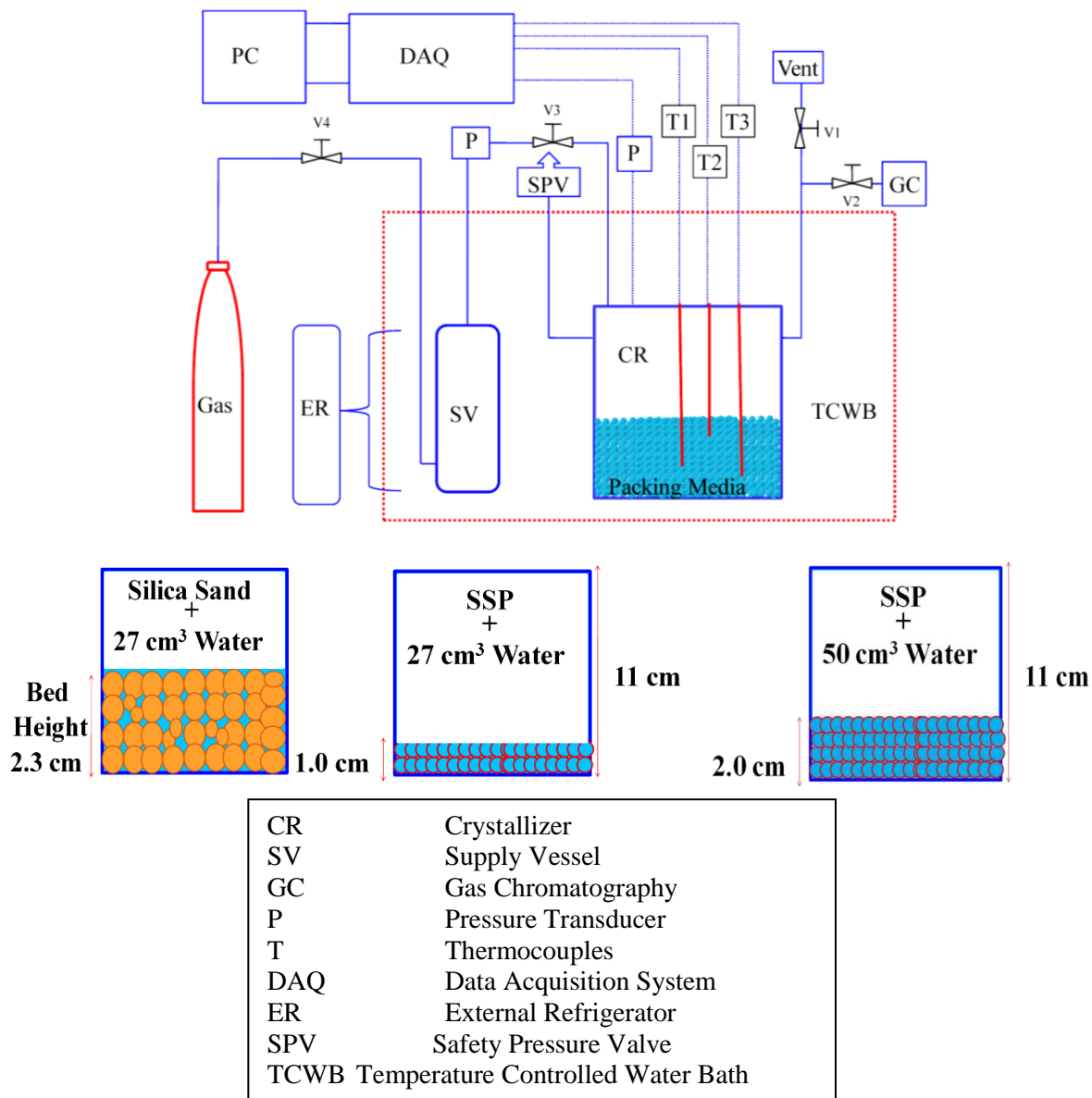


Figure 4.1. Schematic of the experimental apparatus along with the location of thermocouples in the crystallizer and bed height for both packing media

Hydrate formation experiments were conducted in a batch mode with fixed amount of water at constant temperature and the results were used to propose a conceptual continuous HBGS process. The data acquisition system (Make: Micro Technics) is coupled with a computer to record the data. Other relevant details like placement of safety valve, vent, supply vessel, gas chromatography etc. are shown in figure 4.1.

4.3. Experimental Procedure (for Fuel gas system)

4.3.1. Preparation of Silica sand Bed:

180g of silica sand as a fixed bed media was used for each experiment; volume of water required to fill the void spaces was calculated to be $\sim 0.2 \text{ cm}^3/\text{g}$. Accordingly, 36 cm^3 of water is required for 100% saturation; however Babu et al. and Kumar et al. have reported that lower water saturation in the packing leads to better hydrate growth and water to hydrate conversion (Babu et al., 2013c). Thus 27 cm^3 water / SDS solution equivalent to 75% saturation was premixed with the sand and the mixture was transferred to the reactor. This arrangement leads to a bed height of 2.3 cm (figure 4.1)

4.3.2. Preparation of metallic Bed:

27 cm^3 of SDS solution was added to 43 g stainless steel structured packing for hydrate formation; this arrangement results in a bed height of 1 cm (figure 4.1). The volume of water used has been kept constant (27 cm^3) so as to compare the hydrate growth rate in different packing media (Silica sand and SSP) for $\text{CO}_2 + \text{H}_2$ mixture. Experiments for $\text{CO}_2 + \text{H}_2 + \text{H}_2\text{S}$ gas mixture were conducted with 50 cm^3 of SDS solution (bed height of $\sim 2 \text{ cm}$, 70g SSP).

4.3.3. Hydrate formation/dissociation procedure

Detailed description of the procedure for hydrate formation is given elsewhere in the chapter 2, in brief the procedure is as follows. A fixed quantity of liquid solution (27 cm^3 and 50 cm^3 for $\text{CO}_2 + \text{H}_2$ and $\text{CO}_2 + \text{H}_2 + \text{H}_2\text{S}$ experiments respectively) was used along with calculated amount of packing material (silica sand and SSP) in a 500 cm^3 SS-316 crystallizer (CR). CR was placed inside the temperature controlled water bath; any air impurity in the CR was flushed out with the fuel gas mixture by repeated pressurization and depressurization sequence prior to the experiment. Once the experimental temperature is achieved, CR is pressurized by the fuel gas mixture to pre determined experimental pressure (7.0 MPa and 7.8 MPa for $\text{CO}_2 + \text{H}_2$ and $\text{CO}_2 + \text{H}_2 + \text{H}_2\text{S}$ experiments respectively). At this point, gas uptake measurement was initiated. All the gas uptake measurements were carried out in batch mode with a fixed amount of water or SDS solution at constant temperature of $\sim 273.65 \text{ K}$ and 274.5 K for $\text{CO}_2 + \text{H}_2$ and $\text{CO}_2 + \text{H}_2$

+ H₂S gas mixture respectively. Drop in the reactor pressure was measured to calculate the gas consumption during hydrate formation. Temperature and pressure of the reactor were recorded every 5 seconds through a data acquisition system connected to a computer. The pressure of the CR starts to drop upon hydrate formation, which was used to measure the moles of gas uptake for hydrate formation experiment.

At the end of the hydrate formation experiments, the hydrate decomposition kinetics was studied at temperatures of 293.15 K. During the hydrate dissociation process, the pressure inside the reactor increased as the gas was released from the solid hydrates. The increase in the pressure in the reactor was recorded every 5 s and this was used to measure the gas-release kinetics.

4.4. Calculation for the amount of gas consumed during hydrate formation

The total number of moles of the gas that have been consumed for hydrate formation was calculated by following equation

$$(\Delta n_{H,\downarrow})_t = V_{CR} \left[\frac{P}{zRT} \right] - V_{CR} \left[\frac{P}{zRT} \right]_t \quad (1)$$

Where z is the compressibility factor calculated by Pitzer's correlation (Smith et al., 2001); V_{CR} is the volume of the gas phase of the crystallizer; P & T are pressure and temperature of the crystallizer.

4.5. Water to hydrate conversion calculation

Conversion of water to hydrate is determined by using the following equation:

$$\text{Conversion of water to hydrate (mol \%)} = \frac{\Delta n_{H,\downarrow} \times \text{Hydration number}}{n_{H_2O}} \times 100 \quad (2)$$

where $\Delta n_{H,\downarrow}$ is the number of moles of gas consumed for hydrate formation at the end of the experiment determined from the gas uptake and n_{H_2O} is the total number of moles of water in the system. Hydration number is defined by the number of water molecules per guest molecule. The hydration number used in the above equation is 7.09 (for CO₂/H₂ gas mixture) (Kumar et al., 2009). The hydration number for pure CO₂ used in the above equation is 7.03 (Linga et al., 2012)

4.6. Calculation for the rate of hydrate formation

Rate of hydrate formation (R_{30} in $\text{mol} \cdot \text{min}^{-1}$) is calculated by fitting the hydrate growth (gas uptake) data verses time for the first 30 min from nucleation point using least-squares method (appendix C, Figure C5)and the normalized rate of hydrate formation (NR_{30}) is calculated as follows

$$\text{Normalized rate of hydrate formation } (NR_{30}) = \frac{R_{30}}{V_w} (\text{mole of gas} \cdot \text{min}^{-1} \cdot \text{m}^{-3}) \quad (3)$$

Where, V_w is the volume of water taken for the experiment in m^3 .

4.7. Results and discussion (for Pure CO₂ system)

Table 4.1 summarizes all the experiments performed during this study; relevant information including experimental pressure & temperature, induction time, duration of experiments, moles of gas consumed at the end of the reaction and water to hydrate conversion is reported. Operating temperature of 274.65 K and pressure 3.0 MPa at this temperature was estimated from CSMGEM. Equilibrium hydrates formation pressure at 274.65 K was found to be 1.49 MPa (Sloan and Koh, 2008).

4.7.1. Comparison of CO₂ hydrate formation kinetics for various fixed bed media (Silica sand, silica gel, SSP-1 and SSP-2)

Figure 4.1 shows the typical gas uptake curve along with the temperature profile for an experiment conducted at 274.65 K and 3.0 MPa pressure. The general shape of the curve agrees with the gas uptake profile described in detail by Natarajan et al. which involve gas dissolution, nucleation and hydrate growth stage (Natarajan et al. 1994). The gas consumption increases till it reaches the saturation level, partly due to decreasing driving force for hydrate formation. The crystallizer is cooled to the experimental temperature by an external refrigerator, thus the overall temperature of the crystallizer remains constant throughout the dissolution phase. However, exothermic nature of hydrate formation results in sudden temperature spike during hydrate nucleation. Multiple temperature spikes as shown in the fig. indicate multiple nucleation events (Babu et al., 2013b,c; Haligva et al., 2010).

Table 4.1. Summary of experiments, induction time, gas consumption and water to hydrate conversion; experimental pressure and temperature used was 3.0 MPa and 274.65 K respectively. Amount of water used for all the experiment was 50 cm³. (Experiments were conducted in batch mode)

System	Exp. No.	Mass of packing, (g)	Induction time (IT) (min)	Avg. Induction time (min) [\pm stdev]	End of Experiment		Final water to hydrate conversion (% mol) [#]
					Time (min)	Mol of gas/mol of water	
SDS / Water	1a (F)	*	411	249.0 (\pm 220)	650	0.093	65.64
	1b(M)	*	100		350	0.077	54.27
	1c (F)	*	NN				
SSP-1 / SDS / Water	2a (F)	14.5	46	37.5(\pm 26)	160	0.079	55.7
	2b(M)	14.5	36		160	0.080	56.7
	2c (F)	14.5	92		146	0.092	64.7
	2d(M)	14.5	36		200	0.084	59.2
SSP-2 / SDS / Water	3a (F)	60	230	207 (\pm 105)	350	0.104	73
	3b(M)	60	90		200	0.110	77.4
	3c (F)	60	300		480	0.106	75
	3d(M)	60	45		200	0.106	74.4
Silica gel / SDS / Water	4a (F)	55	3	17.3 (\pm 15.6)	165	0.059	41.6
	4b (F)	55	15		300	0.067	47.6
	4c (F)	55	34		300	0.059	41.6
Silica sand/ SDS / Water	5a (F)	250	4.5	4.8 (\pm 4)	136	0.093	65.5
	5b(M)	250	1		147	0.096	67.6
	5c (F)	250	9		133	0.096	67.9

* Indicates no packing

[#]Hydration no. of 7.03 was used for calculation (Linga et al., 2012)

NN= No nucleation for 800 minutes

F=Fresh experiment, M= Memory experiment

Table 4.2. Comparison of gas uptake measurement and initial rate of hydrate growth for STR (stirred tank reactor) and other fixed bed media, relevant experimental details are also included.

S.No.	Contact mode	P _{exp.} (MPa)	Temperature (K)	Exp. Time for max. gas consumption (min)	Gas uptake (mol of gas/mol of water)	NR ₃₀ (moles of gas.min ⁻¹ .m ⁻³) approx	Ref.
(1)	STR	3.1	274.15	4110	0.0389	16	Linga et al., 2012
(2)	STR	3.0	274.15	840	0.0380	12	Lirio et al., 2013
(3)	STR with 500 ppm SDS	3.0	274.15	840	0.0450	26	Lirio et al., 2013
(4)	Silica gel (100nm pore)	3.0	274.15	360	0.1290	55	Kang and Lee, 2010
(5)	Silica gel with 100 ppm SDS	3.0	275.15	360	0.1380	74	Kang and Lee, 2010
(6)	Silica gel with 1500 ppm SDS	3.0	275.15	300	0.1220	74	Kang and Lee, 2010
(7)	Silica gel (5nm pore)	3.5	274.15	360	0.0850	50	This Work (Kumar et al., 2013)
(8)	Silica sand	3.1	274.15	2898	0.0904	32	Linga et al., 2012
(9)	Silica sand	3.2	274.15	1440	0.0826	52	Sun and Englezos, 2014
(10)	Silica sand with 1 wt% SDS	3.0	274.65	150	0.0950	80	This work (Kumar et al., 2015)
(11)	SSP-2 with 1 wt% SDS	3.0	274.65	120	0.1000	115	This work (Kumar et al., 2015)

Large number of simultaneous nucleation results in larger temperature spike accompanied by a higher magnitude of gas uptake (Kumar et al., 2013). Hydrate nucleation is followed by the hydrate growth phase. In the experiment shown in Figure 4.2, the hydrate nucleation occurred at ~45 min. This fig. shows a fast gas uptake rate just after hydrate nucleation; moreover, hydrate continues to grow for next 60 min.

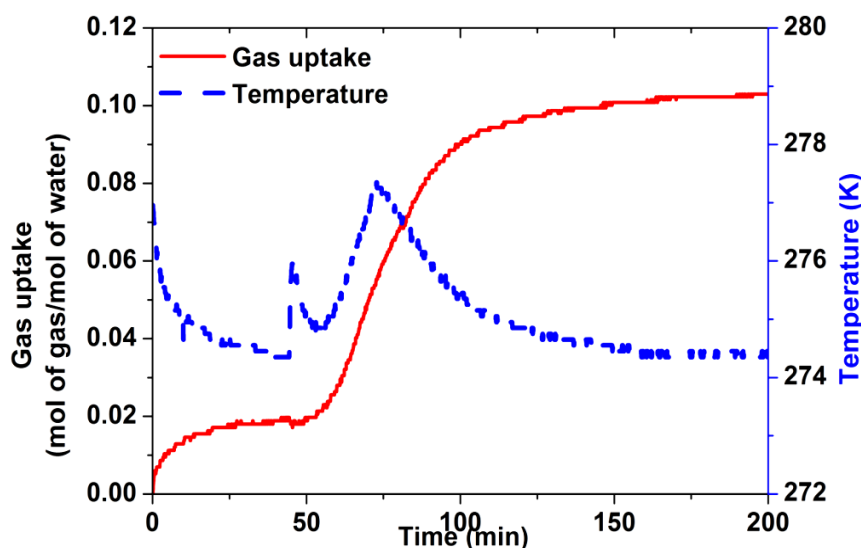


Figure 4.2. Typical gas uptake measurement curve (mol of gas/mol of water) along with temperature profile at 3.0 MPa and 274.65K. (SSP-2/SDS/water system, exp. 3d)

Figure 4.3 compares the growth rate after hydrate nucleation in different fixed bed media used in this study. Time zero in the graph corresponds to nucleation point (induction time) for the experiments. As discussed earlier, 1 wt% of SDS is used as a kinetic promoter (1 wt% SDS was found to be the best concentration to achieve maximum water to hydrate conversion rate and ratio; refer figure C6 in the appendix C). As seen in the figure 4.3, initial rate of hydrate formation is slowest in quiescent system compared to other fixed bed media. As a packing material, silica gel has a very high surface area to volume ratio, however shows least water to hydrate conversion compared to other packing. The silica gel used in this study has a very small pore size of 5 nm and it has been reported in literature that the three phase thermodynamic equilibria of hydrate formation shifts to more extreme conditions in porous media (Kang et al., 2007). It is therefore assumed that water present in the intra particle pores would see a lesser driving force for hydrate formation compared to water present in the inter particle spaces. Thus in all probability, hydrate nucleates from the water available in the inter-particle spaces and growth of solid hydrate on the surface of silica gel blocks the diffusion of

gases to the pores. We believe this phenomenon limits the extent of water to hydrate conversion. This argument leads to the fact that larger silica gel particle with larger pore diameter should improve hydrate formation kinetics (Adeyemo et al., 2010). Figure 4.3 also shows that the initial rate of hydrate growth in the other three packing, SSP-1, SSP-2 and silica sand is much faster compared to silica gel. As shown in table 4.1, water to hydrate conversion in the three packing is ~60%, ~75% and ~65% respectively. Linga et al., have also reported pure CO₂ hydrate formation in silica sand bed (no SDS), showing comparatively slower growth rate while achieving ~64% water to hydrate conversion in 2898 min (48.3h) (Linga et al., 2012). In the current work close to 50% water to hydrate conversion was achieved in ~60 min. Moreover, SSP-2 along with silica sand packing shows slightly better hydrate growth compared to SSP-1 at 3.0 MPa and 274.65 K. Current work clearly shows that SDS enhances hydrate growth rate and achieves similar water to hydrate conversion in much shorter time. Thus it can be said that 1 wt% SDS as used in this study is quite effective in enhancing the rate of hydrate formation. As discussed above, one of the reasons for faster hydrate growth kinetics is due to reduction in the surface tension in presence of SDS, which improves the diffusion of CO₂ resulting in faster hydrate growth (Chen et al., 2007). The lowering in the surface tension reduces the contact angle where a liquid meets a solid surface. Due to lowering of the contact angle with the surfactant, a film-like interface is created on the surface of packing material. This film is believed to be the preferred location for nucleation and initiation of hydrate growth (Yoslim et al., 2010).

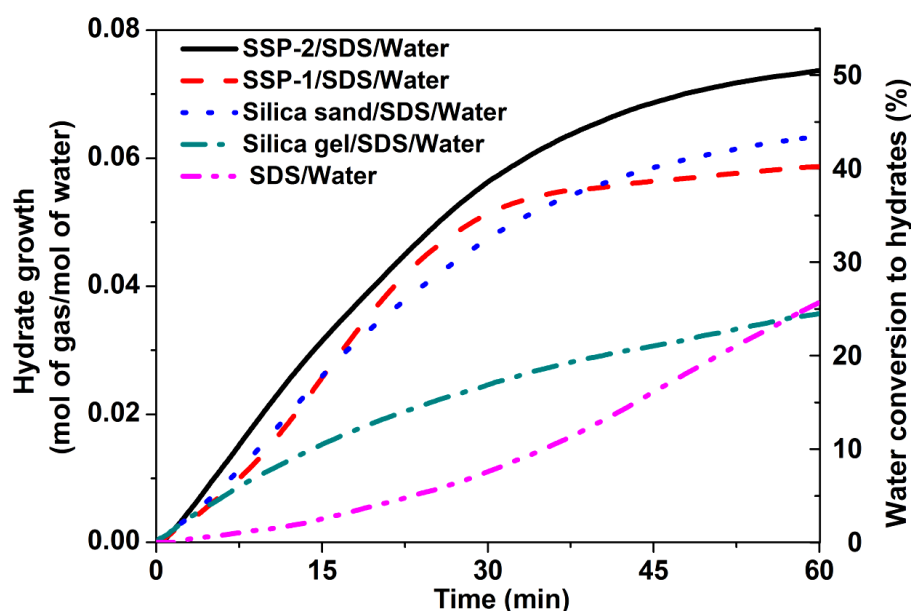


Figure 4.3. Comparison of gas consumption for hydrate growth measured for different fixed bed media. Time zero in the graph corresponds to nucleation point (induction time) for the experiments.

Foam film permeability measurements by Farajzadeh et al. shows that mass transfer rate (transfer of gas to the aqueous phase) remains very high in the presence of SDS (Farajzadeh et al., 2011). CO₂ solubility increases linearly with the surfactant concentration, indicating micellar solubilization at higher concentration of surfactants (Ownby et al., 1997; Ricaurte et al., 2012; Roy et al., 1997). In the absence of any surfactant, hydrate and occluded water creates a slushy hydrate mass which prevents efficient mass transfer of gas through the gas/water interface (Linga et al., 2012), which may not be the case in presence of SDS. However, based on high water to hydrate conversion in quiescent water experiment (table 4.1), it can be said that high water to hydrate conversion in presence of surfactant (SDS) is also due to enhancement of capillarity driven supply of the water from the porous hydrate layer. This allows more and more water to come in contact with hydrate forming gases even in the presence of solid hydrate phase on the interface (Gayet et al., 2005; Okutani et al., 2008; Pang et al., 2007).

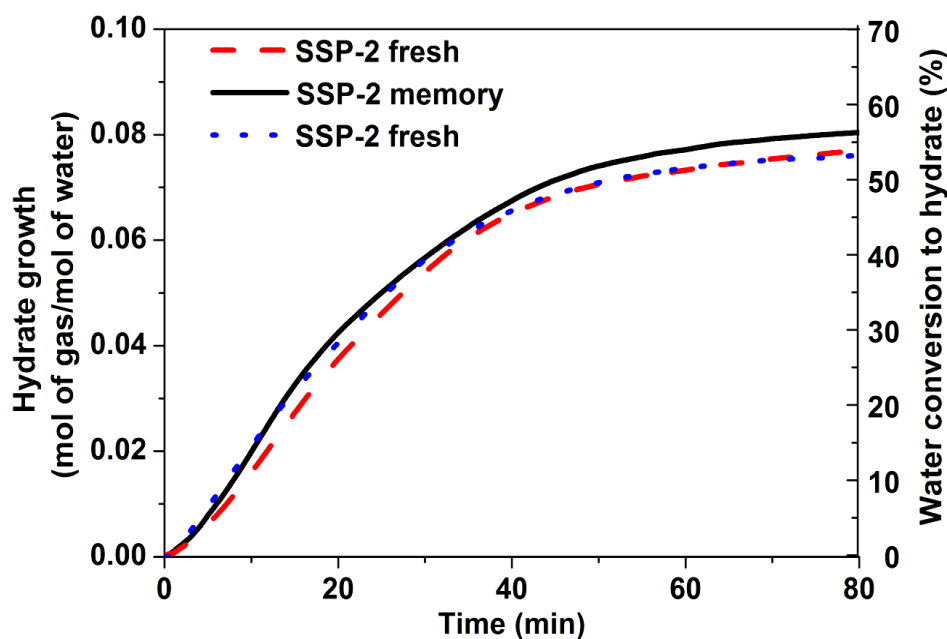


Figure 4.4. Hydrate growth curves (Fresh and memory runs) for SSP-2/SDS system. Time zero in the graph corresponds to nucleation point (induction time) for the experiments. (Experiment No. 3a, 3b and 3c)

Figure 4.4 shows the hydrate growth curves for the three experiments conducted from fresh and memory water for SSP-2 system. Time zero in the graph corresponds to nucleation

point (induction time) for the experiments. As seen in the figure, the hydrate growth curves show very good reproducibility and the growth curves follow the same trend for both fresh and memory water. It can be seen that the rate of gas hydrate formation is linear till about 30 min. We calculated the rate of hydrate formation (R_{30}) by fitting a linear fit for the hydrate growth (gas consumed) data versus time and subsequently calculated the normalized rate of hydrate formation (NR_{30}) using equation 3 (Appendix figure C5). The calculated rates were averaged and presented in figure 4.4 along with the standard deviations for all the systems (Babu et al., 2013a). As seen in figure 4.4, the initial rate of hydrate growth for SSP-2 system is $\sim 115 \text{ mol.min}^{-1}.\text{m}^{-3}$ which is significantly higher than other packing utilized in this work.

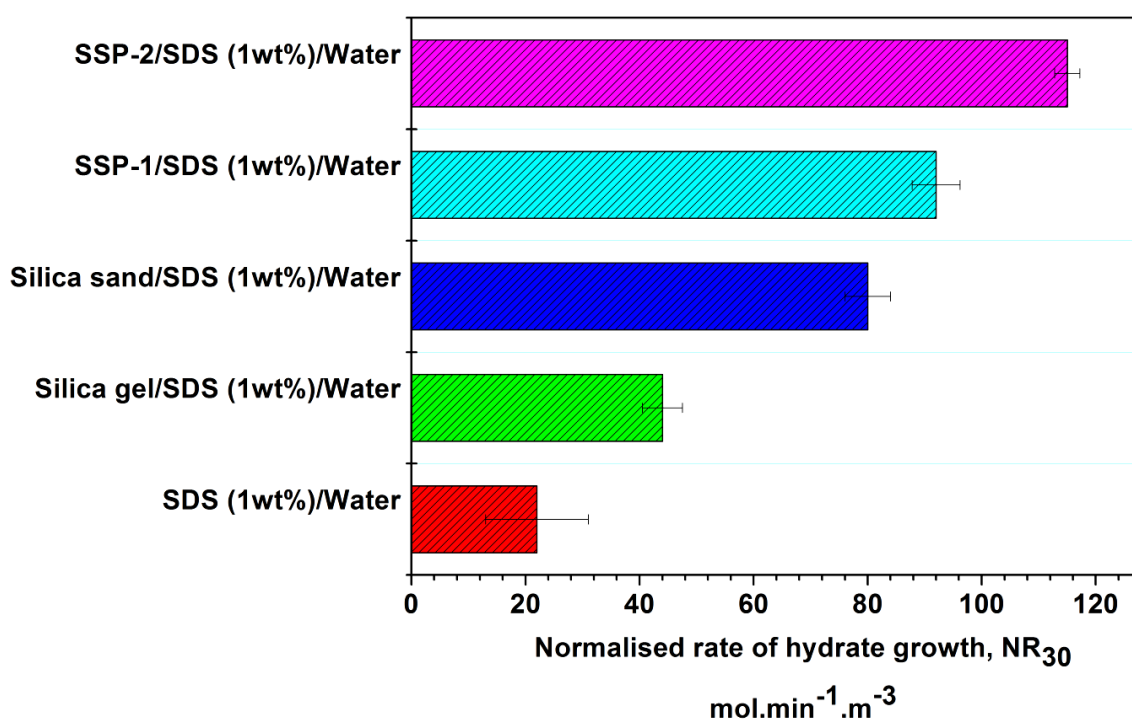


Figure 4.5. Normalized rate of hydrate formation for different fixed bed media, calculated for first 30 min after nucleation.

Figure 4.6 shows the comparison of gas uptake for hydrate growth in terms of milligram of CO_2 consumed per unit mass (g) of material and per unit volume (cm^3) of material, these has been plotted along with CO_2 capture per g of water, for 30 min from induction time. In this fig., the term “material” includes the mass or volume of packing material (in g or cm^3) along with the mass or volume of SDS solution (in g or cm^3) used for hydrate formation experiments, the details are given in table 4.1. As discussed before, density of SS-316 is almost four times that of silica sand and significantly higher density compared to silica gel. Thus it was important to determine how a metallic packing performs compared to less dense silica sand packing. As

seen in figure 4.6 and table 4.1, irrespective of the ways in which CO₂ uptake capacity is determined the two metallic packing SSP-1 and SSP-2 shows better gas uptake kinetics compared to silica gel and silica sand. In the scenario when either weight or volume of the packing is ignored and gas uptake capacity is calculated on the basis of per gram of SDS solution used for hydrate formation, SSP-2 shows comparable gas uptake kinetics with silica sand. Thus this study shows that a non porous metallic packing can substitute silica sand as a packing material in hydrate based gas separation process, which would have better scale up potential compared to silica sand. Highly conductive SS-316 packing can be applied in several gas separation processes where corrosive environment such as fuel gas separation (presence of H₂S) and flue gas separation (presence of SO₂) may potentially degenerate the packing.

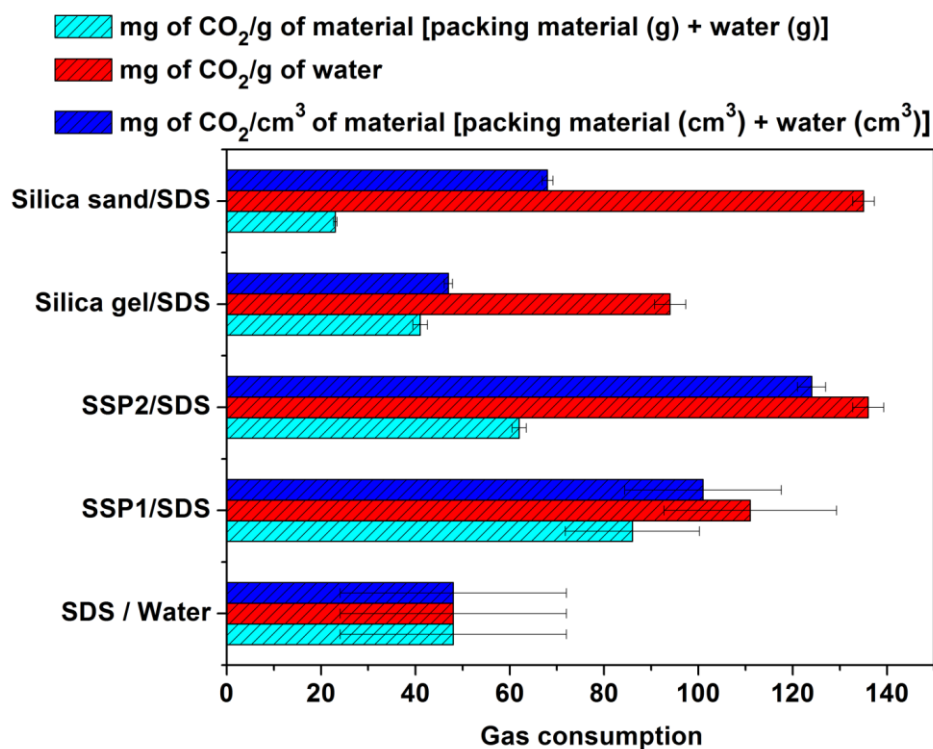


Figure 4.6. Comparison of gas consumption for hydrate growth (average CO₂ uptake) in mg of CO₂ consumed per unit mass of material (g), per unit volume of material (cm³) and per unit mass of water (g) used for hydrate formation. The data shown is for the first 30 min of hydrate growth from induction time (Per unit mass of material includes mass of packing material (g) and water (g) similarly per unit volume of material includes volume of packing material (cm³) and water (cm³).

The induction time in gas hydrate crystallization is an important characteristic of the kinetic studies. Figure 4.7 represents the mean induction time for CO₂ hydrate formation in different packing; as expected induction time being a stochastic phenomenon varies a lot even under

similar operating condition (see table 4.1). Silica gel and silica sand packing shows the shortest induction time compared to relatively non-porous metallic packing SSP-1 and SSP-2, which in turn performs better compared to quiescent system (bulk water). Metallic packing chosen for this work has lower surface area to volume ratio (appendix C) and therefore its performance is not as good as silica sand or silica gel. Shorter induction time for hydrate formation from memory water is favorable for a hydrate based gas separation process, where CO₂ is to be separated from its mixture (Ho et al., 2013; Kumar et al., 2009; Linga et al., 2008). As can be seen from figure 4.7, the average induction time in silica sand system is the lowest followed by silica gel, SSP-1, SSP-2 and quiescent water system. One important conclusion which can be deduced from this measurement is that the presence of SDS and interconnected pores within the packing helps in enhancing the hydrate growth kinetics whereas, efficient dispersion of water in the packing with very high surface area helps in reducing the induction time. Focus of the future work will be to improve the surface area to volume ratio of these metallic packing, which will not only show better hydrate formation kinetics but would also reduce the induction time of hydrate formation. A comparison of initial rate of CO₂ hydrate formation (for the first 30 min after nucleation) from data available in literature is shown in table 4.2, it can be clearly seen that this work shows significantly faster hydrate growth kinetics compared to data reported in the literature.

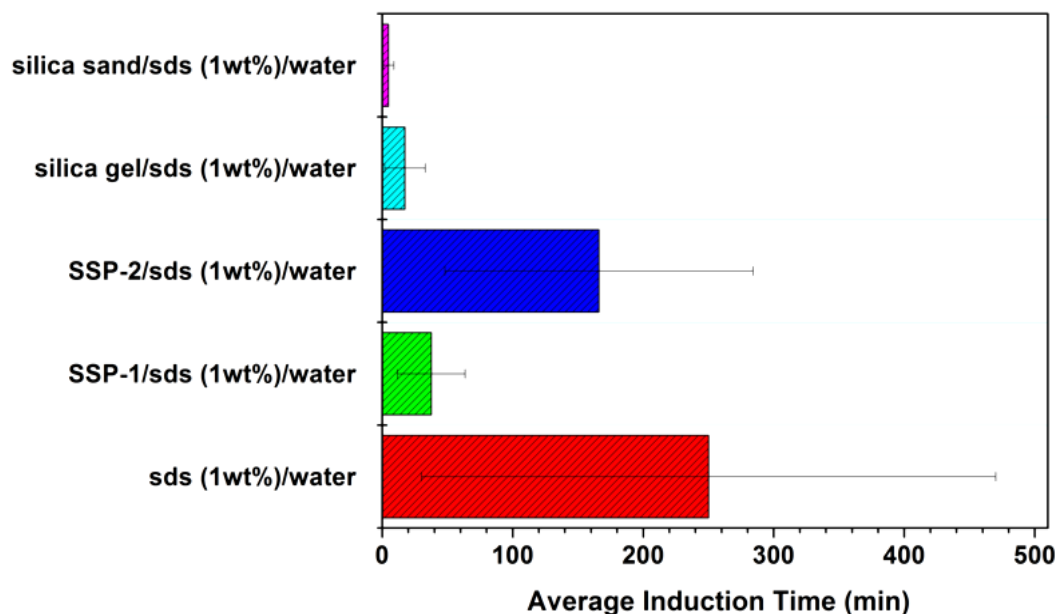


Figure 4.7. Comparison of induction time for different fixed bed media and no media system for hydrate formation

4.8. Results and discussion (for Fuel gas (CO₂ + H₂) system)

4.8.1. Hydrate formation kinetics of fuel gas mixture in silica sand and SSP packing

Table 4.3 summarizes all the experiments performed with CO₂ + H₂ gas mixture during this study; relevant information including experimental pressure & temperature, induction time, duration of experiments, moles of gas consumed at the end of the reaction and water to hydrate conversion have been reported. Equilibrium hydrate formation pressure at 273.9 K is 5.56 MPa (Kumar et al., 2006). It is noted that SDS concentrations do not have any impact on the hydrate phase equilibrium conditions (Song, et al., 2013).

Figure 4.8 presents the hydrate formation/dissociation curve along with temperature profiles obtained with a CO₂ + H₂ + Silica sand + SDS (1wt%) system at 273.65 K and 7.0 MPa. It is important to note that addition of a thermodynamic additive like propane in the fuel gas mixture would ensure a lower operating pressure, which has been studied in detail in one of our previous work (Kumar et al., 2009). Experiments were carried out in batch mode; upon hydrate formation, pressure starts to drop which involves gas dissolution, nucleation and hydrate growth stages. As seen in the figure, hydrate nucleates at 25 minutes which coincides with a sharp increase in temperature (and sudden pressure drop) due to exothermic nature of hydrate nucleation. Pressure drop due to hydrate nucleation and growth continues till there is no driving force for further hydrate growth; at this point a constant pressure profile is observed which typically takes less than 1 h from the formation of stable hydrate nuclei. Hydrates were dissociated by increasing the temperature of the water bath to 293.15K, which initiates hydrate decomposition resulting in rise of the total pressure of the reactor. Figure C7 in the appendix C shows multiple temperature spikes during one such gas uptake run, which indicates multiple nucleation events (Babu et al., 2013a). Multiple nucleations have previously been reported in presence of SDS; Babu et al. reported that without SDS, only one nucleation event occurs in silica sand for fuel gas mixture. Moreover, multiple nucleation results in faster gas uptake rate, however it would also release exothermic heat due to large number of new bond formation necessary for hydrate growth (Babu et al., 2013c). Thus an inefficient heat transfer in the fixed bed media would eventually be a major bottleneck in achieving faster growth kinetics. In the current work it was observed that SSP packing helps by efficiently removing the localized heat during hydrate nucleation; thus enhancing hydrate growth rate. A typical gas uptake profile in SSP packed reactor shows sudden pressure drop after hydrate nucleation. However, the spikes

in the temperature profile obtained in case of SSP system (Figure C8 in the appendix C) are not as sharp as compared to those obtained in case of silica sand system (Figure C7 in the appendix C).

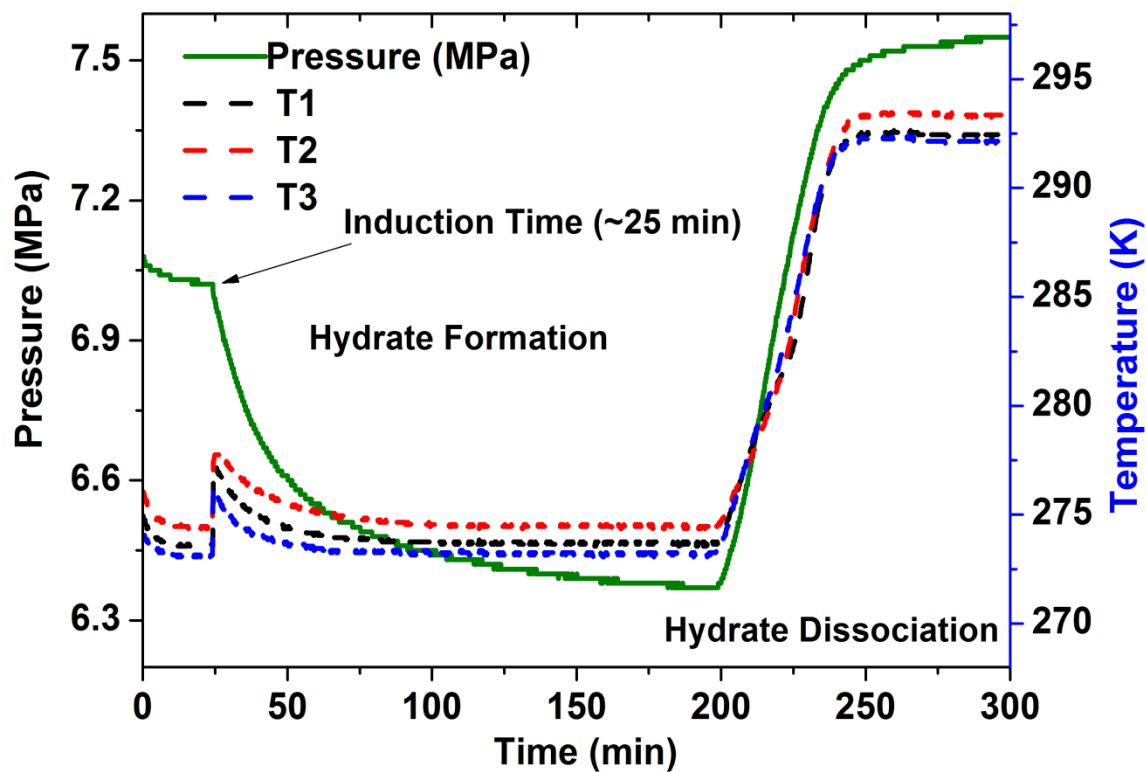


Figure 4.8. A typical hydrate formation (pressure drop) – dissociation (pressure rise at 293.15K) curve along with temperature profile at 7.0 MPa and 273.65 K (Experiment S4)

Table 4.3. Summary of experiments, induction time, gas consumption and water to hydrate conversion; experimental pressure and temperature used was 7.0 MPa and 273.65 K respectively (CO₂+H₂ gas mixture). Amount of water used for all the experiment was 27 cm³.

System	Exp. No.	Induction time (IT) (min)	Normalized rate of hydrate formation, NR ₃₀ (mol.min ⁻¹ .m ⁻³)	End of Experiment		Final water to hydrate conversion (% mol) [#]	Average water to hydrate conversion (% mol±SD)
				Time (min)	Mol of gas/mol of water		
CO ₂ +H ₂ +Silica sand	S1	66	9.8	600	0.031	21.6	26.9±4.6
	S2	48	8.2	600	0.042	30.1	
	S3	20	16	600	0.041	29.1	
CO ₂ +H ₂ +Silica sand+1 wt% SDS	S4	25	100	200	0.090	63.8	57.4±7.9
	S5	5	90.8	120	0.074	52.6	
	S6	36	76	200	0.069	48.8	
	S7	59.7	110	150	0.091	64.6	
CO ₂ +H ₂ +Silica sand+0.5 wt% SDS	S8	840	81	950	0.082	58.2	47.8±7.4
	S9	94	76	200	0.062	44.1	
	S10	30	57	350	0.067	47.8	
	S11	38	47	120	0.058	41.2	
	S12	68	68.5	200	0.047	33.7	
CO ₂ +H ₂ +Silica sand+0.1 wt% SDS	S13	2	40	80	0.047	33.7	26.7±6.6
	S14	10	39.13	100	0.034	24.4	
	S15	332	32	450	0.030	21.6	
	S16	8	31.5	100	0.028	20.0	
	S16	8	31.5	100	0.028	20.0	
CO ₂ +H ₂ +SSP+1 wt% SDS	SP1	2	104	70	0.098	69.6	71.9±4.1
	SP2	1.2	132	60	0.093	65.7	
	SP3	4	83	70	0.106	75.3	
	SP4	NN*					
	SP5	3.4	130	70	0.103	73.1	

[#]Hydration no. of 7.09 was used for calculation (Kumar et al., 2009)

*Not Nucleated till 24h

SD=Standard deviation

Figure 4.9 compares the hydrate growth rate (post nucleation event) in silica sand packing with and without SDS. Three SDS concentrations (0.1, 0.5 and 1 wt%) were used. Average gas uptake data from repeat experiments (3-5 repeat runs) has been presented along with standard deviation (for the first 60 minutes). Time zero in the graph corresponds to nucleation point for all the experiments conducted. As seen in the figure, rate of hydrate formation is slowest in absence of SDS and increases with SDS concentration in the solution. In absence of SDS, only 8-10% water to hydrate conversion was achieved inside the first 60 minutes. These results match quite well with existing information in literature. Babu et al have reported 28-30% conversion in 40 hours, albeit at slightly higher driving force (Babu et al., 2013c). Figure 4.9 also shows that maximum water to hydrate conversion was achieved with 1 wt% SDS; approximately 50% water to hydrate conversion was achieved inside the first 60 minutes (Average water conversion at the end of experiments (4 runs) was 57.4 ± 7.9). This clearly shows that SDS enhances hydrate growth rate and maximizes water to hydrate conversion for fuel gas mixture.

Several mechanisms have been suggested for enhanced hydrate growth rate in SDS solution; increase in gas solubility is one of the likely reasons for enhanced hydrate growth (Ownby, 1997; Ricaurte et al., 2012). The most cited explanation for the enhanced hydrate growth in presence of surfactant is the capillary driven supply of the water from the porous hydrate layer. Capillary driven supply of water to the interface allows more and more water to come in contact with hydrate forming gases even in the presence of solid hydrate phase at the interface.

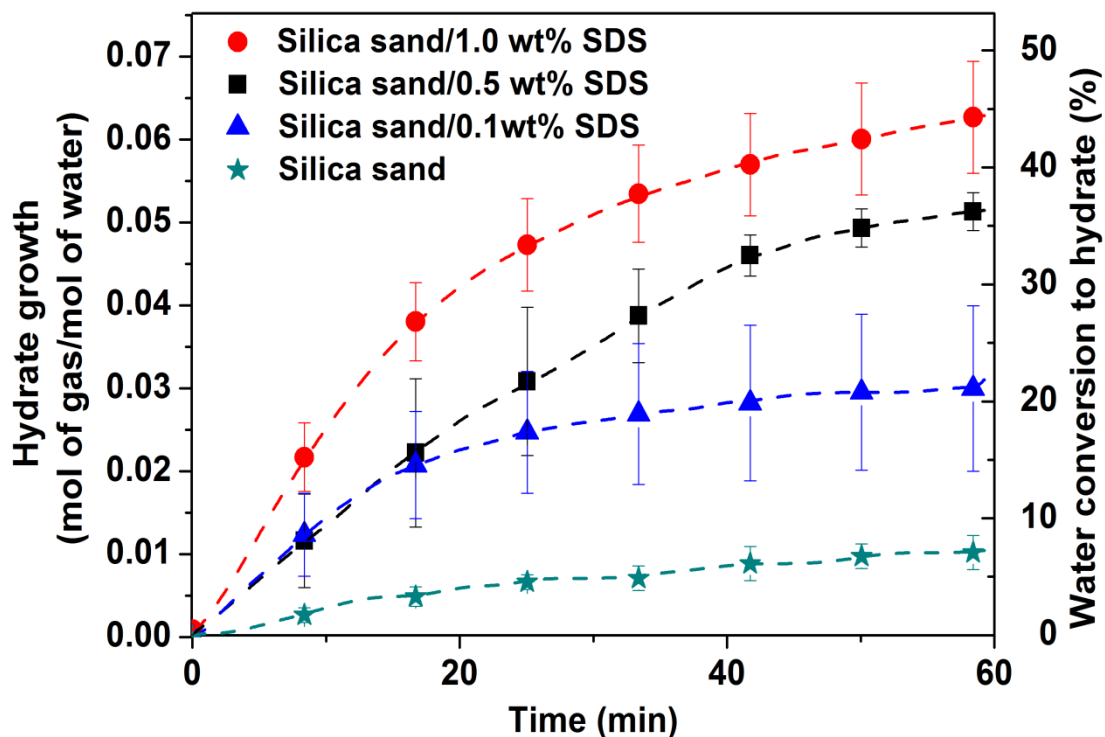


Figure 4.9. Comparison of gas consumption for hydrate growth measured for different concentration of SDS (1, 0.5, 0.1 wt%) in silica sand media. Time zero in the graph corresponds to nucleation point

Figure 4.10 shows some of the gas uptake measurements for experiments conducted in silica sand and metallic packing bed in presence of 1 wt% SDS. Time zero in the graph corresponds to nucleation point (induction time). It can be seen that the initial hydrate growth (for the first 15 minutes after nucleation) is almost the same for both the fixed bed media studied. However, due to efficient heat transfer, the hydrate growth rate in case of metallic packing (SSP) does not slow down and results in significantly higher water to hydrate conversion as compared to silica sand for a fixed time period. The enhanced water to hydrate conversion in SSP can be explained on the basis of bed height and gas cap. As can be seen in figure 4.1, the bed height necessary for 27 cm^3 of water is 2.3 cm for silica sand whereas for SSP it is 1cm. A smaller bed height ensures efficient transfer of hydrate forming gases to the bottom of the reactor thus ascertaining better water to hydrate conversion. Water to hydrate conversion in SSP was found to be 70-73% in one hour of hydrate growth. It is noted that this is the highest conversion ever reported for fuel gas mixture at this scale. The low water to hydrate conversion in silica sand bed for the first hour of hydrate formation is mainly due to mass transfer limitations. A quick review of literature also suggests that change in bed height

significantly alters the hydrate growth rate and in turn, the water to hydrate conversion (Babu et al., 2014b). Most of these studies were reported using silica sand as the fixed bed medium (drop in conversion with bed height); figure C8 in the appendix C represents hydrate growth and water to hydrate conversion along with temperature profile for CO_2+H_2 gas mixture with SSP bed heights of 2.2 cm and 1.0 cm, while keeping the water content of the bed constant. It can be clearly seen from the figure that there is no significant difference in the two gas uptake profiles and water to hydrate conversion is independent of bed height in the case of SSP packing. This result is pivotal to the scale-up potential of the HBGS process. From figures 4.9 and 4.10, it can be seen that the rate of hydrate growth is almost linear till about 30 minutes. We have calculated the rate of hydrate formation (R_{30}) by linearly fitting the hydrate growth (gas consumed) data versus time and subsequently calculated the normalized rate of hydrate formation (NR_{30}) using equation 3. The calculated rates were averaged and are presented in figure 4.11 along with standard deviations for all the systems. As seen in the figure, initial rate of hydrate growth for SSP system in presence of 1 wt% SDS is $\sim 112.3 \pm 23.3 \text{ mol} \cdot \text{min}^{-1} \cdot \text{m}^{-3}$, the mean value is slightly higher than that studied with silica sand packing with 1 wt% SDS ($\sim 94.2 \pm 14.45$). A comparison of gas uptake for hydrate formation (for the first 120 minutes after nucleation) from data available in literature is shown in table 4.4. Gas uptake data as a function of driving force for different fixed bed media as well as employing stirred tank reactor for the HBGS process pertaining to pre-combustion capture of CO_2 has been compared in Figure 4.12. It can be seen that SSP with 1 wt% SDS shows significantly faster hydrate growth kinetics compared to data reported in the literature.

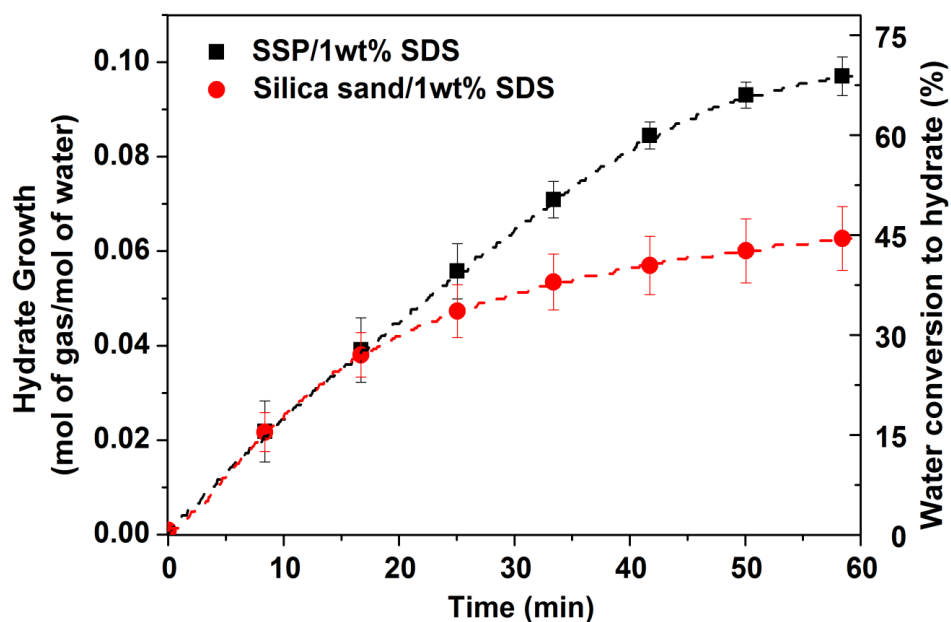


Figure 4.10. Comparison of gas consumption for hydrate growth measured for two different fixed bed media in presence of 1wt% SDS. Time zero in the graph corresponds to nucleation point

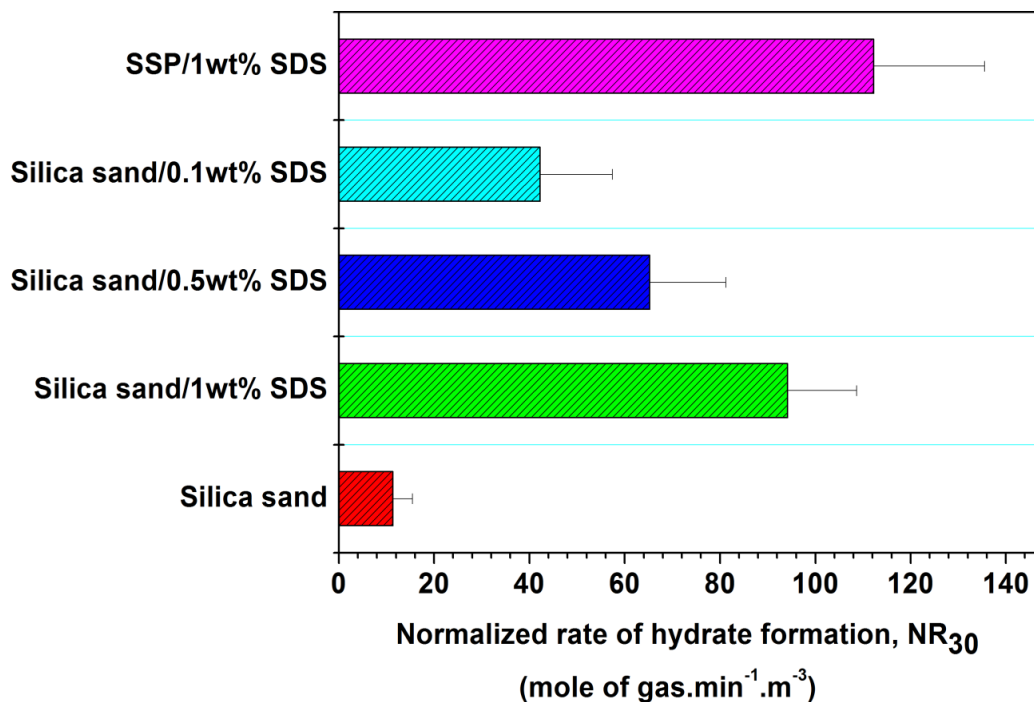


Figure 4.11. Normalized rate of hydrate formation for different fixed bed media with different concentration of SDS, calculated for first 30 minutes after nucleation.

Induction time for gas hydrate formation is an important characteristic of kinetic studies. Table 4.3 and figure C9 (appendix C) represents the induction time for all the experimental runs with average value and standard deviation. Induction time is stochastic phenomenon and the information provided in the figure may change slightly if induction time is averaged over many more experimental runs; nevertheless it gives a good indication of the ease of hydrate nucleation. As seen in the figure and table, SSP packing has the shortest induction time followed by silica sand with 1 wt% SDS. Out of the four experiments carried out in silica sand with 0.5 wt% SDS, one did not nucleate for a long time (Table 4.3). Babu et al. have also reported similar induction time for fuel gas mixture using silica sand and silica gel media (Babu et al., 2013b). Shorter induction time for hydrate formation is highly favorable for a hydrate based gas separation process (HBGS) as it drastically reduces operational costs by reducing the residence time of reaction.

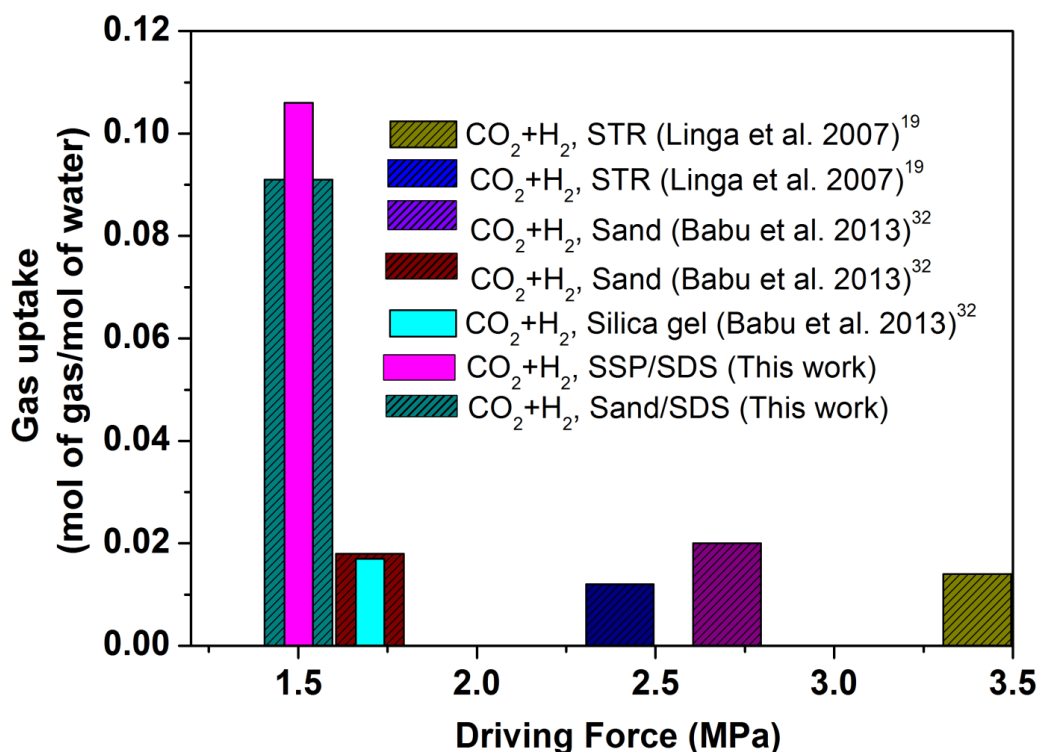


Figure 4.12. Comparison of gas uptake as a function of driving force for different fixed bed media and stirred tank reactor. The data presented is for 120 minutes of hydrate growth.

Table 4.4. Comparison of gas uptake measurement for stirred tank reactor and fixed bed media, relevant experimental details are also included. Data presented is for 120 minutes of hydrate growth (after induction time)

System	Contact mode	P _{exp.} (MPa)	T _{exp.} (K)	Driving Force (~MPa)	Gas consumed (mol/mol of water)	Ref.*
CO ₂ (40)+ H ₂ (60)+Water	Stirred tank	8.5	273.70	3.4	0.014	Linga et al. 2007a
	Stirred tank	7.5	273.70	2.4	0.012	Linga et al. 2007a
	Silica Sand	8.5	274.15	2.7	0.020	Babu et al., 2013b
	Silica Sand	7.5	274.15	1.7	0.018	Babu et al., 2013b
	Silica Gel	7.5	274.15	1.7	0.017	Babu et al., 2013b
	Silica Sand/1wt%SDS	7.0	273.65	1.5	0.091	This Work
	SSP/1wt%SDS	7.0	273.65	1.5	0.106	This Work

*We took utmost care to compare similar data from literature in terms of operating temperature and pressure, please note that a small change in temperature may have a significant impact on gas hydrate kinetics

4.8.2. Hydrate formation kinetics of fuel gas mixture in Copper Foam and Brass packing

Table 4.5 summarizes all the experiments performed with CO₂ + H₂ gas mixture and copper foam & Brass packing during this study; relevant information including experimental pressure & temperature, duration of experiments, moles of gas consumed at the end of the reaction and water to hydrate conversion have been reported.

Figure 4.13 presents the hydrate formation/dissociation cycles (P-T Curves) with temperature profile obtained with CO₂/H₂/copper foam/SDS (1wt%) and CO₂/H₂/brass packing/SDS (1wt%) at 273.65 K and 7.0 MPa. Experiments were carried out in batch mode; upon hydrate formation, pressure starts to drop which involves gas dissolution, nucleation and hydrate growth stages. As seen in the figure 4.13, in fresh run hydrate nucleates quickly which coincides with a sharp increase in temperature (and sudden pressure drop) due to exothermic nature of hydrate nucleation while as can be seen in the figure, rise in temperature due to hydrate nucleation is minimum in copper foam compared to brass packing. Pressure drop due to hydrate nucleation and growth continues till there is not enough driving force for further hydrate growth; at this point a constant pressure profile is observed. An inefficient heat transfer in the fixed bed media would eventually be a major bottleneck in achieving faster growth kinetics (Kumar et al., 2015a). Thus copper foam is found to be a good packing material which helps in efficiently removing the localized heat during hydrate nucleation and enhancing hydrate growth rate. The formed hydrate is dissociated by increasing the temperature of the water bath to 293.15K, which initiates hydrate decomposition resulting in rise of the total pressure of the reactor. After a complete dissociation of hydrates (till we see no further rise in pressure of the reactor) temperature was again set at the experimental temperature (273.65 K) which follow the same trend; gas dissolution, nucleation and hydrate growth. It is evident that figure 4.13 shows the good repeatability.

Table 4.5. Summary of experiments, gas consumption and water to hydrate conversion; experimental pressure and temperature used was 7.0 MPa and 273.65 K respectively.

System	Exp. No.	Amount of water used (cm ³)	End of Experiment		Final water to hydrate conversion (% mol) [#]	Average water to hydrate conversion (% mol±SD)
			Time (min)	Mol of gas/mol of water		
CO ₂ +H ₂ +Brass+1 wt% SDS (1cm bed height)	B1	27	60	0.105	74.4	65.5±6.3
	B2	27	80	0.088	62.4	
	B3	27	80	0.084	60.0	
	B4	27	100	0.092	65.2	
CO ₂ +H ₂ +Cu Foam+1 wt% SDS (1cm bed height)	C1	27	100	0.101	71.6	72.2±6.0
	C2	27	100	0.098	69.5	
	C3	27	100	0.090	63.8	
	C4	27	80	0.099	70.2	
	C5	27	100	0.110	78.0	
	C6	27	120	0.113	80.1	

[#]Hydration no. of 7.09 was used for calculation (Kumar et al., 2009)

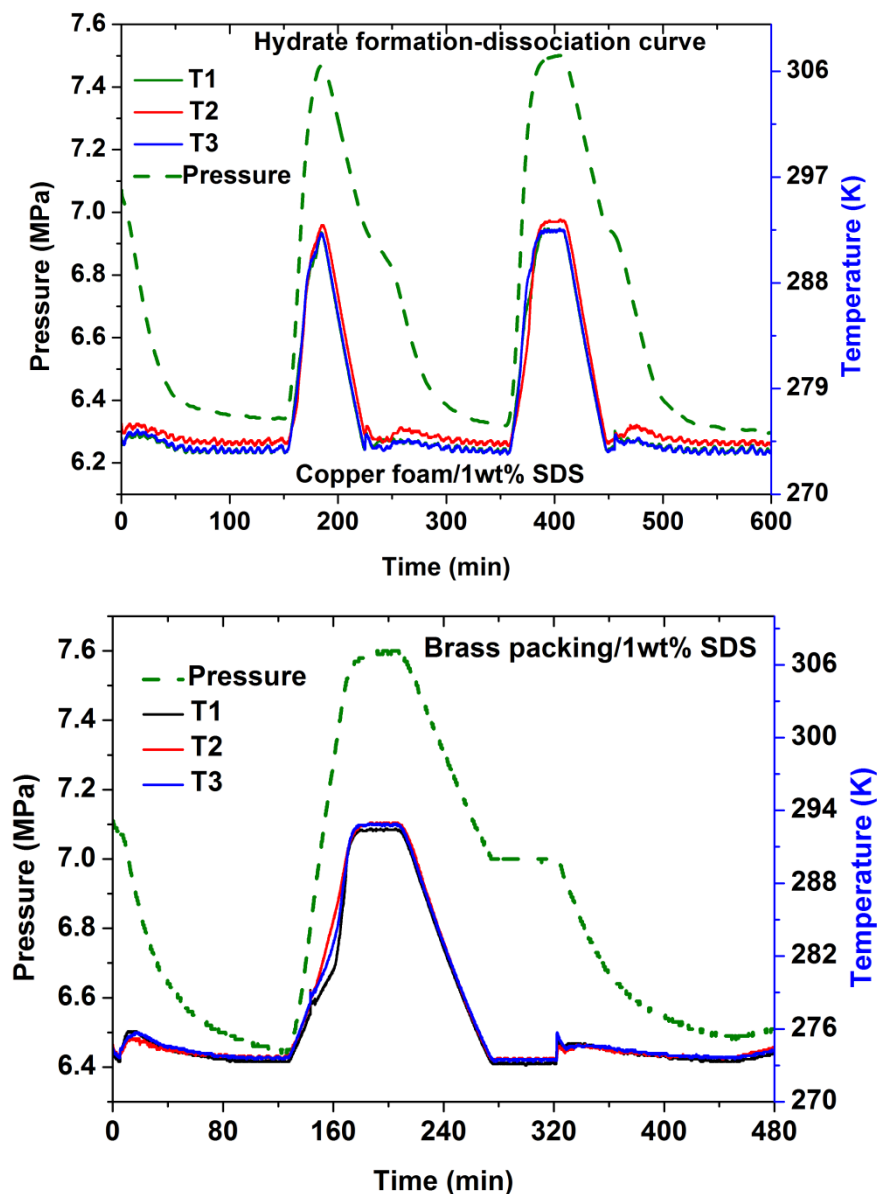


Figure 4.13. Hydrate formation-dissociation curve for copper foam and brass packing in presence of 1wt% SDS, along with temperature profile at 7.0 MPa and 273.65 K

Figure 4.14 represents the morphology of hydrates formed in the copper foam using CO_2/H_2 gas mixture at 7.0 MPa and 273.65 K. Porosity of copper foam was approximately 90- 98% and number of pores per inch (PPI) is 5-120. Pores are interconnected to each other (see figure C3, Appendix C). It is assumed that hydrate nucleated in the pores of copper foam and spread through the interconnected channels. Hydrate crystal growth in the upward direction towards the gas phase is typical of hydrate formation in presence of surfactants which allows water from

the bottom of the reactor to rise through capillary action. Figure 4.14 shows the hydrate growth above the copper foam and grows upward along the crystallizer walls.

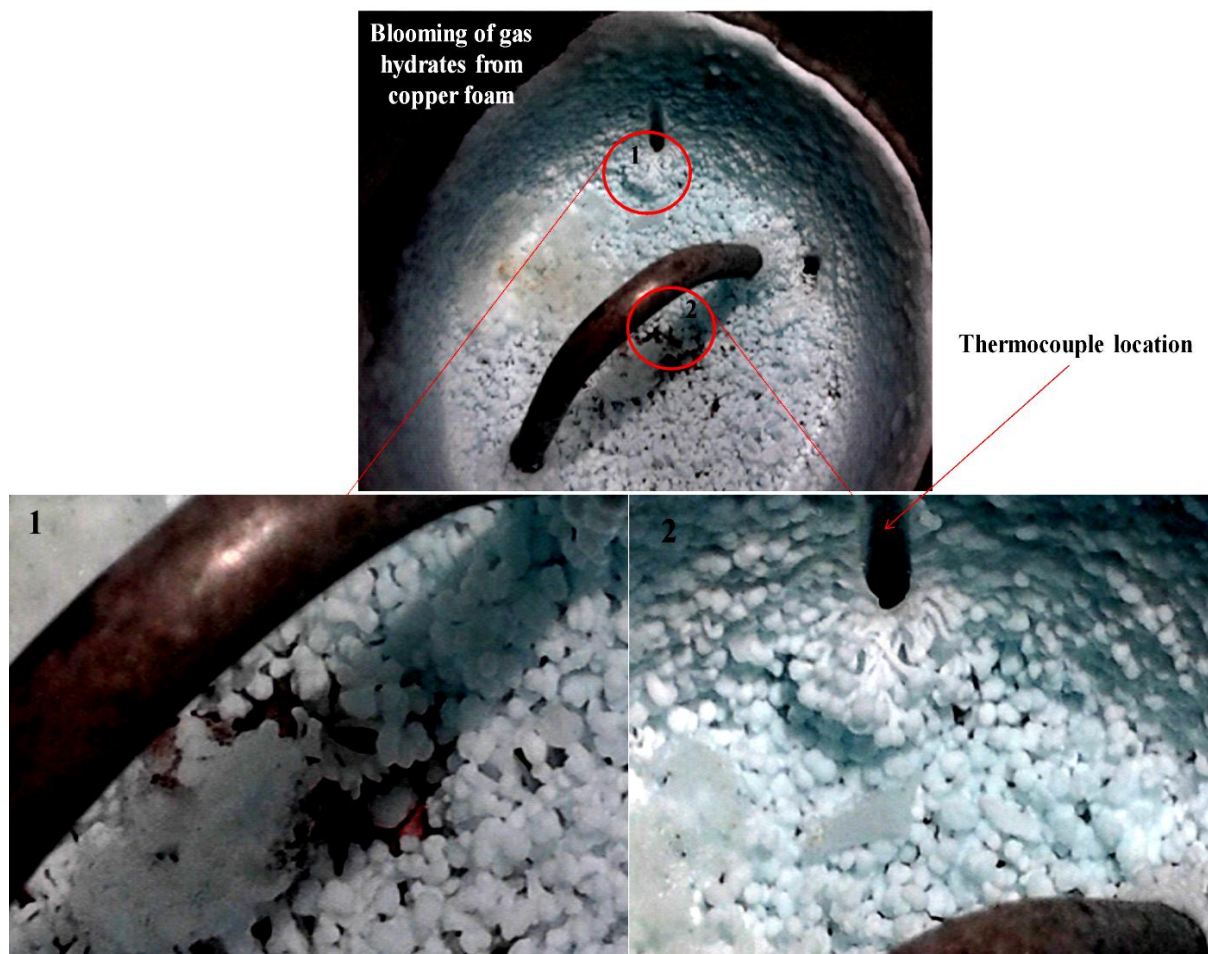


Figure 4.14. Blooming of Hydrates during formation in copper foam at 7.0 MPa and 273.65K

Figure 4.15 shows a typical gas uptake curve (in brass packing) along with the temperature profile conducted at 7 MPa and 273.65 K. In Figure 4.15, the induction time occurred at 90 min. However, induction time (nucleation) is stochastic phenomenon and it depends on number of factors including driving force for hydrate formation. On average it was seen that induction time for hydrates in copper foam was found to be shorter which would be beneficial for HBGS process and CO₂ capture/separation.

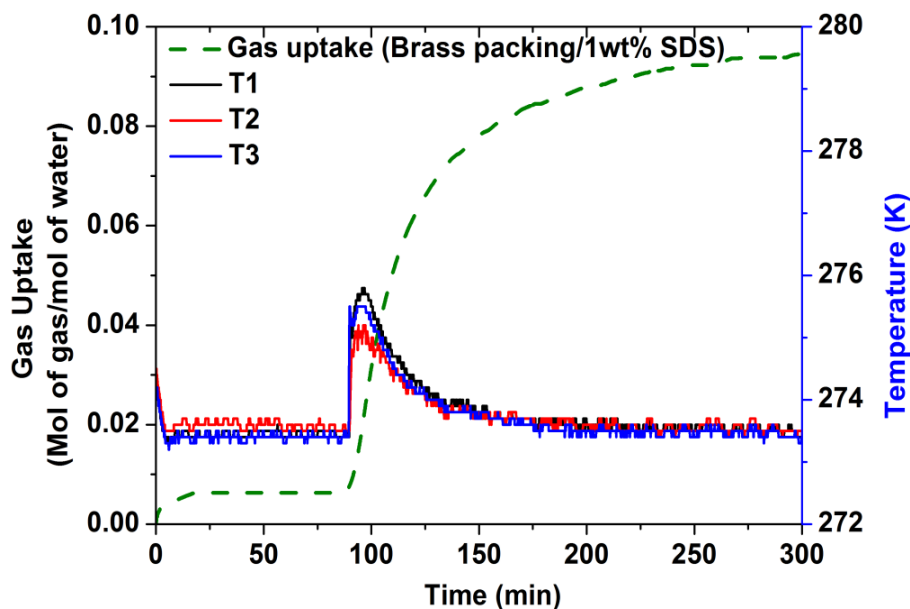


Figure 4.15. Typical gas uptake measurement curve for Brass/1wt% SDS system together with the temperature profile at 7 MPa and 273.65 K

Figure 4.16a compares the hydrate growth in three different fixed bed media (Brass, copper and sand) with 1wt% SDS. It is noted that three different SDS concentrations (0.1, 0.5 and 1 wt%) has already been used in our previous study where 1wt% was found to be the best concentration for enhanced kinetics (Kumar et al., 2015b). Gas uptake data from repeat experiments has been presented with standard deviation (for the first 80 min). Time zero in the graph corresponds to nucleation point for each experiment. As seen in the figure, initial rate of hydrate formation (first 10-20 min) is almost similar in all the packing media. However, after 20 minutes, a significantly higher rate and maximum water to hydrate conversion (~70%) was achieved in metallic bed (brass and copper foam). If one compares the extent of water to hydrate conversion in these experiments, it clearly shows that SDS enhances hydrate growth rate and maximizes water to hydrate conversion. Several mechanisms have been presented in the literature for enhanced hydrate growth rate in SDS solution. The most accepted explanation for the enhanced hydrate growth in presence of SDS is the capillarity driven supply of the water from the porous hydrate layer. Capillary driven supply of water to the interface allows more and more water to come in contact with hydrate forming gases even in the presence of solid hydrate phase at the interface (Okutani et al., 2008, Pang et al., 2007, Kumar, 2013, 2015a).

The calculated normalized rates of hydrate formation (NR_{30}) using equation 3 was averaged and are presented in figure 4.16b along with the standard deviations for all the systems. As seen

in the figure, initial rate of hydrate growth for brass and copper system in presence of 1 wt% SDS is significantly high ~ 141 and 133 and $\text{mol}\cdot\text{min}^{-1}\cdot\text{m}^{-3}$ respectively which are higher than silica sand media. Such a high rate of hydrate growth provides an excellent opportunity to scale up the HBGS process for CO_2 capture/separation from fuel gas mixture. (Babu et al., 2013a).

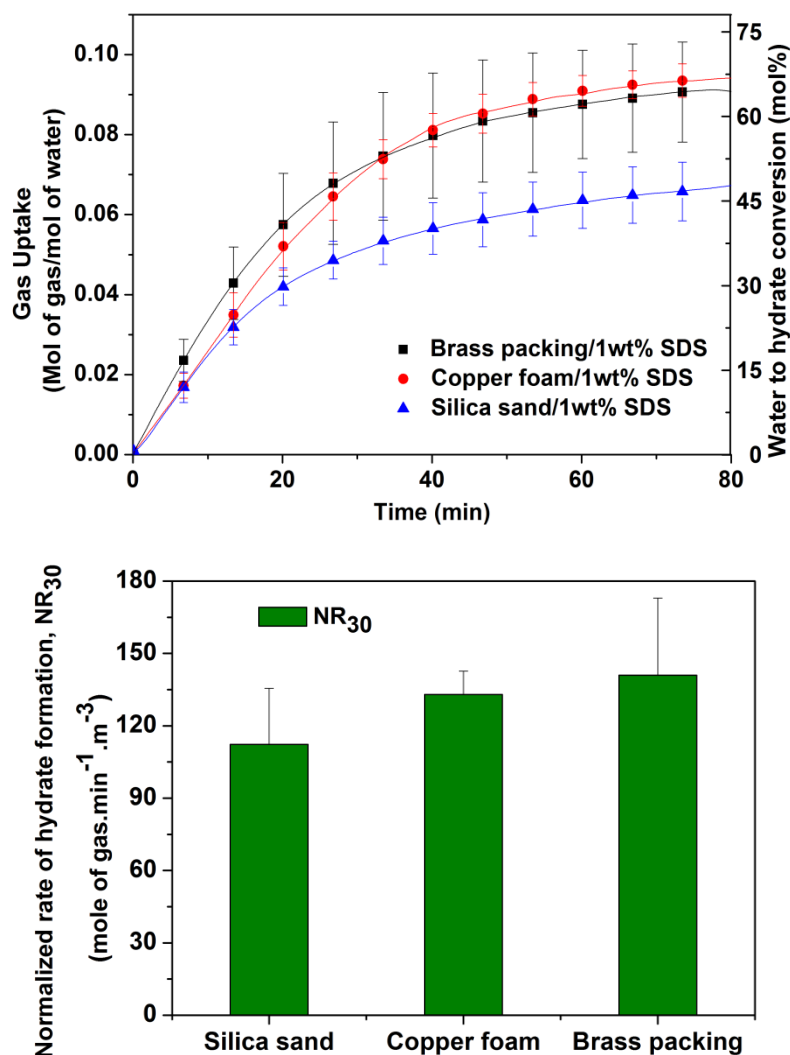


Figure 4.16. (a) Comparison of gas uptake for hydrate growth measured for different fixed bed media (Brass, copper and sand). Time zero in the graph corresponds to nucleation point (induction time) (b) Normalized rate of hydrate formation with 1wt% of SDS, calculated for first 30 min after nucleation.

4.8.3. Hydrate dissociation kinetics of fuel gas mixture in silica sand, Copper Foam and Brass packing

HBGS process involves hydrate formation and decomposition cycle to separate gas mixtures, thus it is important to understand the dissociation profile of the solid hydrate phase in different

fixed bed media utilized in this study. To evaluate the effect of fixed bed media on dissociation kinetics, formed hydrates were decomposed at 20°C (293.15K). This approach resembles a typical thermal stimulation technique of hydrate dissociation. Figure 4.17a shows the normalized gas release in three fixed bed media (silica sand, brass and copper foam) in presence of 1wt% SDS. As can be seen from the figure, the normalized gas release from copper foam is faster compared to brass and silica sand. Normalized rate of gas release was also calculated for first 20 minute (NR₂₀) using equation 4 (below) and are presented in figure 4.17b.

Rate of hydrate dissociation (R_{20} in normalized gas release $\cdot \text{min}^{-1}$) is calculated by fitting the normalized gas release data versus time for the first 20 min during dissociation at 293.15K. (See figure C10, Appendix C)

$$\text{Normalized rate of hydrate dissociation (NR}_{20}) = \frac{R_{20}}{V_w} (\text{normalized gas release} \cdot \text{min}^{-1} \cdot \text{m}^{-3}) \quad (4)$$

Where, V_w is the volume of water taken for the experiment in m^3 .

As can be seen from the figure 4.17b, the initial rate of gas release from hydrates synthesized in copper foam is almost double of hydrates in silica sand and brass packing. However, it should be noted that the porosity of all the three packing's were quite different and a proper comparison of hydrate formation kinetics and decomposition kinetics cannot be made unless we use three different packing material of same porosity.

Sequential images of hydrate formation and dissociation in copper foam bed along with the pressure and temperature profile during hydrate dissociation by thermal stimulation are presented in figure 4.18. It can be clearly seen in the figure that the temperature profile of the thermocouples located in the bed deviates. This is mainly due to endothermic nature of the hydrate decomposition. Sequential images of hydrate formation and dissociation in brass bed along with the pressure and temperature profile during hydrate dissociation by thermal stimulation are also presented in figure 4.19.

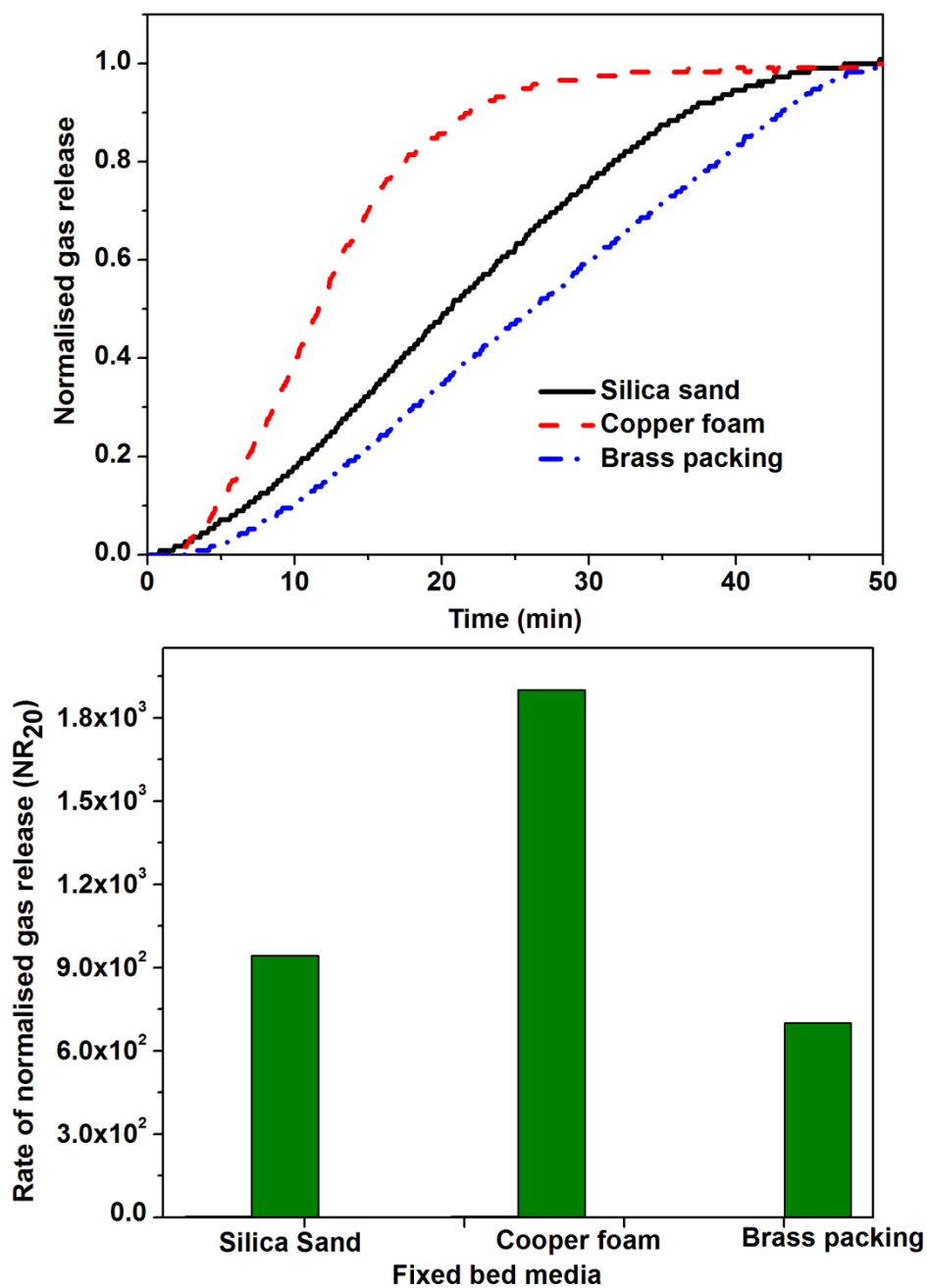


Figure 4.17. (a) Normalized gas release curves for hydrate decomposition in silica sand, copper foam and brass bed. The results are normalized at the dissociation time of 50min for all the experiments. (b) Normalized rate of hydrate dissociation for different fixed bed media with 1wt% of SDS, calculated for first 20 min after nucleation (NR_{20}).

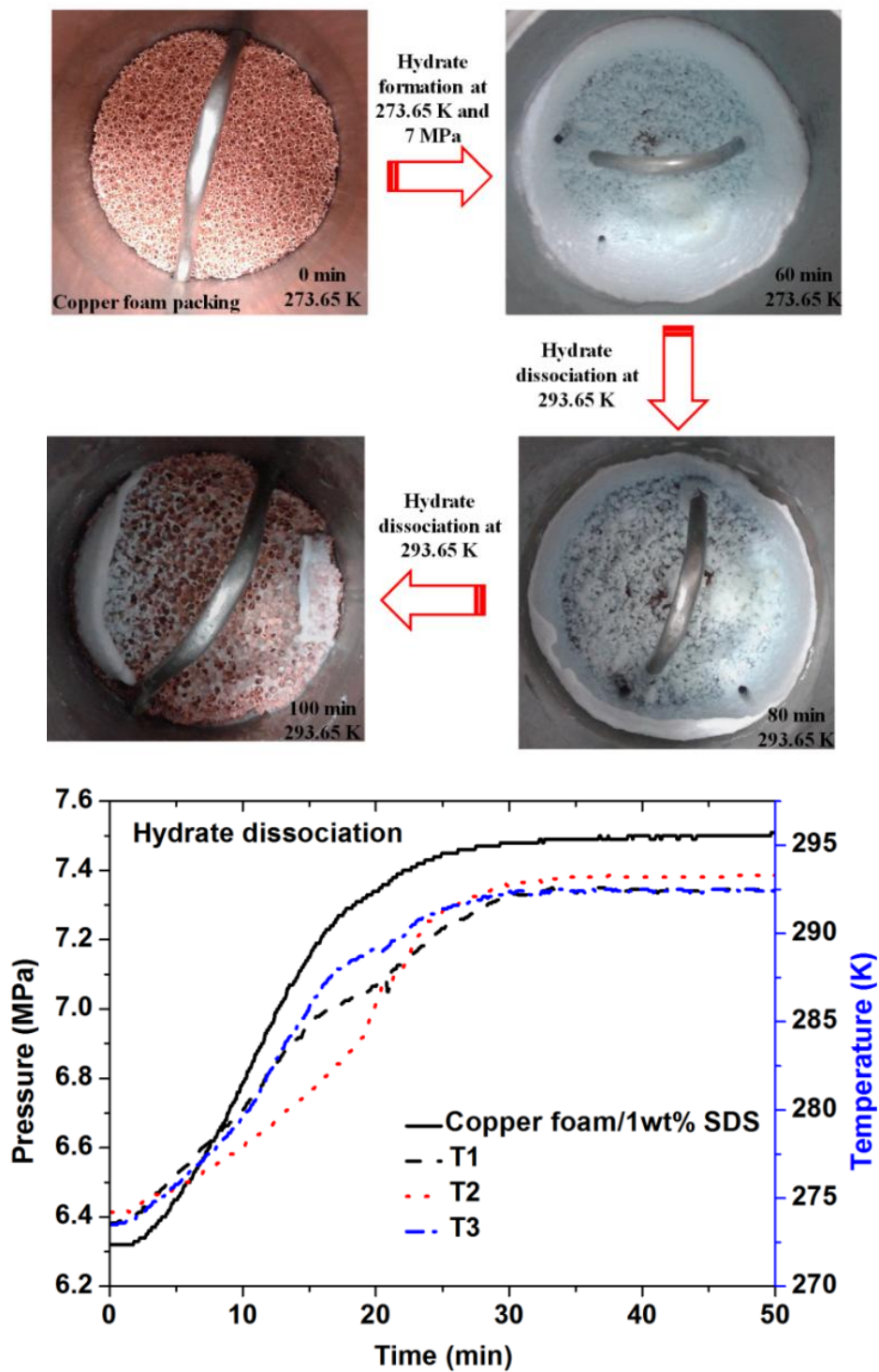


Figure 4.18. Sequential images of hydrate formation and dissociation in copper foam bed along with the pressure and temperature profile during hydrate dissociation by thermal stimulation

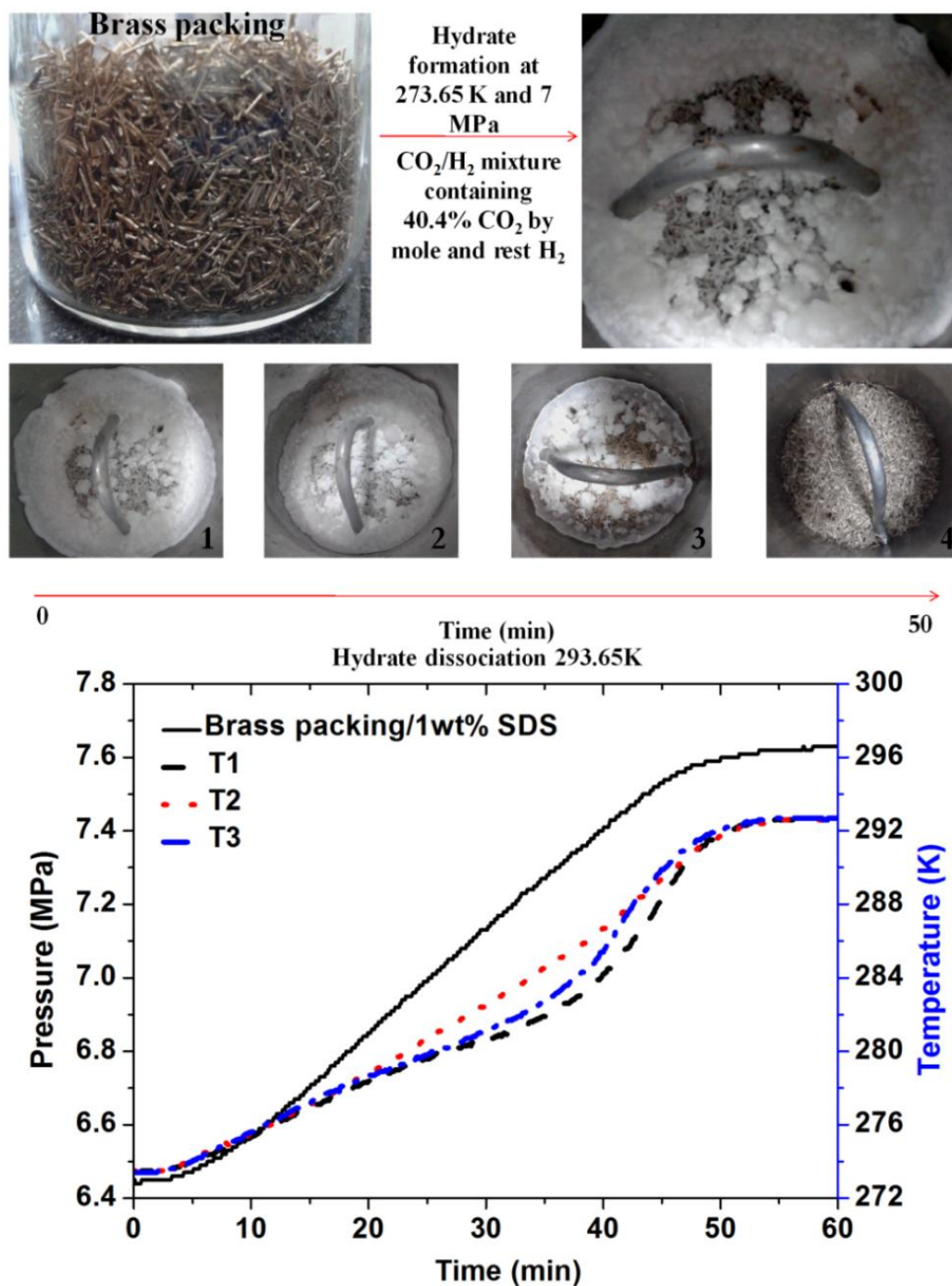


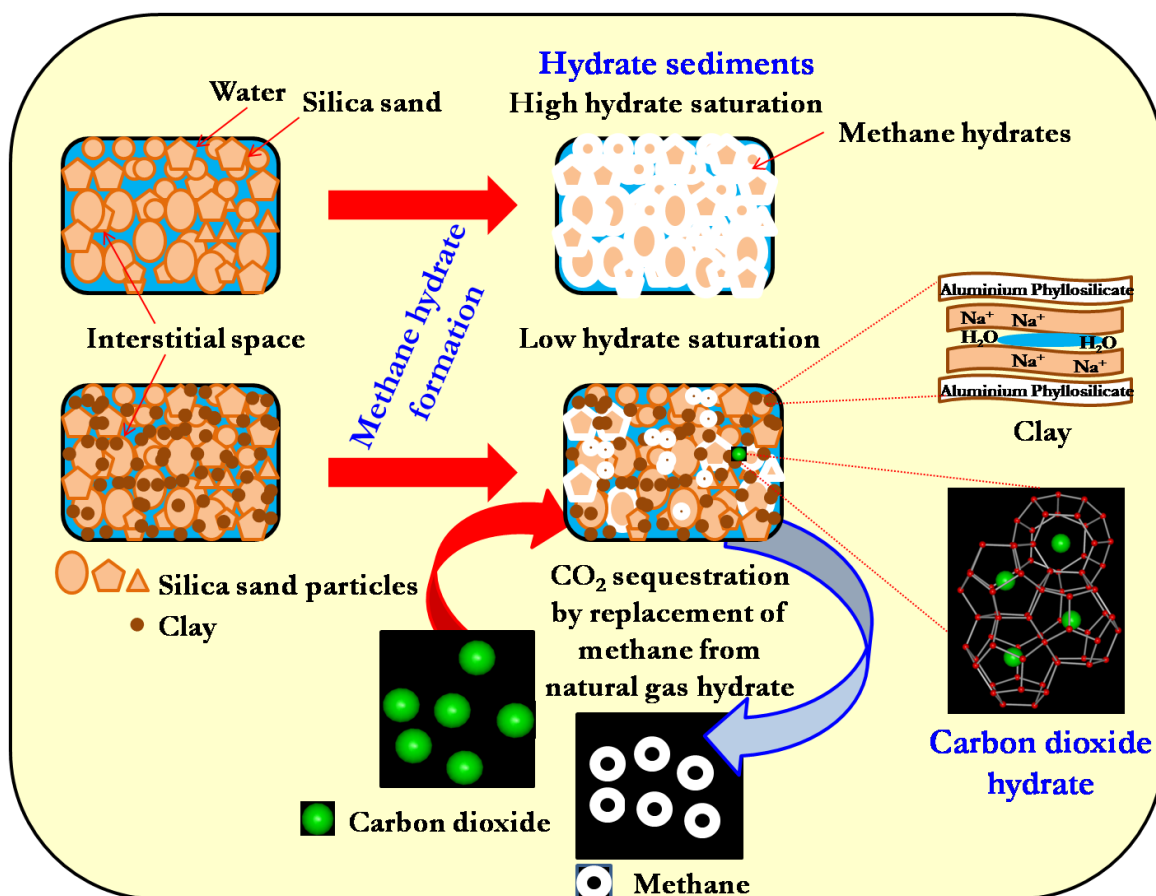
Figure 4.19. Sequential images of hydrate formation and dissociation in brass bed along with the pressure and temperature profile during hydrate dissociation by thermal stimulation

4.9. Conclusions

Hydrate formation and dissociation experiments were conducted in an unstirred reactor to study the kinetics of HBGS process using pure CO₂ and fuel gas (CO₂+H₂) mixture. The unstirred reactor with metallic packing showed better kinetic performance over silica sand packing and stirred tank reactor. The effect of different concentrations of SDS on hydrate formation was investigated; it was conclusively proven that the addition of SDS resulted in a faster rate of hydrate formation. With 1 wt% SDS-water solution and metallic packing, water to hydrate conversion of $\sim 71.0 \pm 4.1$ mol% was achieved for CO₂+H₂ gas mixture. The normalized rate (NR₃₀) of hydrate formation for the first 30 minutes of hydrate growth with metallic packing was calculated to be highest at 7.0 MPa and 273.65 K. This is the highest conversion with maximum rate ever achieved, when forming hydrates with CO₂+H₂ gas mixture. Rate of hydrate dissociation in copper foam was found to be almost double of hydrates synthesized in silica sand and brass packing. However, it should be noted that the porosity of all the three packing's were quite different and for a proper comparison of hydrate formation kinetics and decomposition kinetics porosity should be same. This proposal has been discussed in future work; which will be an important parameter in scaling up the HBGS process for CO₂ capture.

Chapter 5

Carbon dioxide sequestration by replacement of methane from natural gas hydrate reservoir



5. Carbon dioxide sequestration by replacement of methane from natural gas hydrate reservoir⁵

⁵A version of this chapter has been published in following manuscript.

Kumar A, T Sakpal, S Roy, R Kumar, Methane hydrate formation in a test sediment of sand and clay at various level of water saturation, Canadian Journal of Chemistry, 2015, 93(8): 874-881.

5.1. Introduction

As stated in chapter 1, occurrences of natural gas hydrates are predominant and potential reserves of natural gas hydrates are over $1.5 \times 10^{16} \text{ m}^3$ which is distributed all over the earth in the Arctic on land and offshore (Makogon et al., 1971, 2007; Milkov et al., 2004; Kvenvolden et al., 1993; Klauda et al., 2005). For methane recovery from sea bed sediments, it is important to understand the gas hydrate formation and decomposition kinetics. Suitable experiments simulating the natural environment can be conducted in a lab scale setup in test sediment beds of silica sand, sandstone and clay.

It is well known that most of the gas hydrates (methane hydrates) exist in the form of inclusions within sediment (containing silica sand, sand stone, clays etc), with only ~6% naturally occurring bulk hydrates has been reported (Handa et al., 1992). Zhang et al., have speculated that the sediment lithology has a significant impact on the formation conditions and the reaction characteristics of gas hydrates (Zhang et al., 2013). Physical properties of gas hydrate-bearing sediments can obviously be affected by porosity, water and hydrate content (Waite et al., 2002; 2004) and configurations and properties of natural media. It can't be completely simulated through mathematical models alone unless suitable experimental data on laboratory scale is available (Rempel et al., 2011).

Indian National Gas Hydrate Program (NGHP-01) in 2006 which was designed to investigate the geological and geochemical control on gas hydrate occurrence has reported that a significant resource in Indian subcontinent has clay bearing sediments. Most of the "hydrate reservoirs" are dominated by soft clay, clay stone and a little sand in the sediment (Ramana, 2009). In a separate study for NGHP-01, Lee and Collett has found 80% saturated hydrate bearing sediments and 26% hydrate saturated sediments existing simultaneously at the same

drilling site (Lee and Collett, 2009). Most of the study at laboratory scale has been performed on pure silica sand to understand the hydrate formation and decomposition kinetics and thus it is important to understand the effect of clay which might control the extent of hydrate saturation in certain sediments. A reliable assessment of the feasibility of producing natural gas from the earth's naturally occurring hydrates requires several pieces of key information. Through this work it was proposed that at a laboratory scale, formation of methane hydrate in presence of different custom designed porous sediments of varying particle sizes having water in its pores can be performed which would act as a synthetic hydrate bed. In the present work, silica sand and clay were mixed in different proportion with different water saturation levels. Three water saturation levels (100, 75 and 50%) were chosen for hydrate formation. Methane can be recovered from hydrate bearing sediments by depressurization, heating or chemical injection. These methods are based on promoting CH_4 hydrate decomposition by external stimulation. An accurate method for estimating the dissociation rate of methane hydrate would be necessary to predict the methane production rate from a methane hydrate bearing sediment. In particular, the injection of carbon dioxide (CO_2), into hydrate bearing sediments can preferentially liberate some of the enclathrated methane (CH_4), and simultaneously sequester CO_2 in hydrate form. The chemical potential difference between CH_4 and CO_2 hydrates indicates that a mixed hydrate of CH_4 - CO_2 gas mixture is thermodynamically favorable at certain temperature and pressure compared to pure methane hydrate. However, kinetics under field trial and extent of methane replacement are determined by multiple factors, such as

- i. Temperature and pressure condition (refer the hydrate phase diagram of methane and carbon dioxide)
- ii. Mass transfer limitations (permeability, density and viscosity of hydrate bearing sediment) and solubility of CO_2 and CH_4 in sea water
- iii. Heat transfer considerations, which directly affect the local phase boundary (remember gas hydrate formation & decomposition are exothermic and endothermic respectively)
- iv. Structure transition during replacement process and molecular level cage dynamics of CH_4 and CO_2 (it is expected that CO_2 may not like to occupy the small cages due to its size thus putting a limitation on maximum CH_4 exploitation from such reserves).

5.2. Methane hydrate formation

5.2.1. Materials

Methane gas with a certified purity of 99.9% was supplied by De-luxe Industrial Gases, India. Silica sand and clay were purchased from Sakalchand & Company Pune, India. For elemental analysis, Energy Dispersive X-ray analysis (EDAX) of silica sand/clay mixture has been used and data is presented in Appendix D (Figure D1). The particle size distribution of silica sand is in the range of 30–400 μm . Silica sand used in this study is the same as that used by Kumar et al. 2015a. Tap water was used in all the experiments without any purification.

5.2.2. Preparation of silica sand/clay bed

To measure the volume of water required to fill the void spaces, 200 g of silica sand and clay mixture (of known composition) was taken in a plastic beaker as shown in the Appendix D (Figure D2a). A known amount of water in small batches were added in the beaker containing the sand mixture till a layer of free water can be seen at the surface of the sand-clay mixture. The beaker was covered and kept for 30 minutes, so that all the pores of the sand get filled by the water. Once no change in the water layer is observed, the beaker was punctured from the bottom and extra water was removed and collected in a measuring cylinder (figure D2b; Appendix D). The difference of this collected water and total water added in the bottle was taken as water required for 100% saturation. It was found to be $\sim 0.20 \pm 0.025 \text{ cm}^3/\text{g}$ for pure silica sand. Same procedure was applied for mixtures of sand and clay, water saturation in each case is reported in table 5.1.

5.2.3. Apparatus and hydrate formation procedure

Detail description of the fixed bed apparatus (Figure 5.1) and the procedure for hydrate formation are given in chapter 2 (Kumar et al., 2013). Briefly, the procedure is as follow. Pre saturated silica sand /clay mixture with water is charged in the reactor (as per table 5.1) this reactor was then placed in a temperature controlled water bath, the reactor is connected with a vacuum pump which is used to evacuate the reactor of any air impurity. Volume of water required to fill the void spaces of the sand clay mixture is given in table 5.1. Circulating ethylene glycol / water mixture from a Julabo circulator is employed to cool the reactor to desire experimental temperature (274.5 K). Once the desired temperature is reached the crystallizer is pressurized by pure methane gas to pre determined experimental pressure.

Crystallizer is equipped with a WIKA pressure transducer of 0-20 MPa range; along with a Bourdon pressure gauge (WIKA) for a quick look at pressure inside the reactor. To

mimic natural gas hydrate formation, hydrate formation at constant methane pressure were employed. A set of mass flow meter and constant pressure controller (MFC) from Brooks was utilized with a data acquisition system to measure and record the flow rate and pressure inside the reactor. Operating pressure for any experiment was the set point for the MFC and as the pressure inside the reactors dropped due to hydrate formation, an equal amount of gas was supplied through the flow meter to maintain the pressure inside the reactor. The gas flow was accurately measured by the flow meter which was used to create a gas uptake profile for hydrate formation. Some of the experiments were done in batch mode where gas uptake measurements were done by recording the pressure drop inside the CR. For temperature measurement, PT-100 RTDs were inserted inside the CR. Figure 5.1 shows the location of the three RTDs in the CR.

Table 5.1. Summary of all the systems used for hydrate formation experiments along with water saturation level.

System	Sand:Clay ratio	Water saturation (%)	Amount used		Volume of water taken (ml)	# volume of water required to fill the void space with water (100% water saturation) cm^3/g
			Silica sand (g)	Clay(Sod. bentonite) (g)		
I	100:00	100	200	0	40	
II	100:00	75	200	0	30	
III	100:00	50	200	0	20	0.20 \pm 0.025
IV	75:25	100	150	50	42	
V	75:25	75	150	50	31.50	0.21 \pm 0.030
VI	75:25	50	150	50	21	
VII	50:50	75	100	100	33	0.22 \pm 0.045
VIII	50:50	50	100	100	22	
IX	25:75	75	50	150	49.5	0.33 \pm 0.06

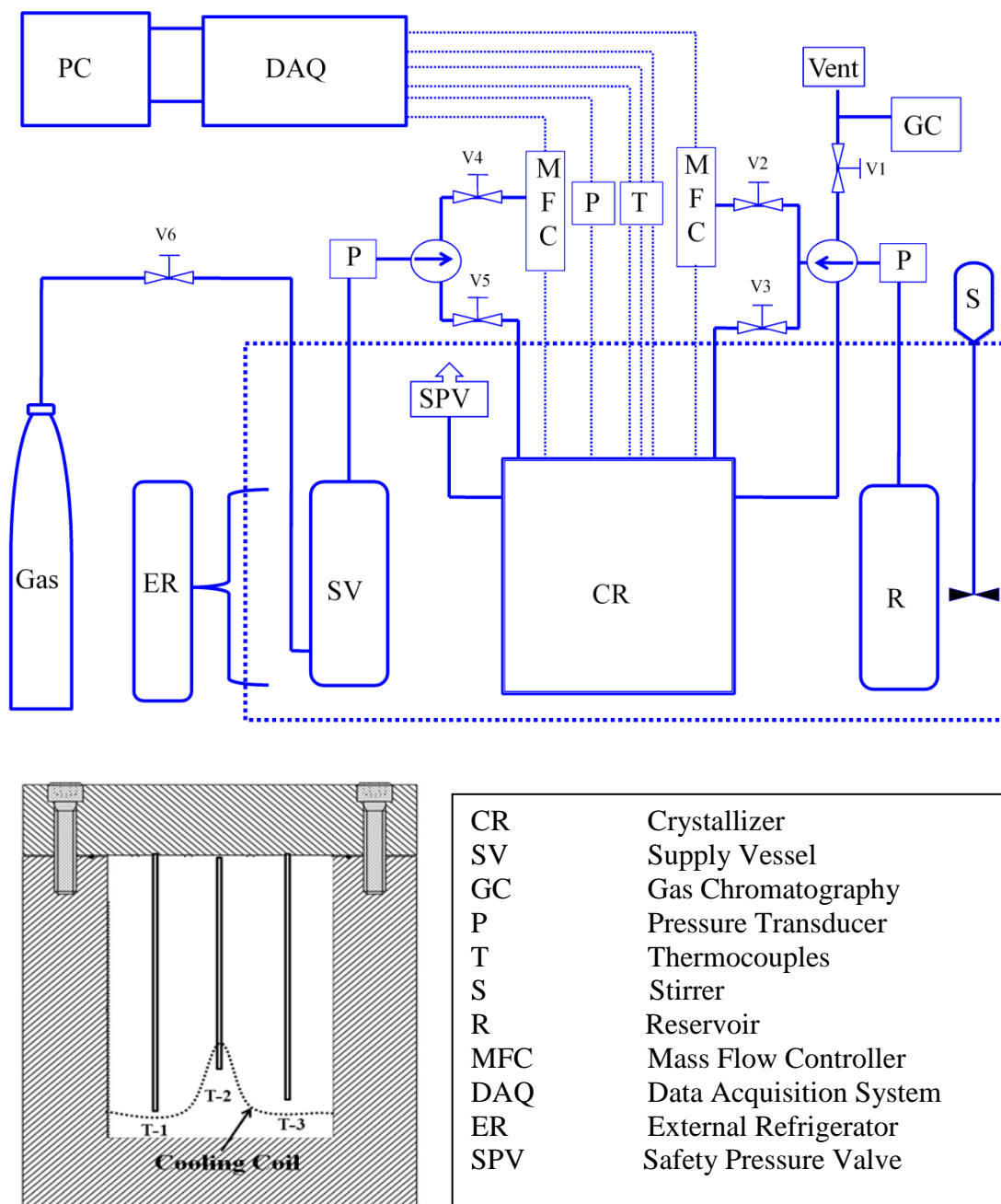


Figure 5. 1. Schematic of experimental setup along with location of thermocouples within the reactor

5.2.4. Calculation for the amount of gas consumed during hydrate formation

Pressure and temperature data were used to calculate the moles of methane consumed in the crystallizer (gas uptake). As the gas in the crystallizer was consumed for hydrate formation, additional gas was supplied from the SV through MFC thus the pressure in the reactor was maintained constant. The number of moles of gas passing through the MFC is recorded with

respect to time. It is important to note that, the gas in the reactor (CR) is supplied from the supply vessel (SV). The supply vessel is also equipped with the pressure gauge, the pressure difference at the start and end of a reaction is noted down to calculate the total amount of gas supplied to the reactor. For this calculation Pitzer's correlation is used. The total number of moles of the gas that have been consumed from the supply vessel for hydrate formation was calculated by equation.

$$n = PV_{SV} / zRT \quad (1)$$

$$Z = 1 + \beta^0 \frac{P_r}{T_r} + \omega \beta^1 \frac{P_r}{T_r} \quad (2)$$

$$\text{Where } \beta^0 = 0.083 - \frac{0.422}{T_r^{1.6}}, \beta^1 = 0.139 - \frac{0.172}{T_r^{4.2}}$$

$$T_r = \frac{T_{\text{exp}}}{T_{\text{critical}}}, P_r = \frac{P_{\text{exp}}}{P_{\text{critical}}}, \omega = \text{Acentric factor}$$

Where z is the compressibility factor calculated by Pitzer's correlation (Smith, J. M, 2001); V_{sv} is the volume of the gas phase of the supply vessel; P & T are pressure and temperature of the crystallizer. This value (moles) was compared with that obtained by the totalizer of the MFC.

5.2.5. Water to hydrate conversion calculation

Conversion of water to hydrate is determined by using the following equation:

$$\text{Conversion of water to hydrate (mol \%)} = \frac{\Delta n_{H,\downarrow} \times \text{Hydration number}}{n_{H_2O}} \times 100 \quad (3)$$

where $\Delta n_{H,\downarrow}$ is the number of moles of gas consumed for hydrate formation at the end of the experiment determined from the gas uptake and n_{H_2O} is the total number of moles of water in the system.

For simple hydrates, the hydration number is related to the fractional occupancy of the large and small cavities, θ_L , and θ_S , respectively as (Sloan and Koh, 2008)

$$\text{Hydration Number } (n) = \frac{46}{6\theta_L + 2\theta_S} \quad (4)$$

The hydration number is the number of water molecules per guest molecule. The hydration number used in the above equation is 6.10 (Tulk et al., 2000).

5.2.6. Calculation of rate of hydrate formation

The rate of hydrate formation is calculated through the forward difference method given below. (Kumar et al., 2014)

$$\left(\frac{d\Delta n_{H,\downarrow}}{dt} \right)_t = \frac{\Delta n_{H,\downarrow(t+\Delta t)} - \Delta n_{H,\downarrow(t)}}{\Delta t}, \Delta t = 30 \text{ min} \quad (5)$$

5.3. Results and discussion

5.3.1. Methane hydrate formation in test sediment

Table 5.2 summarizes the experimental conditions in detail; hydrate formation pressure, water to hydrate conversion, moles of methane consumed to form hydrate and duration of an experiment has been given. Experiments were performed in isothermal and isobaric condition in a semi batch mode, where gas was supplied continuously for hydrate formation. Some of the experiments were conducted in batch mode (reactor was pressurized with a fixed initial pressure) which has been listed in the table as experiment 5b, 6b, 12b and 20b. For the experiment conducted in batch mode, pressure drop data was recorded during hydrate formation experiment. A typical pressure drop data is shown in Appendix D (figure D3). The hydration number used for water to hydrate calculation was 6.10. As seen in the table, water to hydrate conversion depends on the water saturation as well as composition of bed “silica sand and clay”. Irrespective of water saturation level, pure silica sand shows maximum water to hydrate conversion (~60%) while as clay content increase, water to hydrate conversion drops (minimum water to hydrate conversion obtained was ~8% when sand and clay ratio was 25:75). Figure 5.2 shows the methane hydrates in silica sand bed (Brown = silica sand, white = hydrates). Such high conversion of water to hydrates for the methane hydrate formation in sand has been consistently reported in the literature (Linga et al., 2009)

Figure 5.3 represents a typical gas uptake curve along with temperature profile. Exothermic nature of hydrate formation can be seen as sudden increase in temperature during hydrate formation due to release of heat during new bond formation. The time taken for the first hydrate nucleus to start growing is known as the induction time which is stochastic in nature but depends on driving force for hydrate formation (Higher pressure at a given temperature leads to lower induction time). As seen in the temperature profiles, hydrate nucleation occurs at approximately the same time at the three thermocouple locations. Figure 5.3 also shows

evidence of multiple nucleations, where several small temperature rise and a sharp rise in temperature close to 25 h is observed.

Table 5.2. Hydrate formation experiments performed at experimental temperature 274.5 K. Hydration number used for hydrate conversion calculation was 6.10.

System	Exp. No.	End of experiment				
		Exp. Pressure (MPa)	Time (hr)	Methane consumed (mol/mol of water)	Water to hydrate conversion (mol%)	Average conversion (mol%) (\pm std.)
I	1		37	0.047	28.7	
	2		45	0.046	28	
	3	5.75	27	0.026	16	24.87
	4		32	0.044	26.8	(\pm 5.96)
II	5	5.75	37	0.087	53	
	5b		10	0.093	56.5	60.75(\pm 7.49)
	6		37	0.114	69.8	
	6b		12	0.104	63.7	
III	7	5.75	24	0.067	40.8	42.4 (\pm 2.26)
	8		25	0.075	44	
IV	9	5.75	24	0.028	17	22 (\pm 7.07)
	10		14	0.045	27	
V	11	5.75	22	0.038	23.4	32 (\pm 9.40)
	12		23	0.069	42	
	12b		26	0.050	30.3	
VI	13	5.75	16	0.083	50.4	46.4 (\pm 5.64)
	14		24	0.072	42.4	
VII	15	6.10	23	0.038	22.8	23.15
	16		24	0.039	23.5	(\pm 0.46)
VIII	17		25	0.061	37.2	
	18	6.10	35	0.073	43.9	43.52
	19		30	0.085	52	(\pm 6.28)
	20b	5.85	35	0.065	39.5	
IX	21	6.20	15	0.018	12.0	8.5 (\pm 4.94)
	22		15	0.008	5.01	

b= batch mode



Figure 5.2. Methane hydrates in silica sand (Brown=silica sand, white=hydrates)

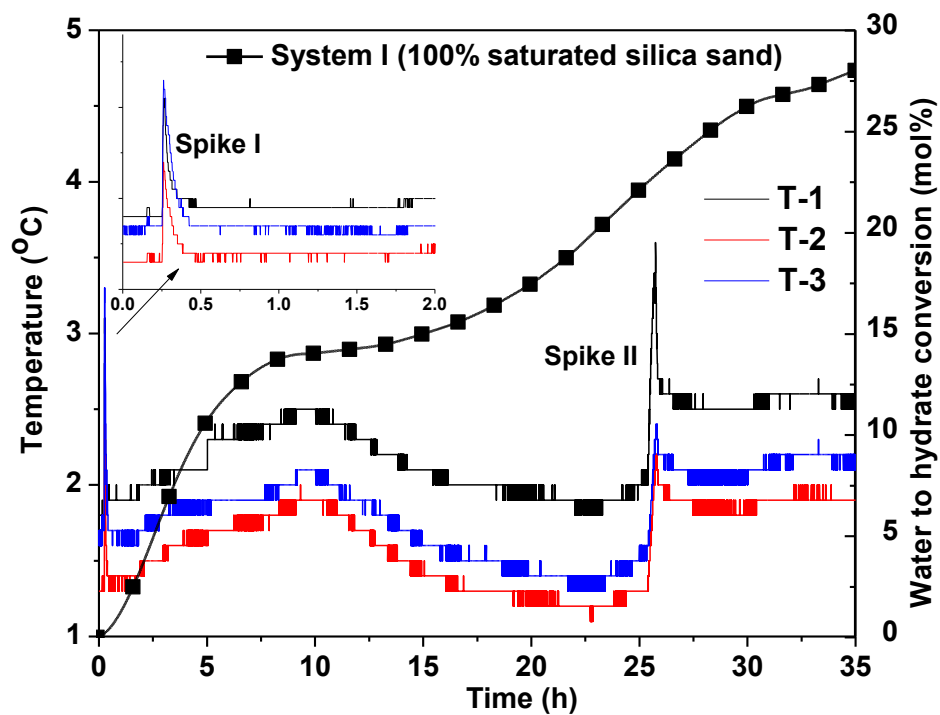


Figure 5.3. Typical gas uptake curve (black symbols) along with temperature profile for hydrate formation in 100% water saturated silica sand (Experiment 1).

Figure 5.4a shows a typical gas uptake measurement during hydrate formation at three different water saturation level in a known amount of silica sand bed. As observed, 100% water saturated silica sand (System I) has the lowest water to hydrate conversion rate compared to two other water saturation levels (75 and 50%, System II and III respectively). Better hydrate conversion at lower water saturation can be attributed to better water to gas contacts in partially saturated sand beds.

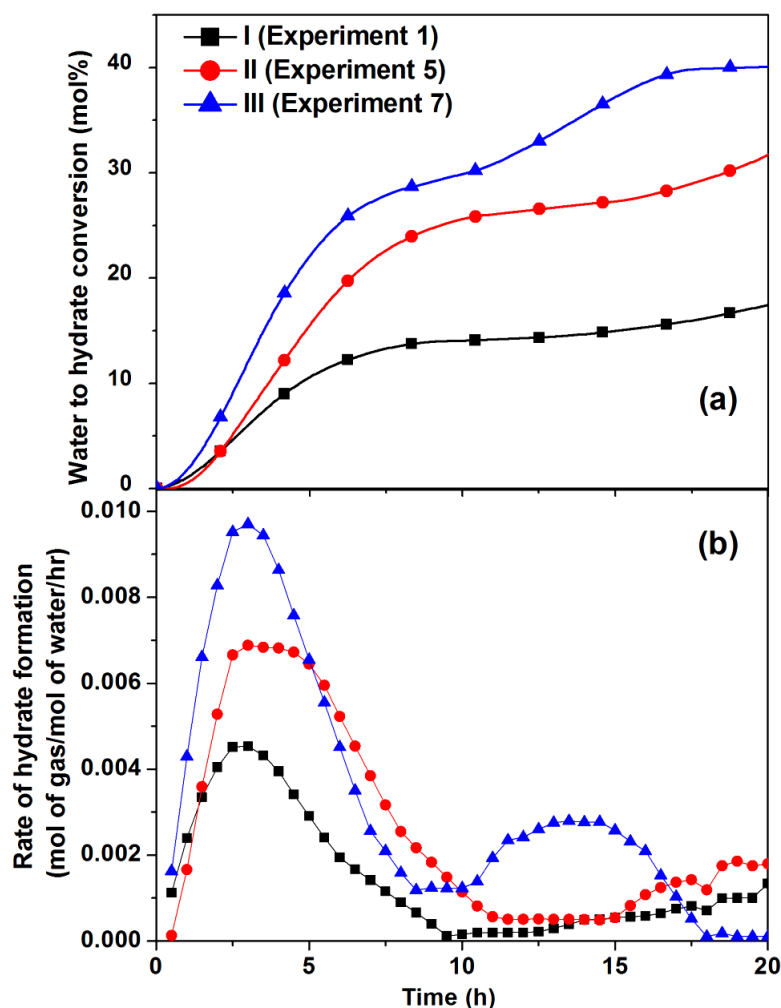


Figure 5.4 (a). Comparison of gas uptake (water to hydrate conversion) for methane hydrate formation with pure silica sand at three different water saturation levels (100, 75 and 50 %, Experiment 1, 5 and 7) (b) Comparison of the rate of methane uptake for the three system

Occurrence of multiple nucleations can also be seen if one plots the rate of gas uptake as a function of time. Figure 5.4b shows the comparison of rate of methane uptake for various water saturated silica sand systems. As seen in the figure, silica sand bed with lower water content

shows sharper hump compared to the other two, which means hydrate formation occurs faster in a bed with lower water saturation. As a result of a higher degree of water dispersion in partially saturated bed, the contact area between water and the gas phase increases, this consequently enhances the rate of hydrate formation. Recently Chari et al., have also reported that hydrate formation kinetics are comparatively faster in partially saturated system compared to water rich sediment (Chari et al., 2013).

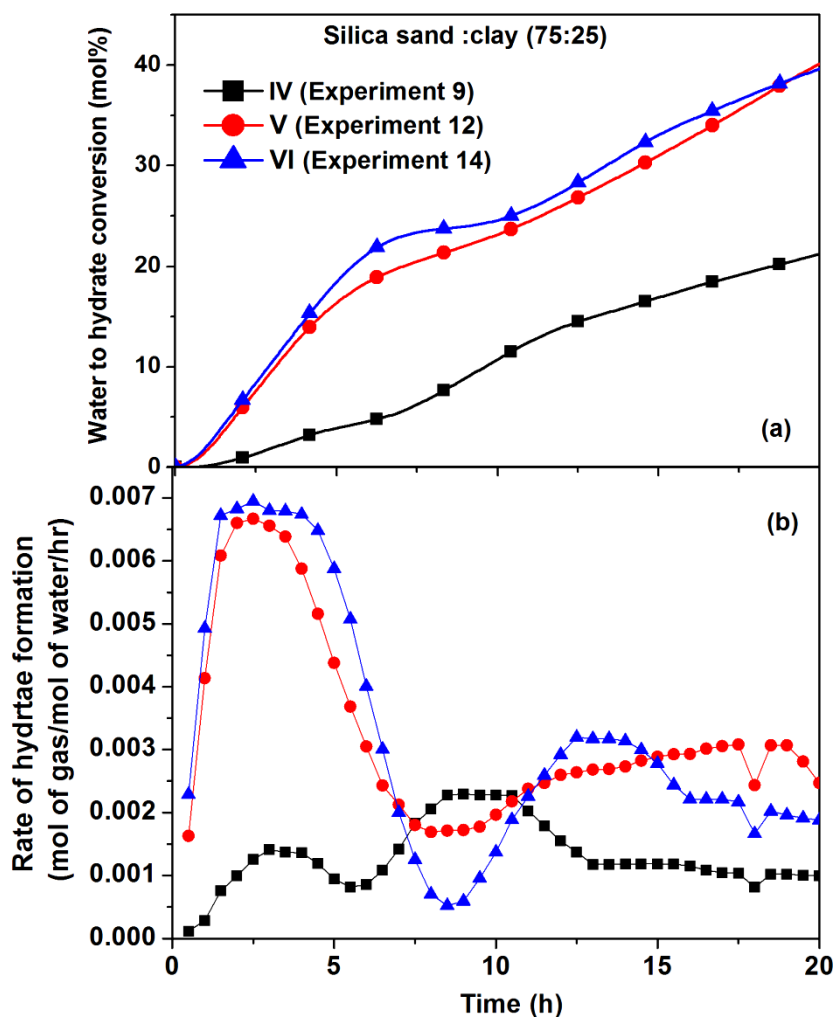


Figure 5.5. (a) Comparison of gas uptake (water to hydrate conversion) for methane hydrate formation conducted with Silica sand-clay mixture (75:25 ratio) at three different water saturation levels (100, 75 and 50 %, experiment 9,12 and 14) (b) Comparison of the rate of methane uptake for the three system

Figure 5.5a represents the comparison of gas uptake (water to hydrate conversion) for methane hydrate formation conducted with silica sand-clay mixture (75:25 ratio) at three different water saturation levels (100, 75 and 50 %, experiment 9, 12 and 14). As seen in the

figure, for 100% water saturated system, the gas uptake is lowest while it is more or less same for 75 and 50% water saturation level. Figure 5.5b represents the rate of hydrate formation for this system. As seen in figure 5.5b, the initial rate of hydrate formation is slower compared to figure 5.4b (System D). In system I (experiment 1), the rate of hydrate formation was found almost four times higher compared to system IV (experiment 9). It shows that addition of clay in the sediment dramatically reduces the hydrate growth rate which was also reported by Lu et al. (Liu et al, 2008). As seen in figure 5.5b, the initial rate of hydrate formation was found almost seven times higher for silica sand-clay mixture (75:25 ratio) at 75 and 50% saturation compared to 100% saturated system.

Figure 5.6a shows the comparison of gas uptake (water to hydrate conversion) for methane hydrate formation conducted with Silica sand-clay mixture (50:50 ratio) at two water saturation levels (75 and 50 %, experiment 15, 17 and 18). As seen in figure 5.6a, experiment 15 and 18 achieves a water to hydrate conversion of ~12 and 25 mol% respectively in first 5 h, while after 7-10 hour upon second nucleation further ~8-16 mol% conversion was achieved. To confirm this observation, one experiment was conducted in batch mode and a similar gas uptake profile was recorded which has been included in the appendix D (Figure D4). This two step hydrate formation is also supported by rate of hydrate formation with two distinguishable humps (figure 5.6b). It was observed that clay (sodium bentonite) upon absorption of water tends to swell and thus reduces the porosity even with partially saturated bed. The swelling property of such clay is due to its 2:1 structure with an octahedral layer sandwiched between two tetrahedral layers which are called smectites. The spacing between these layers is approximately 2 nm and holds various cations on the surface of silicate layers. This narrow and low-charged interlayer can readily accommodate water molecules and can swell as water molecules are intercalated (Uchida et al., 2004). Gaseous molecules are diffused into this confined space and are subsequently involved in forming intercalated gas hydrates (Koh et al., 2012). It can be speculated that higher percentage of clay pulls out the water present in the voids or interstitial spaces of silica sand resulting in lesser water to hydrate conversion rate. It is not easy to postulate the mechanism for hydrate formation in such type of bed as several events are occurring in the bed such as presence of tortuous pathways in the bed, migration of water inside the silica sand bed and those which gets intercalated, transport of gas etc (Linga et al., 2012). An effect of all these different phenomena results in different water to hydrate conversion rate,

figure 5.7 summarizes the comparison of final water to hydrate conversion in all the test sediments.

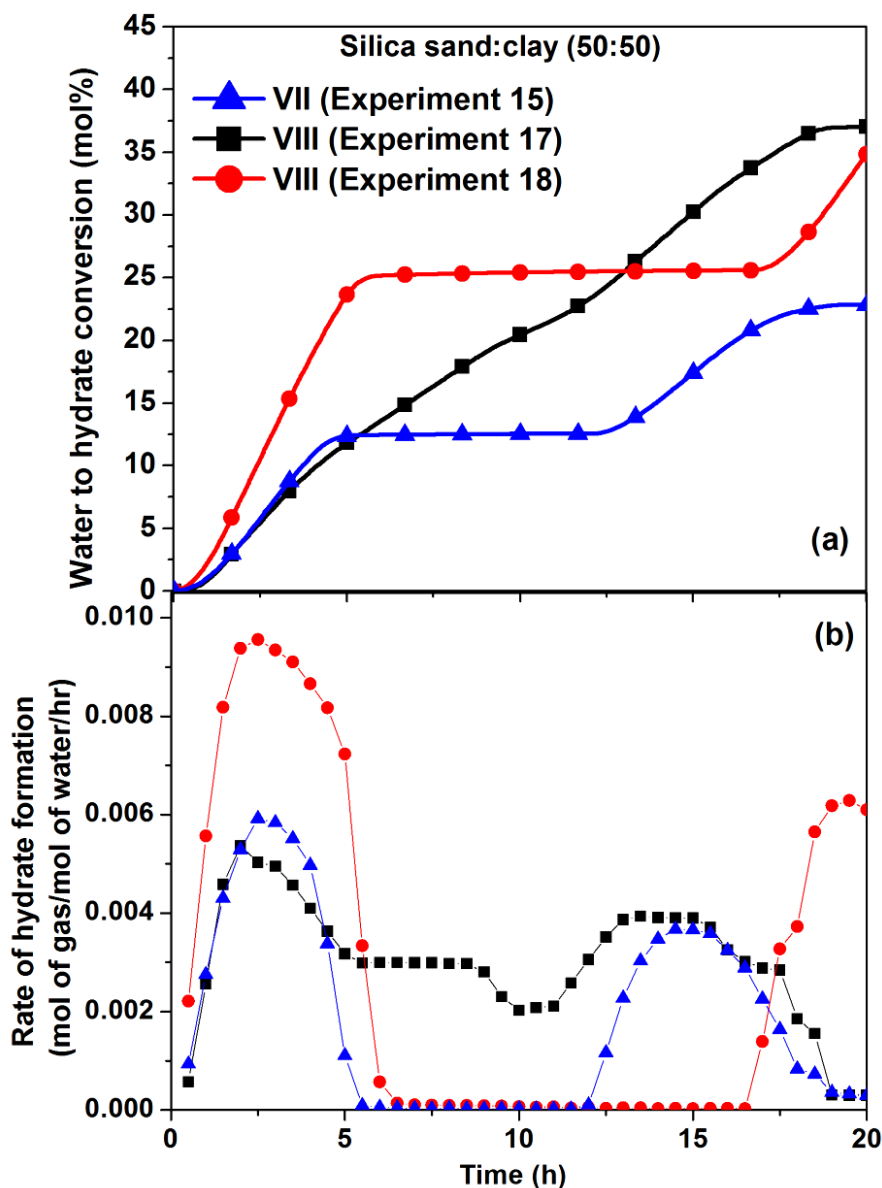


Figure 5.6. (a) Comparison of gas uptake (water to hydrate conversion) for methane hydrate formation conducted with Silica sand-clay mixture (50:50 ratio) at two water saturation levels (75 and 50 %, experiment 15, 17 and 18) (b) Comparison of the rate of methane uptake for the same system

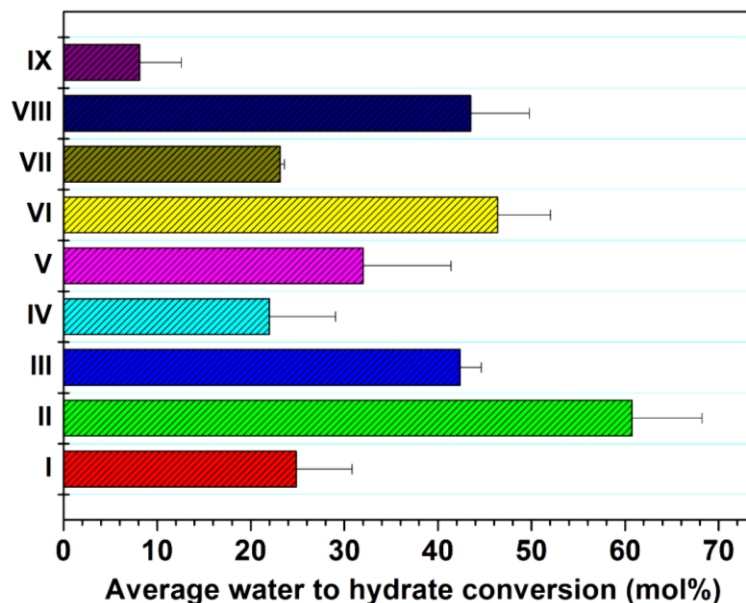


Figure 5.7. Comparison of water to hydrate conversion for methane hydrate formation conducted in same apparatus with silica sand-clay mixtures and pure silica sand at different water saturation levels

5.4. CO₂ Sequestration and Methane recovery from marine gas hydrates through carbon dioxide replacement

5.4.1. Thermodynamic Feasibility of Replacement

Typical phase diagrams of methane gas and carbon dioxide (gas/liquid) hydrate formation are shown in Figure 5.8. In the diagram, areas A and B are above the equilibrium curve of H₂O-hydrate-CO₂ and below that of H₂O-hydrate-CH₄, thus thermodynamically CO₂ hydrate can exist at such conditions whereas CH₄ hydrate would decompose at these temperature and pressure conditions. It is expected that phase boundary of CH₄ and CO₂ mixed hydrate will lie in these region and thus it can be concluded that CO₂ hydrate is more stable than CH₄ hydrate under these conditions. However looking at the region marked with C, it clearly shows that the three phase boundary of liquid CO₂-water -hydrate is less stable than methane-hydrate-water and thus trying to pump CO₂ in liquid phase and expecting methane in return will not be thermodynamically favorable. Also mass transfer limitation with two immiscible liquid phases will negatively impact the kinetics of such replacement process.

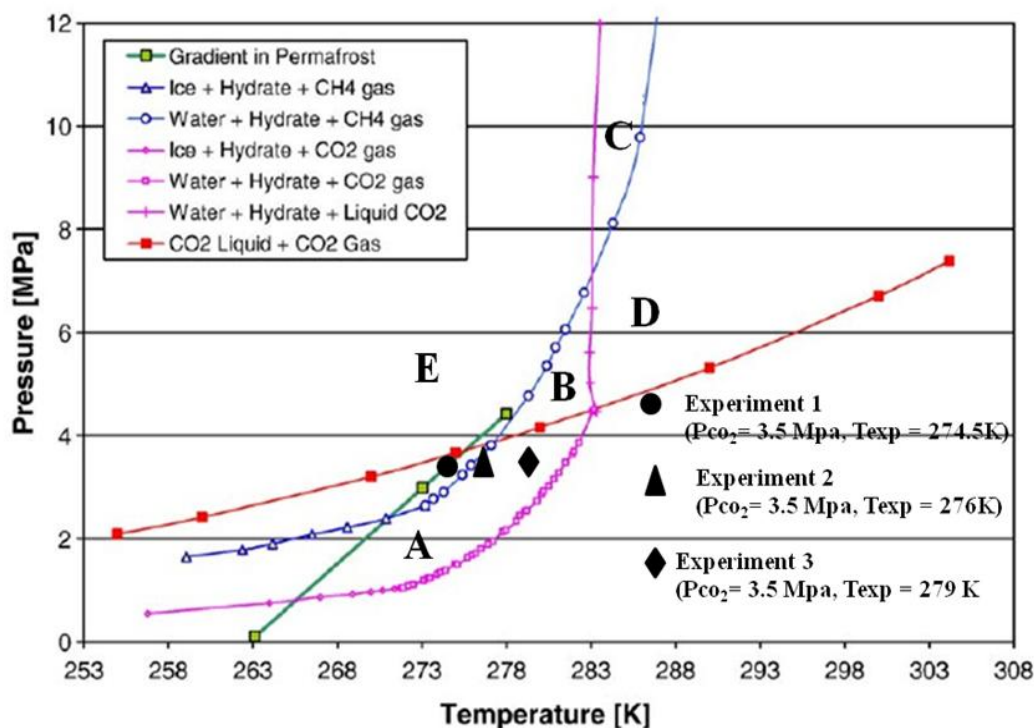


Figure 5.8. Hydrate formation conditions of carbon dioxide and methane modified from Goel,2006 .

In zone B, CO₂ hydrate can exist while CH₄ hydrate cannot. However, this zone is very narrow and the actual natural gas hydrate reservoirs are usually not located in this zone. Therefore, in the present study, as shown in Figure 5.8, the experimental conditions (P and T) are in the zone A. In all the cases CO₂ is in gaseous phase. Table 5.3 lists the various properties of methane and carbon dioxide hydrates (Jung et al., 2010).

Table 5.3. Properties of methane hydrates and carbon dioxide hydrates

Properties	CH ₄ Hydrates	CO ₂ Hydrates
Structure	sI 5 ¹² (S).5 ¹² 6 ² (L). 46 H ₂ O (Sloan and Koh,2008)	sI 5 ¹² (S).5 ¹² 6 ² (L). 46 H ₂ O (Sloan and Koh,2008)
Stoichiometric ratio or hydration number, (number of H ₂ O molecules per number of gas molecules)	5.75 (100% cage occupancy) (Sloan and Koh,2008); 5.81–6.10 [1.9–9.7 MPa, 263–285 K] (Circone et al. 2005)	5.75 (100% cage occupancy) (Sloan and Koh,2008); 6.57 [1.5 MPa, 273 K] (Klapproth et al. 2003)
Cage occupancy	100% Large cage; 70% Small cage; [10 MPa, 273 K] (Klapproth et al. 2003)	100% Large cage; 50% Small cage,[1.5 MPa, 273 K] (Klapproth et al. 2003)
Cavity size (Å)	7.9, 8.66 (Sloan and Koh,2008)	7.9, 8.66 (Sloan and Koh,2008)
Guest size (Å)	4.36 (Sloan and Koh,2008)	5.12 (Sloan and Koh,2008)

Lattice constant a (Å)	11.95 [10 MPa, 271.15 K] (Klapproth et al. 2003)	12.07 [273.2 K] (Uchida et al. 1999)
Heat capacity (kJ kg ⁻¹ K ⁻¹)	2.031 [263 K] (Waite et al. [2009]) 2.077 [270 K] (Handa [1986] and Yoon et al. [2003])	No data found
Thermal conductivity (W m ⁻¹ K ⁻¹)	0.68 [273 K] (Waite et al. 2009) 0.49 [263 K] (Sloan and Koh, 2008)	0.49 [263 K] (Sloan and Koh, 2008)
Thermal diffusivity $\alpha = \frac{k}{\rho c_p}$ (m ² s ⁻¹)	1.1 × 10 ⁻⁷ (Waite et al. [2007])	No data found
Heat or enthalpy of dissociation and formation H (kJ mol ⁻¹)	52.7–56.9 [273 K] (Waite et al. [2009]; 53 (independent of P&T) (Anderson [2003, 2004].)	63.6–57.7 (±1.8) (at quadruple points) (Anderson [2003, 2004].)
Density ρ (kg m ⁻³)	929 [263 K] (Waite et al. 2009) 940 (Sloan and Koh, 2008) 910 [273 K] (Waite et al. [2009])	1110–1090 (Aya et al. 1997) [30 MPa]; 1054 (Uchida et al. [1999])
Water volume expansion upon hydrate formation V_{hyd}/V_w (For CH ₄ -CO ₂ replacement)	1.234 (n = 6; d CH ₄ hyd = 930 kg m ⁻³ ; 100% occupancy)	1.279 (n = 6; d CO ₂ hyd = 1100 kg m ⁻³ ; 100% occupancy)
Coefficient of thermal expansion α (K ⁻¹)	sI hydrate 7.7 × 10 ⁻⁵ [200 K] (Sloan and Koh, 2008); 2.64 × 10 ⁻⁴ (Klapproth et al. [2003])	sI hydrate 7.7 × 10 ⁻⁵ [200 K] (Sloan and Koh, 2008)

5.4.2 CH₄ hydrate formation and CH₄-CO₂ hydrate replacement procedure

It is important to prepare the representative hydrate-bearing sediments sample before the replacement experiment which has been discussed in detail in section 5.2 and 5.3.

After the CH₄ hydrate formation was completed (typically a 24 hr experiment is carried out at different temperature to maximize water to hydrate conversion through better thermodynamics at lower temperature and better kinetics at higher temperature). Study of methane recovery kinetics by CO₂ replacement is carried out by first depressurizing the reactor to a pressure slightly above the equilibrium pressure of pure CH₄ hydrate to ensure no methane decomposition due to depressurization and then pressurizing the reactor with CO₂ by injecting the gaseous CO₂ into the reactor. The free gaseous CH₄ in the pore is expected to get swapped by CO₂, thus creating a CO₂ rich environment around methane hydrate. This rise in chemical potential of CO₂ surrounding the methane hydrate leads to local instability, and the entire

system is expected to move toward a new equilibrium where CH₄ molecules from the solid gas hydrate phase gets swapped provided there is enough driving force in terms of thermodynamics. During the swap process CO₂ was continued to be injected into the CR until a predefined pressure was attained (P_{CO₂}=3.5 MPa), the pressure was chosen to ensure that CO₂ is in gaseous phase. It is assumed that the methane hydrate cavities have to be destroyed to release gas molecules and form new cages for CO₂ gas hydrates. The composition of the gaseous phase was analyzed by gas chromatograph at different time intervals, which shows an increase in methane fraction and drop in CO₂ mole fraction the gaseous phase. The kinetics of this process reduces with time and if no change in gas phase composition is observed for a period of 24 hours the experiment is stopped. At the end of the experiment, temperature was increased up to 25 °C in order to decompose the hydrate phase for a mass balance analysis by analyzing the gaseous phase which has changed due to release of gases from the solid hydrate phase.

5.4.3. Calculations for CH₄ release and CO₂ consumed during replacement process

The mole of methane and carbon dioxide in the gas phase are calculated by the following equation 6 and 7 respectively.

$$n_{CR}^{CH_4} = x_{CR}^{CH_4} \cdot n_{CR}^{Gas} \quad (6)$$

$$n_{CR}^{CO_2} = x_{CR}^{CO_2} \cdot n_{CR}^{Gas} \quad (7)$$

Where $x_{CR}^{CO_2}$ is the mole fractions of CO₂ and $x_{CR}^{CH_4}$ mole fractions of CH₄ in the CR which were analyzed by gas chromatograph, The corresponding mole of CH₄ and CO₂ in the CR were named as $n_{CR}^{CH_4}$ and $n_{CR}^{CO_2}$ respectively. n_{CR}^{Gas} is the mole of gas (Gas mixture of CH₄ and CO₂) in the CR

5.5. Methane – carbon dioxide replacement

After methane hydrate formation, the replacement process was started as discussed earlier. Table 5.4 summarizes all the results obtain during replacement process and experimental conditions. As shown in table two systems are chosen for replacement experiments one is pure silica sand at 75% water saturation and other is silica sand clay mixture (75:25 ratio) at 75% saturation. Replacement experiments are performed at three different experimental temperatures (1.5, 3 and 6°C).

Table 5.4. Summary of CH₄-CO₂ replacement experiments

System	Experiment No.	Temperature (K)	Mol of methane in hydrate phase	Mol of methane released after replacement	Initial Mol of CO ₂	Methane Recovery (%)	
S-75	*1a	274.5	0.142	0.038	0.45	27	
SC-72-75	*1b	274.5	0.0985	0.034	0.41	30	
SC-72-75	2a (Stage I)	276.0	0.086	0.0162	0.27	19	Total Rec. 37 %
SC-72-75	2b (Stage II)	279.0	0.086	0.015	0.23	18	

*Note – *In experiment 1a and 1b, gaseous phase (CH₄) was released to atmospheric pressure at -5 oC while in other experiments the pressure in the reactor was maintained at the equilibrium pressure of methane hydrate*

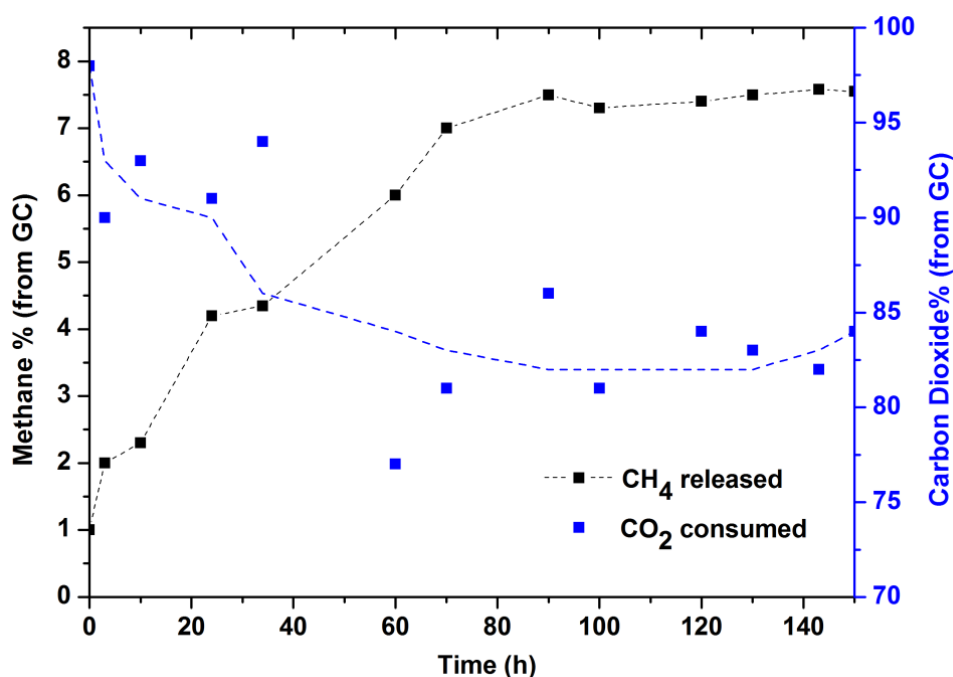
Figure 5.9 summarize and compares the results obtained through the replacement process for experiment 1a (Silica sand at 75% water saturation) and 1b (Silica sand and clay mixture (75:25) at 75% water saturation). As seen in the figure methane concentration increases with time and CO₂ decreases which means that there is considerable CO₂ hydrate formation.

As seen in figure 5.9, CH₄ hydrate dissociation in the initial stage is high but after some time it become slow. This may be because of CO₂ injection which initiates some heating effect i.e difference of heat of formation of CO₂ hydrates and heat of dissociation of methane hydrates. As seen in figure, a scattered data was obtained in this study, considering the size of the reactor the data obtained is not bad and it can be seen that there is a drop of CO₂ composition in the gaseous phase as time progresses. In each case, data has been fitted with a polynomial which shows a good fit for methane recovery with a good R² values. Total methane recoveries obtain in the experiment 1a and 1b are 27 and 30% respectively due to replacement of methane hydrate to CO₂ hydrates. To recover all the methane, at the end of replacement process, the temperature of the crystallizer is increased up to 25 °C at which all the hydrates dissociated. Almost 84% methane is recovered at the end, methane loss during sampling process (GC analysis) and during CO₂ injection makes up for the mass balance.

During the experimentation it was observed that the replacement process is mainly influenced by two factors, thermodynamic condition and efficient mass/heat transfer. In the initial stage, the first factor is dominant because the diffusion barrier of the solid hydrate is very little and can be ignored; but in the later stage, the diffusion barrier is dominant because of the increasing of hydrate layer thickness and limited porosity which is filled by a gas like CO₂ which has very poor thermal conductivity. CH₄ hydrate dissociation, fresh nucleation of CO₂ hydrate and replacement of CH₄ by CO₂ each of these processes occurs simultaneously and

each of these process have independent temperature profile which, at engineering scale can only be studied as lumped parameter. Figure D6 (Appendix D) shows the gas phase analysis for CH₄-CO₂ replacement for SC-72-75 System at 276 (stage I). As seen in figure, the rate of methane hydrate dissociation is too slow and on ~70h only 19% methane is recovered (Table 5.4). The reasons of the slower replacement rate with time can be explained as follows.

1. The replacement process should occur at gaseous CO₂-CH₄ hydrate interface for better mass transfer and higher kinetics.
2. However for a partially saturated marine gas hydrate, which has a significant portion of free water either in liquid phase or in solid ice phase, reacts with the available CO₂ (and in absence of any gaseous CH₄) and forms CO₂ hydrate. Thus changing the boundary to solid CO₂ hydrate-solid CH₄ hydrate and thus significant release of CH₄ is not observed.
3. However if the temperature of such a system is raised to a suitable value where thermodynamics of methane hydrate is unfavorable, it is expected that better methane recovery kinetics can be observed. This can be done by simultaneously giving a thermal stimulation along with CO₂ pressurization.



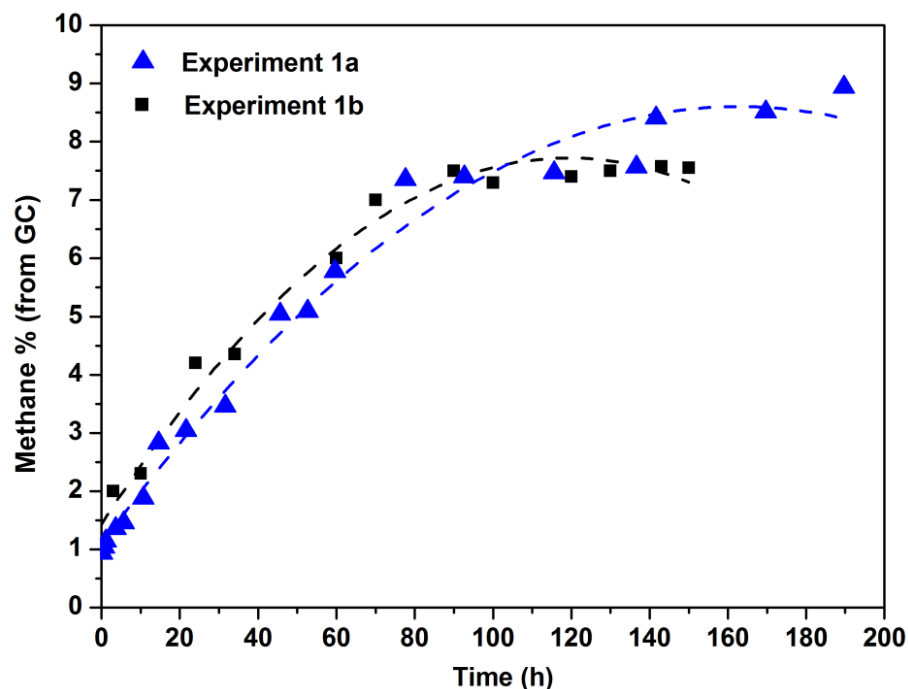


Figure 5.9. Release of methane due to hydrate dissociation and CO_2 consumption due to CO_2 hydrate formation (silica sand and clay mixture (75:25) at 75% water saturation) (experiment 1b) and its comparison with S-75 system (Exp. 1a)

5.6. Conclusion

Methane hydrate formation experiments were carried out in test bed of silica sand & clay under different water saturation which suggests that presence of clay reduces the hydrate formation kinetics significantly. Lower water saturation shows higher water to hydrate conversion rate in pure sand bed as well in sand-clay mixture. The injection of carbon dioxide (CO_2), into hydrate bearing sediments liberates some of the enclathrated methane (CH_4), and simultaneously sequesters CO_2 in hydrate form. Thus CO_2 replacement as seen from this work looks quite feasible at laboratory scale but the process of replacement is quite slow. One can certainly expect methane to get released from such a process; however the process needs to be optimized for temperature, pressure and concentration of CO_2 in the aqueous phase. Kinetics of replacement process needs to be improved. For such improvements, future work has been recommended in the next chapter.

Chapter 6

6. Summary of Conclusions, Recommendations for Future Work and CSIR-800 project

This thesis explores Hydrate Based Gas Separation Process for CO₂ capture from its mixed component. Majority focus of the thesis was to enhance the hydrate formation kinetics and water to hydrate conversion in an un-stirred configuration. Several packing materials has been studied for effective distribution of water and gas in the fixed bed setup to enhance mass transfer and suitable additives (surfactant) were utilized for enhancing the water to hydrate conversion by ensuring better gas/liquid contact. (Kumar et al, 2013). This thesis provides the impact of impurities like fly ash, SO₂ and H₂S on the kinetics and separation efficiency of HBGS process for separation and capture of CO₂ from flue gas and fuel gas mixture (Kumar et al., 2014, 2015a). In addition to this thesis also provides the suggestions for the scale-up of HBGS process for successful commercialization of CO₂ capture from fuel gas mixture and economically viable sequestration option for captured CO₂ via methane recovery from natural gas hydrate reservoirs under the sea bed (Kumar et al., 2015b,c).

6.1. Summary of Conclusions

Feasibility of the Hydrate Based Gas Separation (HBGS) process for CO₂ capture/separation followed by simultaneous sequestration of the captured CO₂ alongwith release of methane from methane hydrate sediment (energy production with CO₂ sequestration) was investigated experimentally. Initially, CO₂ hydrate formation in porous fixed bed media (silica gels) with nonionic, cationic and anionic surfactant has been investigated. Silica gel with high surface area has significant effect on the rate of hydrate formation. Among the three surfactants, anionic (SDS) shows higher hydrate formation rate. It is concluded that in presence of silica gel and anionic surfactant, the rate of gas uptake considerably enhanced. For a commercial hydrate based gas separation (HBGS) process, a fixed bed reactor is more economical compared to a stirred tank reactor. However the impact of impurities such as fly ash, SO₂ and H₂S also plays an important role in HBGS process. Gas hydrate formation experiments from flue gas mixtures (CO₂/N₂/ Fly ash and CO₂/N₂/ SO₂) and Fuel gas mixture (CO₂+H₂+H₂S) were carried out to study the impact of these impurities (fly ash, SO₂ and H₂S)

on the thermodynamics and kinetics of hydrate formation. Additional kinetic & thermodynamic promoters were added in the liquid phase to reduce the operating pressure and enhance the hydrate formation kinetics. In the presence of fly ash impurity no significant shift in the hydrate equilibrium pressure was observed. The two additives used in this work, a thermodynamic promoter (THF) and a kinetic promoter (SDS) showed a synergic effect on hydrate formation kinetics at a comparatively lower operating pressure. Additionally, it was found that the presence of SO_2 shifts the hydrate equilibrium to milder conditions. However, the rate of hydrate formation was very slow which was further enhanced in the present study using a thermodynamic promoter (5.56 mol% THF) and a kinetic promoter (SDS). It was also found that addition of H_2S in fuel gas mixture (CO_2+H_2) shifts the hydrate formation equilibrium condition to the milder conditions (shifting towards the high temperature and low pressure). However presence of 1 mol% H_2S in the gas mixture does not enhance the overall efficiency of HBGS process. However, it was noted that suitable material of construction needs to be selected to avoid corrosive effect of H_2S and SO_2 on the packing medium if a fixed bed arrangement is being utilized for such separation. To scale-up the HBGS process for successful commercialization of CO_2 capture from fuel gas mixture, hydrate formation experiments were conducted in an unstirred reactor to study the kinetics of HBGS process using fuel gas mixture. The unstirred reactor with metallic packing (SS-316, Brass, and Copper foam) showed better kinetic performance over silica sand, silica gel packing and stirred tank reactor. The effect of different concentrations of SDS on hydrate formation was investigated; it was conclusively proven that the addition of SDS resulted in a faster rate of hydrate formation. On the basis of the experimental results, a conceptual process flow diagram of the HBGS process has been proposed for continuous removal of carbon dioxide from a fuel gas mixture at the plant scale. An economically viable sequestration option for captured CO_2 was also identified through lab scale experimentation in a test sediment of silica sand & clay where methane hydrates were replaced by CO_2 hydrates. CO_2 replacement as seen from this work looks quite feasible. One can certainly expect methane to get released from such a process; however it is going to be expensive to pump a gas like CO_2 compared to water at higher pressure. However, if there is a monetary benefit and under Kyoto protocol regime this becomes quite attractive as, some of the economical burden can be offset by monetary advantage one gets from carbon dioxide credit.

6.2. Conceptual protocol for potential application (continuous removal of carbon dioxide from a fuel gas mixture)

Based on the experimental results obtained in the present study, metallic packing used in this work has been identified as a superior fixed bed medium for the HBGS process. Metallic packing was also found to be efficient in removing the exothermic heat of hydrate formation thus allowing for a two stage hydrate based gas separation (HBGS) process as shown in figure 6.1a. The conceptual process flow diagram of the proposed HBGS process is a continuous process suitable for carbon dioxide separation from fuel gas mixture. The HBGS process comprises two thermodynamic phase changes; a hydrate formation stage to convert most of the liquid water into solid hydrate phase through selective enclathration of CO₂ from fuel gas mixture, followed by a hydrate decomposition stage which converts the solid hydrate phase back into liquid water and CO₂ rich gas. The proposed process runs in a fixed bed arrangement and operates like a conventional tray dryer; the process begins with the hydrate formation stage wherein, water soaked packing material is loaded in trays #1, #2, #3 and trays #4, #5, #6 (figure 6.1b) which is then brought in contact with fuel gas mixture. At suitable temperature, pressure and residence time, selective enclathration of CO₂ is achieved, leaving behind a CO₂ rich solid hydrate phase and H₂ rich gas phase. Gas phase is sent to H₂ storage tank and hydrate containing trays use a pivot to move to the decomposition chamber (marked as trays #1', #2', #3' and #4', #5', #6' in figure 6.1b). Hydrates are allowed to decompose in this chamber at suitable temperature to recover CO₂ rich gas phase. For polishing the H₂ rich gas stream (to obtain pure H₂ gas) after hydrate formation in stage one, a suitable polymeric membrane (polyamides) can be utilized. The CO₂ rich phase which is obtained after hydrate decomposition is collected in a CO₂ storage vessel through a throttling process to obtain pure CO₂ gas (figure 6.1a). The throttling process results in cooling of gas due to positive Joule Thompson coefficient of CO₂ which can be utilized to offset the cooling cost for hydrate formation. There are two advantages of this arrangement, firstly a metallic bed ensures efficient heat transfer for hydrate formation and decomposition stages; passing a coolant (to maintain temperature of the reaction) at the bottom of the tray is also quite feasible as it will be easy to implement the same mechanically. The second advantage of the process is that with this tray dryer like arrangement, bed clogging due to solid hydrate formation and resulting flow blockages can be bypassed. Large surface area necessary for better water to gas contact (for

tackling higher flow rate of fuel gas mixture) can be created by just increasing the numbers of trays.

It is proposed that better hydrate growth kinetics can be achieved with use of suitable additives like 1 wt% SDS as reported in this work. Process economics can further be optimized by utilizing the positive Joule-Thompson coefficient of carbon dioxide gas when a high pressure fuel gas mixture from an IGCC unit is throttled to a lower operating pressure as required for a HBGS process. As discussed in our earlier work, utilization of a suitable thermodynamic additive like propane, tetrahydrofuran etc. can reduce the operating pressure of the HBGS process.

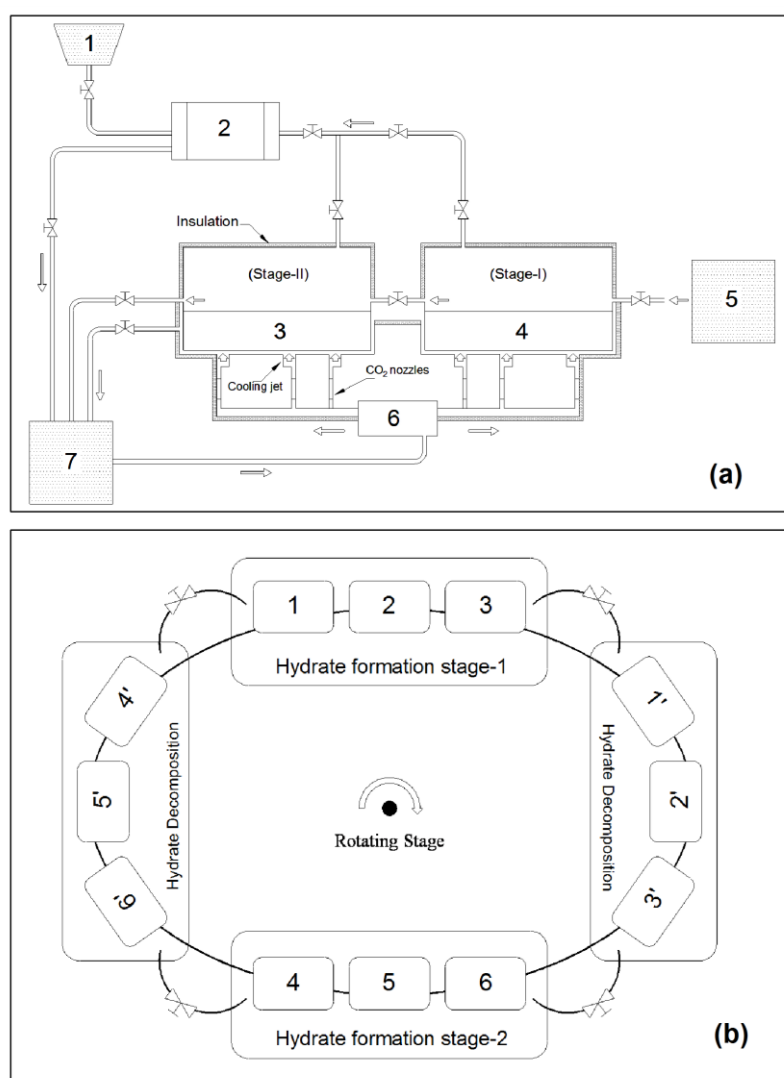


Figure 6.1. (a) Schematic flow sheet for CO₂ capture and separation using HBGS process

1. H₂ gas, 2. Membrane separator, 3 & 4. Metallic packing bed, 5. Feed gas (CO₂+H₂), 6. Throttling process, 7. CO₂ gas

(b) Schematic of continuous HBGS process for gas separation

6.3. Recommendations for Future Work

The following recommendations are proposed for future work.

1. In our study, Surfactant (SDS) was found to be a good candidate to enhance the hydrate formation rate. Suitable mechanism of surfactant action needs to be verified at molecular level. Role of kraft point temperature and CMC of surfactants in hydrate formation needs to be investigated.
2. HBGS process needs to be demonstrated on a large scale (pilot scale) and cost analysis compared to mature CO₂ capture technologies need to be evaluated.
3. In our study, impact of impurities like fly ash, SO₂ and H₂S on thermodynamics and kinetics were demonstrated. Molecular level work (such as cage occupancy) needs to be performed. Structural and compositional characterization studies needs to be carried out by Powder X-ray Diffraction (PXRD), ¹H Magic Angle Spinning (MAS) NMR, ¹³C MAS NMR, mass spectrometry, Fourier Transform Infrared Spectroscopy (FT-IR) (with attenuated total reflection) and Raman spectroscopy.
4. As can be seen in this study, CO₂ replacement process looks quite feasible however kinetics was found to be very slow. Suitable additives along with CO₂ or CO₂/N₂ in gaseous form or along with water in solution form are certainly needed to enhance the kinetics of such a replacement process.
5. From technical point of view many questions are unanswered like, how the kinetics of such replacement will improve once first few layer of methane hydrate has been replaced by CO₂ hydrate. Clearly it will only be possible if methane in the inner core sees a potential gradient from surrounding CO₂ molecule. Some of these studies need to be done through simulation as molecular scale.

6.4. CSIR-800 Project: A novel approach for seawater desalination: Hydrate based desalination (HBD) process

The major objective of the CSIR-800 project is to create and nurture a sense of social consciousness and responsibility by participation in Science & Technology activities. The two major focus areas of CSIR-800 are to enhance income and to improve the quality of life of the 800 million people of India.

To improve the quality of life Potable Water supply is one of the ways which was carried out by hydrate-based desalination (HBD) process.

The HBD process is based on a liquid to solid phase change of water such as a freezing method. In other words, a physical reaction coupled with an exclusion of ions by the hydrogen bonding of water molecules during hydrate formation is the core of the HBD process. It is also important to separate the solids (hydrates) from the remaining liquid phase (brines) in the process after hydrate formation. A schematic of the HBD process is shown in Figure 6.1 which represents the separation of solid hydrate.

The specific objectives are as follow:

- I. Process development for HBD process in minimum capital/ operating costs
- II. Process will be employed for simultaneous CO₂ capture and desalination
- III. Utilization of LNG cold energy hydrate formation
- IV. Eco-friendly process with maximum water recovery

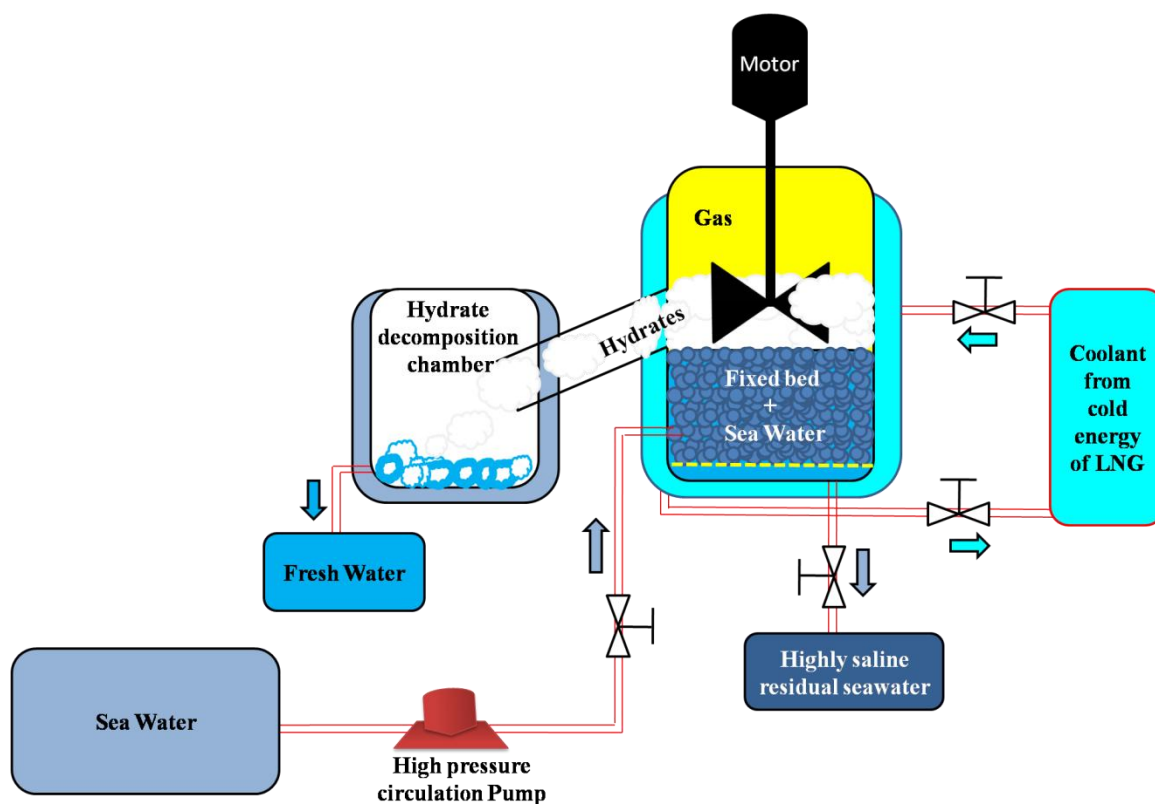


Figure 6.2. Schematic of the apparatus for hydrate-based desalination (HBD) process

7. References

- Aaron, D.; Tsouris, C. Separation of CO₂ from flue gas: A review. *Separ Sci Technol* **2005**; *40*, 321.
- Adeyemo, A.; Kumar, R.; Linga, P.; Ripmeester, J.; Englezos, P. Capture of carbon dioxide from flue or fuel gas mixtures by clathrate crystallization in a silica gel column. *Int J Greenh Gas Con* **2010**, *4*, 478.
- Anderson, G. K. Enthalpy of dissociation and hydration number of carbon dioxide hydrate from the Clapeyron equation, *J. Chem. Thermodyn.*, **2003**, *35*, 1171.
- Anderson, G. K. Enthalpy of dissociation and hydration number of methane hydrate from the Clapeyron equation, *J. Chem. Thermodyn.*, **2004**, *36*, 1119.
- Babu, P.; Ho, C.Y.; Kumar, R.; Linga, P. Enhanced kinetics for the clathrate process in a fixed bed reactor in the presence of liquid promoters for pre-combustion carbon dioxide capture. *Energy*, **2014a**, *70*, 664.
- Babu, P.; Kumar, R.; Linga, P. A new porous material to enhance the kinetics of clathrate process: application to pre-combustion carbon dioxide capture. *Environ. Sci. Technol.* **2013a**, *47*, 13198.
- Babu, P.; Kumar, R.; Linga, P. Medium Pressure Hydrate Based Gas Separation (HBGS) Process for Pre-Combustion Capture of Carbon Dioxide Employing a Novel Fixed Bed Reactor. *Int. J. Greenh. Gas Con.* **2013b**, *17*, 206.
- Babu, P.; Kumar, R.; Linga, P. Pre-Combustion Capture of Carbon Dioxide in a Fixed Bed Reactor using the Clathrate Hydrate Process. *Energy* **2013c**, *50*, 364.
- Babu, P.; Kumar, R.; Linga, P. Unusual behavior of propane as a co-guest during hydrate formation in silica sand: Potential application to seawater desalination and carbon dioxide capture. *Chem. Eng. Sci.* **2014b**, *117*, 342-351.
- Barchas, R.; Davis, R. The Kerr-Mcgee Abb Lummus Crest Technology for the Recovery of CO₂ from Stack Gases. *Energ. Convers. Manage.* **1992**, *33*, 333.
- Bishnoi, P.R.; Natarajan, V. Formation and decomposition of gas hydrates. *Fluid Phase Equilibria*, **1996**, *117*, 177.
- Caskey, J. A.; Barlage Jr, W. B. A Study of the Effects of Soluble Surfactants on Gas Absorption using Liquid Laminar Jets. *J. Colloid Interface Sci.* **1972**, *41*, 52.
- Chapel, D.; Ernest, J.; Mariz C. Recovery of CO₂ from Flue Gases: Commercial Trends. Canadian Society of Chemical Engineers annual meeting. 1999, Saskatoon, Saskatchewan, Canada (http://www.netl.doe.gov/publications/proceedings/01/carbon_seq/2b3.pdf).
- Chari, V. D.; Raju, B.; Prasad, P. S. R.; Rao, D. N. Methane hydrates in spherical silica matrix: Optimization of capillary water. *Energy Fuels*, **2013**, *27*, 3679.
- Chen, H.W.; Ku, Y.; Lin, S.Y.; Chang, C.Y. Effect of sodium dodecyl sulfate (SDS) on bubble characteristics and ozone transfer in a bubble column. *J. Chin. Inst. Chem. Eng.* **2007**, *30*, 155.
- Chopra, N.N. "Gas hydrate An unconventional Trap in Fore Act regions of the Andaman offshore" *Bulletin of ONGC*, 1985, 22.
- Circone, S.; Kirby, S. H.; Stern, L. A. Direct measurement of methane hydrate composition along the hydrate equilibrium boundary, *J. Phys. Chem. B*, **2005**, *109*, 9468.
- CO₂ emissions from fuel combustion Highlights, International Energy Agency (IEA), France, 2014. (www.iea.org)
- Collett and co workers., *USGS, ICICI Securities* 2008. (<http://www.naturalgaseurope.com/methane-hydrates-and-the-potential-natural-gas-boom>)

- Daraboina, N.; Ripmeester, J. A.; Englezos, P. The Impact of SO₂ on Post Combustion Carbon Dioxide Capture in Bed of Silica Sand through Hydrate Formation. *Int. J. Greenh. Gas Con.* **2013**, *15*, 97
- Davidson, D. W. *Clathrate Hydrates, In Water: A Comprehensive Treatise*, Plenum Press, 1973.
- Davydov, A.; Chuang, K. T.; Sanger, A. R. Mechanism of H₂S Oxidation by Ferric Oxide and Hydroxide Surfaces, *J. Phys. Chem. B.* **1998**, *102*, 4745-4752
- Dawson, M. Silica sand: *Foundry requirements and classification*. Cast Metal Service Pty. Ltd., Queensland Australia, 2004, 5.
- Deaton, W. M.; Frost, E. M. *Gas hydrates and their relation to the operation of natural-gas pipelines* U.S. Dept. Interior; 1946.
- Diwan, P.; Yaqoot. M. *Energy management*, Pentagon energy earth, India. 2010, 254.
- Englezos, P. Clathrate Hydrates. *Ind. Eng. Chem. Res.* **1993**, *32*, 1274.
- Englezos, P.; Ngan, Y. T. Effect of Polyethylene Oxide on Gas Hydrate Phase Equilibria. *Fluid Phase Equilib.* **1994**, *92*, 271.
- Fan, S. S.; Li, S. F.; Wang, J. Q.; Lang, X. M.; Wang, Y. H. Efficient Capture of CO₂ from Simulated Flue Gas by Formation of TBAB or TBAF Semiclathrate Hydrates. *Energy Fuels* **2009**, *23*, 4202.
- Farajzadeh, R.; Muruganathan, R.M.; Rossen, W.R.; Krastev, R. Effect of gas type on foam film permeability and its implications for foam flow in porous media. *Adv. Colloid Interface Sci.* **2011**, *168*, 71.
- Folger, P.; *Carbon Capture: A Technology Assessment*, CRS (Congressional Research Service) Report for Congress, 2013.
- Fuhrhop, J.H.; Koning, J. *Membranes and Molecular Assemblies: The Sykinetic Approach*. The Royal Society of Chemistry, Cambridge, UK, 1994.
- Gayet, P.; Dicharry, C.; Marion, G.; Graciaa, A.; Lachaise J.; Nesteroy, A. Experimental Determination of Methane Hydrate Dissociation Curve up to 55 MPa by Using a Small Amount of Surfactants as Hydrate Promoter. *Chem. Eng. Sci.* **2005**, *60*, 5758.
- Goel N. In situ methane hydrate dissociation with carbon dioxide sequestration: Current knowledge and issues, *J. Petroleum Sci. Eng.* **2006**, *51*, 169.
- Halgiva, C.; Linga, P.; Ripmeester, J. A.; Englezos, P. Recovery of Methane from a Variable Volume Bed of Silica Sand/Hydrate by Depressurization. *Energy Fuels*, **2010**, *24*, 2947.
- Handa, Y. P. Compositions, enthalpies of dissociation, and heatcapacities in the range 85 to 270 K for clathrate hydrates of methane, ethane, and propane, and enthalpy of dissociation of isobutane hydrate, as determined by a heat-flow calorimeter, *J. Chem. Thermodyn.*, **1986**, *18*, 915.
- Handa, Y. P.; Stupin, D. Y. Thermodynamic properties and dissociation characteristics of methane and propane hydrates in 70- Å-radius silica gel pores. *J. Physical Chem.* **1992**, *96*, 8599.
- Hanwright, J.; Zhou, J.; Evans, G. M.; Galvin, K. P. Influence of Surfactant on Gas Bubble Stability. *Langmuir* **2005**, *21*, 4912.
- Herzog, H. J.; Drake, E.; Adams, E. *CO₂ Capture, Reuse, and Storage Technologies for Mitigating Global Climate Change*. 1997.
- Ho, L. C.; Babu, P.; Kumar, R.; Linga, P. HBGS (Hydrate Based Gas Separation) Process for Carbon Dioxide Capture Employing an Unstirred Reactor with Cyclopentane. *Energy* **2013**, *63*, 252.
- <http://www.epa.gov/climatechange/ccs/>.
- IPCC Report, "Carbon dioxide capture and storage, IPCC Special report." Intergovernmental Panel on Climate Change, 2005.

- Jones, F.E.; Schoonover, R.M. *Hand book of mass measurement*, CRC Press, Florida, 2002, 170.
- Jung, J. W.; Nicolas Espinoza, D.; Carlos Santamarina J. Properties and phenomena relevant to CH₄-CO₂ replacement in hydrate-bearing sediments, *J. Geophysical Research*, **2010**, *115*, B10102.
- Kalogerakis, N.; Jamaluddin, A. K. M.; Dholabhai, P. D.; Bishnoi, P. R.. *Effect of Surfactants on Hydrate Formation Kinetics*, SPE 25188, presented at SPE International Symposium on Oilfield Chemistry; New Orleans, LA, USA, 1993
- Kang, S.P.; Lee, H.; Lee, C.S.; Sung, W.M. Hydrate phase equilibria of the guest mixtures containing CO₂, N₂ and tetrahydrofuran. *Fluid Phase Equilibria*, **2001a**, *185*, 101.
- Kang, S.P.; Lee, J.W. Kinetic behaviors of CO₂ hydrates in porous media and effect of kinetic promoter on the formation kinetics. *Chem. Eng. Sci.* **2010**, *65*, 1845.
- Karaaslan, U.; Parlaktuna, M. PEO-A new hydrate inhibitor polymer. *Energy Fuels*. **2002**, *16*, 1391.
- Karaaslan, U.; Parlaktuna, M. Promotion Effect of Polymers and Surfactants on Hydrate Formation Rate. *Energy Fuels*. **2000a**, *16*, 1416.
- Karaaslan, U.; Parlaktuna, M. Surfactants as Hydrate Promoters? *Energy Fuels*. **2000b**, *14*, 1107.
- Kim, C. Y.; Escudro, A. A.; Bedzyk, M. J. Interaction of H₂S with α -Fe₂O₃(0001) surface, *Surface Sci.* **2007**, *601*, 4966–4970.
- Klapproth, A. E.; Goreshnik, D.; Staykova, H.; Klein; Kuhs, W. F. Structural studies of gas hydrates, *Can. J. Phys.*, **2003**, *81*, 503.
- Klara, S. M.; Srivastava, R. D. US DOE integrated collaborative technology development program for CO₂ separation and capture, *Environ. Prog.* **2002**, *21*, 247.
- Klauda, J. B.; Sandler, S. I. Global distribution of methane hydrate in ocean sediment. *Energy Fuels*. **2005**, *19*, 470.
- Koh, D. Y.; Kang, H.; Kim, D. O.; Park, J.; Cha, M.; Lee, H. Recovery of methane from gas hydrates intercalated within natural sediments using CO₂ and a CO₂/N₂ gas mixture. *ChemSusChem*. **2012**, *5*, 1443.
- Kumar, A.; Sakpal, T.; Roy, S.; Kumar, R. Methane hydrate formation in a test sediment of sand and clay at various level of water saturation, *Canadian J Chem.* **2015c**, *93*, 874.
- Kumar, A.; Kumar, R. Role of Metallic Packing and Kinetic Promoter in Designing a Hydrate Based Gas Separation Process. *Energy Fuels*, **2015b**, *29*, 4471.
- Kumar, A.; Sakpal, T.; Linga, P.; Kumar, R. Enhanced carbon dioxide hydrate formation kinetics in a fixed bed reactor filled with metallic packing. *Chem. Eng. Sci.* **2015a**, *122*, 85.
- Kumar, A.; Sakpal, T.; Linga, P.; Kumar, R. Impact of fly ash impurity on the hydrate based gas separation process for carbon dioxide capture from a flue gas mixture. *Ind. Eng. Chem. Res.* **2014**, *53*, 9859.
- Kumar, A.; Sakpal, T.; Linga, P.; Kumar, R. Influence of contact medium and surfactants on carbon dioxide clathrate hydrate kinetics. *Fuel*, **2013**, *105*, 671.
- Kumar, R.; Linga, P.; Ripmeester, J.A.; Englezos, P. Two-Stage Clathrate Hydrate/Membrane Process for Precombustion Capture of Carbon Dioxide and Hydrogen. *J Environ Eng-Asce*, **2009**, *135*, 411.
- Kumar, R.; Wu, H.; Englezos, P. Incipient Hydrate Phase Equilibrium for Gas Mixtures Containing Hydrogen, Carbon Dioxide and Propane. *Fluid Phase Equilib.* **2006**, *244*, 167.
- Kutergin, O.B.; Mel'nikov, V.P.; Nesterov, A.N. Surfactant effect on the mechanism and kinetics of gas hydrate formation. *Doklady Acad. Sci.* **1992**, *323*, 549.

- Kvenvolden, K. A. Gas hydrates; Geological perspective and global change. *Reviews of Geophysics*, **1993**, *31*, 187.
- Lee, M. W.; Collett, T. S. *J. Geophys. Res. B: Solid Earth*, **2009**, *114* (B7), 1.
DIO: 10.1029/2008JB006237.
- Leporcher, E. M.; Peytavy, J. L.; Mollier, Y.; Sjoblom, J.; Labes-Carrier, C. *Multiphase transportation: hydrate plugging prevention through crude oil natural surfactants*. SPE Annual Technical Conference and Exhibition, New Orleans, LA, USA, 1998.
- Li, S.; Fan, S.; Wang, J.; Lang, X.; Wang, Y. Clathrate Hydrate Capture of CO₂ from Simulated Flue Gas with Cyclopentane/Water Emulsion. *Chinese J. Chem. Eng.* **2010**, *20118*, 206.
- Li, X.S. ; Xu, C.G.; Chen, Z.Y.; Wu, H.J. Hydrate-based Pre-combustion Carbon Dioxide Capture Process in the System with Tetra-n-butyl Ammonium Bromide Solution in the presence of Cyclopentane. *Energy*, **2011**, *36*, 1394.
- Linga, P.; Adeyemo, A.; Englezos, P. Medium-pressure clathrate hydrate/membrane hybrid process for post combustion capture of carbon dioxide. *Environ. Sci. Technol.* **2008**, *42*, 315.
- Linga, P.; Daraboina, N.; Ripmeester, J.A.; Englezos, P. Enhanced rate of gas hydrate formation in a fixed bed column filled with sand compared to a stirred vessel. *Chem. Eng. Sci.* **2012**, *68*, 623.
- Linga, P.; Haligva, C.; Nam, S. C.; Ripmeester, J. A. Recovery of Methane from Hydrate formed in a Variable Volume Bed of Silica Sand Particles. *Energy Fuels*, **2009**, *23*, 5508.
- Linga, P.; Kumar, R.; Englezos, P. Gas hydrate formation from hydrogen/carbon dioxide and nitrogen/carbon dioxide gas mixtures. *Chem. Eng. Sci.* **2007**, *62*, 4268.
- Linga, P.; Kumar, R.; Englezos, P. The clathrate hydrate process for post and pre combustion capture of carbon dioxide. *J.Hazard.Mater.* **2007**, *149*, 629.
- Linga, P.; Kumar, R.; Lee, J.D.; Ripmeester, J.; Englezos, P. A new apparatus to enhance the rate of gas hydrate formation: application to capture of carbon dioxide. *Int. J. Greenh. Gas Control*, **2010**, *4*, 637.
- Link, D.; Ladner, E.P.; Elsen, H.A.; Taylor, C.E. Formation and Dissociation Studies for Optimizing the Uptake of Methane by Methane Hydrates. *Fluid Phase Equilibr.* **2003**, *211*, 10.
- Lirio, C.F.D.S.; Pessoa, F.L.P.; Uller, A.M.C. Storage capacity of carbon dioxide hydrates in the presence of sodium dodecyl sulfate (SDS) and tetrahydrofuran (THF). *Chem. Eng. Sci.* **2013**, *96*, 123.
- Liu, C. L.; Lu, H. L.; Ye, Y. G.; Ripmeester, J. A.; Zhang, X. H. Raman spectroscopic observations on the structural characteristics and dissociation behavior of methane hydrate synthesized in silica sands with various sizes. *Energy Fuels* **2008**, *22*, 3986.
- Makogon, Y. F. *Hydrates of Natural Gas*. Pennwell books, Tulsa, Okla. (Translated by Cieslewicz, W. J.), 1981.
- Makogon, Y. F.; Holditch, S. A.; Makogon, T. Y. Natural gas hydrates; A potential energy source for the 21st century. *J. Petrol. Sci. Eng.* **2007**, *56*, 31.
- Makogon, Y. F.; Trebin, F. A.; Trofimuk, A. A.; Tsarev, V. P.; Cherskii, N., Detection of a pool of natural gas in a solid (hydrated gas) state. *Doklady Academy Sci.* **1971**, *196*, 206.
- Matson, S. L.; Herrick, C. S.; Ward, W. J. Progress on the selective removal of H₂S from gasified coal using an immobilized liquid membrane. *Ind. Engg. Chem. Process Design and Develop.* **1997**, *16*, 370.
- Mattson, E. *I.V.A. Medd.* **1963**, *137*, 100.

- Mel'nikov, V.P.; Nesterov, A.N.; Feklistov, V.V. Formation of gas hydrates in the presence of additives consisting of surface-active substances. *Khimiia v Interesakh Ustoichivogo Razvitiia*, **1998**, *6*, 102.
- Melnikov, V.P.; Nesterov, A.N. *Water migration during gas hydrate formation in porous media*. In: Proceedings of the International Symposium on Ground Freezing and Frost Action in Soils, 1997, 391.
- Milkov, A. V.; Dickens, G. R.; Claypool, G. E.; Lee, Y. J.; Borowski, W. S.; Torres, M. E.; Xu, W. Y.; Tomaru, H.; Trehu, A. M.; Schultheiss, P. Co-existence of gas hydrate, free gas, and brine within the regional gas hydrate stability zone at hydrate ridge (Oregon margin): Evidence from prolonged degassing of a pressurized core. *Earth Planetary Sci. Letters*, **2004**, *222*, 843.
- Mori, Y.H. Recent Advances in Hydrate-Based Technologies for Natural Gas Storage--A Review. *J. Chem. Ind. Eng. (China)*, **2003**, *54*,17
- Natarajan, V.; Bishnoi, P.R.; Kalogerakis, N. Induction phenomena in gas hydrate nucleation. *Chem. Eng. Sci.***1994**, *49*, 87.
- National Energy Technology Laboratory. *Cost and Performance Baseline for Fossil Energy Power Plants Study*, Volume 1: Bituminous coal and natural gas to electricity, DOE/NETL-2007/1281, 2007. Available online: <http://www.netl.doe.gov>
- Nohra, M.; Woo, T. K.; Alavi, S.; Ripmeester, J. A. Molecular Dynamics Gibbs Free Energy Calculations for CO₂ Capture and Storage in Structure I Clathrate Hydrates in the Presence of SO₂, CH₄, N₂, and H₂S Impurities. *J. Chem. Thermodyn.* **2012**, *44*, 5.
- Okutani, K.; Kuwabara, Y.; Mori, Y.H. Surfactant effects on hydrate formation in an unstirred gas/liquid system: An experimental study using methane and sodium alkyl sulfates. *Chem. Eng. Sci.* **2008**, *63*, 194.
- Owby, D.W.; Prapaitrakul, W.; King, A.D. The Solubility of carbon dioxide and nitrous oxide in aqueous solutions of cetyltrimethylammonium bromide, sodium dodecyl sulphate, sodium 1-heptanesulfonate, and sodium perfluorooctanoate. *J. Colloid Interface Sci.* **1997**, *125*, 526.
- Ramana, M. V.; Ramprasad, T.; Paropkari, A. L.; Borole, D. V.; Rao, B. R.; Karisiddaiah, S. M.; Desa, M.; Kocherla, M.; Joao, H. M.; Lokabharati, P.; Gonsalves, M. J.; Pattan, J. N.; Khadge, N. H.; Babu, C. P. Multidisciplinary investigations exploring indicators of gas hydrate occurrence in the Krishna–Godavari Basin offshore, east coast of India. *Geo-Mar. Lett.* **2009**, *29*, 25.
- Rempel, A. W. *J. Geophys. Res.* **2011**, *116* (B10), 1. DOI: 10.1029/2011JB008484.
- Ricaurte, M.; Torré, J.P.; Asbaï, A.; Broseta, D.; Dicharry, C. Experimental data, modeling, and correlation of carbon dioxide solubility in aqueous solutions containing low concentrations of clathrate hydrate promoters: application to CO₂–CH₄ gas mixtures. *Ind. Eng. Chem. Res.* **2012**, *51*, 3157.
- Ripmeester, J. A.; Ratcliffe, C. I.; Klug, D. D.; Tse, J. S., Molecular Perspectives on Structure and Dynamics in Clathrate Hydrates. International Conference on Natural Gas Hydrates, 1994, 715, 161.
- Ripmeester, J. A.; Tse, J. S.; Ratcliffe, C. I.; Powell, B. M. A New Clathrate Hydrate Structure. *Nature*, **1987**, *325*, 135.
- Ripmeester, J. In 3rd International Hydrate Conference (Ed, Holder, B. E.) NYAS, Salt Lake City, 2000, 912.
- Roy, S.; Mehra, A.; Bhowmick, D. Prediction of solubility of nonpolar gases in micellar solutions of ionic surfactants. *J. Colloid Interface Sci.* **1997**, *196*, 53.

- Seo, Y. T.; Lee, H. Structure and guest distribution of the mixed carbon dioxide and nitrogen hydrates as revealed by X-ray diffraction and C-13 NMR spectroscopy. *J. Physical Chem. B*, **2004**, *108*, 530.
- Seo, Y.T.; Moudrakovski, I.L.; Ripmeester, J.; Lee, J.W.; Lee, H. Efficient recovery of CO₂ from flue gas by clathrate hydrate formation in porous silica gels. *Environ. Sci. Tech.* **2005**, *39*, 2315.
- Shah, D.O. *The World of Surface Science. In Chemical Engineering Education*, Anderson, T.J. Ed.; American Society for Engineering Education: Washington, DC, 1977.
- Sloan, E. D.; Fleyfel, F. Hydrate Dissociation Enthalpy and Guest Size. *Fluid Phase Equilib.* **1992**, *76*, 123.
- Sloan, E. D.; Koh, C. A. *Clathrate hydrates of natural gases*, 3rd ed. CRC Press. New York, USA, 2008.
- Smith, J. M.; Van Ness, H. C.; Abbott, M. M. *Introduction to chemical engineering thermodynamics*. New York: McGraw-Hill, Inc; 2001.
- Song, Y.; Wang, X.; Yang, M.; Jiang, L.; Liu, Y.; Dou, B. Study of selected factors affecting hydrate-based carbon dioxide separation from simulated fuel gas in porous media. *Energy Fuels* **2013**, *27*, 3341–3348.
- Spencer, D. F.; Tam, S. S.; Deppe, G.; Currier, R. F.; Young, J. S.; Anderson, G. K. *Proceedings of 19th Annual International Pittsburgh Coal Conference*: Pittsburgh, PA, 2002.
- Sun, D.; Englezos, P. Storage of CO₂ in a partially saturated porous medium at gas hydrate formation conditions. *Int. J. Greenh. Gas Control*. 2014, *25*, 8.
- Suradkar, Y.R.; Bhagwat, S.S. CMC Determination of an Odd Carbon Chain Surfactant (C₁₃E₂₀) Mixed with Other Surfactants Using a Spectrophotometric Technique. *J. Chem. Eng. Data*. **2006**, *51*, 2031.
- Sweny, J. W.; Valentine, J. P. *Physical solvent stars in gas treatment/purification. Chemical Engineering* (New York, NY, United States) 1970, *77*, 54.
- Takahashi, T., Goldberg, D., and Mutter, J. C., *International Symposium on Deep Sea Sequestration of CO₂*, Tokyo, Japan, 2000.
- Takeya, S.; Hori, A.; Hondoh, T.; Uchida, T. Freezing-Memory Effect of Water on Nucleation of CO₂ Hydrate Crystals. *J. Phys. Chem. B* **2000**, *104*, 4164.
- Teresa, L.; Tarbuck and Geraldine L.; Richmond. Adsorption and Reaction of CO₂ and SO₂ at a Water Surface, *J. Am. Chem. Soc.* **2006**, *128*, 3256.
- Torre, J. P.; Ricaurte, M.; Dicharry, C.; Broseta, D. CO₂ Enclathration in the presence of Water-Soluble Hydrate Promoters: Hydrate Phase Equilibria and Kinetic studies in Quiescent conditions. *Chem. Eng. Sci.* **2012**, *82*, 1.
- Tulk, C. A.; Ripmeester, J. A.; Klug, D. D. *Gas Hydrates* **2000**, *912*, 859. DOI: 10.1111/j.1749-6632.2000.tb06840.x.
- U.S. Department of Energy, *DOE/NETL Carbon Dioxide Capture R&D Annual Technology Update, Draft, National Energy Technology Laboratory, Pittsburgh, PA, April 2010; hereafter "DOE, Carbon Dioxide Capture*
- Uchida, T.; Ebinuma, T.; Kawabata, J.; Narita, H. Microscopic observations of formation processes of clathrate-hydrate films at an interface between water and carbon dioxide, *J. Cryst. Growth*, **1999**, *204*, 348.
- Uchida, T.; Ikeda, I. Y.; Takeya, S.; Kamata, Y.; Ohmura, R.; Nagao, J.; Buffett, B. A. Kinetics and Stability of CH₄–CO₂ Mixed Gas Hydrates during Formation and Long-Term Storage. *Chem. Phys. Chem.* **2005**, *6*, 654.

- Uchida, T.; Takeya, S.; Chuvilin, E. M.; Ohmura, R.; Nagao, J.; Yakushev, V. S.; Istomin, V. A.; Minagawa, H.; Ebinuma, T.; Narita, H. *J. Geophys. Res.*, **2004**, *109* (B5), 1. DOI:10.1029/2003JB002771.
- Udachin, K. A.; Ripmeester, J. A. A complex clathrate hydrate structure showing bimodal guest hydration. *Nature*, **1999**, *397*, 420.
- Vannerberg, N. G.; Sydberger, T. Reaction Between SO₂ and Wet Metal *Surfaces, Corrosion sci.* **1970**, *10*, 43.
- Veluswamy, H.P.; Kumar, R.; Linga, P. Hydrogen storage in clathrate hydrates: current state of the art and future directions. *Appl. Energy*. **2014**, *122*, 132.
- Verrett, J.; Servio, P. Evaluating surfactants and their effect on methane mole fraction during hydrate growth. *Ind. Eng. Chem. Res.* **2012**, *51*, 13149.
- Vögtle, F. *Supramolecular Chemistry*. Wiley, Chichester, 1991.
- Waite, W. F., et al. Physical properties of hydrate-bearing sediments, *Rev. Geophys.*, **2009**, *47*, RG4003.
- Waite, W. F.; DeMartin, B. J.; Kirby, S. H.; Pinkston, J.; Ruppel, C. D. Thermal conductivity measurements in porous mixtures of methane hydrate and quartz sand. *Geophys. Res. Lett.* **2002**, *29*, 82.
- Waite, W. F.; Stern, L. A.; Kirby, S. H.; W. J. Winters, Mason, D. H. Simultaneous determination of thermal conductivity, thermal diffusivity and specific heat in sl methane hydrate, *Geophys. J. Int.*, **2007**, *169*, 767.
- Waite, W. F.; Winters, W. J.; Mason, D. H. Methane hydrate formation in partially water-saturated Ottawa sand. *Am. Mineral.* **2004**, *89*, 1202.
- Yamasaki, A. A New CO₂ Ocean Sequestration Scenario via a Crystallization Process of CO₂ Hydrate Particles," Proceedings of DEEP SEA & CO₂, *International Symposium on Deep Sea Sequestration of CO₂*, Tokyo, Japan, 2000.
- Yang, D.; Le, L. A.; Martinez, R.J.; Currier, R.P.; Spencer, D.F. Kinetics of CO₂ hydrate formation in a continuous flow reactor. *Chem. Eng. J.* **2011**, *172*, 144.
- Yang, D.; Le, L.A.; Martinez, R.J.; Currier, R.P.; Spencer, D.F.; Deppe, G. Heat Transfer During CO₂ Hydrate Formation in a Continuous Flow Reactor. *Energy Fuels*, **2008**, *22*, 2649.
- Yang, L.; Fan, S.; Wang, Y.; Lang, X.; Xie, D. Accelerated formation of methane hydrate in aluminum foam. *Ind. Eng. Chem. Res.* **2011**, *50*, 11563.
- Yang, M.; Song, Y.; Jiang, L.; Zhu, N.; Liu, Y.; Zhao, Y.; Dou, B.; Li, Q. CO₂ Hydrate Formation and Dissociation in Cooled Porous Media: A Potential Technology for CO₂ Capture and Storage. *Environ. Sci. Technol.* **2013**, *47*, 9739.
- Yoslim, J.; Linga, P.; Englezos, P. Enhanced growth of methane propane clathrate hydrate crystals with sodium dodecylsulfate, sodium tetradecylsulfate, and sodium hexadecylsulfate surfactants. *J. Cryst. Growth.* **2010**, *313*, 80.
- Zhang, J. S.; Lo, C.; Somasundaran, P.; Lu, S.; Couzis, A.; Lee, J. W. Adsorption of Sodium Dodecyl Sulfate at THF Hydrate/Liquid Interface. *J. Phys. Chem. C* **2008**, *112*, 12381.
- Zhang, J. S.; Lo, C.; Somasundaran, P.; Lee, J. W. Competitive Adsorption Between SDS and Carbonate on Tetrahydrofuran Hydrates. *J. Colloid Interface Sci.* **2010**, *341*, 286.
- Zhang, J.S.; Lee S.; Lee, J.W. Kinetics of Methane Hydrate Formation from SDS Solution. *Ind. Eng. Chem. Res.* **2007a**, *46*, 6359.
- Zhang, P.; Wu, Q.; Yang, Y. Characteristics of methane hydrate formation in artificial and natural media. *Energies*, **2013**, *6*, 1233.

- Zhong, D.L.; Ding, K.; Yan, J.; Yang, C.; Sun, D.J. Influence of Cyclopentane and SDS on Methane Separation from Coal Mine Gas by Hydrate Crystallization. *Energy Fuels*. **2013**, *27*, 7258.
- Zhong, Y.; Rogers, R.E. Surfactant Effects on Gas Hydrate Formation. *Chem. Eng. Sci.* **2000**, *55*, 4187.

Appendix A

BET Analysis of silica gels

Quantachrome autosorb automated gas sorption system was used for BET analysis of the silica gels in nitrogen environment. The nitrogen adsorption-desorption isotherms at 77K of the silica gels are shown in Figure A1a. The isotherms were classified as the type IV adsorption-desorption defined by IUPAC which gives useful information through its hysteresis loop [1,2]. For this study, the pore diameters were estimated from the pore size distribution curves obtained either from adsorption (Fig. A-1b) or from desorption (Fig. A-1c) branch of N₂ isotherm by BJH [3] method and DH [4] method. Table A-1 lists the BET specific surface area (m²/g), average pore diameter (nm) and pore volume (cc/g) of silica gels. Silica gel with similar pore diameter was chosen for this study, however as shown in Table A-1 there is a significant difference in the surface area, type C silica gel has a higher surface area compared to type A and type B. As shown in Fig. A-1a, the adsorbed volume in type A silica gel is less than the others, because of larger particle size distribution. Fig. A-1b and A-1c provide the BJH adsorption and desorption pore size distribution respectively. The pore diameter shown in Table A-1 is the average estimated from BJH and DH methods.

Reference

- [1] Sing KSW, Everett DH, Haul RW, Moscou L, Pierotti RA, Rouquerol J et al. Reporting physisorption data for gas/solid systems with special reference to the determination of surface area and porosity. *Pure Appl Chem* 1985;57:603.
- [2] Katsumi K. Determination of pore size and pore size distribution 1. Adsorbents and catalysts, *J of Mem Sci* 1994;96:59-89
- [3] Barrett EP, Joyner LG, Halenda PP. The determination of pore volume and area distributions in porous substances. I. Computations from nitrogen isotherms. *J Am Chem Soc* 1951;73:373.
- [4] Dollimore D, Heal GR. An improved method for the calculation of pore size distribution from adsorption data. *J Appl Chem* 1964;14:109.

Table A-1 N₂ adsorption-desorption analysis of silica gels

Silica gel type	Mesh size	Particle size distribution (µm)	Average Pore diameter (nm)	Pore volume (cc/g)	Surface area (m ² /g)

A	60-120	125-250	5.7	0.815	567
B	100-200	75-150	5.3	0.880	669
C	230-400	40-65	4.5	0.920	817

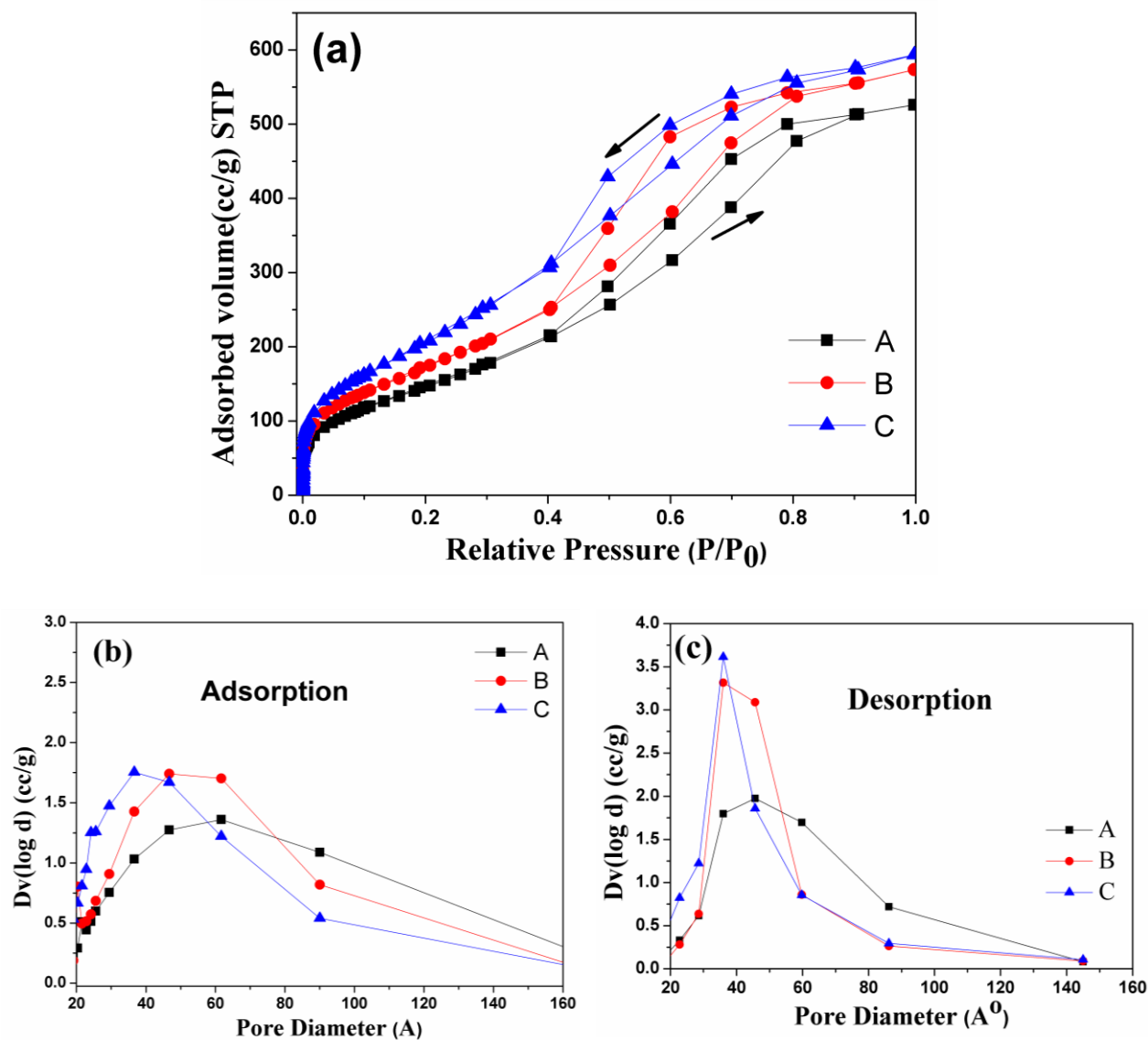


Figure A1. (a) Adsorption – desorption isotherms at liquid nitrogen temperature with a conventional gas adsorption approach. Silica gels of type A, B and C used in the current study were used for BET analysis; small hysteresis observed is typical of silica gel. (b) BJH adsorption pore size distribution curve (c) BJH desorption pore size distribution

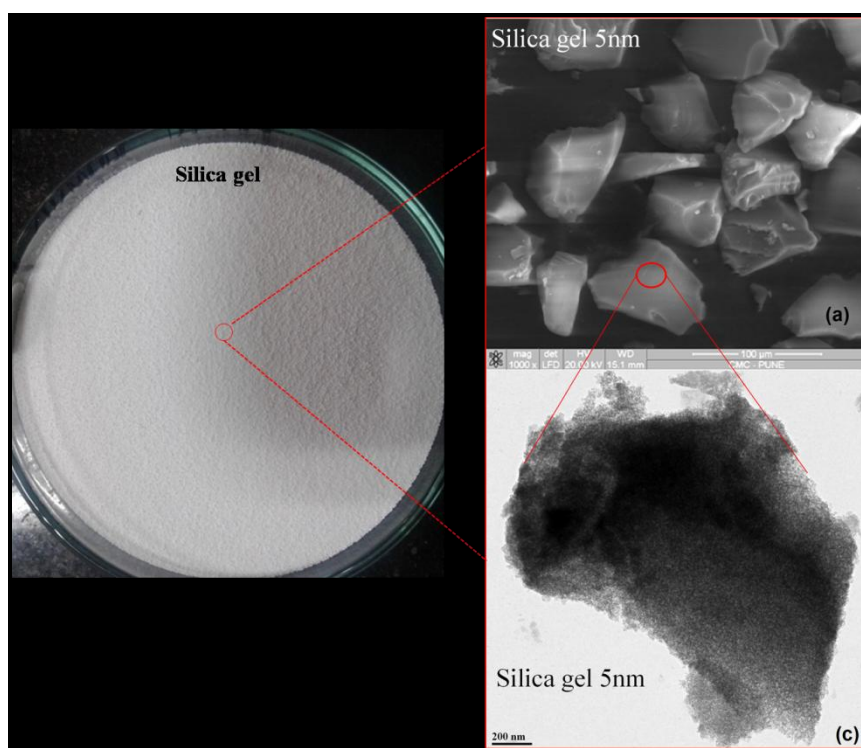


Figure A2: A representative photograph of silica gel (5 nm pore size) along with SEM and TEM image



Figure A3: A representative photograph of experimental setup

Appendix B

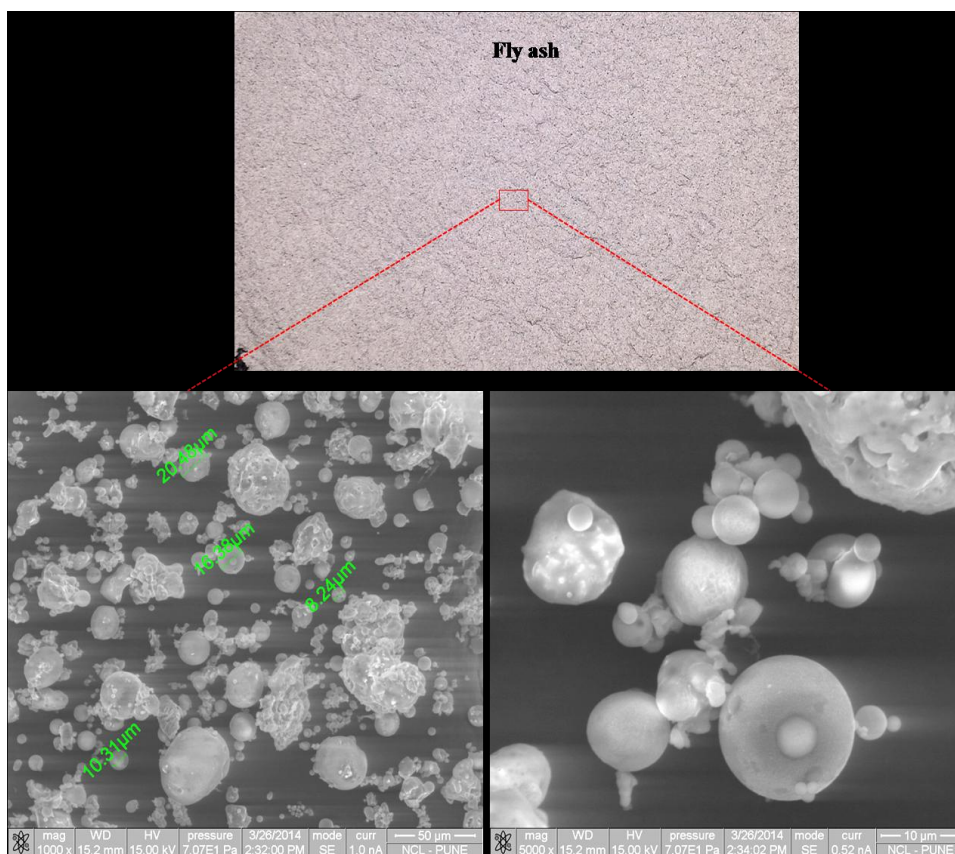


Figure B1: A representative photograph of fly ash along with SEM images

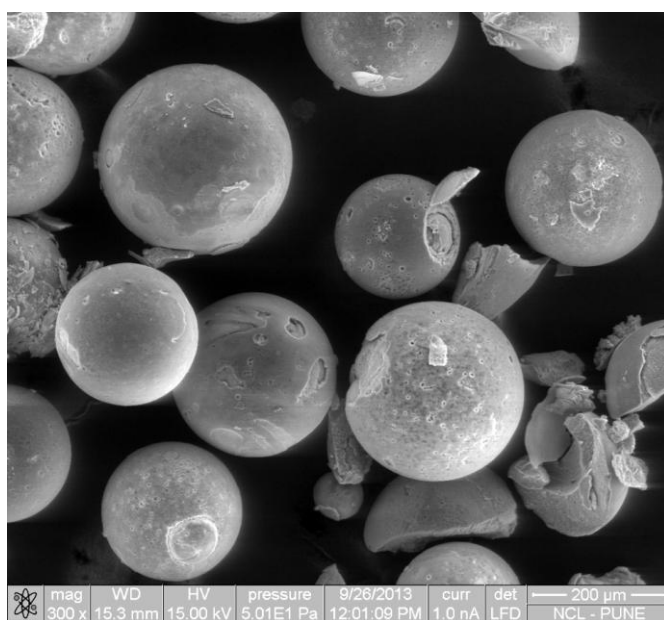


Figure B2: Scanning Electron Microscopy image of spherical silica gel

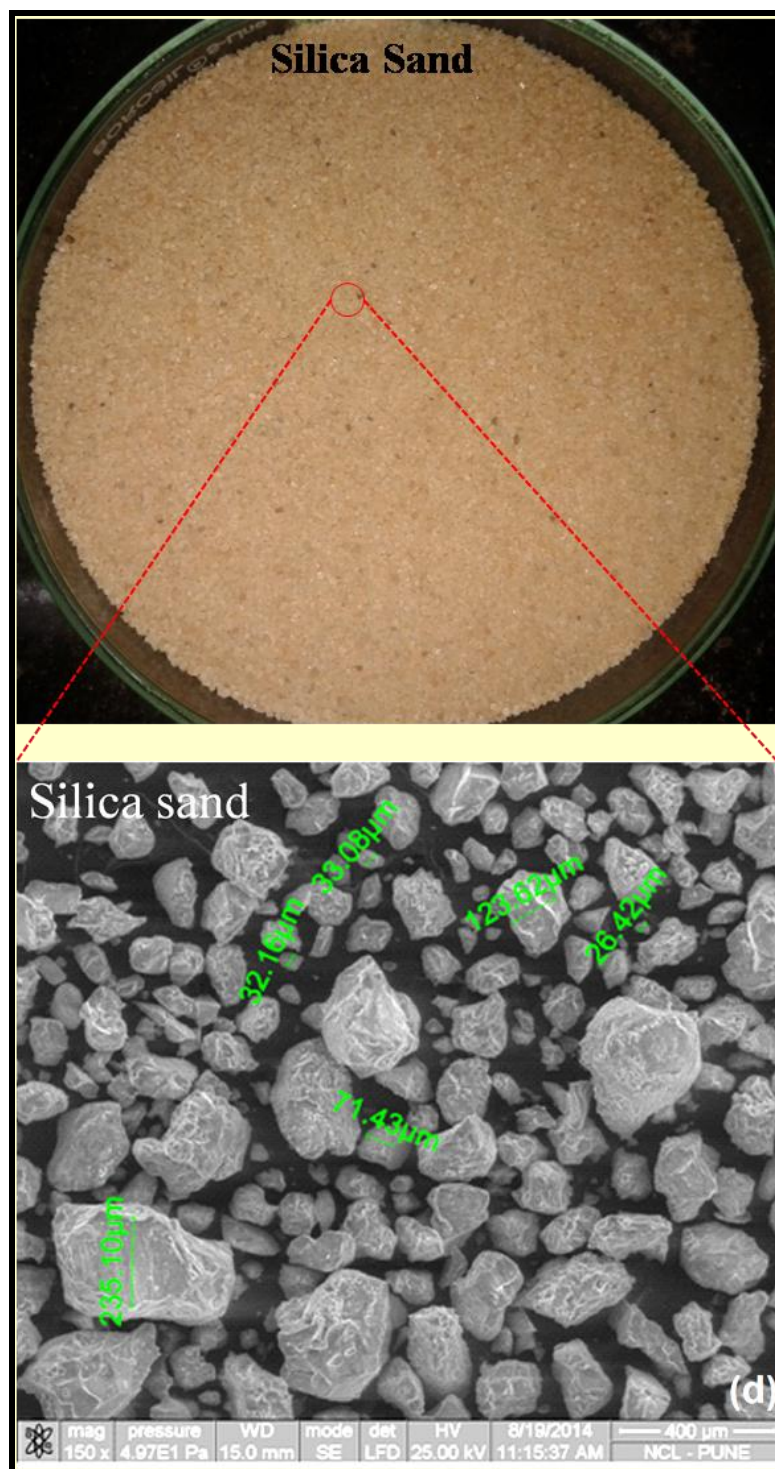


Figure B3: A representative photograph of silica sand along with SEM image

Appendix C

Figure C1: A representative photograph of the SSP-1 (SS-316) random packing

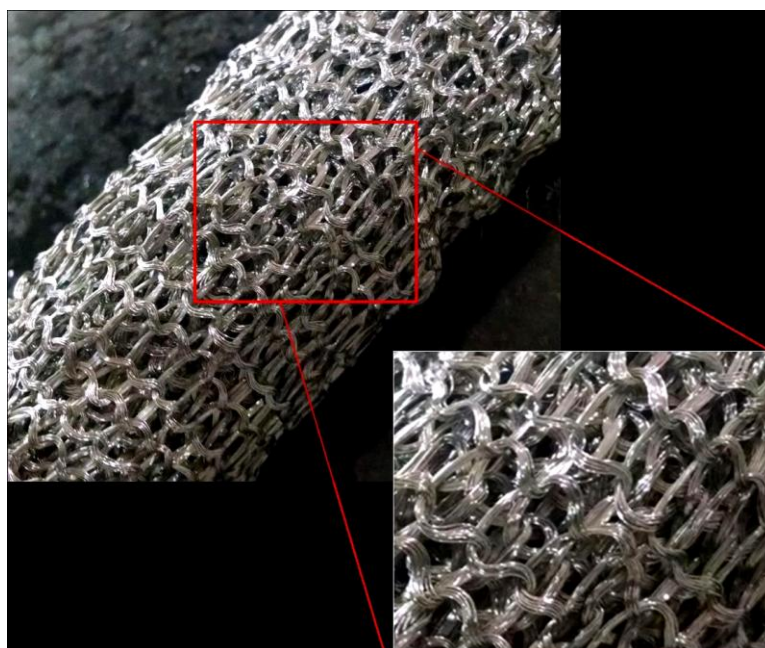


Figure C2: A representative photograph of the SSP-2 (SS-316) structured packing

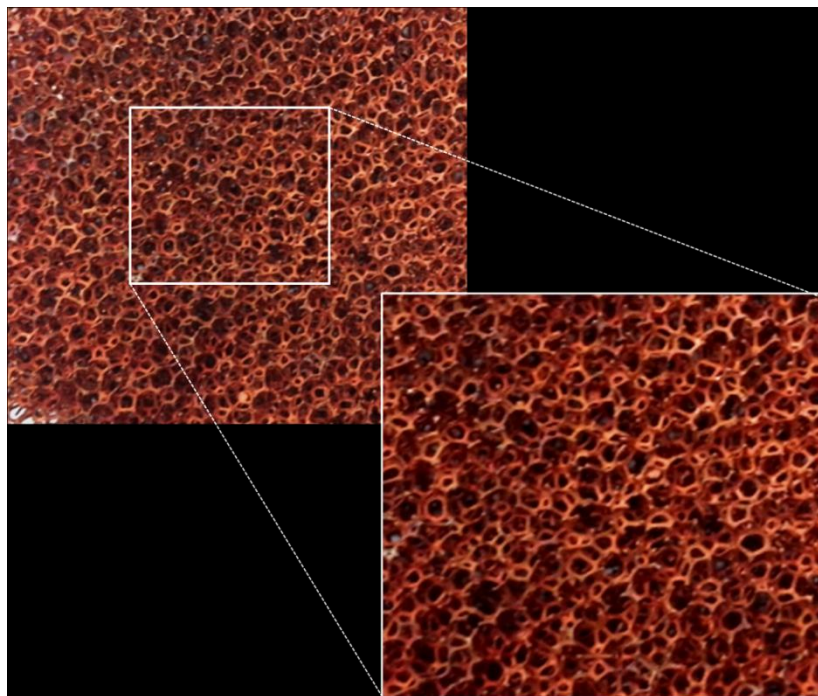


Figure C3: A representative photograph of the copper foam used in this study



Figure C4: A representative photograph of the brass packing used in this study

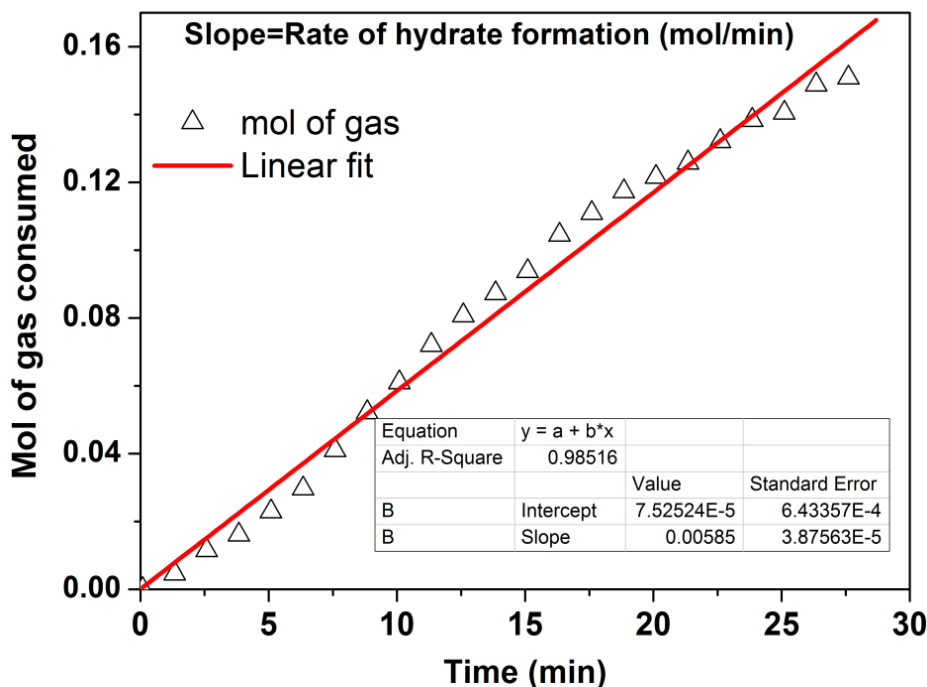


Figure C5. Rate of hydrate formation (R_{30} in $\text{mol} \cdot \text{min}^{-1}$) is calculated by fitting the hydrate growth (gas uptake) data versus time for the first 30 min from nucleation point

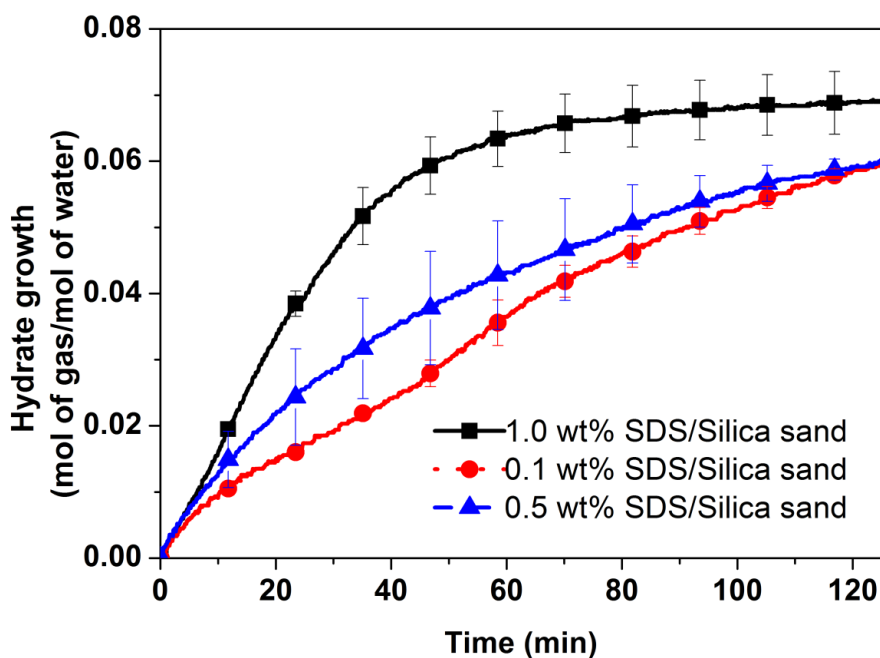


Figure C6: Effect of SDS concentration (0.1%, 0.5% and 1.0% by weight) on the rate of hydrate growth (CO_2 hydrate) in silica sand packing; operating temperature of 274.65 K and pressure 3.0 MPa

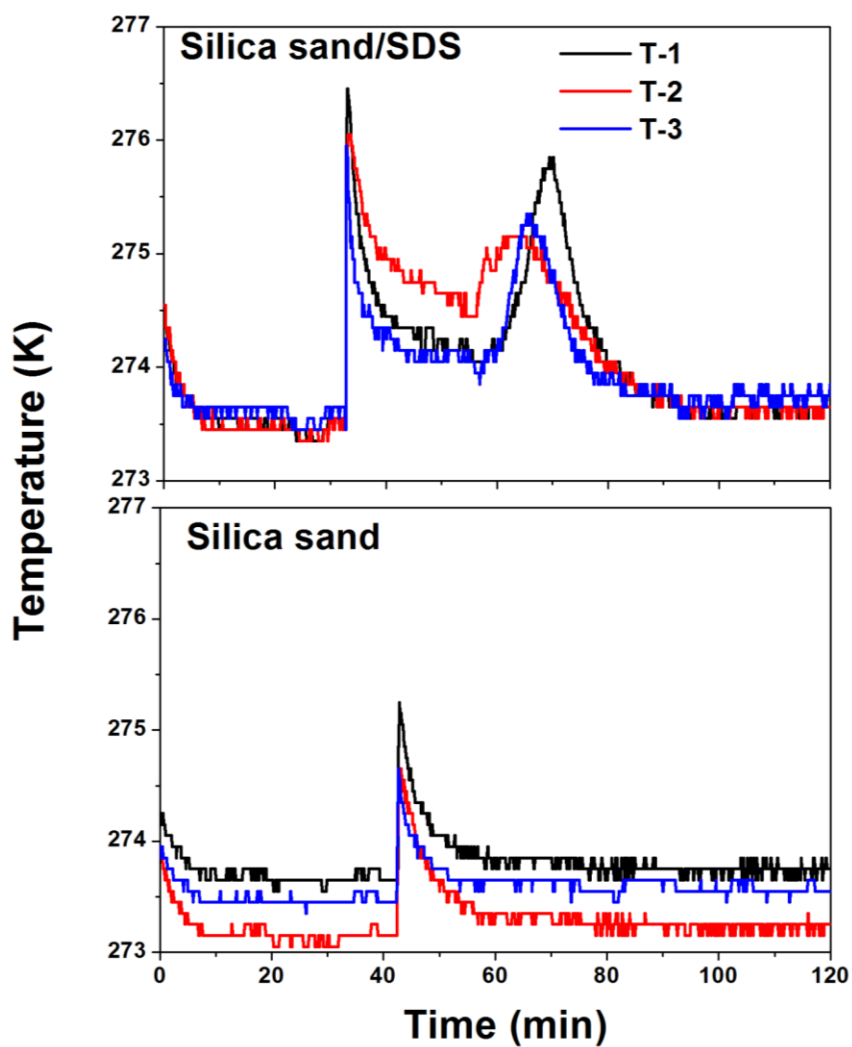


Figure C7: Comparison of temperature profile for two different systems (Silica sand and silica sand+1wt% SDS)

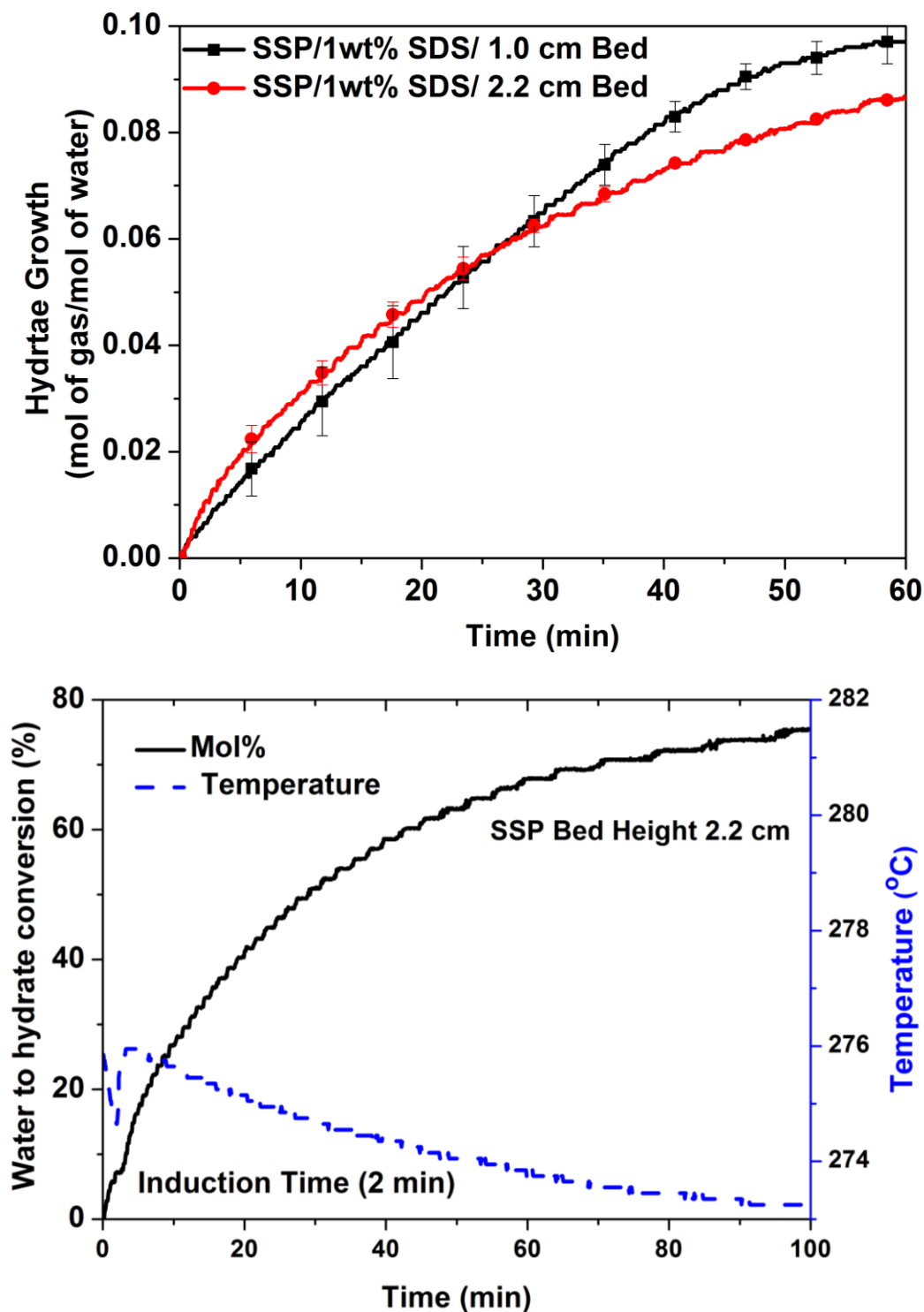


Figure C8: Effect of SSP bed height on hydrate growth and water conversion to hydrate along with temperature profile from CO_2/H_2 mixture at 7.0 MPa and 273.65 K. The average data along with standard deviation are presented. It is noted that amount of water taken for both bed was same (27 cm^3)

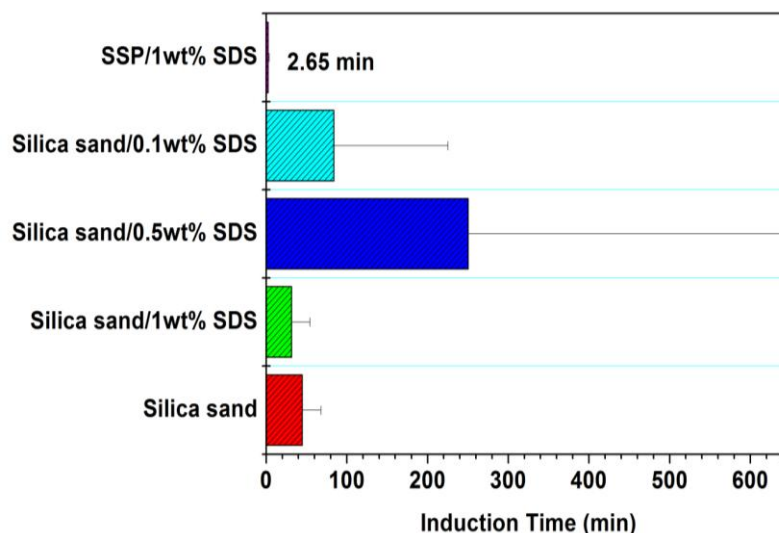


Figure C9: Comparison of induction time for different fixed bed media and different concentration of SDS for hydrate formation.

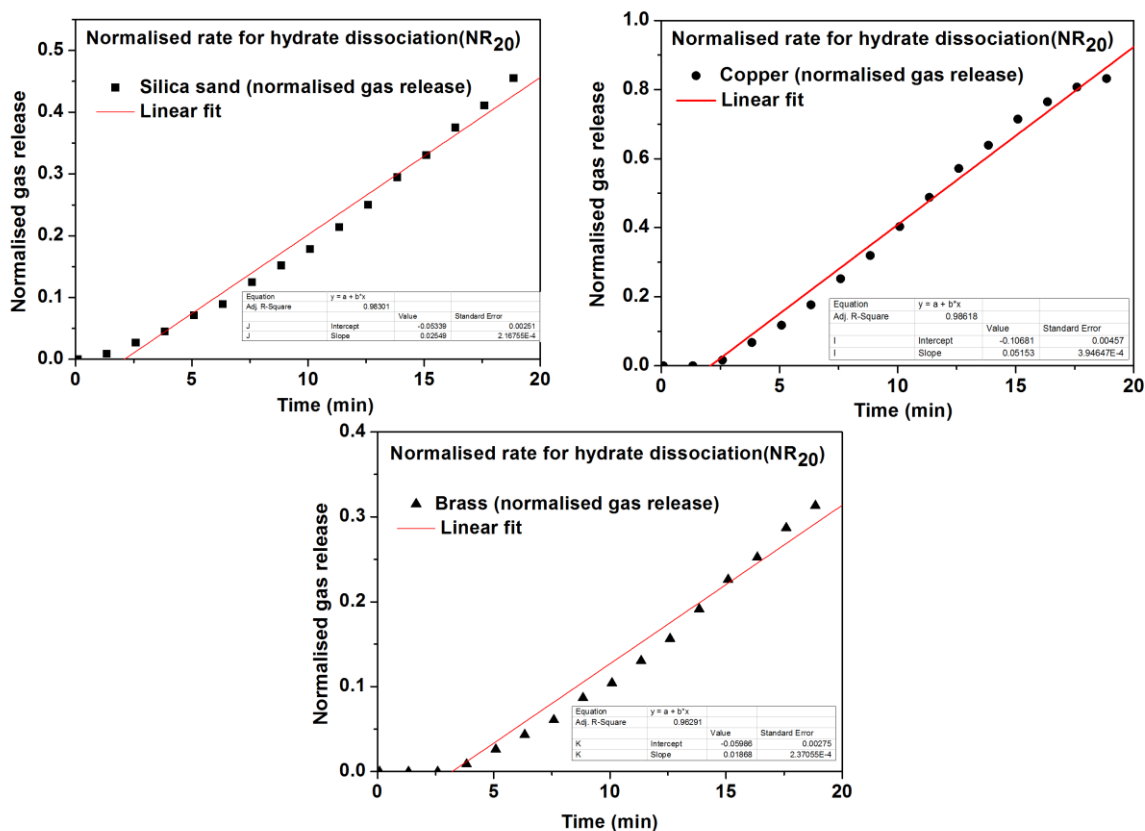


Figure C10: Rate of hydrate dissociation (R_{20} in normalized gas release $\cdot \text{min}^{-1}$) is calculated by fitting the normalized gas release data verses time for the first 20 min during dissociation at 293.15K

Appendix D

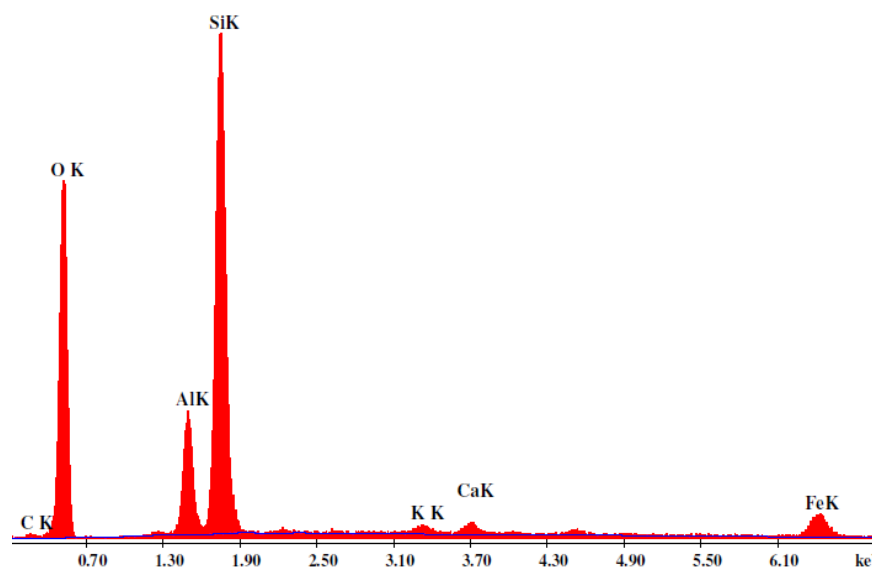


Figure D1. Energy Dispersive X-ray analysis (EDAX) of silica sand/clay (75/25%) mixture



Over saturated silica sand

Layer of extra water



Removal of extra water
in a measuring cylinder

Figure D2. (a) Over saturated silica sand with a layer of extra water (b) Removal of extra water from silica sand and collection in a measuring cylinder.

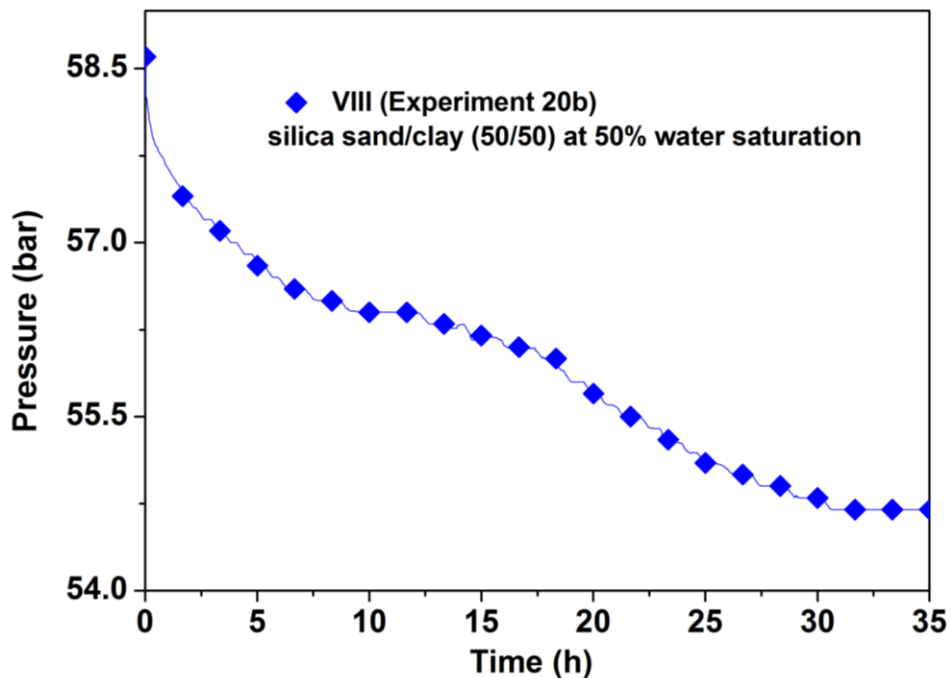


Figure D3. Pressure drop during methane hydrate formation conducted with Silica sand-clay mixture (50:50 ratio) at 50% water saturation level. (Experiment 20b)

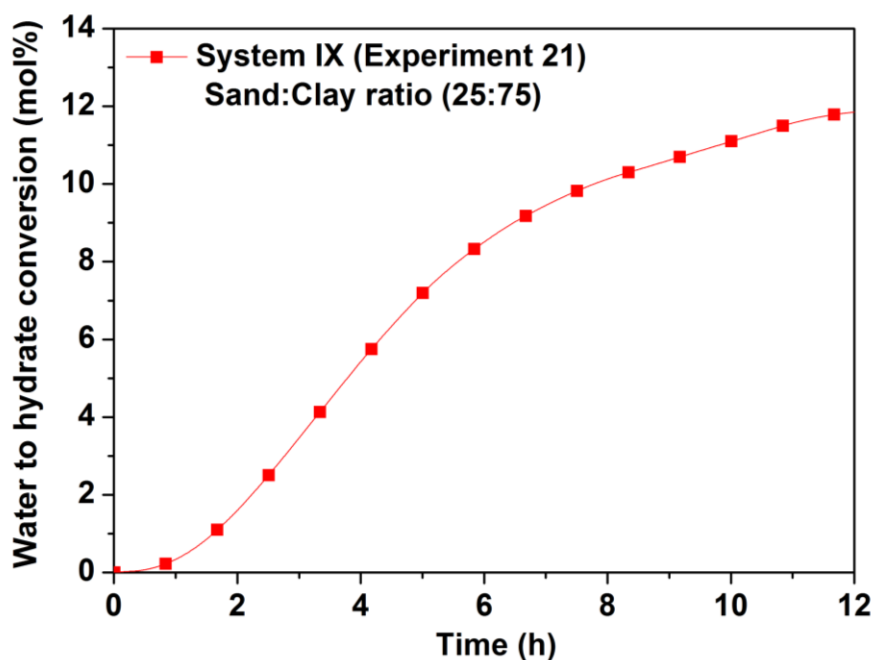


Figure D4. Water to hydrate conversion for methane hydrate formation conducted with Silica sand-clay mixture (25:75 ratio) at 75% water saturation level (experiment 21)

Gas Chromatography Calibration

Before starting the experiments, GC is calibrated each time with different composition of gases as shown in figure D5. Figure D5 shows the calibration curve for CO₂ and CH₄ with a good Adjusted R² of 0.999.

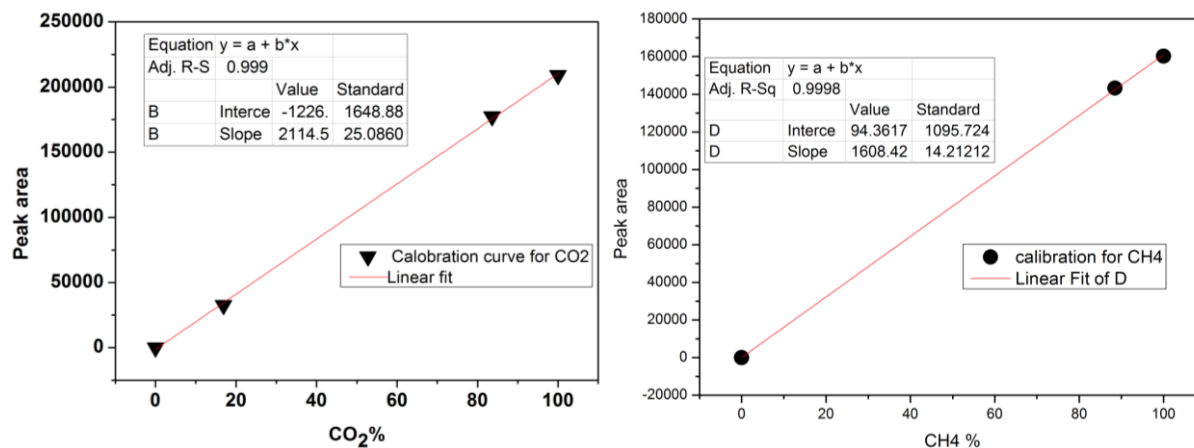


Figure D5. Calibration curve for CO₂ and CH₄

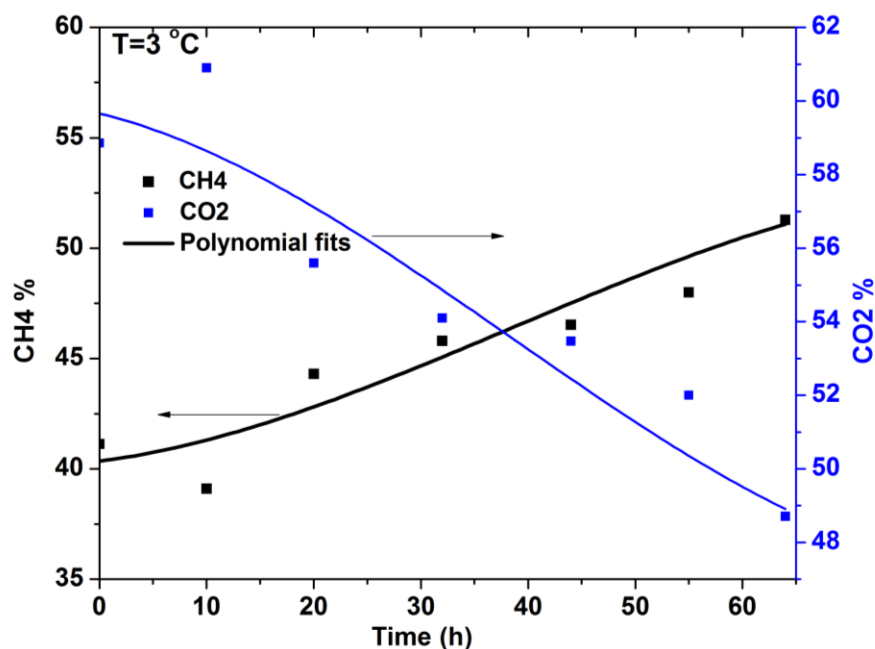


Figure D6. CH₄-CO₂ replacement for SC-72-75 System at 276 (Experiment 2a)

Curriculum Vitae

Asheesh Kumar

C/O Dr. Rajnish Kumar

Gas Hydrate group-Chemical Engineering and Process Development Division

CSIR- National Chemical Laboratory, Pune-411008, India

Tel: +91-7507977028 (M) 00-91-20-2590 3090 (O)

Email: asheeshku@gmail.com, asheesh.kumar@ncl.res.in



Educational qualification

- Ph.D, NCL Pune (2013-2015)
- M.Tech (Advanced Chemical Analysis, IIT Roorkee, India, 2010) (CGPA 8.53)
- M.Sc. (Chemistry, CCS University Meerut, India, 2007) (70.89%)
- Graduation (B.Sc) CCS University Meerut, India, 2004 (68.50%)

Professional experience

- Faculty in Department of Chemistry, Mewar University, Chittorgarh Rajasthan, India (Sep.2010 to Oct. 2011)

Research experience

- **Project Assistant in NCL Pune** (From Oct.2011 to Dec. 2012)
During this period, I worked on DST project “Process development for CO₂ capture from flue and fuel gas mixture by gas hydrate formation”.
- **Internship in National Chemical Laboratory (NCL) Pune** (25 may to 23 July 2009)
Topic: Preparation and Characterization of chitosan-silver nanocomposites
Supervisor: (Prof.) Dr. R.P Singh, Polymer science &engineering division, National chemical laboratory Pune.
- **M.Tech Project in Indian Institute of technology (IIT) Roorkee** (July 2009 to June 2010)
Topic: Preparation of carbonaceous materials using Organometallic compounds for hydrogen storage
Supervisor: Prof. Mala Nath Department of chemistry IIT Roorkee.

Research Interest

Gas hydrates, Methane recovery, CO₂ Capture and Storage, CO₂ Sequestration, Flow assurance, Material chemistry

Contribution in the field of research (Gas Hydrate)

- Ph.D in the field of Gas Hydrate, thesis title is “**Gas Hydrate Studies for Carbon Dioxide Capture and Methane Recovery**”. (2013-2015)
Supervisor: Dr. Rajnish Kumar, Senior Scientist-NCL Pune.
- Successfully completed one year project entitled “**Development studies for kinetics of methane recovery from natural gas hydrate**” sponsored by GAIL India Ltd. (2012-13)
- Worked on another gas hydrate project entitled “**Process development for CO₂ capture from flue and fuel gas mixture**” sponsored by Department of Science & Technology (DST) India. (2011-2014)

Awards/Fellowships

- Received fellowship of MHRD, INDIA by Gate (2008-2010)
- CSIR-Senior Research Fellowship, INDIA (2014)
- Certificate of appreciation by IPFACE Venture center Pune for “PATENT CERTIFICATE COURSE FOR SCIENTIST & ENGINEERS” 2014
- NCL RF-AGNIMITRA MEMORIAL BEST POSTER Award 2014, during National Science Day Celebrations
- Awarded as “*Elsevier Reviewer Recognition*” by Journal of Natural gas Science & Engineering. (2015)

Achievements

- CSIR-NET 2008
- Gate-2008
- Organized a conference on Novel Developments in Medicinal Chemistry-2011, in Mewar University (As Co Convener)

Publications

1. **Asheesh Kumar**, Gaurav Bhattacharjee, B. D. Kulkarni and Rajnish Kumar, Role of surfactants in promoting gas hydrate formation, *Ind. Eng. Chem. Res. (ACS)* **2015**, DOI: 10.1021/acs.iecr.5b03476.
2. **Asheesh Kumar**, Tushar Sakpal, Gaurav Bhattacharjee, Anupam Kumar, Rajnish Kumar, Impact of H₂S Impurity on Carbon Dioxide Hydrate Formation Kinetics in Fixed Bed Arrangements, *Ind. Eng. Chem. Res. (ACS)* **2015**, (DOI: 10.1021/acs.iecr.5b04079)

3. **Asheesh Kumar**, Rajnish Kumar, Role of Metallic Packing and Kinetic Promoter in Designing a Hydrate Based Gas Separation Process, *Energy & Fuels (ACS)*, **2015**, doi: 10.1021/acs.energyfuels.5b00664.
4. **Asheesh Kumar**, Tushar Sakpal, Rajnish Kumar, Influence of Low-Dosage Hydrate Inhibitors on Methane Clathrate Hydrate Formation and Dissociation Kinetics, *Energy Technology (Wiley)*, **2015**, doi/10.1002/ente.201500004. [Citations-2]
5. **Asheesh Kumar**, T Sakpal, S Roy, R Kumar, Methane hydrate formation in a test sediment of sand and clay at various level of water saturation, *Canadian Journal of Chemistry*, **2015**, doi.10.1139/cjc-2014-0537 [Citations-3]
6. Gaurav Bhattacharjee, **Asheesh Kumar**, Tushar Sakpal, and Rajnish Kumar, Carbon Dioxide Sequestration: Influence of Porous Media on Hydrate Formation Kinetics, *ACS Sustainable Chem. Engg. (ACS)*, 2015, 3 (6), 1205-14. [Citations-3]
7. **Asheesh Kumar**, Tushar Sakpal, Praveen Linga, Rajnish Kumar, Enhanced carbon dioxide hydrate formation kinetics in a fixed bed reactor filled with metallic packing, *Chem. Eng. Sci.* **2015**, 122, 78-85. [Citations-6]
8. Amit Arora, **Asheesh Kumar**, Gaurav Bhattacharjee, Pushpendra Kumar, Chandrajit Balomajumder, Effect of different fixed bed media on the performance of sodium dodecyl sulfate for hydrate based CO₂ capture. *Materials & Design*, **2015**, doi:10.1016/j.matdes.2015.06.049.
9. **Asheesh Kumar**, Tushar Sakpal, Praveen Linga, Rajnish Kumar, Impact of Fly Ash Impurity on the Hydrate-Based Gas Separation Process for Carbon Dioxide Capture from a Flue Gas Mixture, *Ind. Eng. Chem. Res. (ACS)* **2014** 53 (23), 849–9859. [Citations-9]
10. **Asheesh Kumar**, Tushar Sakpal, Praveen Linga, Rajnish Kumar, Influence of contact medium and surfactants on carbon dioxide clathrate hydrate kinetics, *FUEL*, **2013**, 105: 664-671.[Citations-51]
(Listed as a “Highly Cited Paper” by Essential Science Indicators since February 2014
(Top 1% in Engineering in 2013) by Thomson Reuters)
11. M Nath, **Asheesh Kumar**, A Mallick, Microporous Carbonaceous Materials Incorporated with Metal (Ti, V and Zn) for Hydrogen Storage, *Materials Science Forum*, **2013**, 755, 111-117.
12. Tushar Sakpal, **Asheesh Kumar**, Sanjay Kamble, Rajnish Kumar Carbon dioxide capture using amine functionalized silica gel, *IJCA*, **2012**, 1214-1222. [Citations-3].
13. **Asheesh Kumar**, Praveen Linga, Rajnish Kumar, Carbon Dioxide Capture From A Flue Gas And Fuel Mixture By Hydrate Formation In Silica Gel And Silica Sand Media, In proceeding of: International Conference on Gas Hydrates, **At Beijing, China**,; 08/2014. [Citations-3]
14. Nilesh Choudhary, **Asheesh Kumar**, Vikesh Singh Baghel Sudip Roy, Rajnish Kumar, Methane Hydrate Dissociation By Thermal Stimulation In Presence Of Kinetic Inhibitors: Experiments And Molecular Dynamics Simulation, In proceeding of: International Conference on Gas Hydrates, **At Beijing, China**; 08/2014 [Citations-1]
15. Amit Arora, **Asheesh Kumar**, Chanderjit Balmajumder, Rajnish Kumar, Maneet Kaur, Pushpendra Kumar, Influence of Zeolites On Carbon Dioxide Gas Hydrate Formation

Proceedings of the International Conference on Gas Hydrates, **Beijing, China**; 08/2014. [\[Citations-1\]](#)

16. Tushar Sakpal, **Asheesh Kumar**, Praveen Linga, Rajnish Kumar, Amine enriched silica gel: An efficient adsorbent for post combustion carbon dioxide capture (PCCC). *Chemical Engineering & Technology*, **2015**, ([Under Review](#)).

Patents/Books/Reports/General articles etc.

- [1] Gas Hydrate Based Gas Separation Process Using Fixed Bed Setup, Patent application No. 445/DEL/2015 (**Under process**)
- [2] Mala Nath, **Asheesh Kumar**, Arjit Mallick, Development and Characterization of Carbonaceous Materials Incorporated with Metal (Ti, V and Zn) –Organic Compounds for Hydrogen Storage, Characterization of Minerals, Metals, and Materials, 277–284, **2012**, Publisher **John Wiley & Sons, Inc.**

Conferences

1. **Asheesh Kumar**, Gas Hydrate studies for CO₂ capture and methane recovery at **Humboldt Kolleg** on sustainable development: mega trends of the 21st century, Humboldt academy, Pune chapter, Nov 19-21, Goa. (**Poster presentation**).
2. **Asheesh Kumar**, Rajnish Kumar, Impact of H₂S impurity in pre-combustion capture of carbon dioxide using the clathrate hydrate process, 13th International Conference on Carbon Dioxide Utilization (ICCDU XIII), July 5-9, 2015, **National University of Singapore**, Singapore. (**Oral Presentation**)
3. **Asheesh Kumar**, Praveen Linga, Rajnish Kumar, Carbon dioxide capture from a flue and fuel gas mixture by hydrate formation in a fixed bed reactor, 17th CRSI National Symposium in Chemistry, February 06-08, 2015, **CSIR-NCL, Pune (Poster presentation)**.
4. **Asheesh Kumar** and Rajnish Kumar, Gas hydrate: Applications to methane recovery from marine natural gas hydrate reserves, 2014, **NCL Pune**. (Poster presentation on national science day) (**Best poster Award**).
5. **Asheesh Kumar** and Rajnish Kumar, Kinetics of gas hydrate formation in fixed bed reactor compared to stirred tank reactor International Conference on Advances in Chemical Engineering (ACE 2013), February 22-24, 2013. **IIT Roorkee, India (Oral Presentation)**
6. **Asheesh Kumar** and Rajnish Kumar, Kinetics Of Methane Clathrate Hydrate Formation, Decomposition And Methane Recovery Using Test Sediment, ChEmference'12, December 10-11, 2012, **IIT Bombay, Powai (Oral Presentation)**
7. **Asheesh Kumar**, Tushar Sakpal, Rajnish Kumar, Influence of additives on carbon dioxide clathrate hydrate kinetics in silica gel media, 2012, **NCL Pune**. (**Poster presentation** on national science day)
8. **Asheesh Kumar**, Nilesh Choudhary, Rajnish Kumar, Gas Hydrates: Carbon dioxide sequestration and Methane recovery, 2013, **NCL Pune**. (**Poster presentation** on national science day)
9. **Asheesh Kumar**, Nilesh Choudhary, Praveen Linga, Sudip Roy, Rajnish Kumar, Methane Hydrate Dissociation in Presence of Kinetic Hydrate Inhibitor through Experiments and Molecular Dynamics Simulation, **14 AIChE Annual Meeting; Atlanta GA, USA**, 11/2014. (**Oral Presentation**)

10. **Asheesh Kumar**, Rajnish Kumar, Carbon Dioxide Capture and Storage in Various Fixed Bed Media, FIERY ICE 2014, 9th International Methane Hydrate R&D (IMHRD) Workshop, CSIR - **National Geophysical research Institute Hyderabad** - INDIA; 11/2014. (**Poster presentation**)
11. Gaurav Bhattacharjee, **Asheesh Kumar**, Rajnish Kumar, FIERY ICE 2014, 9th International Methane Hydrate R&D (IMHRD) Workshop, CSIR - **National Geophysical research Institute Hyderabad** - INDIA; 11/2014. (**Poster presentation**)
12. S. K. Starling and **Asheesh Kumar**; Applications of shortest-pulse x-rays/ultra-fast x-ray beams in different field of science; 4th conference on Recent trends in instrumental methods of analysis, *IIT Roorkee*, 2011, p54. (Oral Presentation)
13. **Asheesh Kumar**; Vijay Rana and R.P.Singh; Preparation, characterization and antimicrobial activity of chitosan-silver nanocomposites; 1st conference on Novel Developments in Medicinal Chemistry, *Mewar University Chittorgarh*, Rajasthan, 2011, p39. (Oral Presentation)

References

Dr. Rajnish Kumar

Senior Scientist,
Chemical Engineering and Process
Development Division,
CSIR-National Chemical Laboratory,
Pune-411008, India.
Tel- +91 2025902734,
E-mail- k.rajnish@ncl.res.in

Dr. Praveen Linga

Assistant Professor
Department of Chemical and
Biomolecular Engineering
National University of Singapore
4 Engineering Drive 4, Block E5 02-
23, Singapore 117586
Tel- 65-6601 1487 (DID) 65-6779
1936 (Fax)
E-mail- praveen.linga@nus.edu.sg
(E) www.nus.edu.sg (W)